NAVAL POSTGRADUATE SCHOOL
Monterey, California

THESIS

NUMERICAL PREDICTION OF MARINE FOG USING THE COUPLED OCEAN/ATMOSPHERE MESOSCALE PREDICTION SYSTEM (COAMPS)

by

John L. Dumas

March 2001

Thesis Advisor:	Douglas K. Miller
Second Reader:	Wendell A. Nuss

Approved for public release; distribution is unlimited

20010614 117

REPORT DOCUMENTATION PAGE	Form Approved OMB No. 0704-0188

Public reporting burden for this collection of information is estimated to average 1 hour per response, including the time for reviewing instruction, searching existing data sources, gathering and maintaining the data needed, and completing and reviewing the collection of information. Send comments regarding this burden estimate or any other aspect of this collection of information, including suggestions for reducing this burden, to Washington headquarters Services, Directorate for Information Operations and Reports, 1215 Jefferson Davis Highway, Suite 1204, Arlington, VA 22202-4302, and to the Office of Management and Budget, Paperwork Reduction Project (0704-0188) Washington DC 20503.

1. AGENCY USE ONLY *(Leave blank)*	2. REPORT DATE March 2001	3. REPORT TYPE AND DATES COVERED Master's Thesis

4. TITLE AND SUBTITLE: Title (Mix case letters) Numerical Prediction of Marine Fog Using the Coupled Ocean/Atmosphere Mesoscale Prediction System (COAMPS)	**5. FUNDING NUMBERS**
6. AUTHOR(S) John L. Dumas	
7. PERFORMING ORGANIZATION NAME(S) AND ADDRESS(ES) Naval Postgraduate School Monterey, CA 93943-5000	**8. PERFORMING ORGANIZATION REPORT NUMBER**
9. SPONSORING / MONITORING AGENCY NAME(S) AND ADDRESS(ES) N/A	**10. SPONSORING / MONITORING AGENCY REPORT NUMBER**

11. SUPPLEMENTARY NOTES *The views expressed in this thesis are those of the author and do not reflect the official policy or position of the Department of Defense or the U.S. Government.*

12a. DISTRIBUTION / AVAILABILITY STATEMENT Approved for public release; distribution is unlimited	**12b. DISTRIBUTION CODE**

13. ABSTRACT ***(maximum 200 words)***

The U.S. Navy's requirement for a computer prediction system for marine fog and stratus dates back to the 1970s when meteorological models were being introduced to the fleet. The Naval Research Laboratory's Coupled Ocean/Atmosphere Mesoscale Prediction System (COAMPS) is a leap forward in the Navy's numerical modeling ability but it still does not show great skill in fog forecasting. COAMPS has been "tuned," or adjusted for certain constants and parameterizations, so that it has the minimum error for the maximum area. This tuning is a common practice for all numerical models. The objective of this thesis is to determine if changes can be made to the existing COAMPS code based on reasonable physical experiments for a specific location to help solve the numerical fog forecasting problem. The effectiveness of these experiments was first measured by comparing a modeled cloud edge to satellite imagery of Monterey, California taken during a week in August 2000 under a variety of foggy conditions. Comparisons were also made with observations taken from an aircraft, land stations and a vertical profiler. The experiments, specifically those regarding changes to the autoconversion and turbulent kinetic energy schemes, showed that while a perfect solution has not been found, it is possible to modify the model physics codes and optimize its performance in a specific region.

14. SUBJECT TERMS Mesoscale Modeling, Model Verification, COAMPS, Fog, Stratus, Forecasting	**15. NUMBER OF PAGES** 182
	16. PRICE CODE

17. SECURITY CLASSIFICATION OF REPORT	18. SECURITY CLASSIFICATION OF THIS PAGE	19. SECURITY CLASSIFICATION OF ABSTRACT	20. LIMITATION OF ABSTRACT
Unclassified	Unclassified	Unclassified	UL

NSN 7540-01-280-5500

Standard Form 298 (Rev. 2-89)
Prescribed by ANSI Std. 239-18

THIS PAGE INTENTIONALLY LEFT BLANK

Approved for public release; distribution is unlimited

NUMERICAL PREDICTION OF MARINE FOG USING THE COUPLED OCEAN/ATMOSPHERE MESOSCALE PREDICTION SYSTEM (COAMPS)

John L. Dumas
Lieutenant Commander, United States Navy
B.S., University of Notre Dame, 1988

Submitted in partial fulfillment of the
requirements for the degree of

MASTER OF SCIENCE IN METEOROLOGY AND PHYSICAL OCEANOGRAPHY

from the

NAVAL POSTGRADUATE SCHOOL
March 2001

Author: _____
John L. Dumas

Approved by: _____
Douglas K. Miller, Thesis Advisor

_____
Wendell A. Nuss, Second Reader

_____ for
Carlyle H. Wash, Chairman
Department of Meteorology

THIS PAGE INTENTIONALLY LEFT BLANK

ABSTRACT

The U.S. Navy's requirement for a computer prediction system for marine fog and stratus dates back to the 1970s when meteorological models were being introduced to the fleet. The Naval Research Laboratory's Coupled Ocean/Atmosphere Mesoscale Prediction System (COAMPS) is a leap forward in the Navy's numerical modeling ability but it still does not show great skill in fog forecasting. COAMPS has been "tuned," or adjusted for certain constants and parameterizations, so that it has the minimum error for the maximum area. This tuning is a common practice for all numerical models. The objective of this thesis is to determine if changes can be made to the existing COAMPS code based on reasonable physical experiments for a specific location to help solve the numerical fog forecasting problem. The effectiveness of these experiments was first measured by comparing a modeled cloud edge to satellite imagery of Monterey, California taken during a week in August 2000 under a variety of foggy conditions. Comparisons were also made with observations taken from an aircraft, land stations and a vertical profiler. The experiments, specifically those regarding changes to the autoconversion and turbulent kinetic energy schemes, showed that while a perfect solution has not been found, it is possible to modify the model physics codes and optimize its performance in a specific region.

THIS PAGE INTENTIONALLY LEFT BLANK

TABLE OF CONTENTS

I. INTRODUCTION 1
  A. OBJECTIVES 1

II. BACKGROUND 5
  A. FOG FORECASTING ON THE CALIFORNIA COAST 5
  B. THE PHYSICS OF MARINE FOG 8
    1. An Ideal Fog Sequence 8
  C. MESOSCALE NUMERICAL WEATHER PREDICTION 9
    1. Predictability and Error 9
    2. Model Description 11
  D. THE EXPERIMENTS 12
    1. Radiation Experiments 13
    2. Turbulent Kinetic Energy Experiments 16
    3. Autoconversion Experiment 17
    4. Combination Experiments 18

III. THE OBSERVATIONAL DATA AND SYNOPTIC WEATHER PICTURE 19
  A. THE OBSERVATIONAL DATA 19
    1. Satellite Data and Related Methodology 19
    2. Aircraft Data: The MUSE Flights 22
    3. Aircraft Data: Methodology 24
    4. Station Observations and ETA Model Data 26
    5. Profiler Data and Related Methodology 27
  B. THE SYNOPTIC WEATHER PICTURE 28
    1. Introduction 28
    2. The Upper and Middle Atmosphere (300, 500, 700 mb) 28
    3. The Lower Atmosphere (850 mb) 29
    4. Surface 30
    5. Summary 31

IV. THE RESULTS 33
  A. COMPARISON WITH SATELLITE DATA 34
    1. Methodology and Comments 34
    2. General Findings: 37
  B. VERTICAL PROFILE COMPARISONS 37
    1. Methodology and Comments 37
    2. General Findings: 40
  C. COMPARISON WITH AIRCRAFT DATA 40
    1. Methodology and Comments 40
    2. General Findings: 44

V. CONCLUSIONS AND RECOMMENDATIONS 45
  A. CONCLUSIONS 45
  B. SUMMARY OF CONTRIBUTIONS 45

C. RECOMMENDATIONS 46
APPENDIX A. TABLES 49
APPENDIX B. FIGURES 75
APPENDIX C: ADDITIONAL FIGURES 119
LIST OF REFERENCES 155
INITIAL DISTRIBUTION LIST 159

LIST OF TABLES

Table 2-1: Fog Occurrences vs. Petterssen's Statistical Index (Petterssen, 1938) 49
Table 2-2: Leipper LIBS Method Fog Forecasting Guidelines (Leipper, 1995) 49
Table 2-3: COAMPS 2.0 Specifications (From, FNMOC) 51
Table 2-4: The Vertical Structure of the Experimental COAMPS Model 52
Table 3-1: Minimum Detectable Thickness as a Function of Drop Radius 53
Table 3-2: Summary of the Five MUSE Flights of Interest 55
Table 3-3: Text Table for Flight 17 56
Table 3-4: Text Table for Flight 20a 57
Table 3-5: Text Table for Flight 20b 58
Table 3-6: Text Table for Flight 22a 59
Table 3-7: Text Table for Flight 22b 60
Table 4-1: Ft. Ord Profiler Inversion Statistics, RMS Error Comparison 61
Table 4-2a(1): Aircraft Data Comparison Table, Flight 17 62
Table 4-2a(2): Aircraft Data Comparison Table, Flight 17 63
Table 4-2b(1): Aircraft Data Comparison Table, Flight 20a 64
Table 4-2b(2): Aircraft Data Comparison Table, Flight 20a 65
Table 4-2c(1): Aircraft Data Comparison Table, Flight 20b 66
Table 4-2c(2): Aircraft Data Comparison Table, Flight 20b 67
Table 4-2d(1): Aircraft Data Comparison Table, Flight 22a 68
Table 4-2d(2): Aircraft Data Comparison Table, Flight 22a 69
Table 4-2e(1): Aircraft Data Comparison Table, Flight 22b 70
Table 4-2e(2): Aircraft Data Comparison Table, Flight 22b 71
Table 4-3: Aircraft Data Comparison Table, Correlation Average By Flight 72
Table 4-4: Aircraft Data Comparison Table, Correlation Standard Deviation By Flight 72
Table 4-5: Summary of Experiments 73

THIS PAGE INTENTIONALLY LEFT BLANK

LIST OF FIGURES

Figure 2-1: Fog Formation Through the Stratus-Lowering Process (Pelié *et al.* , 1979) 75
Figure 2-2: Fog Formation Over Warm Water (Pelié *et al.* , 1979)..... 75
Figure 2-3: Fog Formation Through Convergence and Cooling (Pelié *et al.*, 1979)..... 76
Figure 2-4: Physical Processes Relevant to Offshore Fog (Koracin *et al.*, 1999)..... 76
Figure 2-5: Physical Processes Involved in Fog Production (Zwack and Tardiff, 1999)..... 77
Figure 2-6: The Vertical Spacing of Experimental and Operational COAMPS..... 78
Figure 2-7: The COAMPS Model Grids..... 79
Figure 2-8: The Model Terrain..... 79
Figure 2-9: The COAMPS Radiation Routines 80
Figure 2-10: COAMPS Model Skew-T Diagram for CON Valid at 17/12Z..... 80
Figure 2-11: Cloud Droplet Spectra (Rogers and Yau, 1989)..... 81
Figure 3-1: Location of Data Sites and Topography in the Monterey Bay Area..... 81
Figure 3-2: Detectable Cloud Thickness as a Function of Drop Radius..... 82
Figure 3-3: Detectable Cloud Thickness and Model CLDW Values..... 82
Figure 3-4: The MUSE Aircraft Survey Track (Paduan and Ramp, 2000)..... 83
Figure 3-5: MUSE Aircraft Measured Air Temperatures (Paduan and Ramp, 2000) 84
Figure 3-6: MUSE Aircraft Measured Dew Point Temperatures (Paduan and Ramp, 2000)..... 85
Figure 3-7: MUSE Aircraft Measured Winds (Paduan and Ramp, 2000) 86
Figure 3-8: MUSE Aircraft Measured Sea Surface Temperatures (Paduan and Ramp, 2000)..... 87
Figure 3-9: Track and Altitude for Flight 20a..... 88
Figure 3-10: U and V Speed Outliers for Flight 20a..... 88
Figure 3-11: Filtered U and V Speeds for Flight 20a..... 89
Figure 3-12: Areas of High and Low Wind Speed for Flight 20a..... 89
Figure 3-13: 3-km Points Numbered Along Track for Flight 20a 90
Figure 3-14: Numbered Data Points Selected for Flight 20a..... 90
Figure 3-15: Ft. Ord Surface Station Observations, 17 August 91
Figure 3-16: Del Monte Beach Surface Station Observations, 17 August..... 91
Figure 3-17: GOES-10 Satellite Image 17 August, 1445Z..... 92
Figure 3-18: Ft. Ord Profiler for 17 August..... 92
Figure 3-19: Composite Profile 17-24 Aug 93
Figure 3-20: Inversion Strength as Measured by Height/Thickness..... 93
Figure 3-21: ETA Synoptic Picture, 300mb at 17/00Z..... 94
Figure 3-22: ETA Synoptic Picture, 300mb at 23/00Z..... 94
Figure 3-23: ETA Synoptic Picture, 500mb at 17/00Z..... 95
Figure 3-24: ETA Synoptic Picture, 500mb at 23/00Z..... 95
Figure 3-25: ETA Synoptic Picture, 850mb at 17/00Z..... 96
Figure 3-26: ETA Synoptic Picture, 850mb at 23/00Z..... 96
Figure 3-27: ETA Synoptic Picture, Surface at 17/00Z..... 97
Figure 3-28: ETA Synoptic Picture, Surface at 23/00Z..... 97
Figure 3-29: ETA Synoptic Picture, Surface (with Observations) at 23/00Z..... 98

Figure 3-30: Buoy M4 Station Observations for 23Aug00 98
Figure 4-1: CON CLDW vs. Satellite Cloud Edge at 17/15Z 99
Figure 4-2: CLDW Comparison: CON, AC1, TK1, TK2 at 18/00Z 100
Figure 4-3: CLDW Comparison: CON, AC1, LW1, LW2 at 18/00Z 101
Figure 4-4: CLDW Comparison: CON, AC1, SW1, SW2 at 18/00Z 102
Figure 4-5: CLDW Comparison: CON, AC1, CB1, CB3 at 18/00Z 103
Figure 4-6: CLDW Comparison at 17/15Z 104
Figure 4-7: CLDW Comparison at 18/00Z 105
Figure 4-8: CLDW Comparison at 20/15Z 106
Figure 4-9: CLDW Comparison at 21/00Z 107
Figure 4-10: CLDW Comparison at 22/15Z 108
Figure 4-11: CLDW Comparison at 23/00Z 109
Figure 4-12: Rain Water Comparison at 21/00Z 110
Figure 4-13: Inversion Temperature Comparison Plot 111
Figure 4-14: Inversion Height Comparison Plot 111
Figure 4-15: Profiler vs. CON Model on 17Aug 112
Figure 4-16: SST of the CON Model at 18/00Z 113
Figure 4-17: 10m Air Temperature of the CON Model at 18/00Z 113
Figure 4-18: Skew-T Diagram Showing the Change from CON toTK1 to TK2 114
Figure 4-19: The Position of the Chosen Points for Flight 20b 115
Figure 4-20: Correlation of Temperature Data, CON for Flight 20b 115
Figure 4-21: Correlation of Temperature Data, AC1 for Flight 20b 116
Figure 4-23: Wind Difference Plot for CON and Flight 20b 117
Figure C-1: The Synoptic Picture, ETA Model 500mb at 17/00Z 119
Figure C-2: The Synoptic Picture, ETA Model 850mb at 17/00Z 119
Figure C-3: The Synoptic Picture, ETA Model SFC at 17/00Z 120
Figure C-4: The Synoptic Picture, GOES-10 1m Vis. Image at 17/00Z 120
Figure C-5: The Synoptic Picture, ETA Model 500mb at 17/12Z 121
Figure C-6: The Synoptic Picture, ETA Model 850mb at 17/12Z 121
Figure C-7: The Synoptic Picture, ETA Model SFC at 17/12Z 122
Figure C-8: The Synoptic Picture, GOES-10 1m Vis. Image at 17/1345Z 122
Figure C-9: The Synoptic Picture, ETA Model 500mb at 18/00Z 123
Figure C-10: The Synoptic Picture, ETA Model 850mb at 18/00Z 123
Figure C-11: The Synoptic Picture, ETA Model SFC at 18/00Z 124
Figure C-12: The Synoptic Picture, GOES-10 1m Vis. Image at 18/00Z 124
Figure C-13: The Synoptic Picture, ETA Model 500mb at 18/12Z 125
Figure C-14: The Synoptic Picture, ETA Model 850mb at 18/12Z 125
Figure C-15: The Synoptic Picture, ETA Model SFC at 18/12Z 126
Figure C-16: The Synoptic Picture, GOES-10 1m Vis. Image at 18/1430Z 126
Figure C-17: The Synoptic Picture, ETA Model 500mb at 19/00Z 127
Figure C-18: The Synoptic Picture, ETA Model 850mb at 19/00Z 127
Figure C-19: The Synoptic Picture, ETA Model SFC at 19/00Z 128
Figure C-20: The Synoptic Picture, GOES-10 1m Vis. Image at 19/00Z 128
Figure C-21: The Synoptic Picture, ETA Model 500mb at 19/12Z 129
Figure C-22: The Synoptic Picture, ETA Model 850mb at 1912Z 129

Figure C-23: The Synoptic Picture, ETA Model SFC at 19/12Z 130
Figure C-24: The Synoptic Picture, GOES-10 1m Vis. Image at 19/1430Z 130
Figure C-25: The Synoptic Picture, ETA Model 500mb at 20/00Z 131
Figure C-26: The Synoptic Picture, ETA Model 850mb at 20/00Z 131
Figure C-27: The Synoptic Picture, ETA Model SFC at 20/00Z 132
Figure C-28: The Synoptic Picture, GOES-10 1m Vis. Image at 20/00Z 132
Figure C-29: The Synoptic Picture, ETA Model 500mb at 20/12Z 133
Figure C-30: The Synoptic Picture, ETA Model 850mb at 20/12Z 133
Figure C-31: The Synoptic Picture, ETA Model SFC at 20/12Z 134
Figure C-32: The Synoptic Picture, GOES-10 1m Vis. Image at 20/1400Z 134
Figure C-33: The Synoptic Picture, ETA Model 500mb at 21/00Z 135
Figure C-34: The Synoptic Picture, ETA Model 850mb at 21/00Z 135
Figure C-35: The Synoptic Picture, ETA Model SFC at 21/00Z 136
Figure C-36: The Synoptic Picture, GOES-10 1m Vis. Image at 21/00Z 136
Figure C-37: The Synoptic Picture, ETA Model 500mb at 21/12Z 137
Figure C-38: The Synoptic Picture, ETA Model 850mb at 21/12Z 137
Figure C-39: The Synoptic Picture, ETA Model SFC at 21/12Z 138
Figure C-40: The Synoptic Picture, GOES-10 1m Vis. Image at 21/1430Z 138
Figure C-41: The Synoptic Picture, ETA Model 500mb at 22/00Z 139
Figure C-42: The Synoptic Picture, ETA Model 850mb at 22/00Z 139
Figure C-43: The Synoptic Picture, ETA Model SFC at 22/00Z 140
Figure C-44: The Synoptic Picture, GOES-10 1m Vis. Image at 22/00Z 140
Figure C-45: The Synoptic Picture, ETA Model 500mb at 22/12Z 141
Figure C-46: The Synoptic Picture, ETA Model 850mb at 22/12Z 141
Figure C-47: The Synoptic Picture, ETA Model SFC at 22/12Z 142
Figure C-48: The Synoptic Picture, GOES-10 1m Vis. Image at 22/1430Z 142
Figure C-49: The Synoptic Picture, ETA Model 500mb at 23/00Z 143
Figure C-50: The Synoptic Picture, ETA Model 850mb at 23/00Z 143
Figure C-51: The Synoptic Picture, ETA Model SFC at 23/00Z 144
Figure C-52: The Synoptic Picture, GOES-10 1m Vis. Image at 23/00Z 144
Figure C-53: Ft. Ord Profiler for 17 August 145
Figure C-54: Ft. Ord Profiler for 18 August 145
Figure C-55: Ft. Ord Profiler for 19 August 146
Figure C-56: Ft. Ord Profiler for 20 August 146
Figure C-57: Ft. Ord Profiler for 21 August 147
Figure C-58: Ft. Ord Profiler for 22 August 147
Figure C-59: Del Monte Beach Station Plot for 17 August 148
Figure C-60: Del Monte Beach Station Plot for 18 August 148
Figure C-61: Del Monte Beach Station Plot for 19 August 149
Figure C-62: Del Monte Beach Station Plot for 20 August 149
Figure C-63: Del Monte Beach Station Plot for 21 August 150
Figure C-64: Del Monte Beach Station Plot for 22 August 150
Figure C-65: Ft. Ord Surface Station Plot for 17 August 151
Figure C-66: Ft. Ord Surface Station Plot for 18 August 151
Figure C-67: Ft. Ord Surface Station Plot for 19 August 152

Figure C-68: Ft. Ord Surface Station Plot for 20 August 152
Figure C-69: Ft. Ord Surface Station Plot for 21 August 153
Figure C-70: Ft. Ord Surface Station Plot for 22 August 153

LIST OF ACRONYMS , ABBREVIATIONS AND SYMBOLS

ABL	Atmospheric Boundary Layer
AC1	Autoconversion Experiment One
AOI	Area of Interest
ASL	Above Sea Level
CB1,2,3	Combined Experiment One, Two, Three
CCN	Cloud Condensation Nuclei
CIRPAS	Center for Interdisciplinary Remotely Piloted Aircraft Studies (at NPS)
CLDW	Cloud Liquid Water (model value for a layer)
CNMOC	Commander, Naval Meteorology and Oceanography Command
CON	Control Experiment Run
COAMPS	Coupled Ocean-Atmosphere Mesoscale Prediction System
DMSP	Defense Meteorological Satellite Program
FNMOC	Fleet Numerical Meteorology and Oceanography Center
GOES	Geostationary Operational Environmental Satellite
LCL	Lifting Condensation Level
LW1,2	Longwave Radiation Experiment One, Two
MABL	Marine Atmospheric Boundary Layer
MBARI	Monterey Bay Aquarium Research Institute
MM5	Mesoscale Model Five
MOOS	MBARI Ocean Observatory System
MSRC	Major Shared Resource Center
MUSE	MOOS Upper-Water-Column Science Experiment
MVOI	Multi-Variate Optimum Interpolation
NCAR	National Center for Atmospheric Research
NCEP	National Centers for Environmental Prediction
NOGAPS	Navy Operational Global Atmospheric Prediction System
NORAPS	Navy Operational Regional Atmospheric Prediction System
NPS	Naval Postgraduate School
NRL	Naval Research Laboratory
SPAWAR	Space and Naval Warfare Systems Command
SST	Sea Surface Temperature
SW1,2	Shortwave Radiation Experiment One, Two
TK1,2	Turbulent Kinetic Energy Experiment One,Two
μm	Abbreviation for microns (1×10^{-6} meters)

THIS PAGE INTENTIONALLY LEFT BLANK

ACKNOWLEDGMENTS

The author would like to thank several individuals and institutions for their assistance during research and the preparation of this thesis. Dr. Darko Koracin of the Desert Research Institute in Reno, NV provided an abundance of resources and suggested areas of study during my initial phases of research on the physics of fog processes. Personnel at the Naval Research Laboratory in Monterey, CA (especially Ms. Tracy Haack, Dr. Timothy Hogan and Dr. Chi-Sann Liou) clarified some of the coding in the COAMPS routines once a thesis direction was decided upon. In the NPS Oceanography Department Dr. Jeffrey Paduan was the source for all of the verification from the MUSE experiment and Mr. Mike Cook authored the MATLAB function that is used to plot the Monterey Bay coastline and assisted with several other programming questions. In the NPS Meteorology Department Dr. Phil Durkee gave me cloud physics and satellite remote sensing training and Dr. Wendell Nuss provided some of his valuable time to be my second reader after having taught mesoscale forecasting.

Above all I would like to thank my thesis advisor, Dr. Doug Miller for his infinite patience and guidance. He was the one who physically made all of the COAMPS coding changes ran the multitude of jobs that made this thesis possible. He educated me in the ways of research and the "baby steps" that can lead to real change. Throughout these many months he has kept me challenged, focused and enthusiastic about this project. I was extremely fortunate he chose me as a thesis student.

This work was supported in part by a grant of computer time from the DOD High Performance Computing Modernization Program at the Army Research Laboratory and Naval Oceanographic Office/MSRC Program.

THIS PAGE INTENTIONALLY LEFT BLANK

I. INTRODUCTION

A. OBJECTIVES

Fog has long been the bane of the mariner. It has been, and remains, a cause of collisions at sea, groundings and errors in navigation. While technology has brought advances such as radar and satellite navigation systems that allow a ship to "see" through the fog, it has also brought new military missions that can be severely impacted by fog or stratus. Flight Operations are cancelled, Strike Operations are delayed to ensure battle damage assessment is possible, and weapon targeting systems can be led astray because of fog. The U.S. Navy's requirement for a computer prediction system for marine fog and stratus dates back to the 1970s when meteorological models were being introduced to the fleet. In 1982 when the first version of the Navy Operational Global Atmospheric Prediction System (NOGAPS) was introduced and it seemed that the ability to predict fog and stratus was getting within reach. But sixteen years later and NOGAPS version 4.0, with its global model resolution of 24 vertical levels and 75km horizontal spacing, fog formation and dissipation were still not able to be skillfully forecast.

There are two main sources of model forecast error. The first results when the model is initialized poorly. Even with satellite remote sensing there is very little observational data compared to the mesoscale complexity present within the atmosphere. Initialization is the process of taking all available observational data, a background atmosphere (model first guess), as well as data to represent terrain features, and making an analysis of the atmospheric conditions at a given time. This serves as a starting point for a forecast. The second source of error lies within the model itself due to model physics and to numerical noise (round-off error). It is the model physics errors that this thesis will examine. In addition to all of the various mathematically and empirically derived equations of atmospheric behavior, "model physics" includes numerous parameterizations of physical processes and properties. Errors due to initialization and model physics will be more fully discussed in Section Two.

A new kind of model was introduced in the early 1990s that could take the fields from a global model and apply them to a nested grid at a much higher resolution. This

nesting ability had been in practice with the Navy's Operational Regional Atmospheric Prediction System (NORAPS) for years, but the new model did much more. The Naval Research Laboratory's (NRL) Coupled Ocean/Atmosphere Mesoscale Prediction System (COAMPS) included non-hydrostatic forecast model components that can be coupled with a hydrostatic ocean model. As presented by Hodur (1997, p. 1413), the models could be "integrated simultaneously so that the surface fluxes of heat, momentum, and moisture are exchanged across the air-water interface every time step." Unfortunately the atmospheric model is still not coupled with the ocean model for operational forecasts but this system clearly is a leap forward in the potential to numerically forecast fog. This integrated coupling is also what will separate COAMPS from the Mesoscale Model Version Five (MM5) developed by Pennsylvania State University and the National Center for Atmospheric Research (NCAR) and other mesoscale models that use fixed ocean parameters throughout a forecast.

Some of the same technological advancements that have allowed COAMPS to exist are now taking the system a step further. Radical improvements in computer speed and communication allow COAMPS to be decentralized. This means that it is no longer necessary for Fleet Numerical Meteorology and Oceanography Center (FNMOC) to run the high resolution COAMPS for all of the Areas of Interest (AOI) around the world and then send the fields to regional centers or ships. Instead, the regional center (or other end-user) can determine its own areas of interest and run its own models on computers located at the centers that receive boundary conditions and NOGAPS or coarse COAMPS input from FNMOC. (It should be noted that there is currently a study in progress to see if communications improvements would allow the computers to be physically located at FNMOC but controlled by the end user, minimizing the personnel required to maintain the overall system. This change would in no way adversely impact the tenants of this thesis.) This ability gives the end-user the flexibility to position the model grids exactly to their liking without having to wait for FNMOC to make adjustments or modify their operational model run. It also allows for additional (or later) observations to be input into the model for analysis that wouldn't otherwise be present due to the time restrictions inherent in a centralized operational run.

This push to run COAMPS at the regional level should prompt one more change to the system. NRL developed COAMPS to initialize from a global model and then "tuned" it, or adjusted certain constants and parameterizations, so that it had the minimum error for the maximum area. This tuning is a common practice for all numerical models. Carrying this process one step further, end-users should now be able to work with NRL to "tune" COAMPS based on probable atmospheric differences between their own specific AOIs and the preset values. These changes could be as detailed as requiring different values and or parameterizations be used for specific seasons in specific regions.

The objective of this thesis is to determine if changes to the existing COAMPS code based on reasonable physical experiments can help solve the numerical fog forecasting problem. Section Two describes the physics of fog formation, the base COAMPS configuration and how these experiments were determined. Section Three introduces the environmental conditions in which the experiments were performed. It covers aircraft and ground data, satellite images and the synoptic model used for initialization. The effectiveness of these experiments is examined in Section Four. This was first measured by comparing a modeled cloud edge to satellite imagery taken during a week in August 2000 under a variety of foggy conditions. Comparisons were also made with observations taken from an aircraft, land stations and a vertical profiler. Based on these comparisons, Section Five presents conclusions regarding the effectiveness of these experiments in solving the fog forecasting problem and recommendations for further research can be made. The experiments performed as part of this thesis, specifically those regarding changes to the autoconversion and turbulent kinetic energy schemes in COAMPS, showed that it possible to modify the model physics code to optimize its performance in a specific region.

THIS PAGE INTENTIONALLY LEFT BLANK

II. BACKGROUND

A. FOG FORECASTING ON THE CALIFORNIA COAST

The difficulties of a fog forecast are many. It is not simply a matter of whether or not fog is present. Questions about its vertical extent and the visibility within it are added to the basic questions of its exact formation and dissipation times. Adding further to this problem on the Pacific coast of the United States is the scarcity of upstream observational data. Researchers have been seeking a solution to this problem in some form or another as long as there have been people living in coastal regions. Leipper (1994) is a general overview of research pertaining to fog research on the U.S. west coast and contains much more extensive listings than those that follow.

Numerical forecast studies will be examined within the sections that describe COAMPS and the experiments. Non-numerical studies using modern meteorological methods and concepts have been published since the 1920s and provide useful tools in understanding the dynamics of fog formation and dissipation for which a numerical model must solve. Blake (1928) noted that fog almost always followed a marked temperature inversion, which he categorized as one of more than five degrees Celsius. He also postulated the inversion was caused by adiabatic heating due to subsidence of air from the high pressure area. Anderson (1931) studied fog using aircraft observations around San Diego and described the "stratus-lowering" process, concluding that fog will result when the initial inversion was sufficiently low (less than ~300m) and cloud top cooling due to longwave radiation persisted. Petterssen (1938) was able to develop a statistical method to forecast fog based on morning weather balloon launches from San Diego and distance from the condensation level of the surface air to the base of the inversion (Table 2-1). Significantly, he tried to convey that fog was not formed by cooling from below but by convection and turbulent mixing in the air under the inversion due to instability in the fog layer because of outgoing longwave radiation from the cloud top. Leipper (1948) offered a physical model of California fog development that included lowering of the inversion by offshore winds as well as growth of the fog layer by longwave radiational cooling at the top. He proposed an ideal four-stage fog sequence on the California coast. This ideal sequence was explored by graduate students working

under Leipper at the Naval Postgraduate School (NPS) in Monterey, California during the 1970s and found to be a good theoretical model of the physical processes. In particular, Backes (1977) expanded this to a five-stage model based on Leipper's statistical measures. This sequence will be described below as it is a useful conceptual tool. Pelié *et al.* (1979) posed four different California fog formation processes: fog developed as a result of lowering (thickening) stratus clouds (Fig. 2-1), fog triggered by instability and mixing over warm water patches (Fig. 2-2), fog associated with low-level mesoscale convergence and longwave radiative cooling (Fig. 2-3), and coastal radiation fog advected to sea via nocturnal land breezes. Leipper (1995) updated his 1948 work in 1995 and presented Leipper Inversion Based Statistics (LIBS) as a method to objectively forecast California fog. Table 2-2 summarizes his new five-phase ideal model which is discussed below.

Koracin *et al.* (1999) was a numerical simulation of offshore fog formation and included interesting results regarding turbulent kinetic energy. They began with a stratus deck over water that was capped by the inversion. At this stage they noted that there were two turbulent areas separated by a zone of minimum turbulence (Fig. 2-4). Longwave radiative cooling from the cloud top to air above it produced turbulence within the cloud, and weak positive heat flux and shear produced turbulence near the sea/air interface. As subsidence decreased the depth of the MABL, the cloud base lost heat to the cooler air below it through longwave cooling and gained heat through shortwave absorption from above (during daylight), for a net cooling effect. When the cloud base was driven low enough the two turbulent zones combined and there was complete mixing from to the surface to the cloud top within a layer of fog. In their simulation, this process took 50 hours and resulted in a saturated layer 250m thick. Once the layer had been formed, increased turbulence (increased because now the net cooling is out of the cloud top, destabilizing the layer) caused the depth of the mixed layer to increase. However, the vertical growth was also associated with the entrainment of drier air from above the inversion which would serve to dissipate the cloud. Their simulations showed that in the presence of moderate or significant subsidence the entrainment (and dissipation) was approximately balanced by the layer's turbulence (and growth), and that the fog could be

maintained for several days. The turbulence within the fog acted to control the fate of the fog.

Koracin *et al.* (2000) was a study of the stratus-lowering process already described by Anderson (1931) and Pelié *et al.* (1979), but was fairly unique in that it took a Lagrangian approach to a numerical simulation. Rather than focusing on a single area over time, they followed a "slab" of marine-layer air over a two-day period as it moved over the waters from the California-Oregon border to the California Bight near Santa Barbara. They noted a long list of physical processes "germane to the formation" of fog. Of particular interest their simulation showed that longwave radiative cooling at the stratus top was the primary mechanism for cooling and mixing the entire marine layer, confirming the assertion of a number of theorists. They noted the increase in turbulence at the air/sea boundary over warmer sea surface areas, but showed that this was of secondary importance compared to cloud-top cooling and subsidence – suggesting that a high-resolution ocean model is not necessarily going to contribute greatly to the forecast skill. Their simulation showed that there may be an optimum inversion strength (10-15°C) conducive to fog formation, with weaker inversions (5°C) inducing more cloud-top longwave cooling and more liquid water but delaying the stratus-to-fog transition while stronger inversions (20°C) quickly dissipated fog. In this study, the inversion base was placed between 600m and 700m based on a sounding from Oakland. They showed that the moisture content of the air above the inversion alters cloud-top longwave cooling and therefore influences the formation and evolution of fog. As will be shown, the moisture content was not handled correctly by COAMPS during these simulations as the model was making the air above the inversion excessively dry.

Figure 2-5 does a good job of depicting nearly all of the processes that must be considered when forecasting the formation of fog, whether by traditional, statistical or numerical methods. These include longwave and shortwave radiation, autoconversion processes and turbulent kinetic energy – all of which became the focus of the experiments for this thesis.

B. THE PHYSICS OF MARINE FOG

1. An Ideal Fog Sequence

As a precursor to the formation of fog, the semi-permanent Eastern Pacific (EastPac) High will move to the northeast from its normal position. This makes the isobars at the surface roughly perpendicular to the California coast. Anticyclonic (clockwise) circulation about the high pressure center brings dry continental air over the moist and cool coastal region. This air is heated adiabatically as it subsides and the result is warm and dry offshore (from the North-Northeast in the Monterey Bay area) flow causing a low-level inversion. This corresponds to Leipper's (1995) "Phase One." The weather should be become clear with little or no sea breeze and low level warming.

By "Phase Two" the offshore flow has moved the marine layer well offshore and a surface inversion will be present. The EastPac High then begins to retreat to its normal position and the offshore flow will decrease. Surface winds will swing to Northwesterly and the surface air temperature will cool and strengthen the inversion. Fog will occur where the inversion height is greater and over cold water. The marine layer will thicken, partly because of longwave radiational cooling from its top and the associated increased instability within the layer. Fog may clear over most areas during the day leaving haze present, but return at night.

During "Phase Three" the inversion base rises to 400 meters in height as the air column above the marine layer cools. The winds back to Northwesterly and increase and fog becomes thicker - covering larger areas and extending farther inland at night. Low stratus is evident during the afternoon. By "Phase Four" the inversion has become so high (above 400 meters) that fog will no longer form, but stratus may still be present overhead. Offshore flow will cease as the EastPac High has returned to its normal position. The air above the inversion continues to cool, and the inversion will increase in height and decrease in strength. By "Phase Five" the inversion base has gone so high that even the stratus layer dissipates.

The key to this entire "ideal sequence" is the offshore flow of warm and dry air. The sequence may stop at any phase or even reverse, depending on the strength of this offshore flow. When the offshore flow stops the sequence will progress to conclusion.

This somewhat lengthy discussion has been included because the sequence observed during 17-23 August 2000 in Monterey Bay closely resembles this ideal one and indicates areas to monitor for model performance. From this discussion, modeling the changing wind direction and raising of the inversion base will be especially important if the model is to be able to correctly forecast for fog and stratus. While this ideal sequence is helpful, it is by no means the only method by which marine fog can form. There are other scenarios with markedly different synoptic conditions that give rise to fog, as touched on by Pelié *et al.* (1979), and marine fog is but one of the kinds of fog that requires forecasting. The processes that control radiation, valley, advection, upslope, and steam fog could all have played a factor in creating or maintaining the fog that was visible in the satellite imagery during this case study. Part of the challenge in simulating fog formation lies in the fact there are so many ways in which it may occur. The ideal sequence and stratus-lowering method provide a good conceptual model of the fog formation processes on California's central coast, but cannot used to the exclusion of all others.

C. MESOSCALE NUMERICAL WEATHER PREDICTION

1. Predictability and Error

A forecast's performance is generally measured in terms of accuracy and skill (Nuss, 2000). "Accuracy" is a term used to describe how close the prediction was to the actual physical events – e.g., did it rain when the forecast said it would? "Skill" is the term used to compare the performance of a forecast against a simple forecast based on climatology or persistence. It is possible for several experiments to show improvements in skill versus a control case, yet none of them may be accurate. A typical statistical measure of accuracy and skill is made by comparing the Root Mean Square (RMS) difference, or error, between forecast and verification data to the standard deviation within the verification data itself. For example, if the standard deviation of the high temperature values for a given week is 1.5°C, and the RMS difference between all of the forecast "A" values and verification values was only 2.8°C while forecast "B" had an RMS error of 3.5, forecast "A" could be termed more skillful, but neither would have shown much accuracy.

Three objective approaches that one could take in making a forecast are climatology-based, persistence-based or model-based. Climatology will be generally be the least skillful at analysis time because the real atmosphere rarely exhibits structure equivalent to the mean. But it will show the greatest skill after a long period of time, although it is rarely very accurate. A persistence-based forecast will be the opposite of climatology. It has the greatest initial skill. There is no analysis error because the forecast simply extends the current conditions into the future, but the forecast will have almost no skill after some time has elapsed. Between these two is a numerical model-based forecast. It will show some error at analysis time, a brief period of even greater error while the model brings the initial conditions into dynamic balance with the model physics, then a skillful period as it integrates the necessary equations forward in time. It will be more skillful than persistence and climatology up to some point when it finally can no longer beat a climatology-based forecast. This is due to both initialization errors that propagate through the model and inaccuracies within the numerical model (model physics and numerical noise). As presented in Section One, these two main sources of error may prevent a forecast from being either accurate or skillful - initialization and model physics.

If a model has no first guess or background information about mesoscale conditions, it is termed a "cold" start and requires some extra "spin-up" time to bring the atmospheric equations into equilibrium. If a model is able to blend a previous mesoscale forecast with current observations for an analysis it is termed a "warm" start. Note that a cold start for a mesoscale model uses synoptic-scale model fields during initialization so some large-scale conditions will get in to even a cold start. Whether warm or cold, if this initialization is flawed so too will be the forecast. In a mesoscale simulation of the Los Angeles basin using MM5, Sterbis (2000) noted that neither the cold nor warm starts showed good accuracy, but the cold starts showed more skill suggesting that the warm start was bringing sufficient error from previous forecasts to cause a greater initialization error than the cold start.

Theoretically, for a given set of valid initial conditions, a more complex physics scheme will be able to resolve and forecast mesoscale structure better than a less complex one. This assumes that the added complexity is based on accurate assumptions. Sterbis

(2000) showed this was the case in the MM5 simulation noted above. This added complexity is important at the mesoscale level of forecasting as it may often be necessary for the model to remove error from a poor analysis and prevent it from perpetuating throughout a forecast.

Two problems inherent in all mesoscale predictions that can lead to errors relate to scale. In addition to the obvious reduction in spatial scale when moving from the synoptic to the mesoscale is a reduction in time scale. At some point the physical processes are occurring in such small dimensions of space and time that assumptions and methods used to model at the synoptic scale become invalid. The non-linear behavior of small scale phenomena is extremely difficult to simulate and yet the importance of these processes has led to an entirely new science of chaos theory (Lorenz, 1993). The result is that events at the mesoscale are generally less predictable than those on the synoptic scale.

2. Model Description

The background information for COAMPS has been well documented elsewhere. Hodur (1997) describes the essentials of the system and information regarding research and its present operational status is available through the web sites for NRL (http://www.nrlmry.navy.mil) and FNMOC (http://www.fnmoc.navy.mil). A summary of the COAMPS 2.0 specifications is in Table 2-3. This section emphasizes how the system used for this thesis (referred to as "experimental COAMPS" in this section) differed from the COAMPS currently being used by the Navy (referred to as "operational COAMPS" in this section).

Since the structure within the marine atmospheric boundary layer (MABL) is critical to the formation of fog, we sought to initialize experimental COAMPS with a model having the highest vertical and horizontal resolution possible. The Navy uses fields from NOGAPS to provide the initial and boundary conditions to the outer nest of operational COAMPS. NOGAPS T159 has 159 spectral waves, which translates to horizontal grid spacing of around 75km. It has a total of twenty-four sigma levels throughout the atmosphere with approximately six levels below 850 mb, depending on

terrain elevation The ETA model, run by the National Centers for Environmental Prediction (NCEP), is run at high vertical and horizontal resolution, but some resolution is lost when the fields are made available outside NCEP. Still, those fields available at NPS had comparable horizontal resolution to NOGAPS and an increased vertical resolution, so ETA was chosen as the synoptic model.

Choosing ETA led to another change from operational COAMPS. Initialization of the operational system is through Multi-Variate Optimum Interpolation (MVOI), but this scheme is currently coded to only work with NOGAPS. A similar analysis method, two-dimensional multiquadric interpolation (2DMQ) was used in its place to blend the first guess grid fields and observations with the COAMPS grid fields. Nuss and Titley (1994) explain the details of 2DMQ.

Another change made to the model was to increase its vertical resolution. Operational COAMPS has only 30 sigma levels and this was increased to 45 for experimental COAMPS. Figure 2-6 shows the lower atmospheric sigma levels (below 1600m) in both the experimental and operational configurations as well as plots at every 20 meters and every 50 millibars for reference. The complete sigma-level listing for the model is given in Table 2-4.

A final change to operational COAMPS was an alteration of mixing lengths in the used in the upper atmosphere. This is discussed in the experiments section below.

For this study a quadruply-nested grid configuration was used with horizontal grid spacings of 81km, 27km, 9km and 3km. These grids were centered over the Monterey Bay area and are pictured in Figure 2-7. Figure 2-8 shows the topography used in the inner nest. Note the rather hilly terrain to the north of Monterey Bay. This will play an important role in modifying the air mass moving into the area from the Northwest.

D. THE EXPERIMENTS

When experimental COAMPS was used to model a given day using the configuration described above without modification, it was termed a control run and will be designated "CON" in all subsequent tables and figures. CON was used to simulate all three of the days for which there was verification aircraft data available, the 17th, 20th and

22nd of August 2000. Changes were made to the model's forecast code in a variety of ways as explained below in an attempt to produce a better forecast of fog. The physical processes described in Sections Two A and B, and pictured in Figure 2-5, suggested several areas that could be investigated for possible improvement. A first series of experiments was performed with changes to both longwave and shortwave radiation schemes, autoconversion processes and the turbulent kinetic energy scheme. All of these experiments were performed on the 17th and 20th as these two days had both verification aircraft data and different synoptic conditions. Further experiments were then conducted based on the relative success of the first series. The experiments themselves are described below. The results, including a table summarizing the physical changes and expected effects, are presented in Section Four. All of the experiments (including CON) were run over a forecast simulation period of twenty-four hours using cold start initialization. For that reason the forecast fields prior to the six-hour forecasts were not included in any statistical measures as the model was most likely still in its spin-up phase.

1. Radiation Experiments

Radiative heat transfer is integral to the conceptual fog formation models described earlier in Section Two. Absorbed shortwave radiation transfers energy from the sun to the top of the cloud layer and warms it, leading to cloud dissipation through evaporation. It also warms land and ocean surfaces and can lead to turbulent heat fluxes at the ground/air interface when this heat is re-radiated by the surface back into the air in the lower MABL. Longwave radiational cooling at the top of the stratus-covered MABL destabilized the MABL and is the primary cause of turbulence and mixing within it. This turbulence can lead to the growth of the thickness of a cloud layer, and the growth can lead to its eventual dissipation as dry air is entrained at the cloud top. Because of their importance in the fog processes, both longwave and shortwave radiation experiments were decided to be appropriate.

Hodur (1997) states that radiation parameterization used in COAMPS follows that of Harshvardhan *et al.* (1987) (hereafter simply "Harshvardhan"). The actual code used in the model follows a series of branches as shown in Figure 2-9 that somewhat

corresponds to the flow through the Harshvardhan paper. Very simply put, the first subroutine, "radiat," initializes some information about cloud cover and type and sets some parameters based on climatology before calling on the longwave "rlwxx" and shortwave "rswxx" subroutines. This cloud information is very important because if the model is improperly forecasting an area of clouds to begin with, this will affect the radiation routines that in turn affect the future development of clouds.

Following the longwave branch the next routine is "rlwxx" that does preliminary longwave calculations on coarse and full grids in "rlwcc" and "rlwff" before calling on "rlwrad." Within this routine the model calculates the upward and downward longwave fluxes using the equations presented in Harshvardhan (and calling on the subroutines pictured beneath it). The Harshvardhan parameterization uses Chou and Peng (1983) as the method for parameterizing absorption by carbon dioxide and Chou (1984) as the method for parameterizing absorption by water vapor. Neither of these presented obvious ideas for experimentation, although any parameterization of a physical process can be subject to refinement. One thing did stand out however. Within the emissivity computations for stable and convective clouds there is a diffusivity factor (bdiff) used, according to Haack (2001), to account for the (solid) angle integration in the diffuse transmission function. This value was hard-coded to a value of 1.66 which Hogan (2000) states is a standard. Since changing the cloud's emissivity would ultimately change its longwave radiation properties, this was a likely source for an experiment. Two longwave experiments were made as part of the first series of experiments. The first, dubbed "LW1," decreased the value of bdiff to 4/3 and in LW2 it was increased to 6/3. It is important to note that these changes will only have an impact if the model has any clouds – as they are within a routine that is specific to the presence of clouds. It should also be pointed out that this change was not made to directly state that the bdiff values used as the standard was incorrect. It simply afforded an opportunity to see if changes could be affected by altering a value such as this. By decreasing the emissivity in LW1, the model should decrease longwave radiational cooling by the cloud and subsequently have less turbulent mixing and decreased cloud growth. LW2 should have just the opposite effect and increase the longwave cooling at the cloud top, destabilizing the layer and increasing turbulence and cloud growth.

On the shortwave side of the radiation branch Harshvardhan uses the Lacis and Hansen (1974) method to parameterize both ozone and water vapor absorption. Solar absorption by oxygen and carbon dioxide is neglected, as is the absorption by all trace gases (methane, freons, oxides of nitrogen, etc.). Also neglected are all aerosols other than the clouds themselves. This may be important in a marine environment rich in large diameter sea spray salts aerosols. Any of these could be the subject of further study or experiments

In a simulation using MM5, Mass and Steenburgh (2000) noted that solar absorption overwhelmed infrared cooling in the upper layers of their model stratus in contrast to the numerous findings that longwave cooling should dominate. To correct this they reduced the shortwave absorption in low-level clouds by 45% and achieved a "more realistic spatial distribution and diurnal evolution of boundary layer stratus" (p. 2375). This seemed a promising avenue of experimentation for COAMPS as well so the radiation subroutines were again examined.

Working down the shortwave branch of Figure 2-9 one eventually gets to the subroutine "rcludy" in which the net shortwave flux absorption in each layer is determined according to the equations of Lacis and Hansen (1974). Within these equations is a constant (pizero) that is used to represent the single scattering albedo. According to Liou (2000) this value should be around 0.99. He noted however that the value was actually set to 0.97 due to "some bias problem of NOGAPS at that time." Hogan (2000) amplified this to state that the single scattering albedo factor was decreased to give a total absorption in the atmosphere of solar radiation of 68 Watts/m^2 as an admitted "tune" in the code. Two experiments were made during the first series of experiments based on this scattering albedo. The default COAMPS value is 0.99. Experiment SW1 actually increased the value to 1.0 and SW2 decreased it to the discussed value of 0.97. By increasing the single scatter albedo, SW1 should decrease shortwave absorption, similar to the Mass and Steenburgh experiment, and decrease the cloud dissipation due to evaporation. SW2 would actually increase absorption and was the "tuned" value selected by NRL. This would increase the cloud temperature and dissipation by evaporation.

2. Turbulent Kinetic Energy Experiments

Changes to the radiation schemes ultimately should lead to changes in the turbulent fluxes within the cloud layer. Turbulent kinetic energy (TKE) experiments sought to change the turbulence more directly. In the CON configuration, the TKE above the boundary layer has been estimated, as defined in Walters and Miller (1999), by adjustments to the mixing coefficients, Km and Kh, in order to allow TKE to develop realistically in the stable free atmosphere.

In the analysis of CON fields, spikes were noted in the energy values at the top of the MABL. Experiment TK1 included the changes from operational COAMPS to CON as well as a correction to make the surface boundary layer more shallow by changing how its top is defined. Since different parameters are used depending on whether a model level is within or above the boundary layer, this would affect changes to many of the model's fields, including the elimination of the spikes in TKE observed in CON.

When analysis was performed on the first series of experiments it was observed that TK1 was comparable to CON in correlation and RMS checks against aircraft data, but had smaller RMS errors than CON when compared with the Ft. Ord vertical profiler data for inversion base height and temperature. A Skew-T diagram of the model data from CON (Fig. 2-10) showed an unrealistically dry layer at the 850mb level suggesting that the entrainment above the stratus-topped MABL was too weak and, potentially, turbulent mixing lengths used by the model above the MABL were too small. A follow-on experiment, TK2, contained the modifications of CON and TK1 plus an additional correction to the mixing length values. In the original scheme, a constant value of five meters is used from above the boundary layer to the top of the model. This was replaced with a value that varies linearly from 23m near the top of the surface boundary layer to five meters at the model top. The value of 23m was empirically obtained in experiments in Sweden as explained in Tjernstrom (1993).

3. Autoconversion Experiment

There are a variety of means by which water vapor becomes cloud liquid water and subsequently grows from the smallest of cloud droplets to precipitation size drops. Within the atmosphere there are large concentrations of very small particles (micron or submicron size) that have a natural affinity for water. These particles, called cloud condensation nuclei (CCN), are at the center of the process called heterogeneous nucleation by which water vapor condenses into cloud droplets. The character of these CCN is largely a function of the climate that produces them, and since the cloud droplets are a function of the CCN, it follows that clouds produced in different climates may have different characteristics. For example, continental air masses generally have larger numbers of smaller-sized CCN and a resulting larger number of smaller droplets that are all competing for the water vapor present in a given volume. Figure 2-11 shows the difference in a continental cumulus cloud and a trade-wind cumulus. This relation of CCN, and subsequent cloud characteristics, to their environment suggests that cloud processes should be modeled according to the properties of the air mass in which they form. Kong (1999) and Mecham and Kogan (2000) have both examined the effect of changing the values used in the COAMPS autoconversion process.

Typical cloud droplets are on the order of 10 μm in radius and a typical cloud will be composed of several hundred of them per cubic centimeter. There are three generally accepted means that this cloud structure may become unstable causing the droplets to grow. The first involves the interaction between ice crystals and the droplets and is not important in this study as California fog is formed in a warm air process. The second simply involves droplets colliding and coalescing, or sticking together. As droplets of larger size fall more quickly than smaller droplets they will often overtake the smaller droplet and combine with them. What is interesting is that unless cloud droplets are larger than around 18μm in radius, they are too small to effectively collide enough for this process to produce a cloud in the time span that has been observed in actual cloud formation. To grow a droplet to this size (and afterwards, too) a third process is at work wherein the droplet grows by direct diffusion of water molecules form the vapor onto its

surface. This process is greatly dependent of the vapor pressure and individual droplets are in competition for the available water vapor.

Autoconversion is the transformation process wherein droplets of a given radius grow through spontaneous coalescence to a point where they can generally be precipitated out of a cloud. COAMPS uses the Kessler method to parameterize the warm rain processes, in which a criterion for the cloud water mixing ratio (q_{c0}) is used to determine the beginning of the autoconversion process. This criterion is set to 1g/kg in COAMPS. Kong (1999) writes that this value is more suitable for convective precipitation processes and that it produced unrealistic cloud water content (over 1g/kg) in a California MABL study and reduced q_{c0} to 0.5g/kg. This lower autoconversion criterion produced a more reasonable maximum cloud water mixing ratio (0.6g/kg) and increased significantly the removal of liquid condensate through drizzle which, in turn, improved the fog burnoff process. However, Mechem and Kogan (2000), researchers from the University of Oklahoma's Coastal Meteorology Research Program, noted that a lower autoconversion number resulted in a reduced q_c arising from the scavenging of cloud droplets by drizzle drops and recommended keeping the value of 1g/kg because the lower value made water precipitate out too rapidly in their experiments.

Experiment AC1 directly follows from this discussion and was run by changing the value of the autoconversion criterion from 1g/kg to 0.5 g/kg. This was done in the COAMPS subroutine "adjtq.F" by setting the value of praut2 equal to 0.0005.

4. Combination Experiments

Seeking to combine plausible physical effects, a combined experiment was run that included the AC1 change to the autoconversion criterion as well as the changes to the handling of turbulent kinetic energy from TK1. This experiment was termed CB1 and run simultaneously with the others in the first experiment series. After analysis of the first series of experiments showed that SW2 was showing more skill than TK1 in correlation comparisons a second combination experiment (CB2) was performed using AC1 and SW2. A third combination experiment was made (CB3) that combined AC1 and TK2 after the change in TK2's TKE scheme seemed to show promise.

III. THE OBSERVATIONAL DATA AND SYNOPTIC WEATHER PICTURE

The data used to gauge the model's performance was obtained from a variety of locations throughout the Monterey Bay Area. Since the overall objective was to improve the model's ability to predict fog and stratus, a visual comparison of satellite imagery to model fields was a primary check of its effectiveness. This improvement however could not be at the expense of accuracy in other model fields, so further comparisons would be needed. Numerical comparisons were made with aircraft data and ground stations to check the performance of the model in the horizontal, and with the NPS vertical profiler to gauge its ability to capture the evolution of the marine atmospheric boundary layer (MABL). The locations of the data sites referred to and major topographic features are shown in Figure 3-1 (which may be roughly compared with the model topography in Fig. 2-8). Appendix B contains all of the Figures specifically cited in Section Three. Appendix C includes the majority of the figures used in making the meteorological analysis of this week. Inclusion of all of the data and figures used in this study (including results) would be impractical, but all are available through the Meteorology Department of the Naval Postgraduate School should anyone wish to use it for further research.

A. THE OBSERVATIONAL DATA

1. Satellite Data and Related Methodology

One of the most important model performance checks involved a comparison of the cloud edge visualized by a model variable with a satellite image of the cloud. Since marine fog is often at a temperature very close to the underlying water, visible-spectrum images (0.55-0.90 μm) are often better at showing it than an infrared (10.5-10.6 μm) image. NPS had a ready archive of visible channel Geostationary Operational Environmental Satellite (GOES) images (in "gif" format) with one-kilometer resolution over California and the western United States for this week, so they were chosen as the comparison images. Since the fog edge comparison is a major element in this whole study it is clear in retrospect that the highest resolution images possible should have been used, and preferably in a data format that could be subjected to enhancement.

A basic question which had to be answered in order do this comparison objectively was: What model value of cloud water would correspond to a detectible cloud edge? Some rough calculations were made to quality-control check the results based on the GOES detection ability and the concept of optical depth. Optical depth (δ) is essentially a term used to describe how effective something is at scattering or blocking light. At $\delta = 0$ there would be no interference with light transmittance; the direct transmittance value would be one. As δ increases, the transmittance decreases. A useful reference number is $\delta = 7$ which corresponds to a transmittance of 0.1%, and the point at which the disk of the sun would just become blocked. The GOES sensor should be capable of discerning an object with an optical depth of 0.1 km^{-1} (Durkee, 2001). This is an approximate number and is subject to change with variables like sun angle, but was exact enough for the following rough calculations. Two calculations were made: the detectable cloud layer thickness for a given input of radius and cloud drop concentration, and cloud layer thickness based on model cloud water values.

The first calculation is largely a function of the clouds' ability to scatter light. The equation for the scattering coefficient (σ_s) in the cloud is given by:

$$\sigma_s = \pi \ r^2 \, Q \, N \tag{3-1}$$

where r is the cloud drop radius, Q is the scattering efficiency and N is the number of drops per unit volume. The equation is valid for any consistent units of length. Q asymptotically approaches a value of two for drop radii greater than one micron so it was fixed at two in these calculations. If typical values of r = 10μm and N = 100 drops cm^{-3} are used, σ_s is 0.063 m^{-1}. For reference: a typical CCN has a radius of 0.1μm, a typical cloud drop has a radius of 10μm, a large cloud drop has a radius of 50μm and the conventional borderline between cloud drops and rain drops is 100μm (Rodgers and Yau, 1989).

Optical depth is the product of the scattering coefficient times thickness (ΔZ):

$$\delta = \sigma_s \ \Delta Z \tag{3-2}$$

Using the value of 0.1 km^{-1} as a minimum detectible optical depth and the scattering coefficient obtained from Eq. 3-1, the minimum thickness of a detectible fog

layer would be only 1.6 meters. Table 3-1 shows the results of varying the drop size from 2.5 to 25 μm while holding N and δ constant. Figure 3-2 is a plot of this data and shows the sharp decrease in required thickness when drops increase from five to 15 microns. This information will be used in further calculations below.

The second calculation used the model's value for cloud water content within a layer (CLDW), which can be thought of as the "cloud liquid water path content" (LWP). Preliminary studies were made that examined the cloud water content at individual levels. They showed that almost all of the cloud water was found at or below the 900mb level. Rarely was there any observed at 800mb and never any at 700mb or higher during this study. A layer from the surface up to 700mb (~3000m in a standard atmosphere) was chosen to ensure it would contain all of the LWP that the satellite would observe. Initial comparisons with the image at 17/15Z suggested a value of 0.1 kg/m^2 made a reasonable approximation of the cloud edge, so this was used as a baseline value. Liquid Water Content (LWC) is simply the LWP divided by the path length, Z (3000m in this case). But LWC can also be expressed as:

$$LWC = 4/3\ \rho\ \pi\ r^3\ N \qquad (3\text{-}3)$$

where r and N are the same as in Eq. 3-1 and ρ is the density of water, 1000 kg/m^3. Having obtained a value for LWC from the relation LWC=LWP/Z, one can then solve Eq. 3-3 for N. With the same r = 10μm value as above and the N value obtained from Eq. 3-3, a value for scattering efficiency was found to be $\sigma_s = 0.005\ m^{-1}$. Optical depth values of δ = 0.1, 1 and 7 were used to represent the detectible cloud edge, outer cloud and center cloud respectively and Eq. 3-2 was used to determine the thicknesses. The result was a cloud edge thickness of 20m, outer cloud thickness of 200m and center cloud thickness of 1400m. The process was repeated for model layer cloud water values up to 0.5 kg/m^2. Figure 3-3 is a plot of the detectable edge thickness based on an optical depth of 0.1 for CLDW values from 0.1 to 0.5 kg/m^2 overlaid on the plot of the detectable cloud edge from Figure 3-2. It shows that lower values of CLDW are closer to the expected value of detectable cloud edge for smaller drop sizes and larger CLDW values are better for large drop sizes. Recall in Figure 2-11 that since there were fewer CCN in the trade-wind cumulus cloud, the drops were free to grow to larger sizes. The drop size

in a coastal environment could likely be influenced by the amount of aerosols released into the atmosphere by nearby land sources, but this study assumed larger drop sizes would be likely. All of these results were for a fixed value of N, which would be changing in reality but was held constant here in order to examine the relation of CLDW and detectable cloud edge. The results suggest that CLDW values between 0.1 and 0.5 kg/m^2 are not unreasonable for modeling the edge of the marine fog layer and could be used to define the cloud edge in COAMPS simulations.

2. Aircraft Data: The MUSE Flights

The aircraft data used in this thesis was gathered as part of the Monterey Bay Aquarium Research Institute (MBARI) Ocean Observatory System (MOOS) Upper-Water-Column Science Experiment (MUSE). MUSE coordinated several upper-water-column science projects and included research flights to map sea surface temperature (SST) and over-water wind velocity. The availability of verifying flight-level winds and temperatures during a week in which there were varying fog conditions in the Monterey Bay area made this a very appealing case study for simulation tests using COAMPS.

All flights were conducted with scientific and engineering support from the Navy's SPAWAR System Center-San Diego using a twin-engine Navajo aircraft. The project, as detailed in Paduan and Ramp (2000), involved level flights along a regular grid over Monterey Bay at altitudes between 400 feet and 1000 feet (Fig 3-4). There were five flights during this week that were used extensively in the model analysis: one in the afternoon of August 17th, and morning and afternoon flights on the 20th and 22nd. These flights will be referred to hereafter as 17, 20a, 20b, 22a and 22b respectively. Flight times and other parameters, including a satellite image, are summarized in Table 3-2.

Values of the individual U (East/West) and V (North/South) wind speed components were recorded as well as total wind speed and direction. Temperature, moisture, pressure and a great many other flight variables were also recorded at frequencies between one every second to one every five seconds. Virtual temperature was calculated from the temperature, moisture and pressure measurements using standard

formulas. There was an unfortunate wind instrument failure on Flight 17, but temperature and moisture measurements were good and, as this was a day with a distinct fog event, it was left in the study.

A sense of the overall meteorological conditions may be gained by examining the images prepared by NPS/SPAWAR/CIRPAS based on the flight data. The five panels of Figures 3-5 to 3-8 show the conditions as interpreted from the aircraft data for each of the five flights. (Note: these images are among all of the MUSE data available on the internet at http://www.oc.nps.navy.mil/~icon/collaborations/muse_overflights.htm). They show flight-level air temperature, flight-level dew point temperature, flight-level winds and SST, respectively. Note especially the very warm (Fig. 3-5) and dry (Fig. 3-6) area on the north side of the bay during Flight 17. The mean temperature of 17.4°C during this flight was nearly two degrees warmer than during any other flight. This is most likely due a good deal of adiabatic warming as the air descended from the coastal mountains with winds directed from the north-northwest. The flight-level (~100m) air cooled throughout the week, suggesting the progression of phases in the ideal fog sequence described in Section Two above. The winds on the 17th shown in Figure 3-7 were not measured directly due to the instrument failure previously mentioned. The northwesterly flow at flight level on that date was determined by an indirect calculation and since it was in keeping with other data sources, it was included to show a general trend in the wind pattern. These Flight 17 winds were not used in model verification tests. Additionally, the high-speed winds shown during all flights at the east and west sides of the image may not be accurate, as discovered when the data was being prepared for comparison with model fields. The flight-level winds backed throughout the week and by the 22nd southerly flow was observed over the bay. The synoptic weather discussion that follows in Section Three B discusses the reasons for this reversal. A diurnal heating effect can be seen by comparing the morning "a" flights on the left side of these figures with the afternoon "b" flights on the right. SSTs within Monterey Bay are usually quite cool due to the upwelling of deep waters from the marine canyon that replaces surface waters pushed offshore by Ekman flow from the prevailing northwesterly winds. The SSTs of Figure 3-8 depict a persistent (relatively) warm area on the north side of the bay and the mean temperature rises by about a degree overall

are just the kind of mesoscale fluctuations that may be important in numerically forecasting fog, they were not included in these model runs as the SST input came from the NOGAPS one-degree SST analysis and was held constant through any given forecast.

3. Aircraft Data: Methodology

One of the methods used to check the model's performance across a quasi-horizontal level was to compute its correlation to, and RMS difference from, the aircraft data. To this end the both sets of data had to be put into a similar form. As the commercial computation and graphics software "MATLAB" was going to be used the data fields were written to text files that this program could read. In the process of preparing these files some interesting points were discovered about the aircraft dataset as will now be described. Figures 3-9 through 3-14 complement this discussion and by showing the appropriate plots for Flight 20a. The process was similar for all the days and the Flight 20a plots were simply chosen as representative of all five flights. The 17th would have been used to be consistent with the rest of the this section, but the winds were unavailable for that flight and the following discussion illustrated the data processing method rather than meteorological findings, so the discontinuity of days is not important.

The first step was to plot the aircraft's position and altitude from the data. Figure 3-9 shows that the track kept pretty well to the planned route (Fig. 3-4) but that the altitude fluctuated throughout the duration. As this fluctuation amounted only to a mean standard deviation of 18 meters from the mean of any given flight it did not preclude the idea of assessing model performance across a quasi-horizontal level. The exact method of point comparisons will be described later.

When the U and V wind components were originally plotted over time some questionably high values (greater than 50 m/s) were seen. The series was re-plotted (Fig. 3-10) with any values more than two standard deviations from the mean noted by an asterisk, and the locations of these readings noted on the aircraft's track. In each case it was observed that these points were almost exclusively found during the aircraft's turns as it changed direction back and forth over the bay. Since this brought into question the validity of these readings, these points were removed from the dataset. This is also the

suspected reason for the high wind speeds shown in the MUSE figures and why they were not used for wind verification. A third plot was made after the data had been filtered (Fig. 3-11) that showed a fairly regular sinusoidal pattern of speed over time. Since it was feared that perhaps the aircraft heading somehow influenced the wind readings another plot was made (Fig. 3-12) that showed where the aircraft was reading values above or below the mean. This plot showed that the cause of this variation was more likely due to the topographical effects of the coastline north of the bay as the values shifted whenever the aircraft passed into or out of the lee side of the land. Analysis of the temperature fields showed no degradation during the aircraft's turns and were not filtered in any way.

Since the inner nest of the model was running at a horizontal resolution of three kilometers, it was determined that points chosen along the aircraft path should be separated by at least that same amount. Another plot was made (Fig. 3-13) with numbered points marked every three kilometers along the aircraft's track. This was simply determined as a distance along the track and would not ensure the correct spacing in the turns or from line to line but they would serve well enough as guidelines. Points were then chosen that would provide a fair sampling of the flight path. This was done by including points in the inner and outer bay area and points close to shore. The number of points selected varied from flight to flight but averaged around 21. A text file was made that showed the data at each of these points and was checked to ensure none of those points selected were from the set filtered due to suspect winds. Tables 3-3 to 3-7 show the text files for each of the five flights. Figure 3-14 shows those points chosen along the aircraft's track to be used as verification against the model data. A script was then written that found the nearest data point to the track point and a similar data table was produced. In some cases this model "point" was created by interpolating the values of two to four surrounding points.

Having the aircraft and model dataset for the selected points, statistical measures were now able to be made. The first was to determine the correlation of the model to the aircraft data for each of U-speed, V-speed, total wind speed, wind direction, temperature and virtual temperature. A student-t test based on sample size was made to determine if there was a statistically significant change from the correlation values obtained for the

control run and each experiment. Root Mean Squared (RMS) differences were also calculated so that the models skill could be judged. The results of these tests are detailed in Section Four.

4. Station Observations and ETA Model Data

Additional methods of examining the model performance across a horizontal level was to compare the COAMPS fields with hourly land and buoy station observations and synoptic-scale analyses from the ETA model. The station observations were generally available as prepared time-series plots. Figure 3-15 shows one such plot from the station located on the former Fort Ord Army Base (about ten miles northeast of the Monterey airport) on August 17th. The plot is read with time increasing from right to left. Time is plotted here in UTC, so seven hours must be subtracted to get the local time. Care must be given when comparing figures as the subplots are scaled automatically.

A fairly complete picture of the weather at this site can be gained by combining the information in the different data subplots. For instance, on this day the temperature and dewpoint start to fall and come quite close together at 08 UTC, or 1:00am local time. The longwave irradiance increases, suggesting the presence of clouds until around 15Z. At this time the shortwave irradiance increases with the rising sun, the weak land breeze shifts to a moderate westerly sea breeze, temperatures increase and the clouds dissipate. Figure 3-16 is the plot for the Del Monte Beach station. Note how the moderating influence of the marine air is evidenced here by the fairly constant temperature and dewpoint. While temperature and dewpoint are close throughout the night these beach temperatures are almost four degrees warmer than those at the inland Ft. Ord station. The winds shifted about 45 minutes earlier at the beach and the brief (~30 min) spike in longwave radiation suggest a passing cloud. Figure 3-17 is the satellite image valid at 1445Z and is in excellent agreement with the above assessment as a patch of fog is distinctly visible over most of the bay, extending inland just to the Ft. Ord station but ending north of the Del Monte Beach site.

A final check of the model's performance in the horizontal was made using ETA model fields. These were the same fields used to initialize the cold-start COAMPS runs

A final check of the model's performance in the horizontal was made using ETA model fields. These were the same fields used to initialize the cold-start COAMPS runs on the 17th, 20th and 22nd plus additional analyses. All ETA fields examined were "analysis" vice "forecast" fields and were available every six hours. These fields were used to help describe the synoptic weather pattern during the week and as a rough check of conditions in the Monterey Bay area.

5. Profiler Data and Related Methodology

Located with the surface station at the Ft. Ord site is a vertical profiler. Boundary Layer Profilers are small UHF Doppler radar used primarily to measure vertical profiles of horizontal winds. With the addition of an optional Radio Acoustic Sounding System, virtual temperature profiles up to about 1 km can also be obtained. The profiler at Ft. Ord is located at an elevation of 51 meters above mean sea level (MSL) and provides an excellent look at the vertical temperature and wind structure from that height up to about 1400 meters, or nearly the 850 millibar (mb) pressure-level. Figure 3-18 is the image prepared from the data on the 17th, the same day examined above. The image is read, like the surface station plots, with time increasing from right to left. The designation "low mode" on this chart simply indicates the mode in which the profiler samples the lower atmosphere. The profilers in the NOAA Profiler Network alternate sampling modes between low and high every minute, and switch beam positions (eastward, northward, or vertical) every two minutes. The winds displayed at each height are averaged over the preceding hour. These profiler images can be used to track the pattern of the temperature inversion throughout the week as well as the wind patterns at this station. Note for instance in Figure 3-18 that there is a very strong temperature inversion at 17/00Z, with temperatures increasing from 16°C at its base near 175m to nearly 30°C around 550m. Interestingly, this would correlate with the "stronger" inversion that Koracin *et al.* (2000) noted led to quick dissipation of fog within a shallow marine layer and satellite imagery shows the fog in Monterey is gone by 1930Z. The winds aloft at this time are westerly so this is more likely warm air due to subsidence than from any offshore flow. Figure 3-19 is a composite of the images from the 17th through the 22nd. Although the winds are too

The height of the inversion base was taken as that height at the top of the coldest region on the image just above the lowest elevation of the profiler. The height of the inversion top was the lowest altitude of the warmest region above this cold point. The heights were estimated to within 25m. The temperatures were estimated using the scale on the image and the lowest value a color could represent. For instance if the coldest region above the ground was blue and this color indicated temperatures from ten to twelve degrees then ten was used for inversion base (virtual) temperature. Figure 3-20 is a plot of the change in inversion base and top height throughout the week as interpreted from the images and more clearly shows the increase in the elevation of the inversion base exactly as described in the progression of the ideal fog sequence in Section Two.

B. THE SYNOPTIC WEATHER PICTURE

1. Introduction

A brief discussion of the synoptic weather pattern needs to be given in order to place the mesoscale events within the larger picture. The discussion that follows uses information from each of the four sources described above. It begins on August 17th and goes through the 23rd, spanning the period during which data was collected for model verification. A series of charts covering the 500mb level down to the surface is provided in Appendix C. Upper level charts are not included in this series since the surface pressure features are essentially mirrored aloft in the geopotential fields of isobaric surfaces.

2. The Upper and Middle Atmosphere (300, 500, 700 mb)

At 17/00Z (Fig. 3-21) the polar front jet was flowing cyclonically to the south of an area of low heights in the Gulf of Alaska associated with a surface low pressure system. The 100kt jet maximum at 300mb supporting this low stays well to the north of Monterey and dissipates as it enters an area of more zonal flow over northern Idaho and Montana later in the time series. A trough appears in the 300mb pattern at 21/12Z, extending from Canada south to Mexico by 23/00Z. A broad area of closed low heights

forms off the California-Oregon coastal border within this trough and moves south so that by the 23/00Z it is centered just 400km west of Monterey (Fig. 3-22).

The 5820m contour is a useful reference line on the 500mb sequence as it can be used to show the development of the upper-level trough just seen at the 300mb level. It begins at 17/00Z (Fig. 3-23) as the southernmost contour that is clearly influenced by the low height center in the Gulf of Alaska and can be seen crossing over land at around the Oregon-Washington border. At 19/06Z it has moved into northern California and by 21/12Z it dips south to the San Francisco area. The trough continues to develop and by 23/00Z (Fig. 3-24) it extends along the whole west coast. Note the closed cyclonic circulation pattern that develops at the base of the trough and southerly flow it indicates along the California coast. These southerly coastal winds are modeled all the way down to the 850mb level and were observed during Flights 22a and 22b as well as by the Ft. Ord profiler. The 500mb height gradient over Monterey stays weak throughout the week.

The same trend was observed at the 700mb level (not shown). The heights develop a large trough at 21/12Z and by 23/00Z there is a cyclonic circulation with a closed height center to the west of the circulation center.

3. The Lower Atmosphere (850 mb)

The 850mb chart at 17/00Z (Fig. 3-25) is similar to the 700mb chart, showing the low height area in the Gulf of Alaska and a weak gradient over Monterey. The 1560m height contour begins parallel to the coast of northern California, as discussed in the early phases of the ideal fog sequence and the high temperatures near Monterey (between 20° and 30°C) suggest warming has indeed been occurring before this analysis time. The 23/00Z chart shows (Fig. 3-26) how far the 1560m contour receded to the west allowing the trough to extend southward. Model temperatures over Monterey cool to between 15° and 20°C and the MUSE flights and profiler data confirm this cooling trend. This cooling aloft is a critical part of the ideal fog sequence in that is serves to weaken the inversion and allow the inversion base height to rise. When it has risen high enough, the fog will change to low stratus. Satellite imagery clearly shows the early-week, localized, diurnal

patches change to a solid deck all along the coast by 23/00Z and seems to confirm the evolution of fog into stratus.

4. Surface

The 17/00Z analysis chart (Fig. 3-27) has the same dominating features as all of the upper air charts. The EastPac high pressure cell is at 1031mb and centered about 1500km off the central California coast. The Gulf of Alaska low to the north of it has a central pressure of 998mb and is filling. The surface isobars are nearly perpendicular to much of the northern half of California as described in the early phases of the ideal fog sequence as the cause of offshore flow and warming. There is a very strong thermal gradient along the coastline with surface temperatures of 75°F (ETA 2m temperatures are given in degrees Fahrenheit) just offshore increasing to over 100°F in the interior valleys. Coastal winds are from the north-northwest and running at 15 knots. At each 00Z analysis throughout this series there is a low pressure center positioned in central Nevada. Since the 00Z charts are the afternoon (hot) charts and temperatures in central Nevada are over 100°F these are most likely thermal lows. While they move closer to California throughout the series they never become a dominant features over the central coast. They move closer to California as a result of the EastPac High moving west, they do not cause the movement. A good reference isobar on the surface charts is the 1020mb contour. It begins tangent to northern California and is meridional with a slightly positive tilt. By 23/00Z (Fig. 3-28) this contour is almost 500km offshore as the high pressure cell has moved over 1400km to the west-southwest since 17/00Z. While the coastal winds back from the northwesterlies to a westerly, onshore pattern by 23/00Z, they never back all the way to a southerly the way they did at mid-levels. This was verified with land station observations all along the coast in addition to this model. Figure 3-29 is a larger scale chart at 23/00Z that includes land station reports. One exception is the M4 buoy station that did show the southerly flow. Figure 3-30 is its data time series and shows not only southerly flow for a period on the 22nd, but an increase in speed at the same time. This buoy is far enough offshore (Fig. 3-29) to be less influenced by the thermal gradient. Neither M1 nor M2, both within Monterey Bay showed this southerly wind. It is not uncommon for the marine boundary layer winds to remain influenced by mesoscale

features while the winds aloft respond to the changes in the height fields. In this case the surface winds seem to be following a diurnal land and sea breeze cycle while the winds aloft formed cyclonic cells within the cyclonic curve of the troughs that formed in the wake of the receding EastPac High.

5. Summary

The synoptic-scale pattern seen influencing California on the upper air charts was a reflection of what was occurring at the surface. Isobars paralleled the California coast at the onset and the anticyclonic flow brought northerly, offshore winds descending down into the Monterey Bay area. This warmed the lower levels and strengthened the thermal inversion that caps the MABL. As the EastPac High moved west, all of the upper-level charts showed the development of a trough along the western United States. The cyclonic curvature of this upper-level trough caused small areas of cyclonic upper-level winds and southerly flow along California's west coast. The surface winds in the MABL however became a function of mesoscale effects in the absence of strong synoptic forcing and did not back to southerly flow. The Del Monte Beach station observations for instance showed a consistent sea breeze from 270° except for twice at sunrise when they became northerly and calmer. The effect of the loss of the northerly winds can be seen in the temperature change of the MABL in the composite profiler plot (Fig. 3-19) which shows the boundary layer air cooling and the base of the inversion rising as in the ideal fog sequence. Longwave irradiance both showed increasing cloudiness throughout the week and satellite images indicated that it was fog/stratus.

THIS PAGE INTENTIONALLY LEFT BLANK

IV. THE RESULTS

Perfect model simulation results are fairly easy to document. Unfortunately, the experiments in this study yielded imperfect simulations of the days in question. These presented several possibilities. Were the simulations correct in their fog forecasts but made a poor positional placement within the forecast area? Were they accurate in all things except for the timing of the forecast? Did they show skill along the horizontal but not in the vertical? Or were they just plain wrong? The section below explains some of the methods and results used in an attempt to answer these questions and determine if the primary objective of the thesis had been met and improved skill could be shown in a fog forecast with parameters tuned for a local area. The fact that all of the experiments were consistent in either placing clouds where the satellite showed none, or missing clouds when the satellite does have them, suggests that there is an atmospheric flow condition that the model is missing, perhaps due to poor initialization. The result was that the second-order, relative changes to the fog forecasts produced by the experiments were largely masked by the first order errors in the model's simulation of the mesoscale atmosphere. The general findings will then focus more on the relative changes brought about by altering the model physics between experiments than on the degree to which any one of them accurately forecasted fog.

The first series of eight experiments included AC1, CB1, CON, LW1, LW2, SW1, SW2 and TK1. Each was performed for the 17th and the 20th, with CON also running on the 22nd for later comparisons. The first analysis was a visual comparison of the cloud edge as expressed by the cloud water value, CLDW. This was done for all eight experiments for all three days modeled. The second test was a comparison with the aircraft data winds, temperature and moisture (via virtual temperature). RMS errors and correlation coefficients were calculated for all eight of the experiments were used to determine accuracy and statistically significant changes from CON, but only on two days with different fog patterns as seen by satellite imagery - the 17th and 20th. The third test was a comparison with the profiler data from Ft. Ord to again assess accuracy and skill compared to CON. This test was only performed on the experiments that had shown some skill in the earlier analyses. Three additional experiments, CB2, TK2 and CB3

were also performed and subject to those tests deemed necessary for comparison with the results from the first series. Data from other ground stations and the ETA model was used throughout the analysis to clarify the synoptic situation so that the mesoscale effects could be seen within a broader context. A summary of the physical changes made in all of the experiments and the observed results in presented in Table 4-5.

A. COMPARISON WITH SATELLITE DATA

1. Methodology and Comments

Two tests were made using the satellite imagery and the model fields. The first was to compare the CLDW values forecasted by the experiments to the values somewhere between 0.1 and 0.5 kg/m^2 suggested as likely for a cloud edge obtained by the calculations done in the satellite data portion of Section Three. Since cloud drop size was not measured, a specific forecast value could not be stated before the experiments were performed, but it was hoped that a value, once found, would remain consistent across the three days for any given experiment. Accuracy could be judged by comparing a "reasonable" value against the actual cloud contour in the imagery. Figure 4-1 shows one such test with the CLDW value plotted for CON versus the satellite image at 15Z on the 17th. Note in this image the 0.05 contour does a good job of outlining the edge of the fog present in the bay. Unfortunately, using this value for later forecasts led to gross over-forecasting of fog. These comparison tests also provided an opportunity to judge the sensitivity of the model to the different effects on cloud water produced by the changes to model physics in each experiment.

Figures 4-2 to 4-5 show each of the initial experiments at 18/00Z for comparison. Despite the fact that the simulations suggest the presence of clouds, the satellite image showed none at this time. Any areas on these figures with CLDW values greater than zero can then be taken as forecast areas for clouds when none were observed – termed "false alarms." Since there was so much cloud water indicated in the CON forecast at 18/00Z when the imagery showed no clouds, it was re-run to extend to a 48-hour forecast to ensure the model wasn't simply continuously adding cloud water over time. This 48-hour study ruled out this possible error as it showed a diurnal pattern and decreased

CLDW values after 18/00Z. AC1 is included on each of these four figures as it had the lowest CLDW values and significantly fewer false alarm areas than CON at 18/00Z.

The differences between LW1 and LW2 were very small, showing the model was fairly insensitive to the change in emissivity calculation. Since neither longwave experiment was very different from CON either, they were not chosen to be a part of any combination experiments. What was interesting about the longwave experiments was that their cloud water results were what was expected. LW2 showed, as expected, more cloud water than LW1 presumably because of its increased longwave emissivity and associated cooling and mixing. All of the experiments, in fact, yielded results that were expected based on the physical changes that were made.

SW1 was also too much like CON, thereby ruling it out in a possible combination experiment. SW2 was significantly different than SW1, showing that the model was quite sensitive to the change in the single scattering albedo. In fact, SW2 was almost as good in this case as AC1. These shortwave experiments also showed a difference in COAMPS and MM5, as COAMPS achieved fewer false alarms by decreasing shortwave scattering (thereby increasing absorption) while Mass and Steenburgh (2000) improved MM5 by reducing shortwave absorption by 45%. Because of the good performance of SW2 in this test, and its good correlation results with aircraft data, SW2 was combined with AC1 for the second combination. The CB2 cloud edge results were, however so similar to those of AC1 that little statistical data from CB2 was collected.

While neither the TK1 nor TK2 experiments decreased the false alarm rate as much as AC1 did, they were both better than CON and they also improved the vertical structure of the models so they were incorporated into combination experiments with AC1 (CB1 and CB3, respectively). The addition of TK2 to AC1 was also seen to have an observable and positive effect during the rainwater analysis as described below.

The second test was a skill test to see how each experiment compared with CON to gage their relative merits. Each experiment was checked at the 15 and 24-hour forecast time for each of the three days as visible imagery was available for both of those times and they represent both hot and cold chart times. Figures 4-6 through 4-11 show the comparisons for CON, AC1 and CB3 with the satellite image throughout the three

days. The value used to obtain the best cloud edge at 17/15Z was carried forward for the series. It is important to note on these figures that the thin green contour lines have the same scale in each panel of the six figures, but different shading is used for each experiment. That value determined to best depict the fog edge at 17/15Z was used as the minimum value to be shaded for all six comparisons. While certain experiments showed skill relative to others, none of them achieved a cloud edge matching that in the satellite imagery using a consistent value of CLDW for the three days modeled. The main problem was that all experiments showed values of CLDW high enough to indicate clouds when in fact there were none (false alarms). This was especially true in the San Francisco Bay region and may indicate some regional difference in this area and Monterey Bay.

The fewest over-forecasts came from AC1, but it may cause other problems. Lowering the autoconversion parameter should decrease cloud water amounts as drizzle forms, and this drizzle should aid in dissipating the fog itself. These experiments showed that the cloud water was reduced at the expense of increased rainwater amounts. Figure 4-12 is a comparison plot of rain water values at 1000mb for AC1, CON, CB1 and CB3. No rain or drizzle was reported in any of the land station observations, but only the Monterey station was in a position where the experiments indicated rainwater over land. Ship observations may have actually confirmed the rainwater over the water as drizzle, but were not available during this time as part of the NPS data archives. The areas of rainwater are hypothesized to be seen as false alarms in this case. Note that both the area and amount of rainfall is significantly higher in AC1, CB1 and CB3 than in CON. The AC1 values are as much as five times those of CON. The addition of TK2 to AC1 seemed to have a mitigating influence as CB3 shows less rainwater than AC1 alone, but the values are still well above CON. This could be due to TK2 increasing the likelihood of dry air entrainment at the cloud top due to its increased mixing length just above the boundary layer. This entrainment would then reduce the amount of both cloud water and rainwater.

2. General Findings:

In general, COAMPS simulations showed the correct qualitative trend in increasing the horizontal extent of the stratus coverage from the 17th to the 22nd.

Values between 0.1 and 0.2 kg/m^2 were found to model the cloud edge reasonably well, depending on the experiment. However, within any experiment no value that was found to work well on the 17th could be used in all subsequent forecasts over the three days and still yield consistently good results. Perhaps the CLDW value used to simulate cloud edge actually *should be* changing over time to reflect changes within the cloud structure (droplet size and concentration).

The model's cloud edge depiction was fairly insensitive to the emissivity changes in the LW experiments.

The model's cloud edge depiction was somewhat sensitive to the changes in the TK experiments.

The model's cloud edge depiction was very sensitive to single scatter albedo changes in the SW experiments, and the autoconversion criterion change in the AC experiment.

COAMPS differs from MM5 in that COAMPS improved cloud edge simulation by decreasing shortwave scattering (thereby increasing absorption).

AC1 had the least tendency to over-forecast clouds, but it did so by precipitating out the cloud water as rain water.

Combining TK2 with AC1 (CB3) reduced the amount of suspected false alarms in rain water.

B. VERTICAL PROFILE COMPARISONS

1. Methodology and Comments

A script was written that allowed model fields to be extracted to a text file at positions that corresponded with the data collected by the Ft. Ord profiler. Comparing these two datasets was then possible in a similar fashion to the aircraft data comparisons.

Since what was critical to forecasting fog throughout this week was the height of the base of the inversion and the strength as measured by temperature, these were the fields chosen for direct comparison. Disregarding the 00Z analysis fields produced during the cold start and beginning with the six-hour forecast, the temperature and height of the inversion base and top were obtained every six hours by manual interpretation of the data text file generated, using the same definitions of inversion base and top as previously explained. Figures 4-13 and 4-14 show the inversion temperatures and heights respectively. The Ft. Ord profiler data is shown as a black line. All of the experiments for which the vertical data was gathered are also shown on these figures, which are most useful to see the inversion strength as measured by either height or temperature difference.

Table 4-1 is a summary of the RMS error data pertaining to the profiler comparisons. Most significant to note on this table is the improvement from CON to CB3 in three of the four measurements. It is difficult to compare all of the data for the experiments as those marked with an asterisk on this table were only obtained from the results on the 17th and 20th while the others included the 22nd. There was a tendency for all of the experiments to under-forecast the elevation of the inversion base on the 22nd and this makes those experiments that included this data to appear worse than those that did not. It is important to note from this table that none of the changes made to model physics to improve the cloud edge performance had a significantly adverse effect on these other model parameters.

A script was written to produce a profiler image similar to those of the Ft. Ord profiler. A quick comparison of the vertical wind structure was possible by comparing these two images. One general tendency was noted using a comparison like that shown in Figure 4-15. The winds in the lower levels of these images during the daylight hours show that the model winds were was generally around five knots too weak. Since the wind at these levels and times was primarily a thermally-driven sea breeze, the plots suggested the model was not creating a sufficiently strong thermal gradient. Figure 4-16 shows that the CON model's SST at 18/00Z in the central bay was around 54°F (~12°C). This is fairly close to the 13°C value from approximately the same time obtained during MUSE Flight 17 (Fig. 3-8), although the MUSE data has much more structure. More

important is the air temperature difference at 18/00Z shown in Figure 4-17. Here the CON model's air temperature at ten meter elevation is shown by the green shading to be between 54 and 56°F at the Monterey station, whereas the observation showed 66°F. Since the Ft. Ord profiler site is further inland and consistently warmer than Monterey there may have been an even larger error than this observed ten-degree difference. Such a large thermal difference could be the cause of under-forecasting the wind speed. Why this difference was present could be the subject of further research. Sterbis (2000) noted soil heat budget parameterization as a possible source of MM5 air temperature errors in the Los Angeles basin.

Model data was used to produce a synthetic sounding that was plotted on a Skew-T diagram. Recall from Koracin *et al.* (2000) that the moisture content of the air above the inversion can alter cloud-top longwave cooling and therefore influence the formation and evolution of fog. The entrainment of dry air at the cloud top can be a primary cause of cloud dissipation. Since COAMPS seemed to be over-forecasting clouds based on satellite comparisons, yet was excessively dry above the inversion in Figure 2-10 (CON valid at 17/12), a re-examination of the turbulent mixing length was made that led to experiments TK2 and CB3. One result of scaling the mixing length above the boundary layer with height rather than holding it at a fixed (small) value is to increase the likelihood of mixing across the boundary. Figure 4-18 shows that the two TK experiments did cause the air above the cloud top to be slightly less dry. Here the Skew-T diagrams for a location over the bay and valid at 17/12Z made from the TK1 and TK2 experiments are compared with that of CON. While the changes in the dewpoint temperature curves appear to be slight, the result in modeled cloud edge was readily apparent.

The Skew-T diagrams were generally examined to see if they indicated events that were not seen to be occurring in other data sources. Separate statistics were not kept based on Skew-T comparisons.

2. General Findings:

The inversion base elevation correctly tended to increase throughout the week, but was too low by the end of the week.

The inversion top elevation correctly tended to increase throughout the week, but was almost always too high.

The inversion base temperature correctly tended to decrease throughout the week, but was too cold by the end of the week.

The inversion top temperature correctly tended to decrease throughout the week, but was always too cold.

The winds in the lower 500m were approximately 5kts less than those observed by the profiler during the warmer part of the day.

Skew-T diagrams show the effect of changing the TKE mixing length to a scalable value in experiment TK2 was to alter the temperature structure in the lower MABL in a way that suggests an improvement was made, albeit a small one.

C. COMPARISON WITH AIRCRAFT DATA

1. Methodology and Comments

The limited dataset at the chosen points for each of the MUSE flights, as explained in Section Three, was used to compare with the model data on a quasi-horizontal level. It is important to note that while statistics suggesting an improved forecast were welcomed when they occurred, this analysis of correlation and RMS error statistics was primarily to ensure that the changes made to improve the cloud edge did not adversely affect other forecast variables.

A script was run that selected the model data points closest to the chosen points in both space and time. In some cases the values from two or four adjacent points may have been interpolated to best fit the chosen point. The model output from this set of matching points was then compared to the aircraft set using a MATLAB program. Figure 4-19 is a plot of the chosen points for Flight 20b with the outline of Monterey Bay on the east side of the figure. The program then produced a correlation plot for each variable examined.

These variables are: U-direction wind speed, V-direction wind speed, total wind speed, wind direction, temperature and virtual temperature. Fig. 4-20 is an example of one of these plots showing the correlation of temperature data from the CON experiment and the aircraft data. If there had been perfect correlation between the two datasets, the resulting correlation would have been the dashed line shown with a slope of one. How much the line obtained by a least-squared linear fit of the data pairs differs from this line is then a relative measure of the model's inaccuracy, assuming the aircraft data to be the "truth" for verification purposes. Note that each data point is labeled with the same number used in Figure 4-19, allowing geographic-based analyses to be performed. Once the performance of CON was determined, a student-t test was preformed to see how much change would be necessary for a "statistically significant" change from CON based on the sample size. The results of these tests for each of the five flights, as well as all of the other flight data comparison test information, are summarized in Table 4-2, which is divided into five sections (a-e) corresponding to each flight, and two parts to each section (1 and 2) containing statistics for the entire flight and specific to each parameter. The numbers in the "(b)" and "(w)" columns found in the row for CON indicate those values required to show (b)etter or (w)orse forecast values at the level of statistical significance indicated. For example, Figure 4-21 is the result of the AC1 experiment for temperature for the same flight. Note that its Rxy value is 0.703 compared to the CON value of 0.614. Using the "(b)" column values in Table 4-2 this would indicate a statistically significant better result with between 55% and 75% certainty. Note that the correlation results are very sensitive to changes in only a few points as all of the datasets contain less than 25 points. This is one of the reasons so few of the experiments produced changes with a high level of significance. Additional information available from the plots like Figure 4-20 includes the general bias of the model and specific locations where it was performing well and poorly. These were all analyzed to search for some systematic errors present in the data. For instance, in this case the model showed about a 2°C cold bias in both figures above. They also showed that the model's temperature was too high at point 21. Referring to Figure 4-20 one can see that this point is quite close to the coastline As Flight 20b was late in the day this could indicate that the model was warming this point disproportionately to the others or that the horizontal variation of the

MABL structure was wrong in the model. Further study showed that this point was actually over land in the model terrain database and so it was being heated as such. All of the comparison plots have been archived at the Meteorology Department at NPS along with the rest of the data and the MATLAB analysis programs

In addition to the correlation test, the RMS error was calculated for each flight, experiment parameter. All of these results can also be found in Table 4-2. Continuing with the example from above, the AC1 experiment is again better than CON with an RMS value of 1.7°C compared to 2.13°C value for CON. However, neither of these values is less than the standard deviation of the aircraft chosen point temperature values suggesting they were not accurate. Care must be exercised when making this assessment as the mean and standard deviation values were calculated using all of the points in the chosen (filtered) aircraft's dataset and these are temporally and spatially separated, while the RMS error is a comparison between points at an identical temporal and spatial location in the two data sets.

Two additional plots were made for each flight to try to identify systematic model errors or other trends in the data related to the geography. Figure 4-22 shows a temperature difference at each point. An upward arrow indicates the model is too warm and the length of this arrow corresponds to the magnitude of the difference. Recall from the discussion above that the model showed a cold bias. This figure seeks to show exactly were the model was cold. Only point 21, the point the model actually held over land, is warmer than the aircraft data set in this figure.

The second figure (Fig. 4-23) is a wind comparison plot showing both the wind as measured by the aircraft (as a solid line) and the experiment's wind (dashed). In this case the CON winds are shown to be fairly accurate in direction but slightly over-forecast in the outer bay, but under-forecast closer to land. This tendency to under-forecast the winds was noted on almost all of the later afternoon plots and also during the profiler comparison. The hypothesis that this was due to the insufficient heating of the air over land by the model was explored in the vertical profile results section above.

The general tendencies noted on each day are as follows:

Flight 17: The temperatures were generally in good agreement (no wind data available for comparison). All experiments tended to be cold on points #19-21, all of which are on the north side of the bay in the area of very warm temperatures noted on the MUSE air temperature plot (Fig. 3-5). Virtual temperature tendencies followed temperature. This was true of virtual temperature for all five flights.

Flight 20a: All experiments tended to have high wind speed except for at point #20 (the point the model topography has over land in the center of the bay on the eastern side) where the experiments were 6-7 kts slow. The wind direction was generally good with the exception of points 13 and 19 (north, central bay) which the aircraft showed to be southerly and the models had northwesterly, and point 20 which the aircraft had southwesterly and the model had southerly. The temperatures were generally around one degree too cold. Points #12,13,18,19,20 (all in the interior bay) were in closest agreement with the aircraft.

Flight 20b: All experiments had a generally good correlation on wind speed. Points #13,20,21 (northeast side of the bay) had a much slower speed than the rest of the points. The wind direction was generally good with the exception of these same three points that the model has ~30 degrees too northerly. The temperatures were generally around two degrees too cold except at point #21 (close to location of point 20 in Flight 20a) where the model was 2 degrees too high.

Flight 22a: Both 22a and 22b have a much smaller experiment dataset for comparison as only three experiments were run simulating the 22nd. The wind speed had a generally poor correlation. The wind direction was also poor, with the model indicating northwesterly flow and the aircraft indicating southeasterly. The temperatures were generally around five degrees too cold. This ties in with the profiler comparison which showed that at this time, the modeled inversion base was almost 200m lower than that observed by the profiler.

Flight 22b: The wind speed was generally around 3 kts slow except at points #2 and 3 (northwest bay) where model was 2 kts fast. The wind direction was around 50 degrees too northwesterly except at points #1,2 and 15 (NE side of bay) which had good

correlation. The temperatures were generally around two degrees too cold except at point #1 (NE bay) which was almost five degrees too cold.

2. General Findings:

Points close to land on the northeast side of the bay seemed to often be the outliers on correlation plots, suggesting the terrain effects played a significant role in the mesoscale environment as would be expected.

Of the 160 correlation comparisons, only 17 were statistically significantly different than the control case with a confidence of more than 75%. Fourteen were improvements, mostly to temperatures on Flight 20a and three were degradations to wind speed on Flight 20b. Table 4-3 shows the average correlation values for each flight and, combined with the extremely small (0.05) standard deviations shown in Table 4-4, indicates how similar all of the experiments really were in comparison with the aircraft data. These results, like those in the vertical comparison, show that the physics could be modified by these experimental amounts to improve the cloud edge definition without necessarily degrading performance elsewhere.

The wind direction was generally good early in the week, with the exception of points along the coastline. As the week progressed, the model maintained northwesterly winds while the aircraft data showed winds from the south. Recall the synoptic picture indicated southerly winds down to the 850mb level, but not to the surface. Since the model showed the elevation of the base of the inversion was too low on the 22nd, it is not unreasonable to think that these northerly winds are merely those that would be observed at a lower level (as they were in station observations) rather than incorrect by 180°. That is, the model's northerly winds could be the correct winds from a lower level simply misplaced in the vertical.

The temperatures were generally at least one degree too cold. This would lead to wind speed and direction errors and the winds were greatly influenced by the diurnal land/sea breeze pattern.

The virtual temperature tendencies followed temperature.

V. CONCLUSIONS AND RECOMMENDATIONS

A. CONCLUSIONS

In a sort of bridge between statistical methods and numerical forecasts, Tag and Peak (1996) proposed a machine learning scheme that would take existing statistical rules and apply them to data to make a fog forecast. Given the popularity of automated tactical decision aids this certainly seems likely to happen. It also lends itself to the notion that machines may replace humans in operationally interpreting meteorological data. This is especially relevant in light of the current push within the Naval METOC community to make environmental products another layer of data within the omnipresent GIS systems foreseen in the electronic future. The CNMOC Strategic Plan (1997) calls for this community to "furnish products focused on fine scale tactical and strategic environmental effects which *every warfighter* will understand." But the main problem that Tag and Peak noted in their system was the poor quality of the meteorological input their system was forced to ingest, "the primary limitation comes from the data itself."

This study showed just how far we are from an automated system that can reliably produce a fog forecast. But it also showed that steps can be taken to improve the existing method. The change made to the autoconversion threshold showed great promise in better defining the cloud edge. The change to the turbulent kinetic energy scheme also showed some skill based on the comparisons with profiler data.

B. SUMMARY OF CONTRIBUTIONS

While there was no definitive solution to tune COAMPS to the local area for an optimum fog forecast, there were several insights gained by this study:

In general, COAMPS simulations showed the correct qualitative trend in increasing the horizontal extent of the stratus coverage from the 17th to the 22nd.

The COAMPS fog forecast can be "tuned," to a degree, by changing parameters like autoconversion criterion or shortwave radiation absorption that may be unique to a local area without significantly adversely affecting other forecast variables.

A model parameter (layer cloud water) can be used to approximate a cloud edge with some degree of skill.

COAMPS is capable of successfully simulating the height and temperature changes in the thermal inversion and MABL during a fog/stratus sequence.

Making mixing length a scalable parameter vice a constant can realistically increase cloud-top entrainment for low-level stratus.

COAMPS is very sensitive to changes in the autoconversion criterion and single scatter albedo values and less sensitive to changes in longwave emissivity values.

C. RECOMMENDATIONS

This study provided many interesting results and succeeded in raising many new questions worthy of effort. The recommendations that follow try to achieve three main goals: to make COAMPS better, to make a regionally tuned COAMPS a possibility and to improve the research approach during future studies that may be similar to this.

*** Examine the COAMPS land-surface processes.**

Could different soil parameterizations or land use categories result in more accurate surface temperatures and subsequent coastal winds?

*** Do more regional studies.**

Why were there consistently false alarms in the San Francisco Bay region? Does it have to do with different terrain effects? Does it have to do with an increased aerosol count in the atmosphere due to the proximity of the city? More studies in more regions would provide more information on how to "tune" the code by geographic area.

*** Do more autoconversion experiments.**

The autoconversion experiment showed skill in cloud forecasting at the expense of over-forecasting rain - is there a way to avoid this? Could additionally research seek appropriate values for the criterion by geographic area based on atmospheric properties and availability of CCN?

* **Examine changes to the shortwave radiation schemes.**

The current shortwave radiation scheme does not allow for absorption by any aerosols other than the clouds themselves. Could examining the effect of including aerosol absorption and obtaining appropriate regional aerosol parameters improve the forecast? The model was quite sensitive to changes in the single scatter albedo and showed skill when the value was decreased to allow for increased shortwave heating. Could further experiments improve on the results of SW2?

* **Experiment with model resolution.**

Accurately representing the vertical structure through the MABL is essential to making a fog forecast. Increasing the number of vertical levels may be more important to this end than current efforts to reduce the horizontal grid spacing. Examine the computational cost of increasing the vertical resolution at the expense of the horizontal. Could decreased horizontal resolution and increased vertical help the forecast?

* **Experiment with new initialization schemes.**

What changes will 3DVAR bring to COAMPS? Is it better than 3DMQ? How can NPS student-researchers assist in the evaluation?

* **Try changing the longwave radiation parameterization.**

Even though the longwave experiments of this study showed no improvement over CON, that doesn't mean there is nothing to gain in this area. One area that was not changed but could be the subject of further study was that clouds in this scheme were assumed to completely fill a model layer in the vertical but could be fractionally designated in the horizontal. Given the importance of processes occurring at the cloud top boundary it would seem that this assumption of filling a vertical layer could lead to errors. If, for instance, a cloud was analyzed to be in the level above 750m in operational COAMPS then it would extend all the way to 1100m. This could lead to clouds layers unrealistically extending through the inversion layer or, conversely, for the inversion layer to have dissipated a cloud to a much lower level. One approach to solving this problem is to use more vertical levels, as experimental COAMPS does, but another method may be less computationally expensive. Could changing the longwave radiation

scheme so that clouds can occupy portions of vertical layers be computationally less expensive than increasing vertical resolution?

* **Use more advanced satellite analysis methods.**

Would using satellite data instead of satellite imagery have shown different threshold areas for cloud edge based on threshold values?

* **Study the effects of cloud physics.**

How would altering the concentration of the cloud drops affect the "reasonable" values determined for CLDW? Should a single value of CLDW ever be expected to simulate a cloud edge over time or will physical processes change the structure of clouds too much over time and space?

APPENDIX A. TABLES

(BI-CL)* [meters]	Unbroken Fog	Scattered Fog	Clear
> +400			
300 - 400	3		
200 - 300	9	1	
100 - 200	7		
0 - 100	8	5	
-100 - 0			1
-200 - -100			5
-300 - -200			4
-400 - -300			2
< -400			12

Table 2-1: Fog Occurrences vs. Petterssen's Statistical Index (Petterssen, 1938)

* (BI-CL): BI = base of inversion [m], CL = condensation level [m]

Phase	BI [m]	Conditions
ONE "Initial Conditions"	0	Strong offshore winds; a semi- ovular clear area offshore; zero or near-zero BI; and hot, dry air with very high visibilities ashore. The zero BI is present over the sea when the air temperature (Ta) is greater than the water temperature (Tw). A difference of 5C or more is a good precursor of fog. The low inversion may not show at a land RAOB site where the surface temperature may be abnormally high, but its presence offshore at the same time is critical to fog formation.
TWO "Fog Formation"	0-250	Shallow, cold, dense, often patchy fog at sea approaching the coast in wide bands, possibly touching the coast in mid-afternoon.
THREE "Fog Growth and Extension"	251-400	Deeper, more widespread, less dense fog at sea and more encroachment over land
FOUR "Stratus"	401-800	No fog ashore but a low stratus overcast
FIVE "Clearing"	>801	

Table 2-2: Leipper LIBS Method Fog Forecasting Guidelines (Leipper, 1995)

COAMPS 2.0 Specifications	
Parameter	Information:
Basic equations:	Primitive equations including non- hydrostatic effects
Field formats:	Applications grids are latitude- longitude or cartesian coordinates on horizontal map projection
Variables:	Wind components, potential temperature, mixing ratio, surface pressure, ground temperature, ground wetness, SST
Numerical techniques:	Arakawa C-grid, vertically and horizontally staggered with split explicit time integration
Integration domain:	Regional, surface to sigma (30) = 31500 m (approx. 10 mb)
Horizontal resolution:	User specified, most often 81 x 27 x 9 km, triple nested
Vertical levels:	30 vertical levels on sigma z coordinates
Nested grids:	level of nesting is most often 2 or 3
Forecast time:	Nominally 48 h (72 for European Area)
Initial fields:	An MVOI maps both real and synthetic observations from NOGAPS on the model grid. In the incremental update cycle, analysis increments to the first-guess are interpolated in the vertical to the model vertical levels, and added to the most recent model forecast.
First-guess analysis:	As COAMPS runs in a continuous update cycle, the first-guess fields come from the previous COAMPS forecast
Boundary conditions:	Davies (1976) or Perkey-Kreitzberg (1976) treatment of NOGAPS forecast fields
Orography:	Envelope topography is from the 1 km terrain data base developed from the DMA DTED level 1 data set
Horizontal diffusion:	Fourth-order diffusion applied to all prognostic variables, except the Exner perturbation (pi')
Moisture physics:	Explicit moist physics (Rutledge and Hobbs, 1983) for horizontal grid resolutions less than specified value (typically 10 km). Cumulus convective process (Kain and Fritsch, 1990)
Radiation:	Longwave & shortwave radiation (Harshvardhan, 1987)
Planetary boundary layer:	1.5 order turbulence kinetic energy closure (Deardorff, 1980)

COAMPS 2.0 Specifications (cont.)	
Land surface:	single layer/bucket model
Ocean surface:	COAMPS makes its own SST analysis at the surface every time it runs using optimum interpolation techniques

Table 2-3: COAMPS 2.0 Specifications (From, FNMOC)

Experimental Model Vertical Spacing

Level#	Spacing [m]	Height [m]	Height [ft]	Press [mb]
45	2,000	20,000	65,616.8	55.0
44	2,000	18,000	59,055.1	75.3
43	2,000	16,000	52,493.4	103.2
42	2,000	14,000	45,931.8	141.5
41	2,000	12,000	39,370.1	193.9
40	2,000	10,000	32,808.4	264.6
39	2,000	8,000	26,246.7	356.2
38	1,000	6,000	19,685.0	472.0
37	1,000	5,000	16,404.2	540.4
36	1,000	4,000	13,123.4	616.6
35	700	3,000	9,842.5	701.2
34	400	2,300	7,545.9	765.9
33	300	1,900	6,233.6	805.0
32	200	1,600	5,249.3	835.3
31	100	1,400	4,593.2	856.1
30	100	1,300	4,265.1	866.6
29	50	1,200	3,937.0	877.2
28	50	1,150	3,773.0	882.6
27	50	1,100	3,608.9	888.0
26	50	1,050	3,444.9	893.4
25	50	1,000	3,280.8	898.8
24	50	950	3,116.8	904.3
23	40	900	2,952.8	909.8
22	40	860	2,821.5	914.2
21	40	820	2,690.3	918.6
20	40	780	2,559.1	923.0
19	40	740	2,427.8	927.5
18	40	700	2,296.6	932.0
17	40	660	2,165.4	936.5
16	40	620	2,034.1	941.0
15	40	580	1,902.9	945.5
14	40	540	1,771.7	950.1
13	40	500	1,640.4	954.6

Experimental Model Vertical Spacing (cont)				
12	40	460	1,509.2	959.2
11	40	420	1,378.0	963.8
10	40	380	1,246.7	968.4
9	40	340	1,115.5	973.1
8	40	300	984.3	977.7
7	40	260	853.0	982.4
6	40	220	721.8	987.1
5	40	180	590.6	991.8
4	40	140	459.3	996.6
3	40	100	328.1	1,001.3
2	40	60	196.9	1,006.1
1	20	20	65.6	1,010.9
0	0	0	0.0	1,013.3

Table 2-4: The Vertical Structure of the Experimental COAMPS Model

Note: Height (Z) and Pressure (P) values are based on the U.S. Standard Atmosphere

Drop Radius [μm]	N [drops/cm^3]	δ	Min Detect Thick [m]
2.5	100	0.1	25
5	100	0.1	6.4
10	100	0.1	1.6
15	100	0.1	0.71
20	100	0.1	0.40
25	100	0.1	0.25

Table 3-1: Minimum Detectable Thickness as a Function of Drop Radius

MUSE Flight Information Table					
Flight	**Date**	**Time**	**Mean Alt AGL**	**BI[1]** **SI[2]**	**Satellite**
17	17 Aug 2000	2236Z to 0011Z 3:36 to 4:11pm PDT	109m	300m 14°C	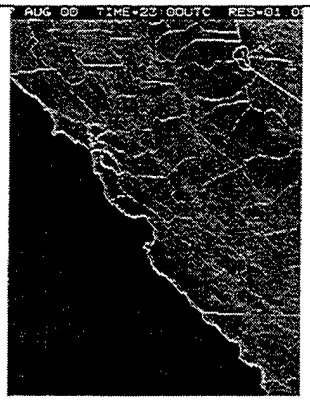
20a	20 Aug 2000	1649Z to 1832Z 9:49 to 11:32am PDT	76m	375m 9°C	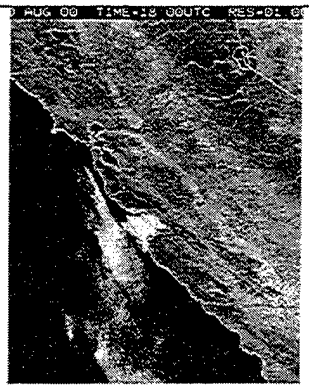
20b	20 Aug 2000	2143Z to 2334Z 2:43 to 4:34pm PDT	84m	375m 8°C	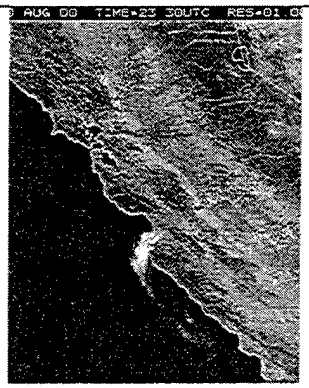

MUSE Flight Information Table (cont.)					
Flight	**Date**	**Time**	**Mean Alt AGL**	**BI[1]** **SI[2]**	**Satellite**
22a	22 Aug 2000	1455Z to 1642Z 7:55 to 9:42am PDT	120m	575m 10°C	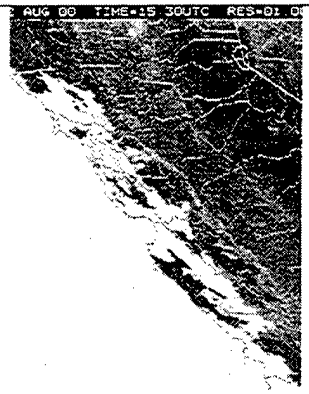
22b	22 Aug 2000	2122Z to 2313Z 2:22-4:13pm PDT	113m	675m 9°C	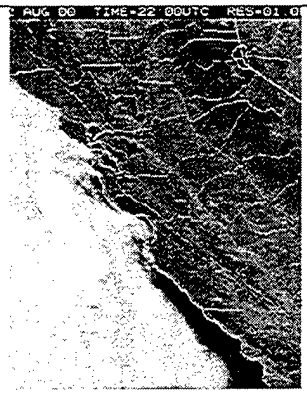

Table 3-2: Summary of the Five MUSE Flights of Interest

NOTES

1. BI=Inversion Base Height [meters]
2. SI=Strength of the Inversion (Top Temperature-Base Temperature) [°C]

#	Date	Time hhmmss [UTC]	La[N]	Lo[W]	Ht[m]	Pr[mb]	U[m/s]	V[m/s]	Wind [m/s]	Wdir [deg]	T [C]	Tv [C]
2	17	223642	36.67	-122.02	124	998.4	NaN	NaN	NaN	NaN	15.18	17.08
7	17	224038	36.67	-122.18	113	999.7	NaN	NaN	NaN	NaN	15.62	17.57
11	17	224333	36.67	-122.3	94.6	1001.9	NaN	NaN	NaN	NaN	15.03	16.91
21	17	225114	36.75	-122.31	98.3	1001.5	NaN	NaN	NaN	NaN	15.08	16.96
25	17	225319	36.75	-122.19	101.9	1001	NaN	NaN	NaN	NaN	16.1	18.13
30	17	225602	36.75	-122.03	94.6	1001.9	NaN	NaN	NaN	NaN	16.1	18.12
42	17	230409	36.78	-122.02	105.6	1000.6	NaN	NaN	NaN	NaN	16.54	18.63
47	17	230805	36.8	-122.17	109.3	1000.2	NaN	NaN	NaN	NaN	19.08	21.55
51	17	231112	36.82	-122.29	113	999.7	NaN	NaN	NaN	NaN	14.74	16.58
60	17	231703	36.86	-122.29	79.9	1003.7	NaN	NaN	NaN	NaN	14.64	16.46
64	17	231908	36.86	-122.17	98.3	1001.5	NaN	NaN	NaN	NaN	19.96	22.58
69	17	232149	36.86	-122.02	120.3	998.9	NaN	NaN	NaN	NaN	20.79	23.56
80	17	232905	36.9	-122.02	127.6	998	NaN	NaN	NaN	NaN	20.25	22.93
85	17	233225	36.9	-122.17	116.6	999.3	NaN	NaN	NaN	NaN	22.11	25.12
89	17	233531	36.9	-122.29	90.9	1002.4	NaN	NaN	NaN	NaN	15.08	16.96
99	17	234212	36.94	-122.28	120.3	998.9	NaN	NaN	NaN	NaN	16.4	18.46
112	17	235119	36.98	-122.3	98.3	1001.5	NaN	NaN	NaN	NaN	16.98	19.13
122	17	235842	37.04	-122.3	101.9	1001	NaN	NaN	NaN	NaN	17.96	20.25
127	18	118	36.97	-122.17	105.6	1000.6	NaN	NaN	NaN	NaN	22.65	25.76
132	18	408	36.94	-122.02	105.6	1000.6	NaN	NaN	NaN	NaN	20.01	22.64
140	18	942	36.84	-121.89	98.3	1001.5	NaN	NaN	NaN	NaN	18.69	21.09

Table 3-3: Text Table for Flight 17

#	Date	Time hhmmss [UTC]	La[N]	Lo[W]	Ht[m]	Pr[mb]	U[m/s]	V[m/s]	Wind [m/s]	Wdir [deg]	T [C]	Tv [C]
1	20	164902	36.68	-122.03	76.3	1004.1	0.14	-0.31	0.35	335.3	13.37	15.04
6	20	165233	36.67	-122.19	76.3	1004.1	5.38	-6.6	8.52	320.7	13.86	15.59
11	20	165553	36.67	-122.35	61.6	1005.9	3.92	-10 5	10.79	338.5	14.35	16.13
23	20	170409	36.76	-122.33	87.3	1002.8	5.18	-9.69	10.99	331.7	14.44	16.24
27	20	170630	36.75	-122.2	76.3	1004.1	4.82	-6.1	7.77	321.6	14.44	16.24
33	20	171000	36.74	-122.02	65.2	1005.4	1.26	-2.52	2.81	333.3	13.17	14.82
47	20	171850	36.81	-122.02	65.2	1005.4	1.09	-0.67	1.28	301.6	13.42	15.09
53	20	172220	36.82	-122.19	109.3	1000.2	2.99	-1.81	3.49	301.1	14.1	15.86
58	20	172516	36.82	-122.33	65.2	1005.4	4.29	-4.78	6.43	317.9	14.2	15.97
70	20	173310	36.86	-122.32	79.9	1003.7	5.45	-7.7	9.44	324.6	13.96	15.7
74	20	173525	36.86	-122.2	61.6	1005.9	4.02	-5.17	6.55	322	13.91	15.64
80	20	173855	36.86	-122.02	68.9	1005	1.02	-0.42	1.11	292.4	13.08	14.72
92	20	174629	36.9	-122.01	68.9	1005	-0.18	0.69	0.71	165	12.98	14.61
98	20	175000	36.9	-122.18	68.9	1005	4.03	-3.78	5.52	313	13.22	14.87
103	20	175310	36.9	-122.32	68.9	1005	7.22	-4.25	8.37	300.4	13.86	15.59
114	20	180031	36.95	-122.32	72.6	1004.5	5.33	-5.42	7.6	315.4	13.81	15.53
127	20	180951	37	-122.32	87.3	1002.8	5.72	-3.88	6.92	304.1	13.61	15.31
144	20	182042	36.99	-122.2	54.2	1006.7	5.36	-5.06	7.37	313.2	13.76	15.47
150	20	182423	36.94	-122.03	72.6	1004.5	0.09	1.47	1.47	183.8	13.42	15.1
158	20	182928	36.87	-121.84	131.3	997.5	7.19	2.67	7.67	249.7	12.88	14.51

Table 3-4: Text Table for Flight 20a

#	Date	Time hhmmss [UTC]	La[N]	Lo[W]	Ht[m]	Pr[mb]	U[m/s]	V[m/s]	Wind [m/s]	Wdir [deg]	T [C]	Tv [C]
10	20	215102	36.68	-121.99	94.6	1001.9	7.65	-6.63	10.12	310.8	13.96	15.7
16	20	215513	36.67	-122.17	83.6	1003.2	9.2	-7.26	11.72	308.2	14.59	16.41
22	20	215913	36.67	-122.34	79.9	1003.7	9.26	-9.8	13.48	316.5	15.52	17.46
34	20	220721	36.76	-122.36	54.2	1006.7	9.67	-9.04	13.23	313	15.08	16.95
41	20	221052	36.75	-122.16	57.9	1006.3	10.21	-12.59	16.21	320.8	14.69	16.52
47	20	221352	36.75	-121.99	57.9	1006.3	9.2	-6.25	11.12	304.1	13.76	15.47
60	20	222150	36.82	-121.99	113	999.7	11.05	-6	12.57	298.4	14.25	16.03
66	20	222600	36.81	-122.16	72.6	1004.5	11.71	-7.26	13.77	301.7	14.25	16.02
73	20	223040	36.81	-122.36	76.3	1004.1	9.87	-10.02	14.07	315.3	15.13	17.02
82	20	223632	36.86	-122.35	94.6	1001.9	10.7	-10.86	15.24	315.3	14.93	16.79
89	20	224003	36.86	-122.15	79.9	1003.7	13.08	-9.71	16.29	306.5	14.1	15.86
94	20	224233	36.86	-122	83.6	1003.2	10.44	-7.17	12.67	304.4	16.35	18.4
105	20	224909	36.91	-121.99	94.6	1001.9	2.93	-3.46	4.53	319.6	17.91	20.19
111	20	225304	36.9	-122.17	76.3	1004.1	12.34	-10.38	16.13	310	14.59	16.41
118	20	225750	36.9	-122.36	87.3	1002.8	9.75	-9.76	13.79	314.9	14.88	16.74
126	20	230313	36.95	-122.35	79.9	1003.7	10.89	-11.99	16.2	317.6	14.93	16.79
144	20	231447	37.01	-122.35	76.3	1004.1	7.71	-11.71	14.02	326.5	14.25	16.03
153	20	232105	37.09	-122.36	54.2	1006.7	8.51	-12.56	15.17	325.7	14.59	16.4
161	20	232516	36.97	-122.16	101.9	1001	11.33	-10.31	15.32	312.2	15.03	16.91
167	20	232822	36.94	-121.99	101.9	1001	3.09	-0.82	3.2	284.8	18.84	21.27
174	20	233254	36.86	-121.84	68.9	1005	0.76	-1.56	1.74	333.9	15.52	17.45

Table 3-5: Text Table for Flight 20b

#	Date	Time hhmmss [UTC]	La[N]	Lo[W]	Ht[m]	Pr [mb]	U[m/s]	V[m/s]	Wind [m/s]	WDir [deg]	T [C]	Tv [C]
7	22	145911	36.68	-121.97	124	998.4	0.45	3.12	3.15	188.5	14.1	15.87
14	22	150316	36.67	-122.17	142.3	996.2	-1.03	2.55	2.74	157.9	15.18	17.09
21	22	150722	36.67	-122.38	120.3	998.9	-1.02	-0.14	1.03	82	15.18	17.08
31	22	151346	36.76	-122.37	153.4	994.9	-2.6	1.84	3.19	125.1	15.32	17.25
38	22	151756	36.75	-122.17	138.7	996.7	-1.22	2.18	2.5	150.6	14.88	16.75
44	22	152132	36.74	-121.99	113	999.7	-0.55	1.24	1.36	155.9	14.64	16.47
56	22	152859	36.81	-121.99	116.6	999.3	-2.51	3.52	4.32	144.3	13.61	15.32
62	22	153229	36.81	-122.17	157	994.5	-2.98	3.13	4.32	136.3	13.61	15.33
69	22	153634	36.82	-122.38	120.3	998.9	-2.55	1.43	2.92	119.1	15.03	16.91
78	22	154217	36.86	-122.36	101.9	1001	-4.43	2.05	4.88	114.8	14.83	16.68
85	22	154622	36.86	-122.17	127.7	998	-4.96	3.84	6.27	127.6	13.47	15.16
92	22	155027	36.86	-121.98	120.3	998.9	-1.06	-0.85	1.36	51.1	13.37	15.05
100	22	155535	36.9	-121.98	127.7	998	-1.16	-0.14	1.17	83	13.71	15.43
107	22	155940	36.9	-122.19	116.6	999.3	-4.56	1.56	4.82	108.8	13.76	15.49
113	22	160302	36.9	-122.37	116.6	999.3	-5.58	5.04	7.52	132	14.54	16.36
122	22	160847	36.95	-122.39	116.6	999.3	-5.83	-2.82	6.47	64.3	14.3	16.09
141	22	162044	37.03	-122.39	135	997.1	-4.67	2.56	5.33	118.7	15.32	17.24
149	22	162550	37.11	-122.38	127.7	998	-6.14	2.5	6.63	112.1	14.88	16.75
157	22	163117	36.97	-122.19	120.3	998.9	-4.69	1.1	4.81	103.2	14.88	16.74
164	22	163538	36.93	-122	116.6	999.3	-2.17	-1.22	2.49	60.8	13.96	15.71
172	22	164045	36.84	-121.83	90.9	1002.4	0.59	1.61	1.72	200.4	14.44	16.24

Table 3-6: Text Table for Flight 22a

#	Date	Time hhmmss [UTC]	La[N]	Lo[W]	Ht[m]	Pr[mb]	U[m/s]	V[m/s]	Wind [m/s]	WDir [deg]	T[C]	Tv [C]
11	22	212852	36.91	-121.89	109.3	1000.2	4.24	2.14	4.75	243.3	16.25	18.29
16	22	213149	36.94	-122.02	124	998.4	2.21	1.54	2.69	235.1	16.25	18.3
21	22	213437	36.96	-122.15	90.9	1002.4	0.77	1.65	1.82	204.9	15.86	17.84
28	22	213835	37.07	-122.31	116.6	999.3	-0.77	6.9	6.94	173.6	15.71	17.68
40	22	214610	37	-122.34	127.6	998	-0.9	5.09	5.17	170	15.18	17.08
55	22	215517	36.94	-122.32	120.3	998.9	-1	6	6.09	170.5	14.59	16.42
66	22	220133	36.9	-122.32	83.6	1003.2	1.27	7.46	7.57	189.7	14.59	16.41
71	22	220415	36.9	-122.18	109.3	1000.2	1.32	4.65	4.83	195.8	15.03	16.91
91	22	221532	36.86	-122.02	127.6	998	2.37	3.2	3.98	216.5	15.22	17.13
96	22	221822	36.86	-122.16	131.3	997.5	2.96	6.25	6.92	205.3	14.93	16.8
102	22	222143	36.86	-122.32	124	998.4	1.97	6.07	6.38	198	15.52	17.46
121	22	223310	36.82	-122.33	127.6	998	2.66	5.16	5.8	207.3	15.22	17.13
127	22	223620	36.82	-122.16	160.7	994.1	3.39	5.3	6.29	212.6	15.96	17.97
132	22	223858	36.81	-122.02	138.7	996.7	3.79	5.26	6.49	215.8	15.42	17.36
137	22	224134	36.81	-121.89	109.3	1000.2	3.99	-0.4	4.01	275.8	15.62	17.57
146	22	224720	36.72	-121.89	79.9	1003.7	6.95	5.26	8.72	232.8	16.3	18.34
151	22	225020	36.74	-122.02	120.3	998.9	5.33	6.54	8.43	219.2	16.15	18.18
157	22	225346	36.75	-122.19	124	998.4	4.06	6.67	7.81	211.3	15.66	17.63
162	22	225636	36.75	-122.32	87.3	1002.8	2.72	4.85	5.55	209.3	15.13	17.01
175	22	230417	36.67	-122.33	109.3	1000.2	1.7	3.18	3.6	208.2	15.03	16.91
181	22	230725	36.67	-122.17	138.7	996.7	3.69	5.42	6.55	214.2	15.71	17.69
186	22	230958	36.67	-122.03	109.3	1000.2	5.44	5.46	7.7	224.9	16.15	18.18
189	22	231129	36.68	-121.95	124	998.4	6.24	6.19	8.79	225.2	16.05	18.07

Table 3-7: Text Table for Flight 22b

Exp	Base Temp Mean 12.72°C SDev 1.49°C	Base Ht Mean 348.04m SDev 149.90m	Top Temp Mean 22.40°C SDev 3.30°C	Top Ht Mean 780.00m SDev 192.71m
AC1	1.64	134.82	3.83	269.16
CON	1.74	133.84	3.86	272.08
CB1*	1.44	95.55	2.89	268.23
CB2	---	---	---	---
CB3	1.61	144.18	3.70	266.99
LW1	---	---	---	---
LW2	---	---	---	---
SW1	---	---	---	---
SW2*	1.31	120.77	3.11	282.94
TK1*	1.40	95.55	2.79	271.02
TK2	1.71	138.66	3.72	269.85

Notes:

1. The mean and standard deviation for the profiler were for all times from 17/00Z to 23/00Z while the RMS errors were only based on the few sample times available (12 for control, 8 for the others so far).

2. Also profiler statistics were taken during a period of changing values, so the mean and standard deviation may not be as meaningful as they would of the conditions were unchanging.

3. A "*" next to an experiment name means the statistics are only for two days of data as these the text file was not made for the 22nd.

Table 4-1: Ft. Ord Profiler Inversion Statistics, RMS Error Comparison

17 Aug (21 Observation Points)
Time of Flight 2236 Z to 0011Z = 3:36pm to 4:11pm Pacific Daylight Time
Mean height AGL 109m, with Standard Deviation 16m (Min 62m, Max 175m)

	Entire Flight		Sample Points	
Variable	Mean	Std	Mean	Std
U-Speed	NA	NA	NA	NA
V-Speed	NA	NA	NA	NA
Wind Speed	NA	NA	NA	NA
Wind Direction	NA	NA	NA	NA
Temperature	17.4	2.5	17.57	2.56
Virtual Temp	19.6	2.9	19.83	2.97

Table 4-2a(1): Aircraft Data Comparison Table, Flight 17

	Flight 17 Statistics					
Exp	U Spd	V Spd	Wind Spd	Wind Dir	Temp	V. Temp
AC1						
Rxy	NA	NA	NA	NA	.11211	.14732
RMS	NA	NA	NA	NA	3.07	3.58
CB1						
Rxy	NA	NA	NA	NA	.079054	.11302
RMS	NA	NA	NA	NA	3.15	3.66
CB2						
Rxy	NA	NA	NA	NA	--	--
RMS	NA	NA	NA	NA	--	--
CB3						
Rxy	NA	NA	NA	NA	.092872	.11962
RMS	NA	NA	NA	NA	3.16	3.70
CON						
Rxy	NA	NA	NA	NA	.079282	.11370
	(w) (b)	(w) (b)	(w) (b)	(w) (b)	(w) (b)	(w) (b)
55%	.NA .NA	.NA .NA	.NA .NA	.NA .NA	.04 .12	.07 .16
75%	.NA .NA	.NA .NA	.NA .NA	.NA .NA	***-.15*** .30	***-.11*** .33
95%	.NA .NA	.NA .NA	.NA .NA	.NA .NA	***-.46*** .57	***-.43*** .60
	.....	.....	.....	.....	.....	.....
RMS	NA	NA	NA	NA	3.14	3.65
LW1						
Rxy	NA	NA	NA	NA	.067558	.10008
RMS	NA	NA	NA	NA	3.17	3.68
LW2						
Rxy	NA	NA	NA	NA	.075168	.10912
RMS	NA	NA	NA	NA	3.15	3.66
SW1						
Rxy	NA	NA	NA	NA	.057683	.089184
RMS	NA	NA	NA	NA	3.21	3.73
SW2						
Rxy	NA	NA	NA	NA	.11381	.15067
RMS	NA	NA	NA	NA	3.05	3.55
TK1						
Rxy	NA	NA	NA	NA	.05905	.092228
RMS	NA	NA	NA	NA	3.20	3.71
TK2						
Rxy	NA	NA	NA	NA	.0486	.074519
RMS	NA	NA	NA	NA	3.28	3.81

Table 4-2a(2): Aircraft Data Comparison Table, Flight 17

20a Aug (20 Observation Points)
Time of Flight 1649 Z to 1832Z = 9:49am to 11:32am Pacific Daylight Time
Mean height AGL 76m, with Standard Deviation 15m (Min 21m, Max 142m)

	Entire Flight		**Sample Points**	
Variable	Mean	Std	Mean	Std
U-Speed	3.4	2.4	3.72	2.35
V-Speed	-4.0	3.8	-3.67	3.54
Wind Speed	6.2	3.8	5.76	3.45
Wind Direction	284	76	299	47
Temperature	13.7	0.6	13.69	0.48
Virtual Temp	15.4	0.7	15.40	0.54

Table 4-2b(1): Aircraft Data Comparison Table, Flight 20a

	Flight 20a Statistics					
Exp	U Spd	V Spd	Wind Spd	Wind Dir	Temp	V. Temp
AC1			high	13 19 20	cold	cold
Rxy	.28068	.80219	.48807	.47611	.02372	***-.0532***
RMS	2.95	3.14	3.99	43	1.23	1.43
CB1						
Rxy	.24841	.79589	.45651	.46004	***-.0562***	***-.1502***
RMS	3.12	3.22	4.17	43	1.21	1.41
CB2						
Rxy	--	--	--	--	--	--
RMS	--	--	--	--	--	--
CB3						
Rxy	.29268	.81076	.50889	.51097	***-.11534***	***-.19799***
RMS	2.90	2.97	3.82	41	1.26	1.45
CON						
Rxy	.29399	.80223	.49584	.49708	***-.5040***	***-.5243***
	(w) (b)	(w) (b)	(w) (b)	(w) (b)	(w) (b)	(w) (b)
55%	.25 .34	.78 .82	.46 .53	.46 .53	***-.54 -.47***	***-.56 -.49***
75%	.00 .50	.70 .88	.29 .66	.29 .66	***-.66 -.30***	***-.68 -.33***
95%	***-.29*** .72	.47 .94	***-.05*** .82	***-.05*** .82	***-.82*** .04	***-.83*** .02
	.....	.....	.....	.....	.....	.....
RMS	2.71	3.09	3.78	43	1.62	1.80
LW1						
Rxy	.31544	.79751	.50141	.48705	***-.3050***	***-.3274***
RMS	2.73	3.02	3.75	43	1.58	1.76
LW2						
Rxy	.31636	.79849	.50252	.48813	***-.2705***	***-.2894***
RMS	2.71	3.00	3.73	43	1.60	1.78
SW1						
Rxy	.32103	.79825	.50490	.48765	***-.2636***	***-.2913***
RMS	2.71	3.00	3.72	43	1.64	1.83
SW2						
Rxy	.30073	.79820	.49466	.48487	***-.3222***	***-.3490***
RMS	2.75	3.01	3.76	43	1.50	1.67
TK1						
Rxy	.28725	.79536	.47811	.45645	***-.3790***	***-.3982***
RMS	2.88	3.02	3.86	44	1.55	1.72
TK2						
Rxy	.32036	.80648	.51954	.52184	***-.33134***	***-.35273***
RMS	2.72	2.85	3.60	41	1.52	1.69

Table 4-2b(2): Aircraft Data Comparison Table, Flight 20a

20b Aug (21 Observation Points)
Time of Flight 2143 Z to 2334 Z = 2:43pm to 4:34pm Pacific Daylight Time
Mean height AGL 84m, with Standard Deviation 24m (Min 25m, Max 267m)

	Entire Flight		**Sample Points**	
Variable	Mean	Std	Mean	Std
U-Speed	9.1	3.4	9.02	3.16
V-Speed	-7.8	4.8	-8.34	3.37
Wind Speed	12.6	4.3	12.41	4.25
Wind Direction	295	54	312	11
Temperature	15.0	1.1	15.10	1.25
Virtual Temp	16.8	1.2	16.99	1.42

Table 4-2c(1): Aircraft Data Comparison Table, Flight 20b

	Flight 20b Statistics					
Exp	U Spd	V Spd	Wind Spd	Wind Dir	Temp	V. Temp
AC1						
Rxy	.81006	.84614	.87164	.49875	.70340	.74420
RMS	3.06	2.67	3.80	13	1.70	1.99
CB1						
Rxy	.62482	.85044	.88948	.44891	.66337	.71462
RMS	2.95	2.76	3.72	12	1.83	2.13
CB2						
Rxy	--	--	--	--	--	--
RMS	--	--	--	--	--	--
CB3						
Rxy	.68367	.84688	.89387	.48666	.61467	.67057
RMS	3.13	3.11	4.11	13	1.95	2.24
CON						
Rxy	.76480	.85291	.89177	.49183	.61387	.66438
	(w) (b)	(w) (b)	(w) (b)	(w) (b)	(w) (b)	(w) (b)
55%	.74 .79	.84 .87	.88 .91	.45 .53	.58 .64	.64 .69
75%	.65 .85	.77 .91	.83 .94	.29 .65	.45 .74	.51 .78
95%	.40 .92	.60 .96	.69 .97	***-.04*** .81	.14 .86	.22 .88
	.....	.....	.....	.....	.....	.....
RMS	3.15	2.88	3.98	13	2.13	2.40
LW1						
Rxy	.76248	.84979	.89170	.49347	.61001	.66022
RMS	3.17	2.92	4.02	13	2.14	2.42
LW2						
Rxy	.77251	.85627	.89382	.49976	.60832	.65921
RMS	3.13	2.85	3.95	14	2.10	2.37
SW1						
Rxy	.75249	.84727	.88352	.49157	.59224	.63904
RMS	3.24	2.92	4.06	14	2.35	2.64
SW2						
Rxy	.81243	.86203	.89202	.51047	.66943	.71914
RMS	2.97	2.74	3.81	12	1.63	1.89
TK1						
Rxy	.49680	.85337	.85816	.44391	.59674	.65257
RMS	3.16	3.05	4.07	13	2.13	2.39
TK2						
Rxy	.5409	.84454	.86806	.47606	.54847	.60375
RMS	3.33	3.34	4.40	14	2.23	2.50

Table 4-2c(2): Aircraft Data Comparison Table, Flight 20b

22a Aug (21 Observation Points)
Time of Flight 1455 Z to 1642Z = 7:55am to 9:42am Pacific Daylight Time
Mean height AGL 120m, with Standard Deviation 15m (Min 73m, Max 197m)

	Entire Flight		**Sample Points**	
Variable	Mean	Std	Mean	Std
U-Speed	-2.7	2.3	-2.79	2.10
V-Speed	1.9	2.5	1.62	1.85
Wind Speed	4.4	2.3	3.76	1.98
Wind Direction	130	50	121	39
Temperature	14.4	0.6	14.43	0.66
Virtual Temp	16.1	0.6	16.24	0.74

Table 4-2d(1): Aircraft Data Comparison Table, Flight 22a

	Flight 22a Statistics					
Exp	U Spd	V Spd	Wind Spd	Wind Dir	Temp	V. Temp
AC1						
Rxy	.37652	***-.22107***	.0094792	***-.14872***	.22754	.22684
RMS	6.78	4.39	2.22	184	4.24	4.70
CB1						
Rxy	--	--	--	--	--	--
RMS	--	--	--	--	--	--
CB2						
Rxy	--	--	--	--	--	--
RMS	--	--	--	--	--	--
CB3						
Rxy	.36358	***-.22447***	***-.030323***	***-.15376***	.27058	.26908
RMS	6.7	4.07	2.15	181	4.62	5.11
CON						
Rxy	.29463	***-.2199***	.19682	***-.1360***	.21188	.21266
	(w) (b)	(w) (b)	(w) (b)	(w) (b)	(w) (b)	(w) (b)
55%	.25 .34	***-.26*** ***-.17***	.15 .24	***-.18*** ***-.09***	.17 .26	.17 .26
75%	.07 .49	***-.43*** .01	***-.03*** .41	***-.36*** .10	***-.02*** .42	***-.02*** .42
95%	***-.27*** .71	***-.67*** .34	***-.36*** .65	***-.62*** .42	***-.35*** .66	***-.35*** .66
	.....	.....	.....	.....	.....	.....
RMS	6.8	4.4	2.1	183	4.5	5.0
LW1						
Rxy	--	--	--	--	--	--
RMS	--	--	--	--	--	--
LW2						
Rxy	--	--	--	--	--	--
RMS	--	--	--	--	--	--
SW1						
Rxy	--	--	--	--	--	--
RMS	--	--	--	--	--	--
SW2						
Rxy	--	--	--	--	--	--
RMS	--	--	--	--	--	--
TK1						
Rxy	--	--	--	--	--	--
RMS	--	--	--	--	--	--
TK2						
Rxy	.31545	***-.23566***	.015457	***-.14022***	.18831	.18926
RMS	6.71	4.02	2.08	178	4.76	5.27

Table 4-2d(2): Aircraft Data Comparison Table, Flight 22a

22b(filtered) Aug (23 Observation Points)
Time of Flight 2122 Z to 2313 Z = 2:22pm to 4:13pm Pacific Daylight Time
Mean height AGL 113m, with Standard Deviation 19m (Min 29m, Max 175m)

	Entire Flight		**Sample Points**	
Variable	Mean	Std	Mean	Std
U-Speed	2.3	2.2	2.75	2.12
V-Speed	4.3	2.1	4.61	2.10
Wind Speed	5.6	1.8	5.78	2.03
Wind Direction	212	32	213	24
Temperature	15.5	0.5	15.54	0.52
Virtual Temp	17.5	0.6	17.49	0.59

Table 4-2e(1): Aircraft Data Comparison Table, Flight 22b

	Flight 22b Statistics					
Exp	U Spd	V Spd	Wind Spd	Wind Dir	Temp	V. Temp
AC1						
Rxy	.32646	***-.20901***	***-.15227***	.01509	.025216	***-.12622***
RMS	2.32	5.42	2.76	65	2.31	2.69
CB1						
Rxy	--	--	--	--	--	--
RMS	--	--	--	--	--	--
CB2						
Rxy	--	--	--	--	--	--
RMS	--	--	--	--	--	--
CB3						
Rxy	.41918	***-.28202***	***-.10651***	.37317	***-.26778***	***-.30085***
RMS	2.05	4.45	3.05	50	2.50	2.94
CON						
Rxy	.29902	***-.29649***	***-.040767***	***-.057138***	***-.32947***	***-.37171***
	(w) (b)	(w) (b)	(w) (b)	(w) (b)	(w) (b)	(w) (b)
55%	.26 .34	***-.33 -.26***	***-.08 -.00***	***-.10 -.02***	***-.37 -.29***	***-.41 -.34***
75%	.09 .49	***-.48 -.08***	***-.26*** .18	***-.37*** .16	***-.51 -.12***	***-.55 -.17***
95%	***-.24*** .70	***-.70*** .25	***-.54*** .48	***-.55*** .46	***-.72*** .21	***-.74*** .17
	.....	.....	.....	.....	.....	.....
RMS	2.22	5.24	2.91	63	2.64	3.04
LW1						
Rxy	--	--	--	--	--	--
RMS	--	--	--	--	--	--
LW2						
Rxy	--	--	--	--	--	--
RMS	--	--	--	--	--	--
SW1						
Rxy	--	--	--	--	--	--
RMS	--	--	--	--	--	--
SW2						
Rxy	--	--	--	--	--	--
RMS	--	--	--	--	--	--
TK1						
Rxy	--	--	--	--	--	--
RMS	--	--	--	--	--	--
TK2						
Rxy	.4785	***-.33956***	***-.17165***	.21817	***-.28212***	***-.29203***
RMS	1.87	4.49	3.41	47	2.94	3.37

Table 4-2e(2): Aircraft Data Comparison Table, Flight 22b

Averages				
Flt	Wind Spd	Wind Dir	Temp	V. Temp
17	NA	NA	0.078	0.111
20a	0.495	0.487	-0.252	-0.293
20b	0.883	0.484	0.622	0.670
22a	0.048	-0.144	0.224	0.224
22b	-0.117	0.137	-0.213	-0.272
Total Avg=	0.262	0.193	0.092	0.088

Table 4-3: Aircraft Data Comparison Table, Correlation Average By Flight

Standard Deviations				
Flt	Wind Spd	Wind Dir	Temp	V. Temp
17	NA	NA	0.022	0.024
20a	0.018	0.020	0.159	0.133
20b	0.013	0.022	0.045	0.043
22a	0.101	0.008	0.035	0.034
22b	0.058	0.196	0.161	0.104
Avg SDev=	0.038	0.049	0.084	0.067

Table 4-4: Aircraft Data Comparison Table, Correlation Standard Deviation By Flight

Exp	Parameter Change	Variable	Expected Result	Observed Result
AC1	Decreased the autoconversion criterion by half	praut= 0.0005	Convert cloud water content to drizzle, improving fog burnoff process	As expected, less cloud water and more rain water observed in AC1 than in CON
CB1	AC1+TK1	AC1+TK1	AC1+TK1	AC1+TK1
CB2	AC1+SW2	AC1+SW2	AC1+SW2	AC1+SW2
CB3	AC1+TK2	AC1+TK2	AC1+TK2	AC1+TK2
CON		bdiff=5/3 pizero=0.99 praut=0.001 const mixing length above MABL of 5m	COAMPS tendency to over-forecast clouds and cloud water	As expected
LW1	Decreased LW emissivity	bdiff=4/3	Decreased LW cooling from cloud top, more stable layer, less cloud growth	As expected, very slightly less cloud water than CON
LW2	Increased LW emmisivity	bdiff=6/3	Increased LW cooling from cloud top, less stable layer, more cloud growth	As expected, more clouds than LW1 and CON
SW1	Increased the single scattering albedo	pizero=1	Increased SW scattering, less SW absorption, less warming, less cloud mass evaporated away	As expected, more cloud water than in CON
SW2	Decreased the single scatter albedo	pizero=0.97	Decreased SW scattering, more SW absorption, more cloud dissipation by evaporation	As expected, less cloud water observed than in SW1 or CON
TK1	Made boundary layer more shallow	Many	Effectively lowers the stratus cloud top height. If this is below the LCL it would decreases the likelihood of clouds.	As expected, less cloud water was observed than in CON
TK2	TK1+ scaled mixing length	TK1+scaled mixing length above the MABL from 23m to 5m at the model top	Increased mixing at top of the MABL, cloud top entrainment and fewer clouds	As expected, less cloud water observed than in TK1

Table 4-5: Summary of Experiments

THIS PAGE INTENTIONALLY LEFT BLANK

APPENDIX B. FIGURES

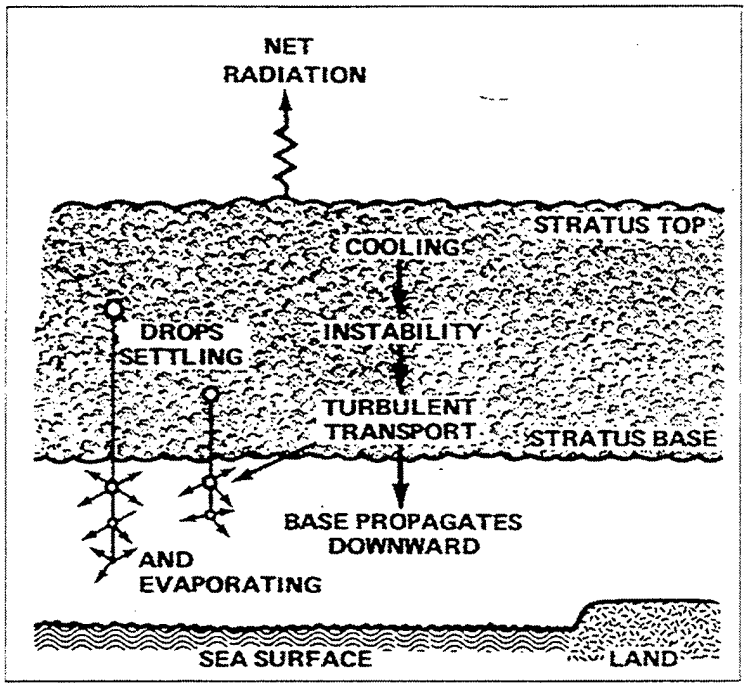

Figure 2-1: Fog Formation Through the Stratus-Lowering Process (Pelié *et al.*, 1979)

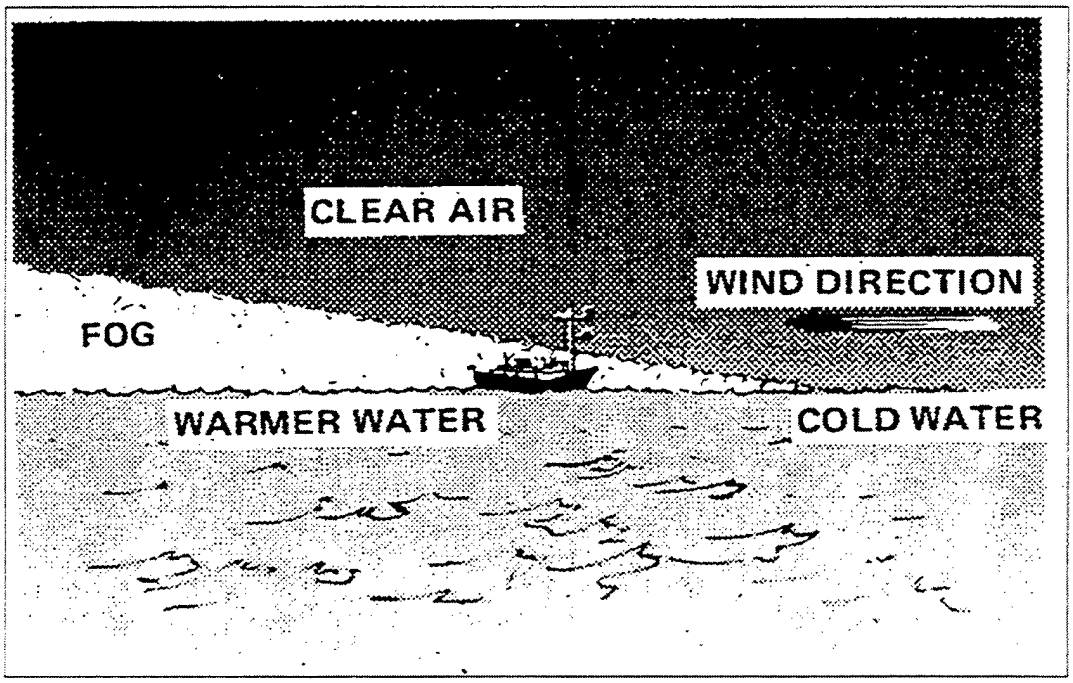

Figure 2-2: Fog Formation Over Warm Water (Pelié *et al.*, 1979)

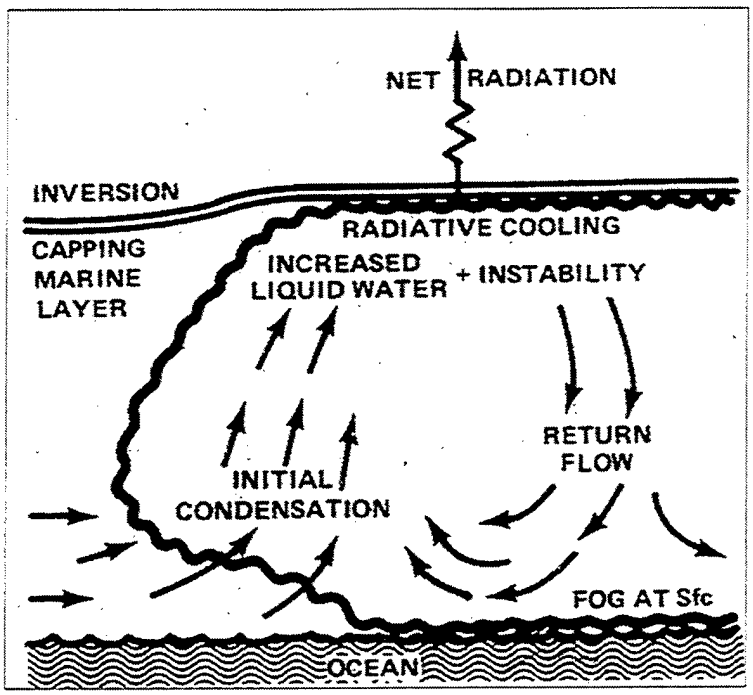

Figure 2-3: Fog Formation Through Convergence and Cooling (Pelié *et al.*, 1979)

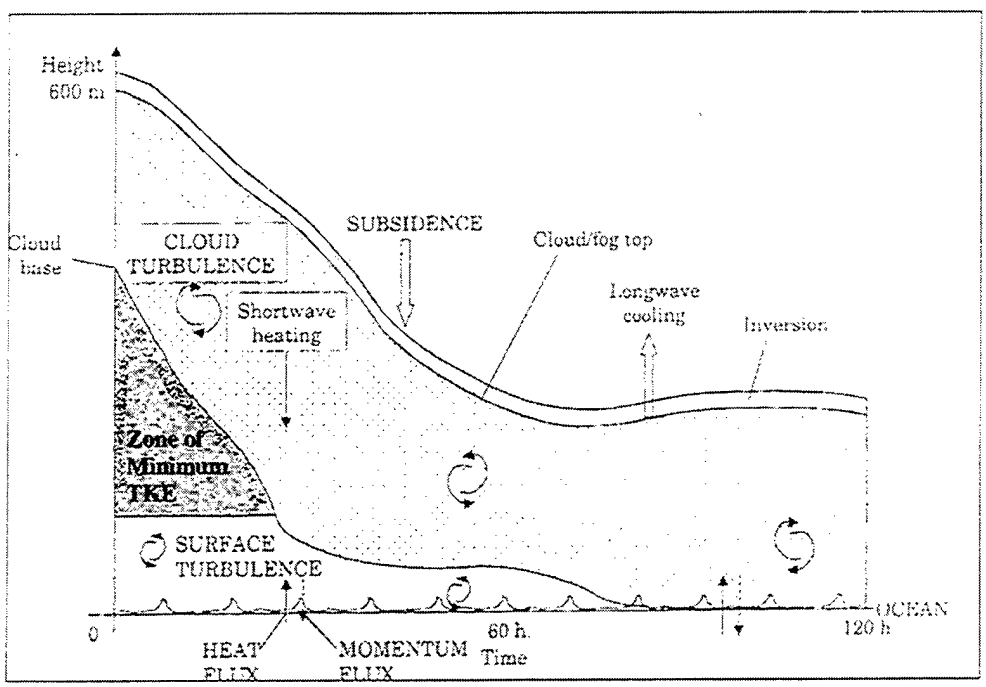

Figure 2-4: Physical Processes Relevant to Offshore Fog (Koracin *et al.*, 1999)

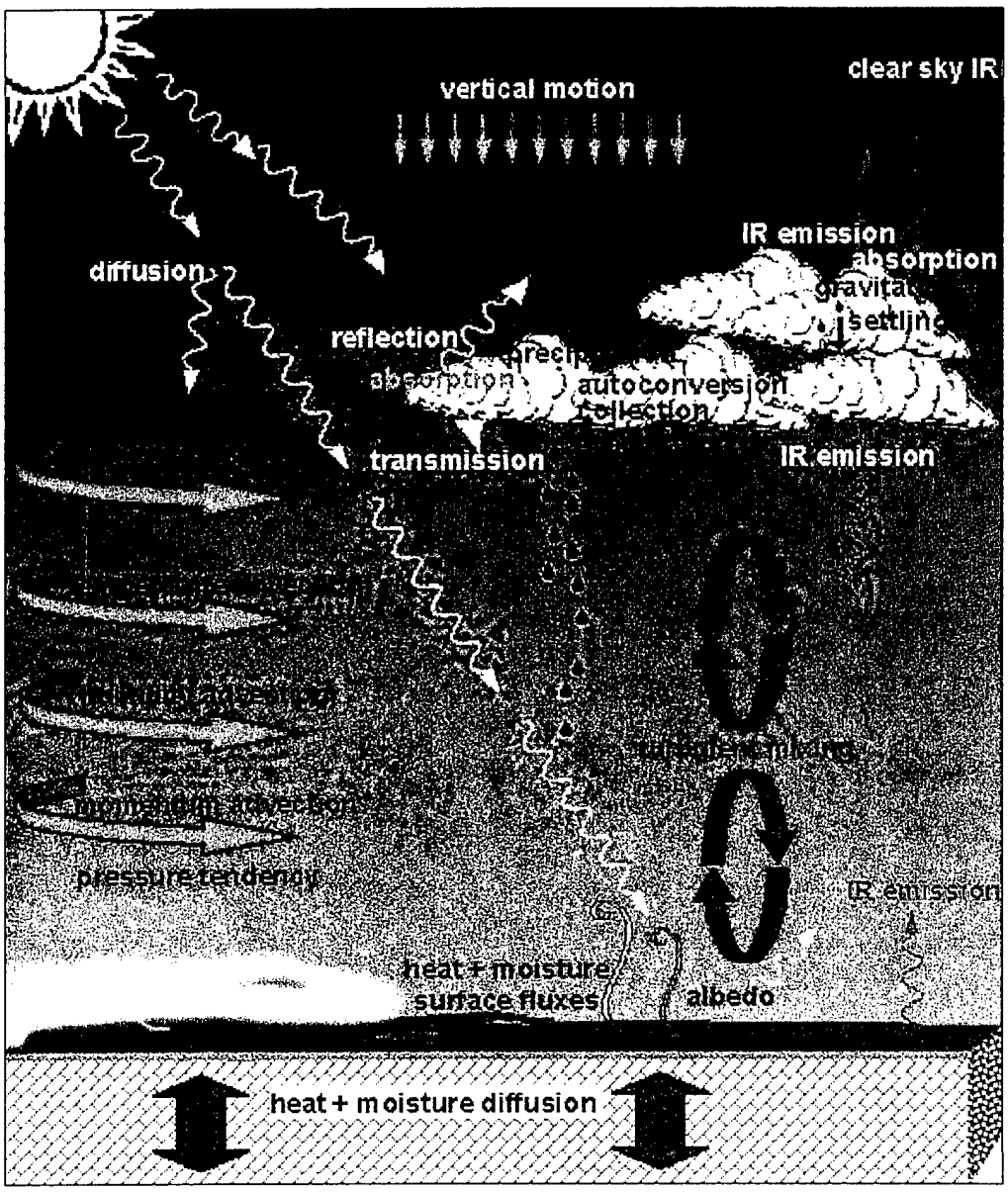

Figure 2-5: Physical Processes Involved in Fog Production (Zwack and Tardiff, 1999)

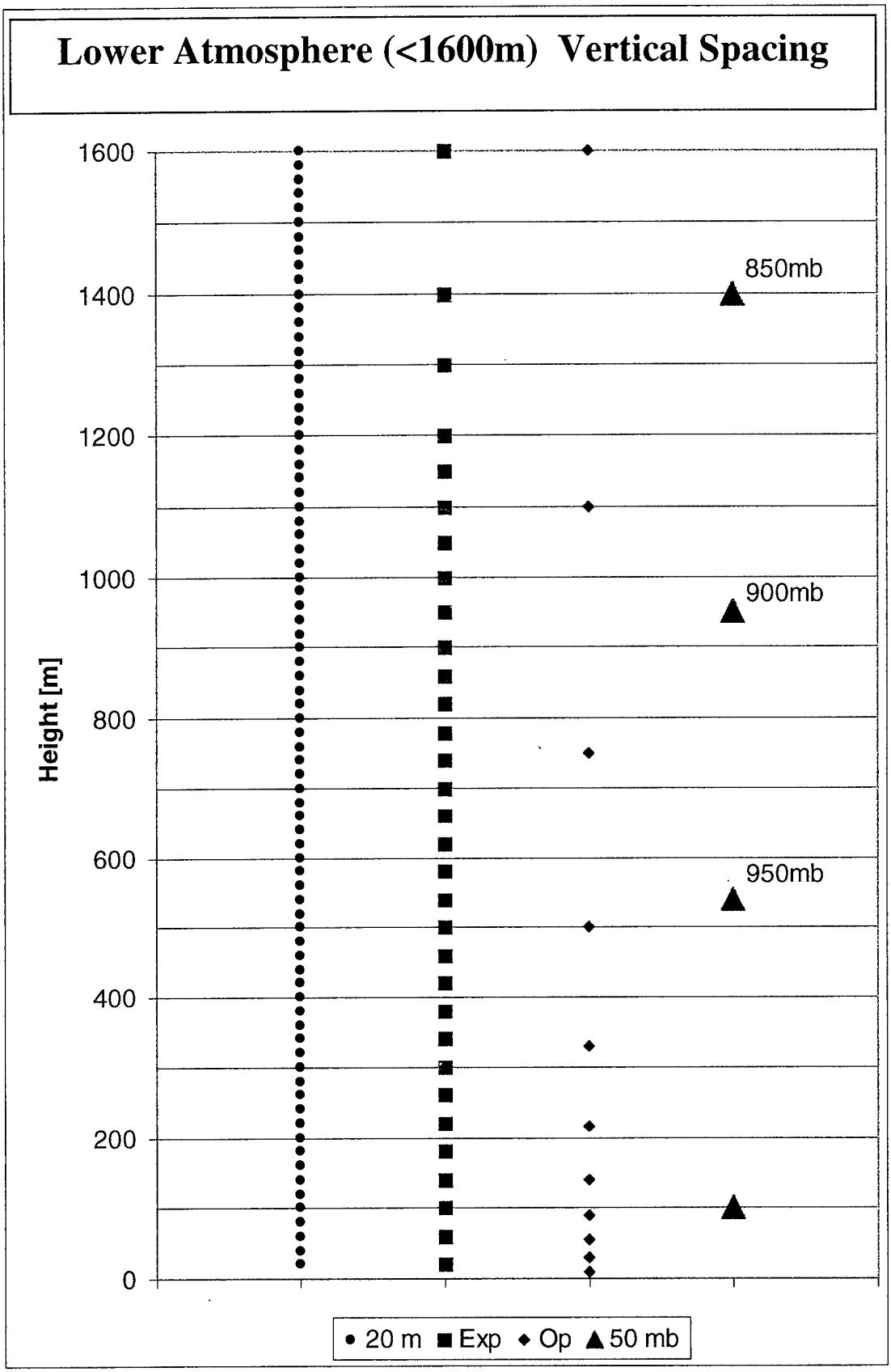

Figure 2-6: The Vertical Spacing of Experimental and Operational COAMPS

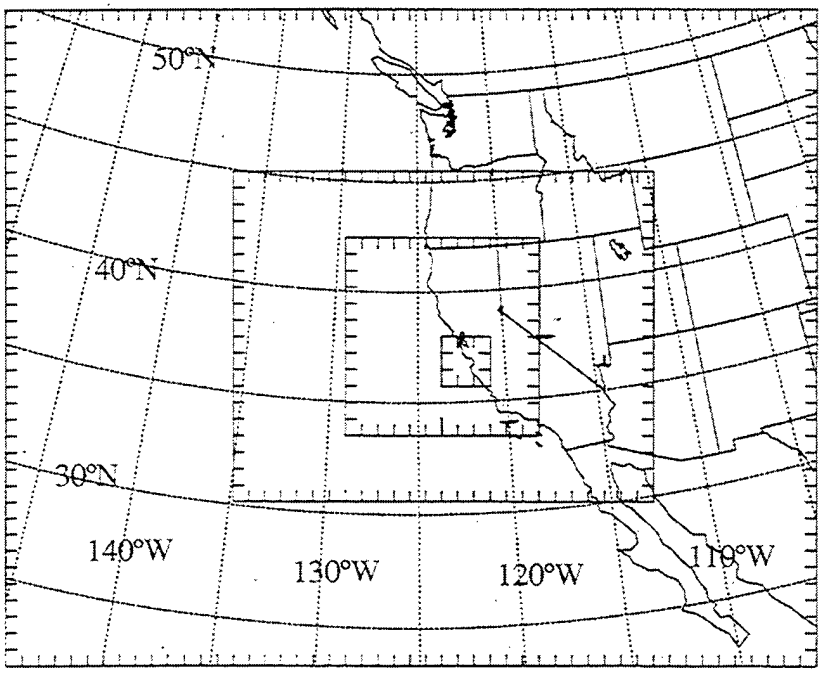

Figure 2-7: The COAMPS Model Grids

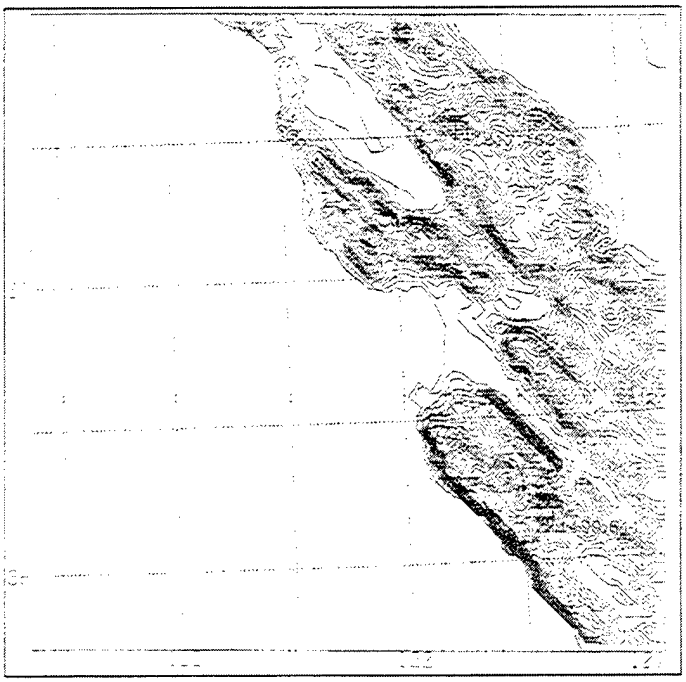

Figure 2-8: The Model Terrain

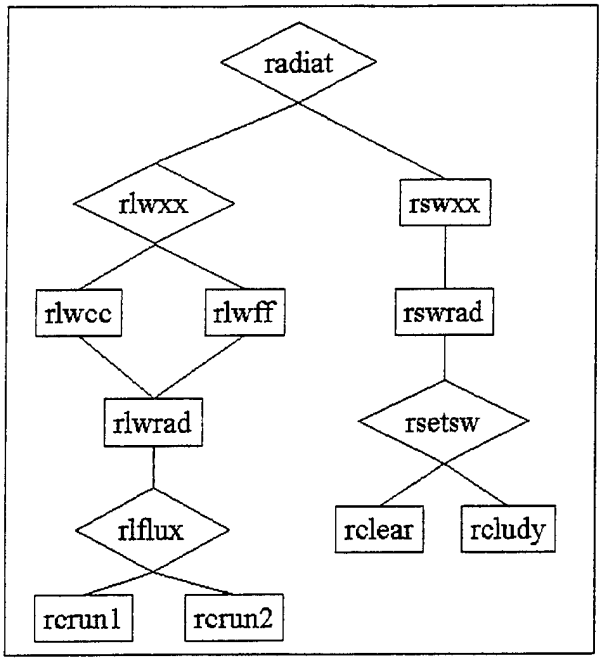

Figure 2-9: The COAMPS Radiation Routines

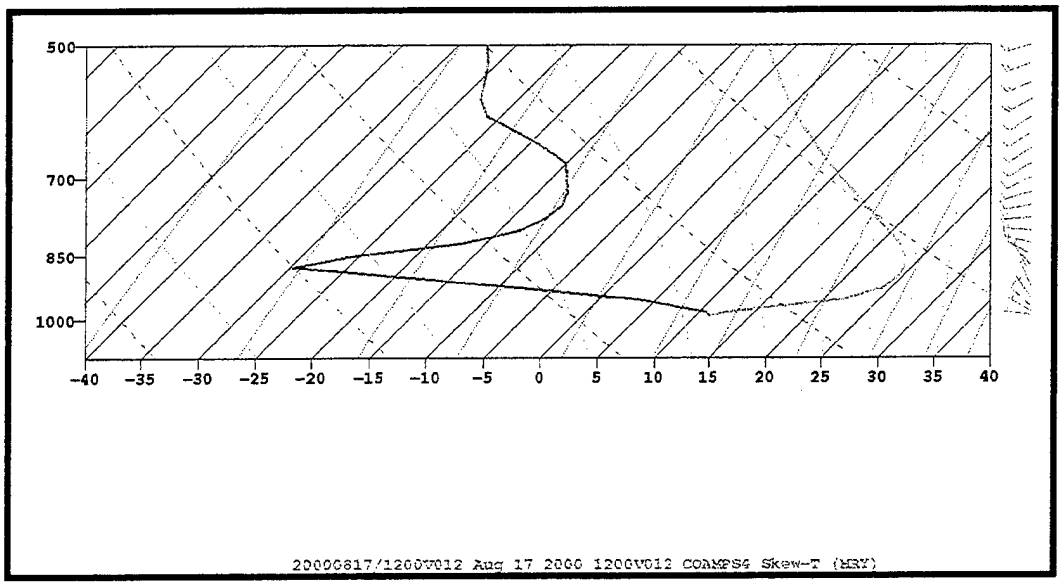

Figure 2-10: COAMPS Model Skew-T Diagram for CON Valid at 17/12Z

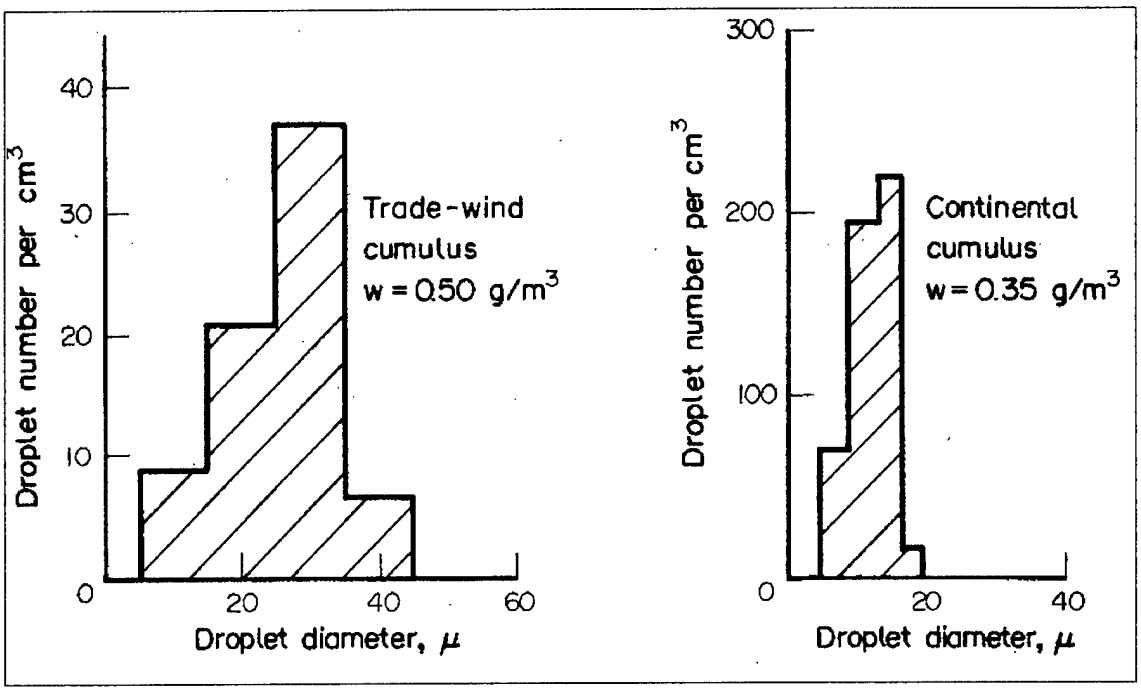

Figure 2-11: Cloud Droplet Spectra (Rogers and Yau, 1989)

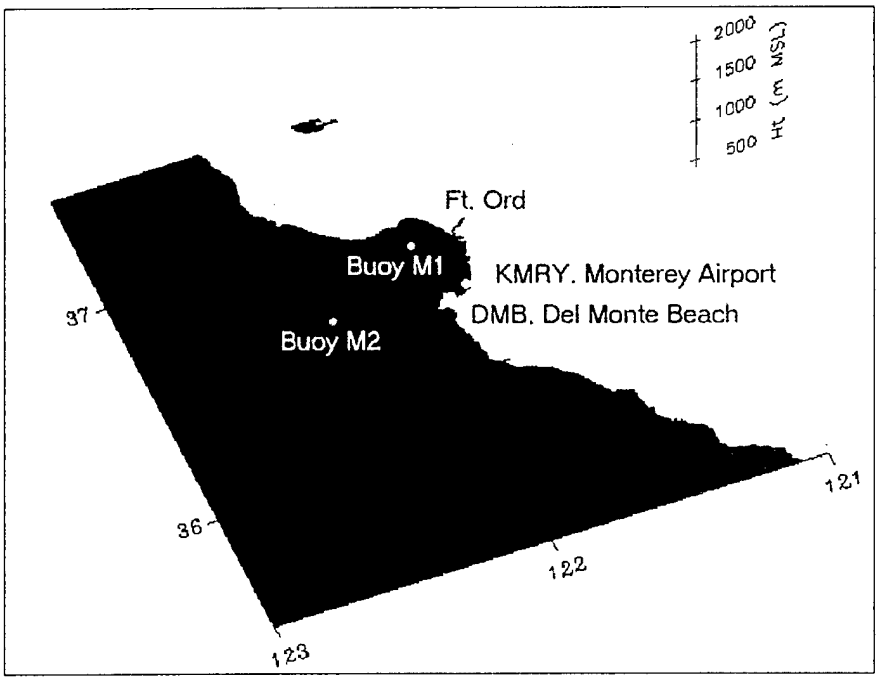

Figure 3-1: Location of Data Sites and Topography in the Monterey Bay Area

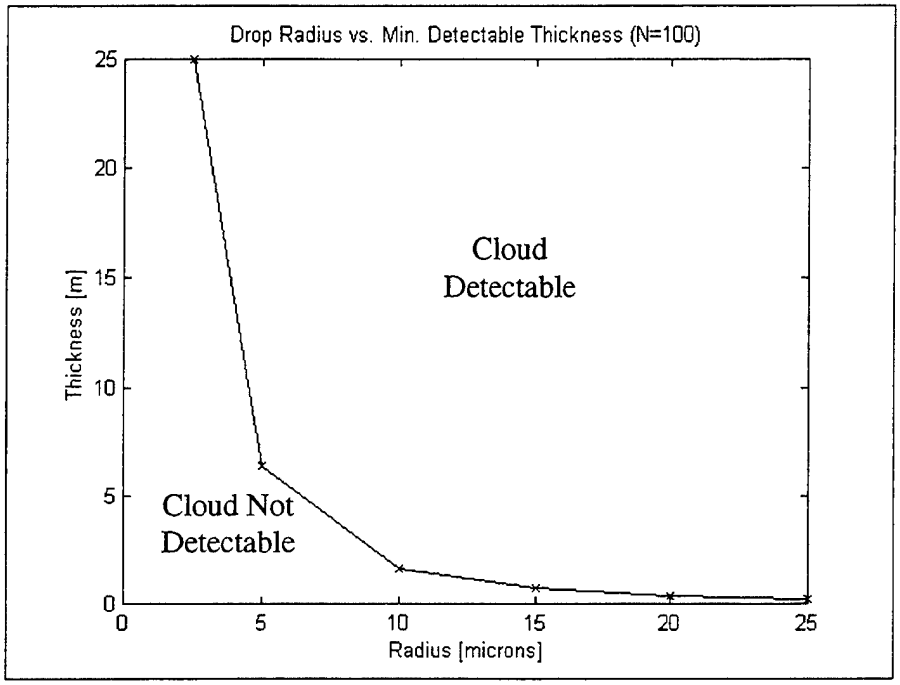

Figure 3-2: Detectable Cloud Thickness as a Function of Drop Radius

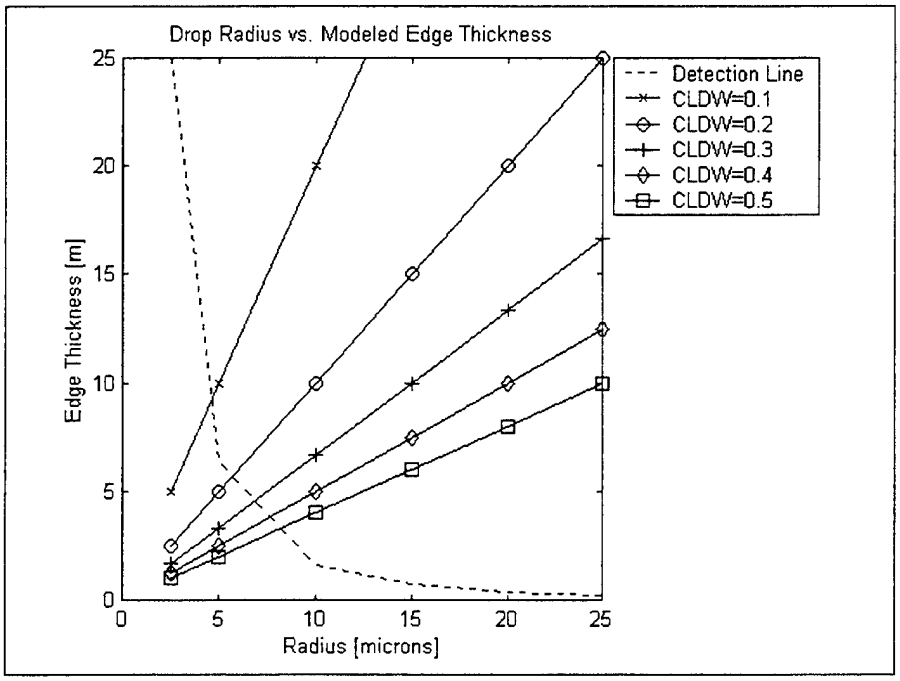

Figure 3-3: Detectable Cloud Thickness and Model CLDW Values

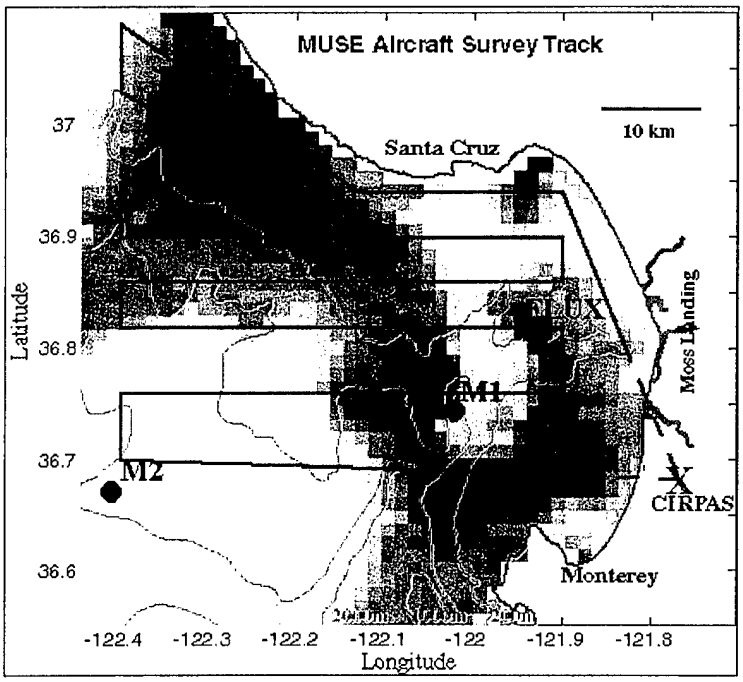

Figure 3-4: The MUSE Aircraft Survey Track (Paduan and Ramp, 2000)

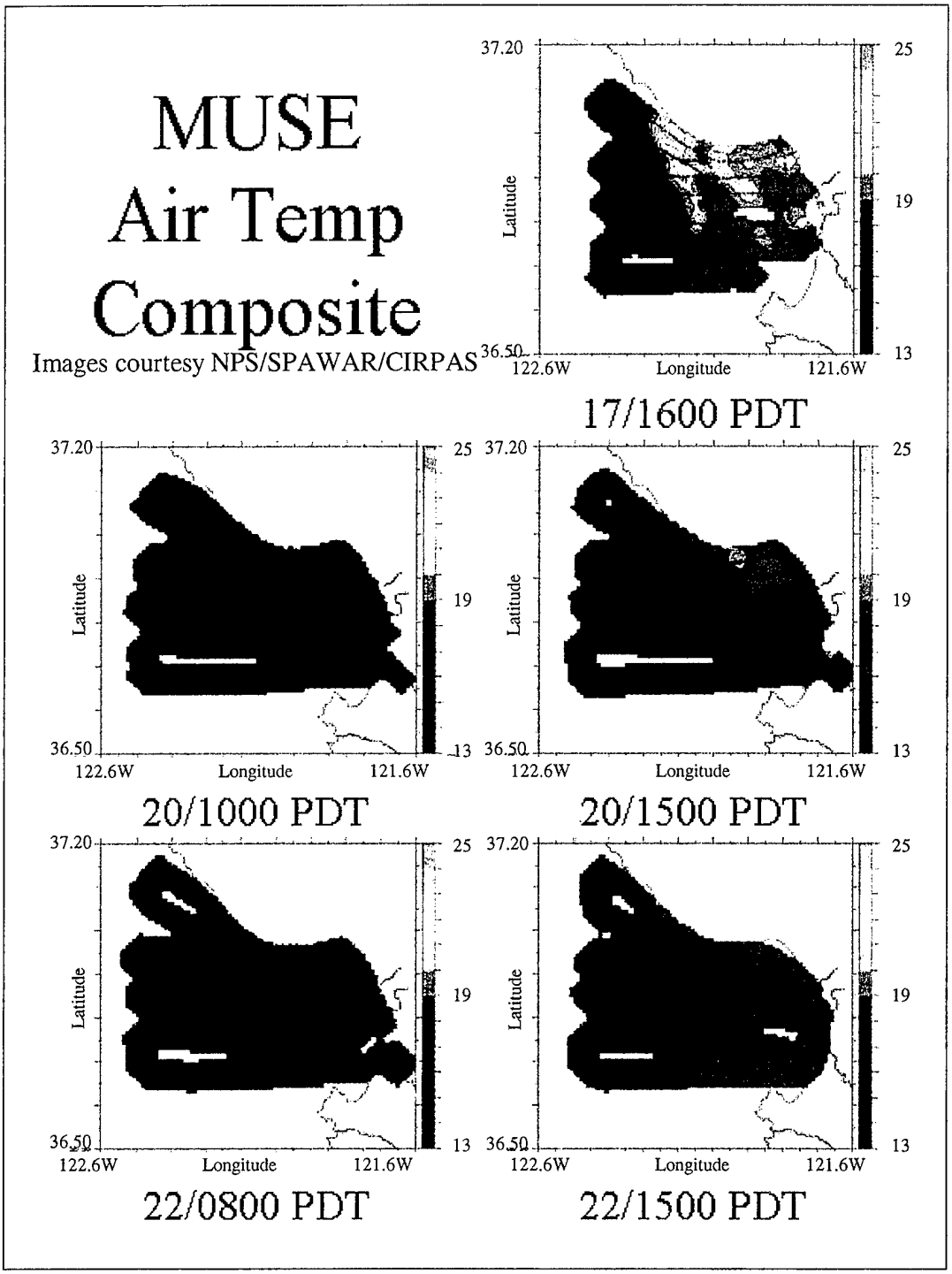

Figure 3-5: MUSE Aircraft Measured Air Temperatures (Paduan and Ramp, 2000)

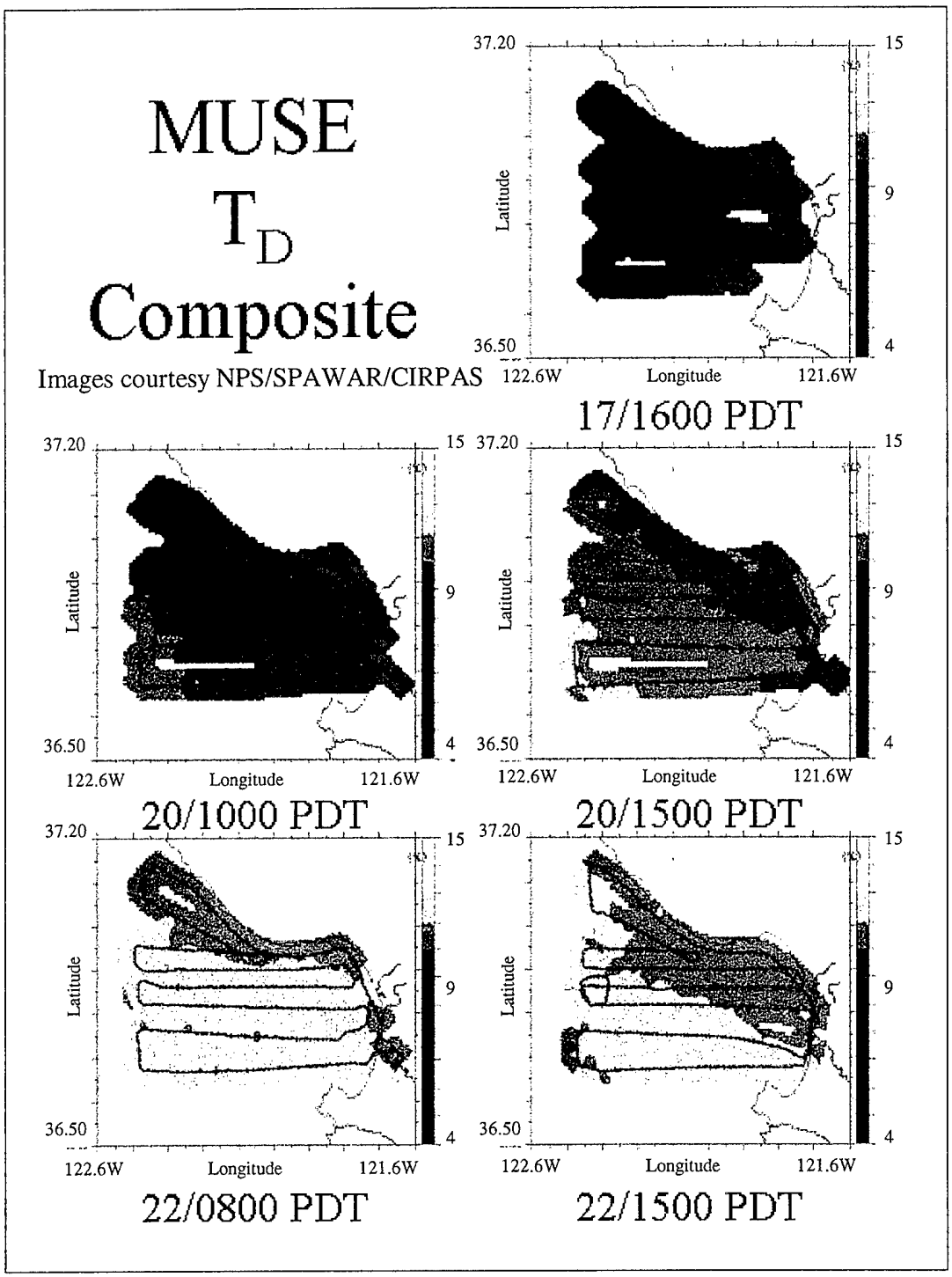

Figure 3-6: MUSE Aircraft Measured Dew Point Temperatures (Paduan and Ramp, 2000)

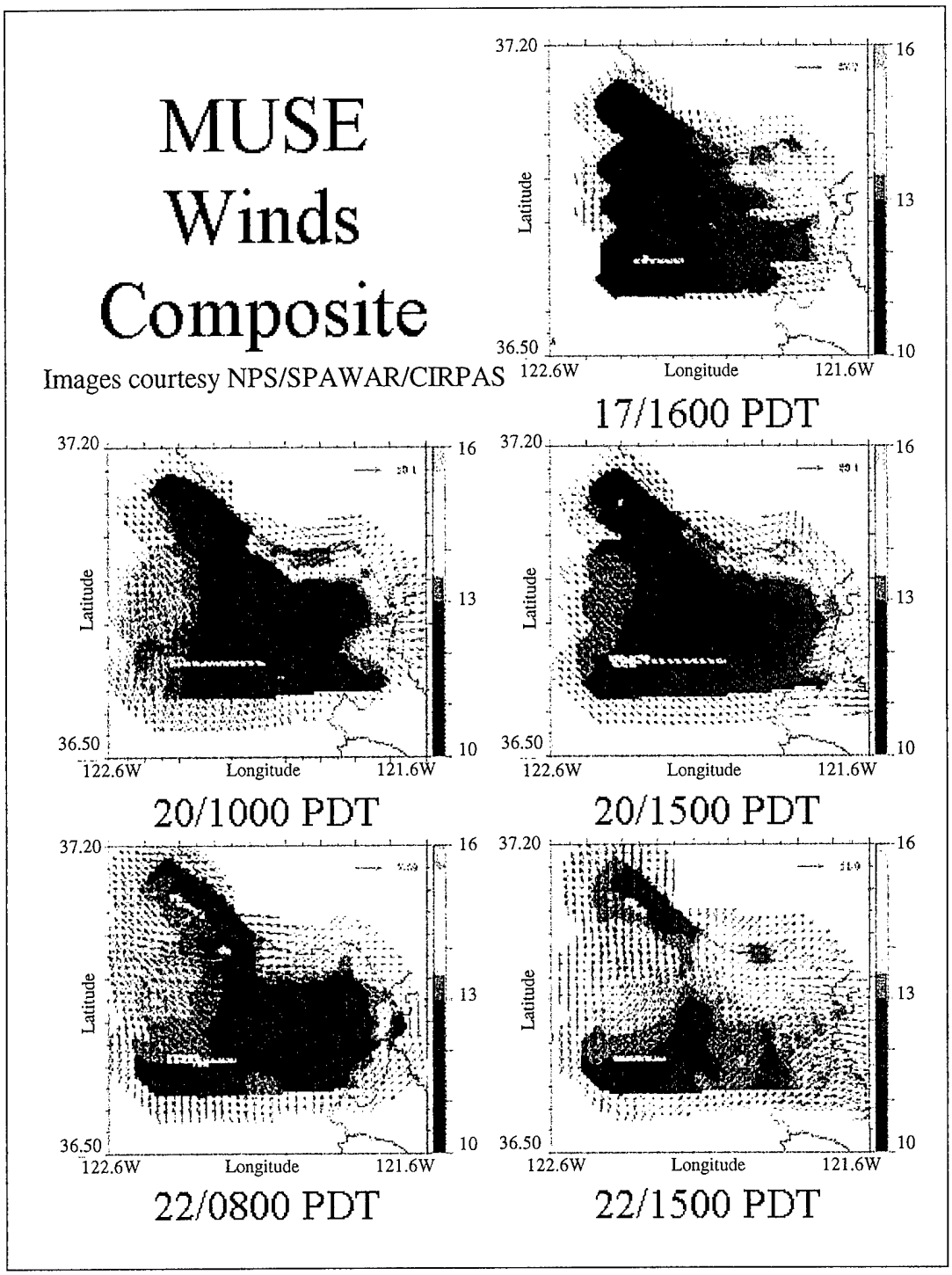

Figure 3-7: MUSE Aircraft Measured Winds (Paduan and Ramp, 2000)

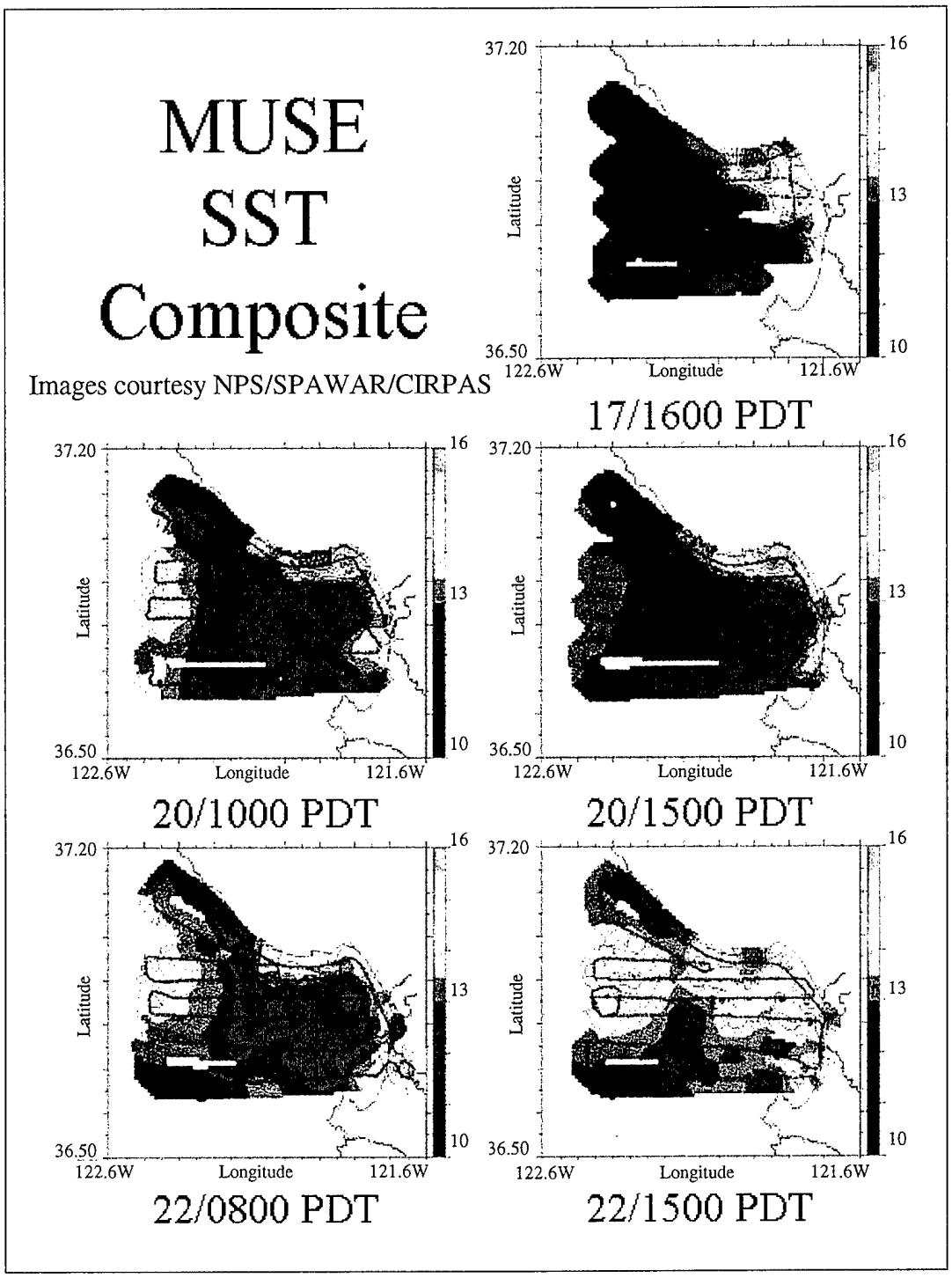

Figure 3-8: MUSE Aircraft Measured Sea Surface Temperatures (Paduan and Ramp, 2000)

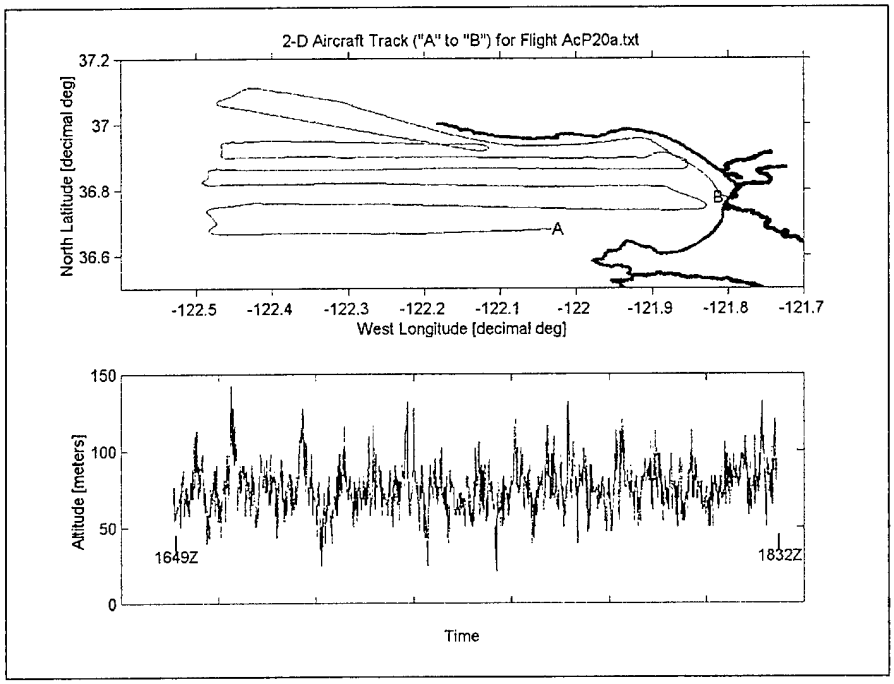

Figure 3-9: Track and Altitude for Flight 20a

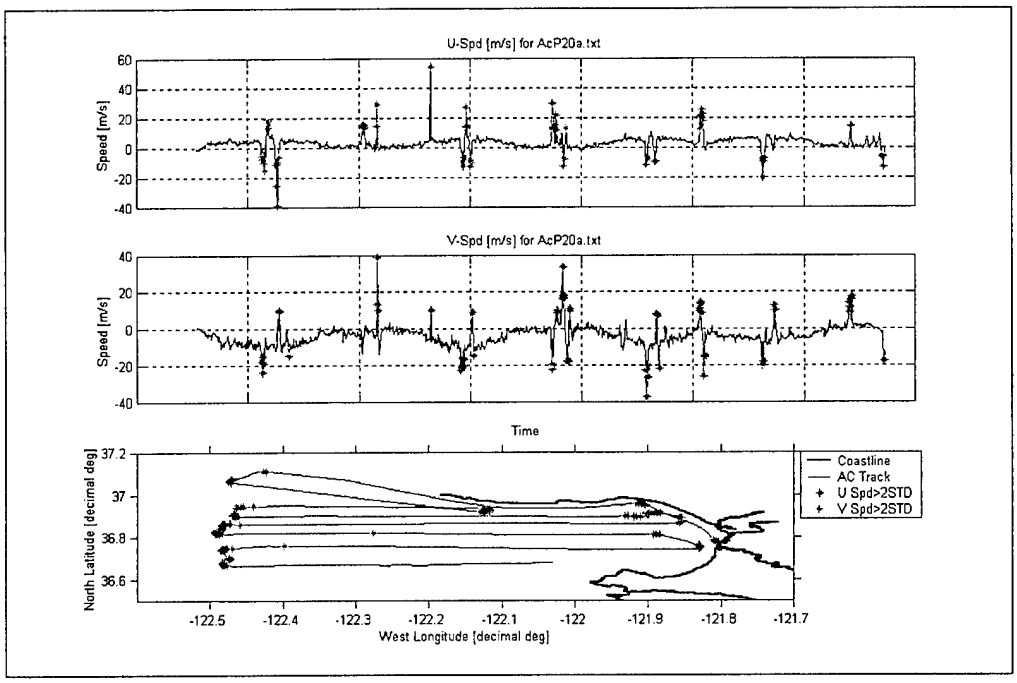

Figure 3-10: U and V Speed Outliers for Flight 20a

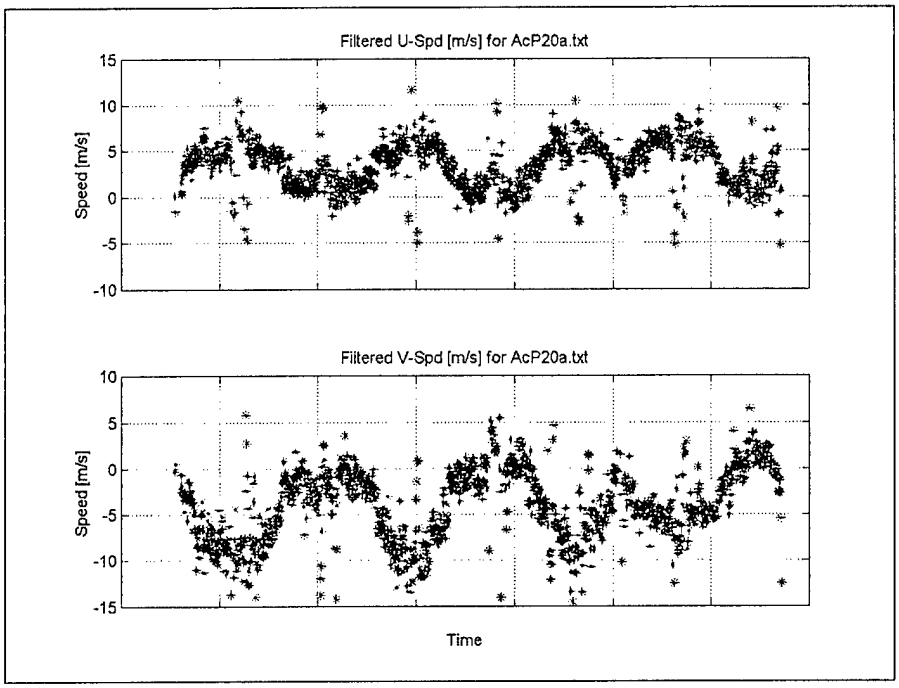

Figure 3-11: Filtered U and V Speeds for Flight 20a

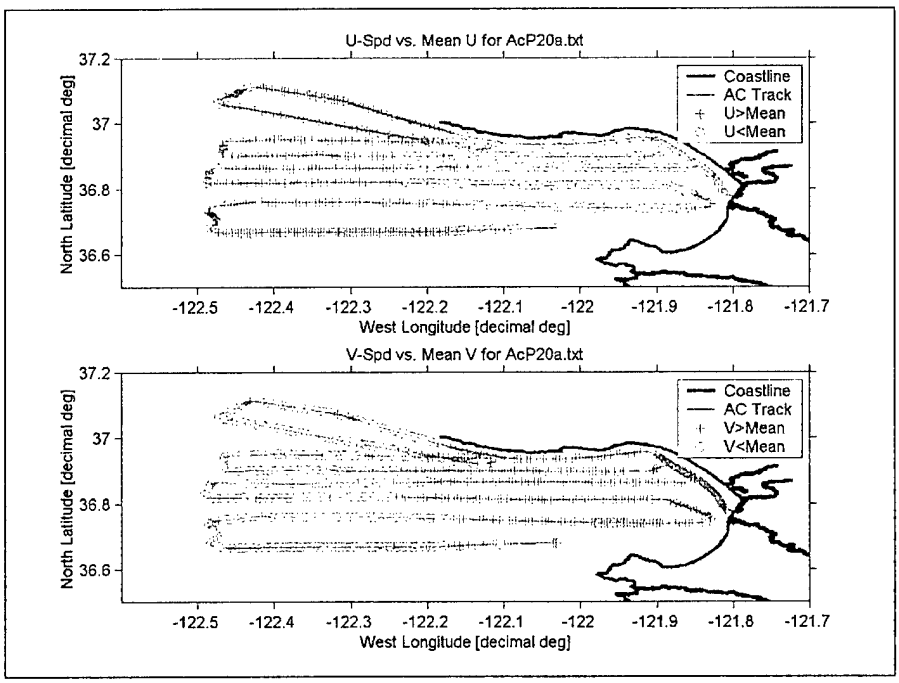

Figure 3-12: Areas of High and Low Wind Speed for Flight 20a

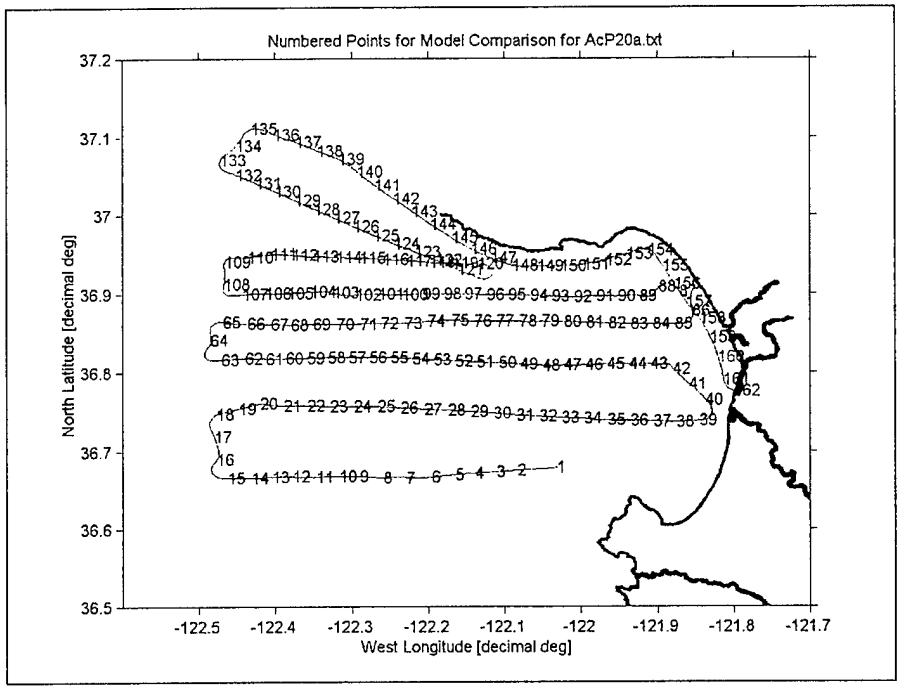

Figure 3-13: 3-km Points Numbered Along Track for Flight 20a

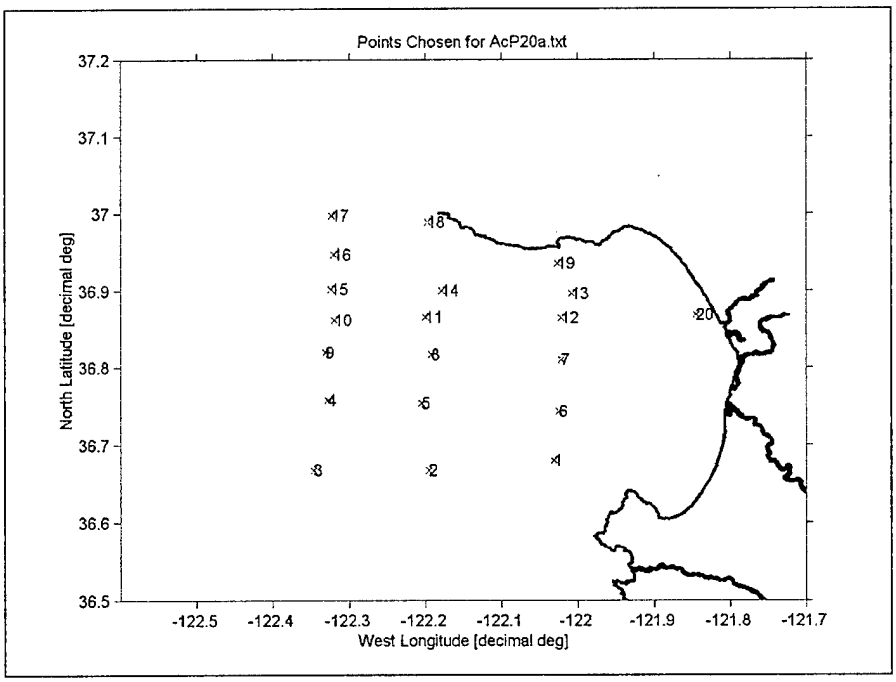

Figure 3-14: Numbered Data Points Selected for Flight 20a

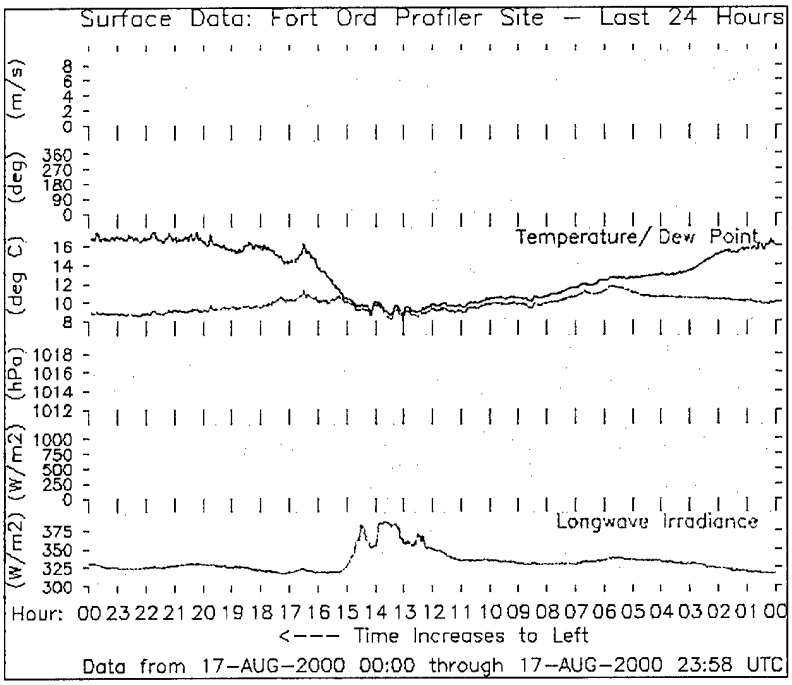

Figure 3-15: Ft. Ord Surface Station Observations, 17 August

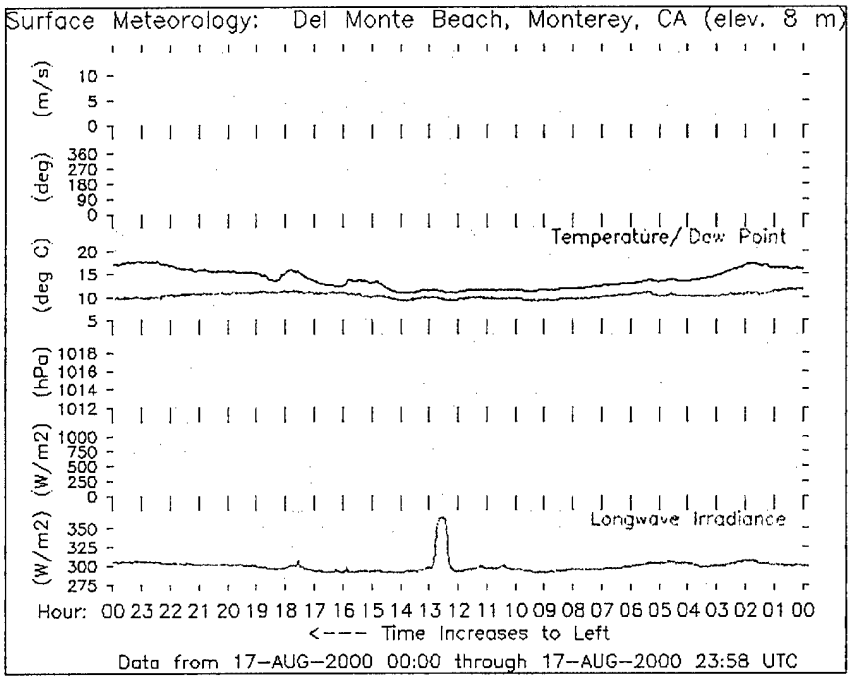

Figure 3-16: Del Monte Beach Surface Station Observations, 17 August

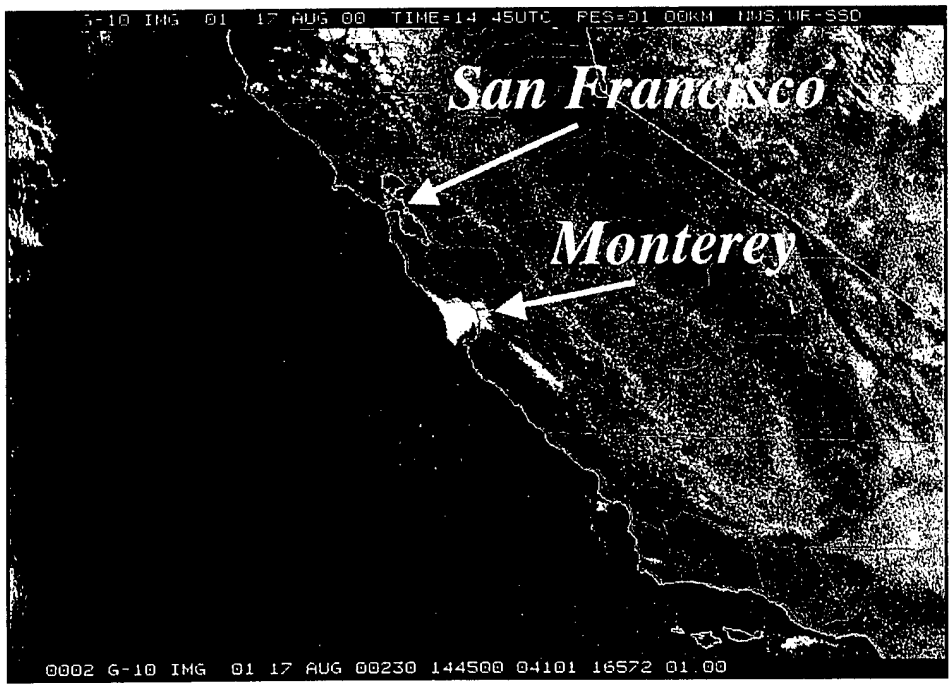

Figure 3-17: GOES-10 Satellite Image 17 August, 1445Z

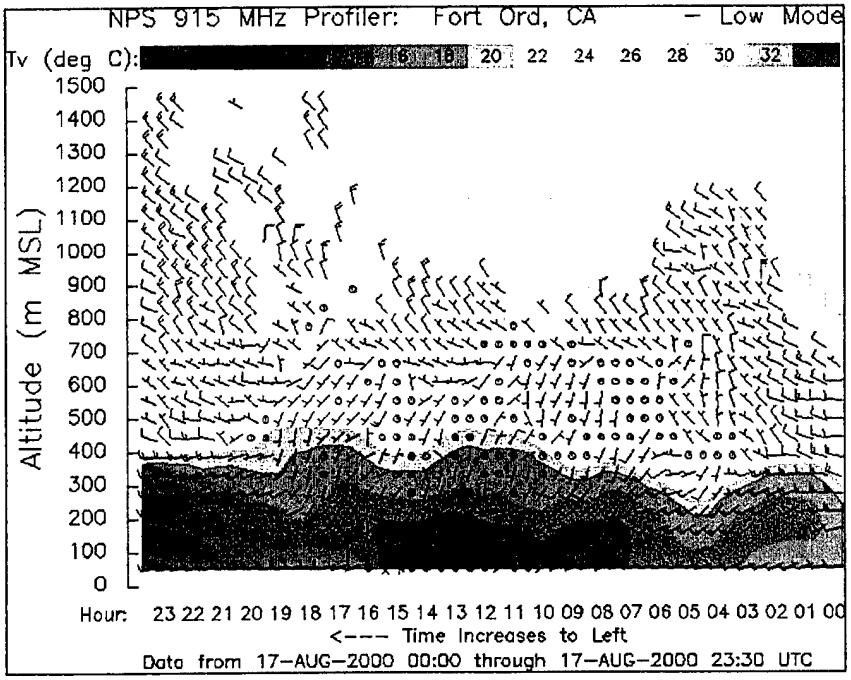

Figure 3-18: Ft. Ord Profiler for 17 August

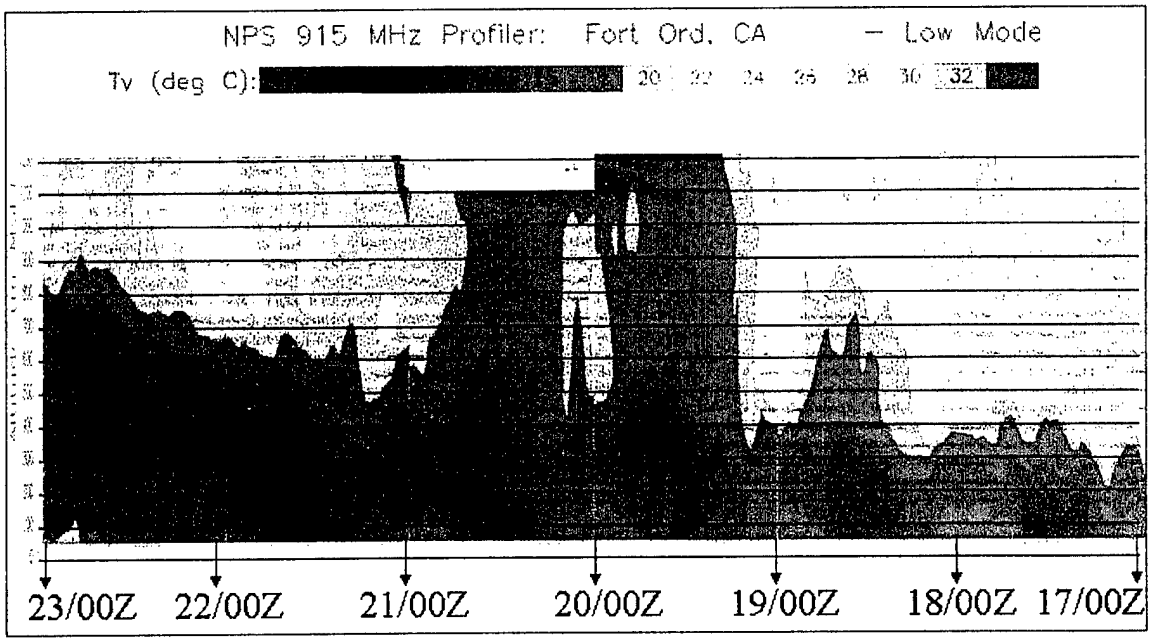

Figure 3-19: Composite Profile 17-24 Aug

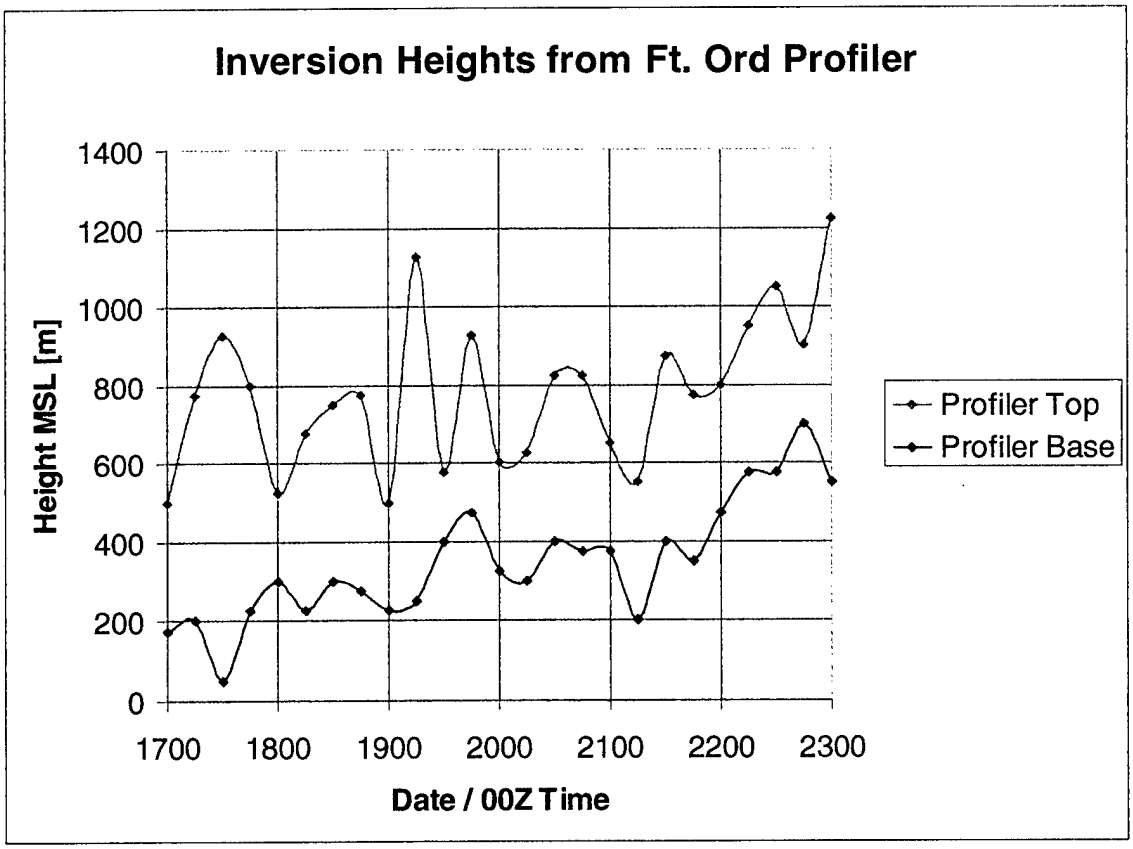

Figure 3-20: Inversion Strength as Measured by Height/Thickness

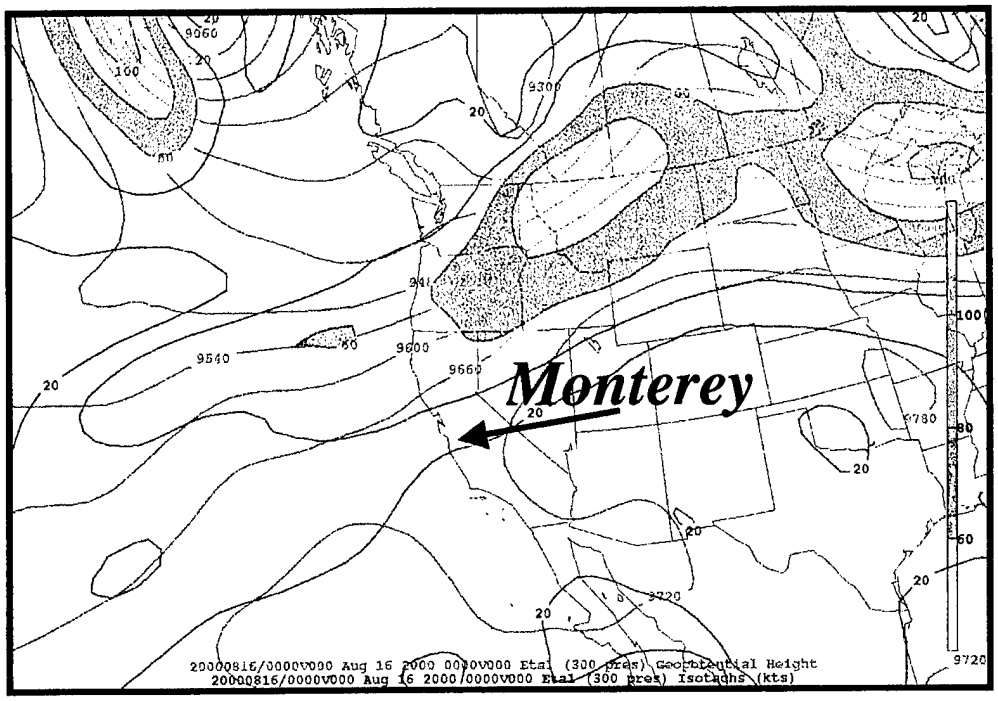

Figure 3-21: ETA Synoptic Picture, 300mb at 17/00Z

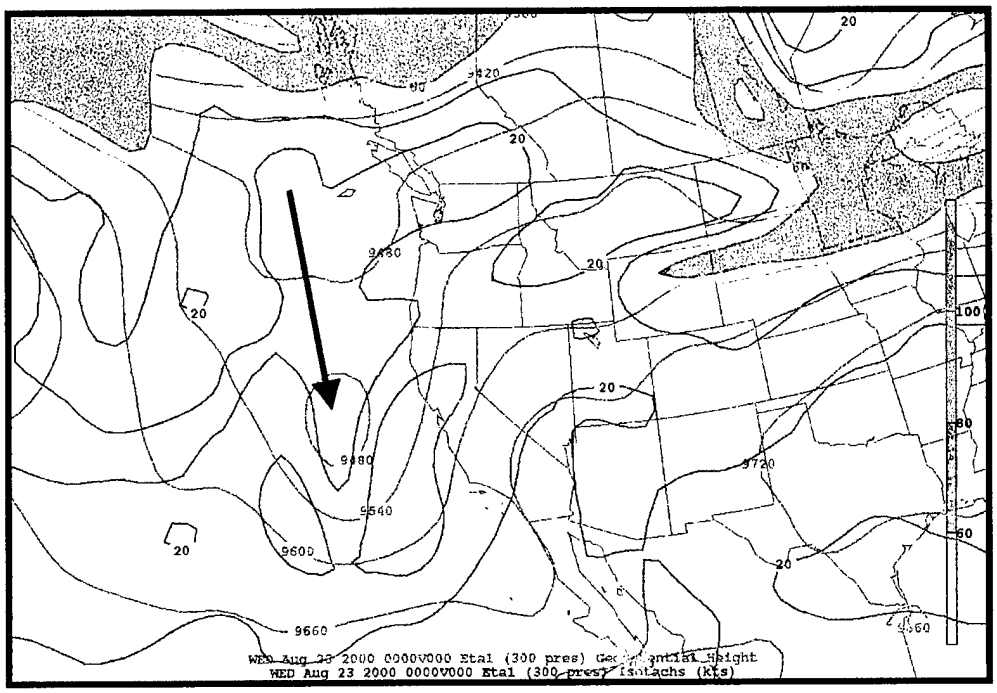

Figure 3-22: ETA Synoptic Picture, 300mb at 23/00Z

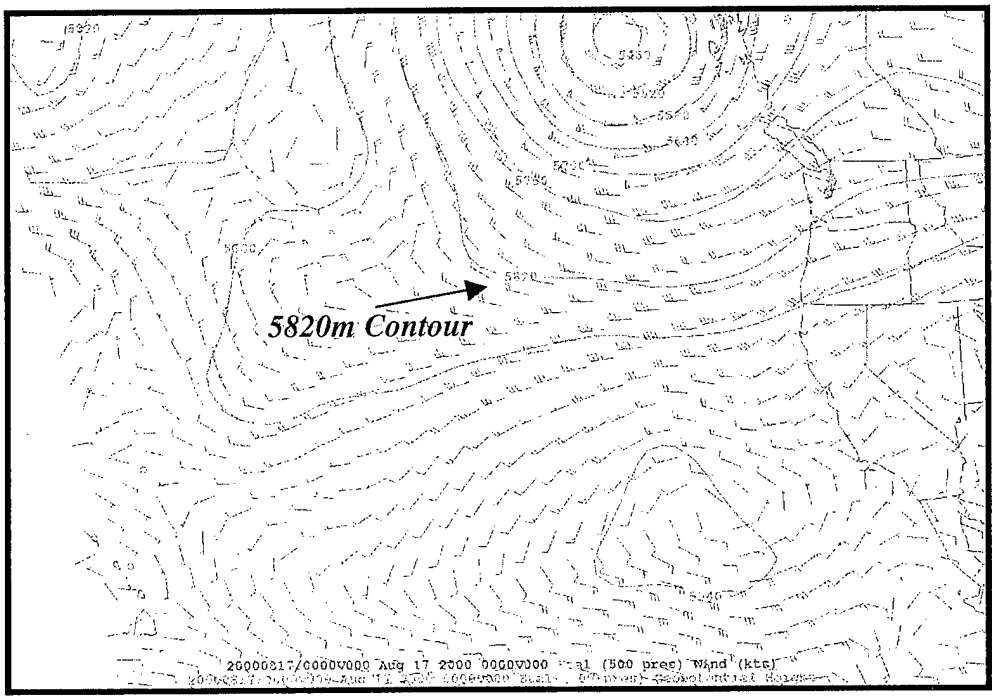

Figure 3-23: ETA Synoptic Picture, 500mb at 17/00Z

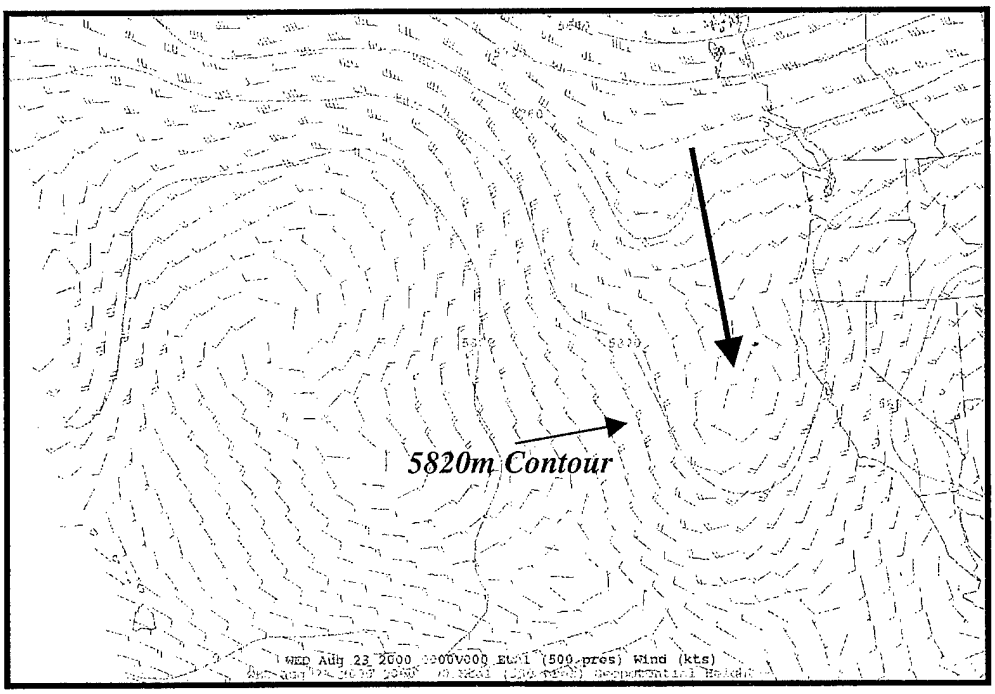

Figure 3-24: ETA Synoptic Picture, 500mb at 23/00Z

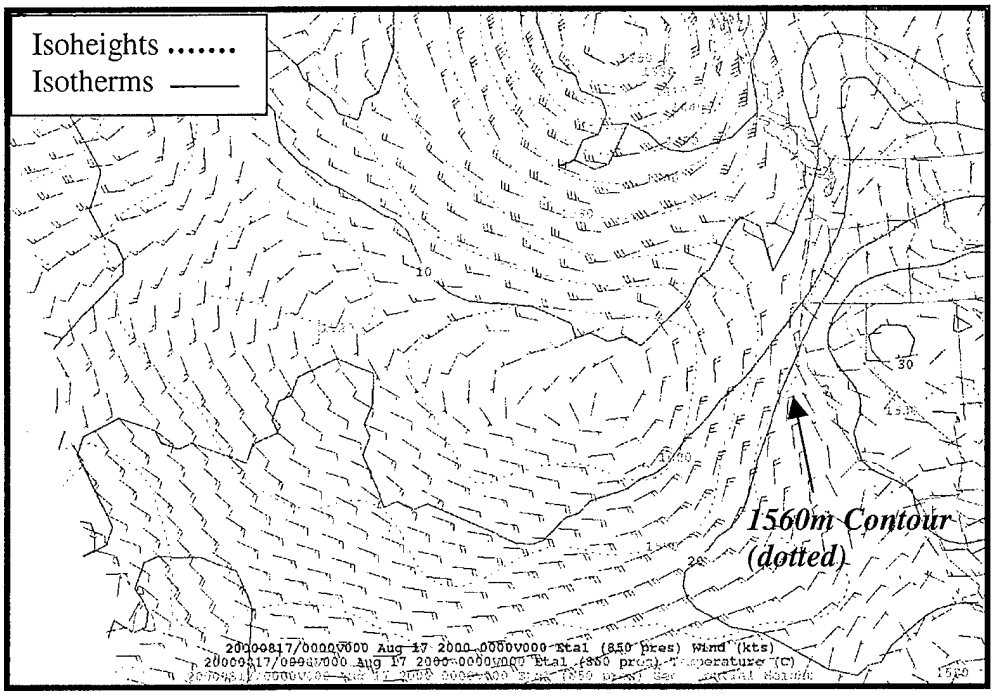

Figure 3-25: ETA Synoptic Picture, 850mb at 17/00Z

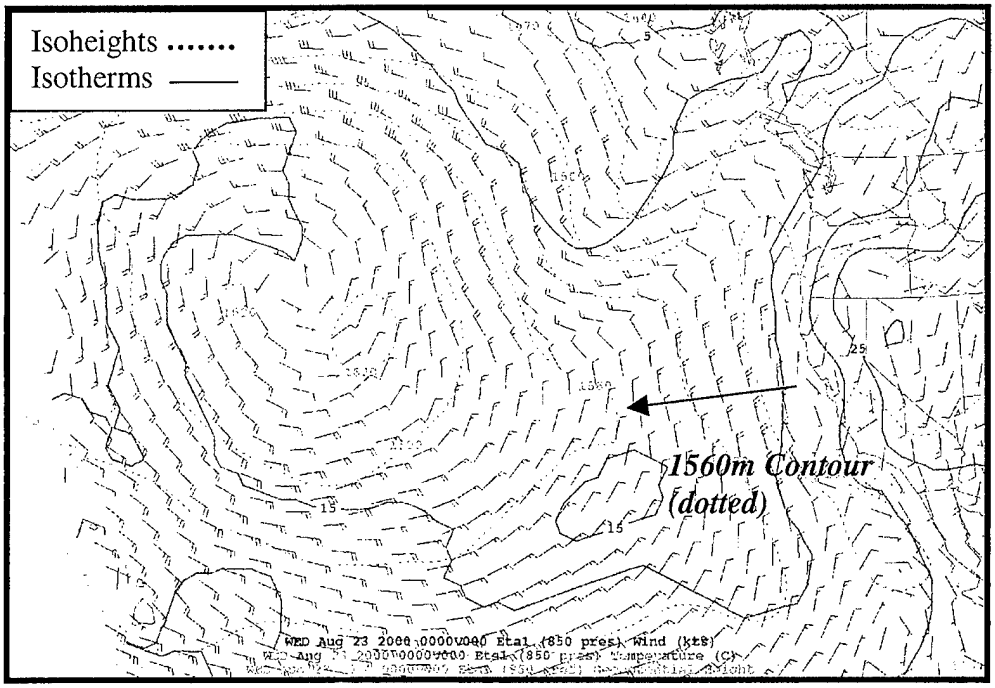

Figure 3-26: ETA Synoptic Picture, 850mb at 23/00Z

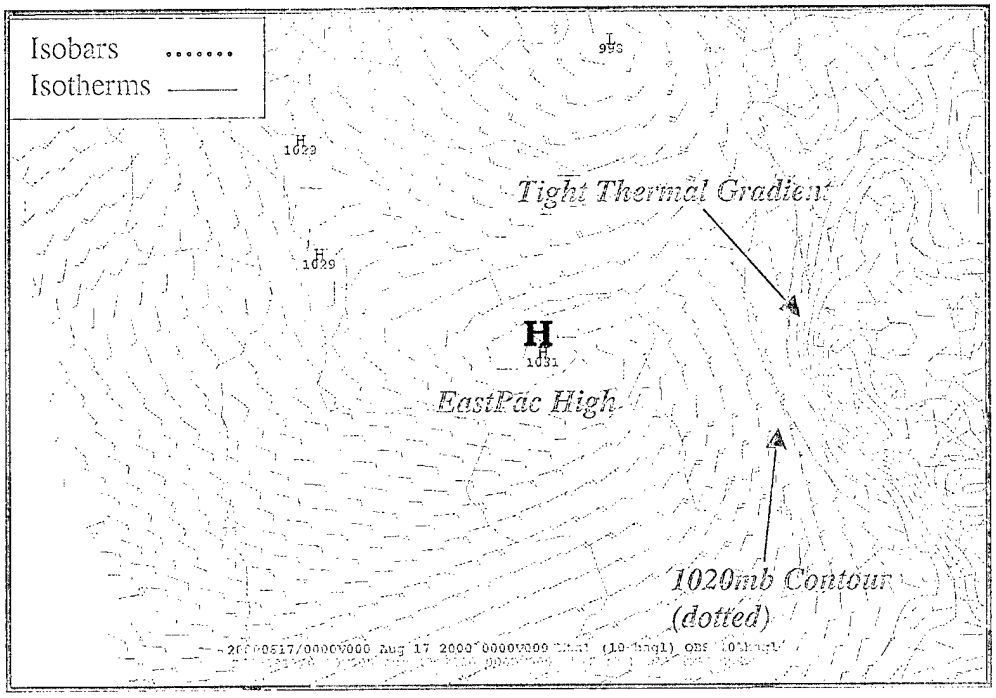

Figure 3-27: ETA Synoptic Picture, Surface at 17/00Z

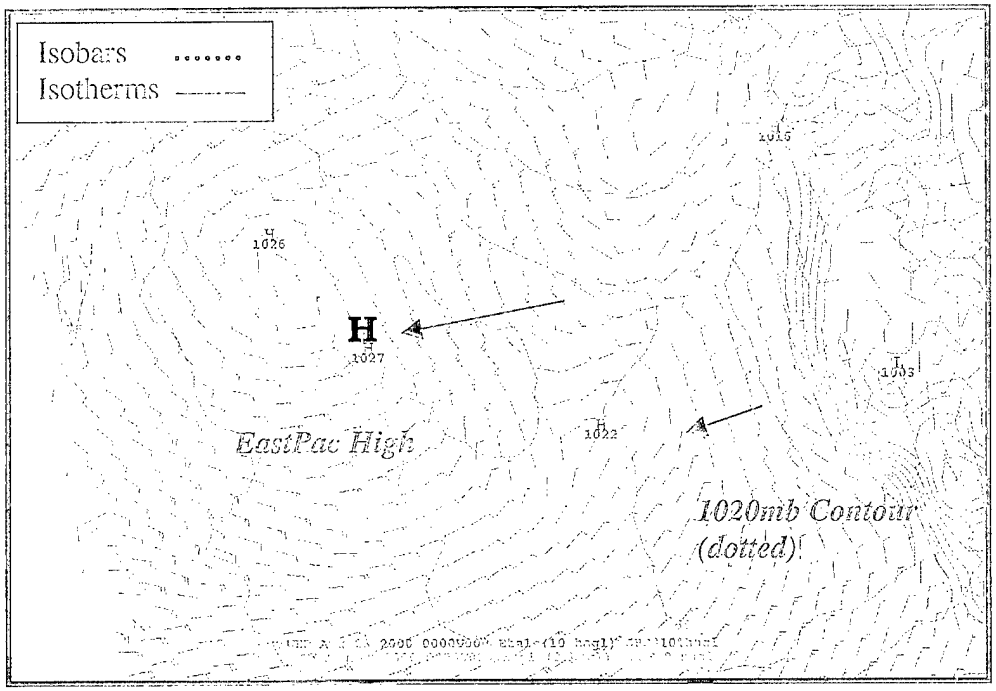

Figure 3-28: ETA Synoptic Picture, Surface at 23/00Z

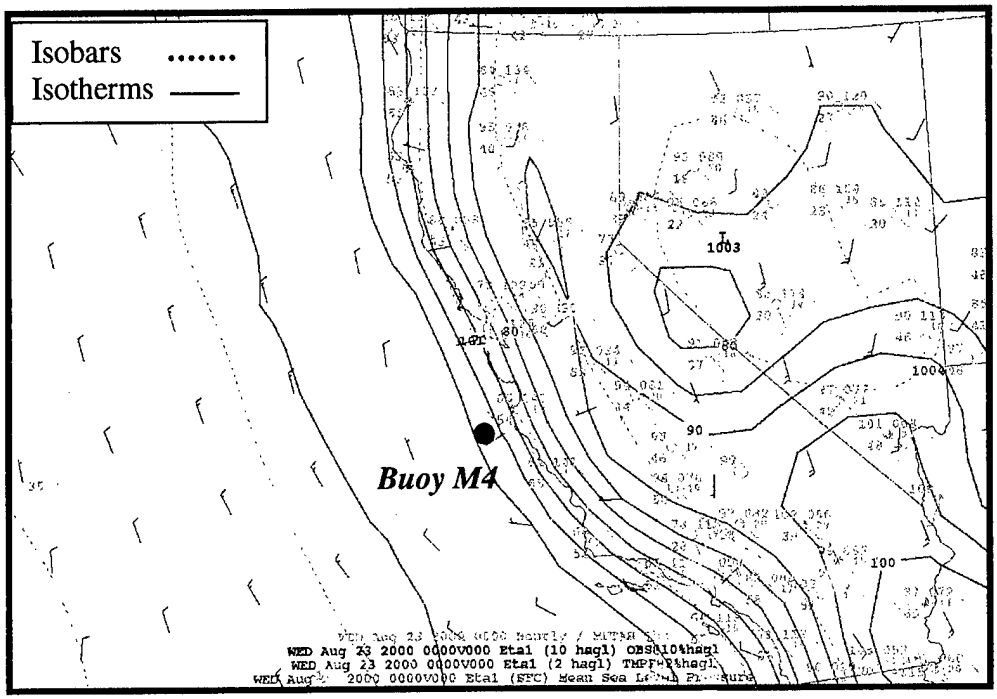

Figure 3-29: ETA Synoptic Picture, Surface (with Observations) at 23/00Z

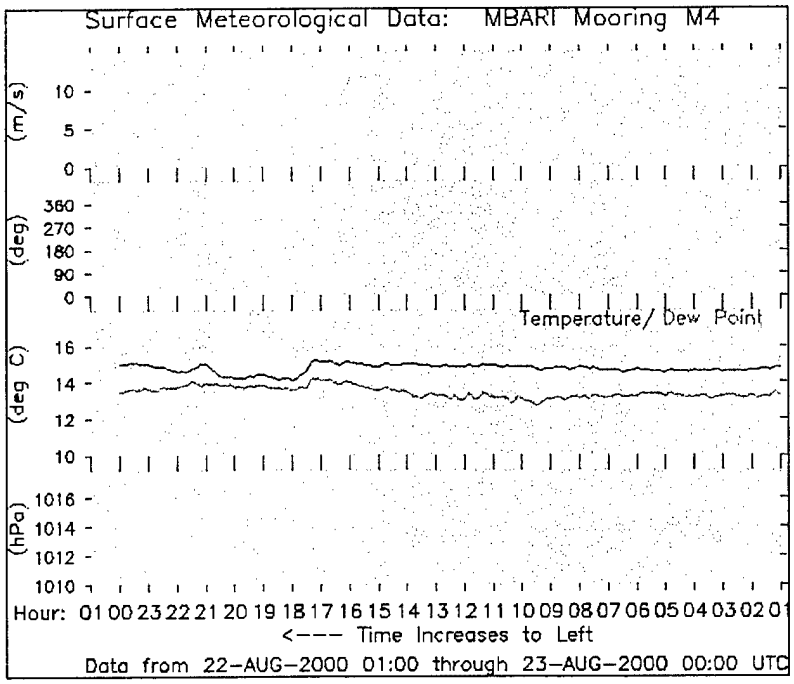

Figure 3-30: Buoy M4 Station Observations for 23Aug00

Figure 4-1: CON CLDW vs. Satellite Cloud Edge at 17/15Z

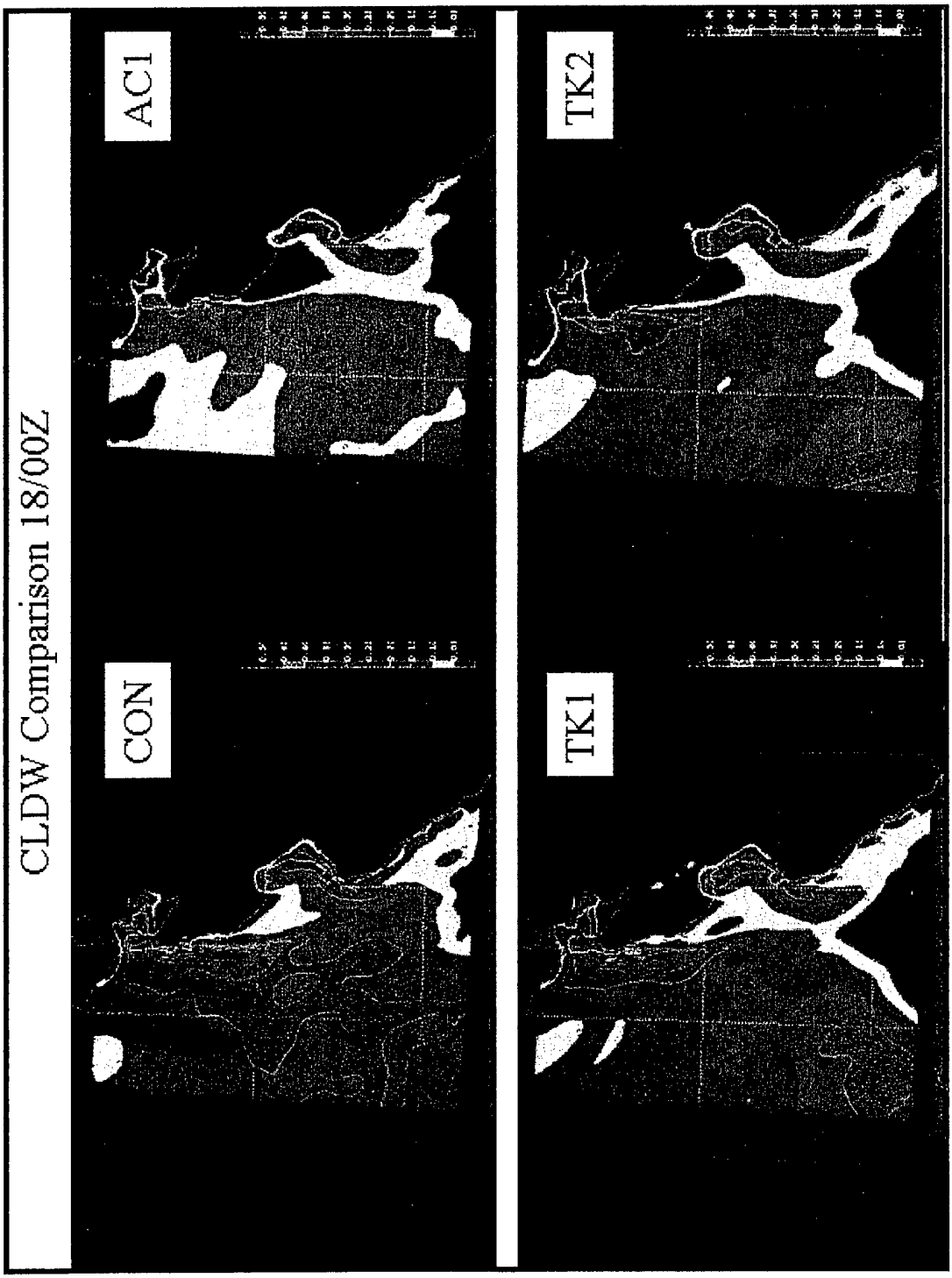

Figure 4-2: CLDW Comparison: CON, AC1, TK1, TK2 at 18/00Z

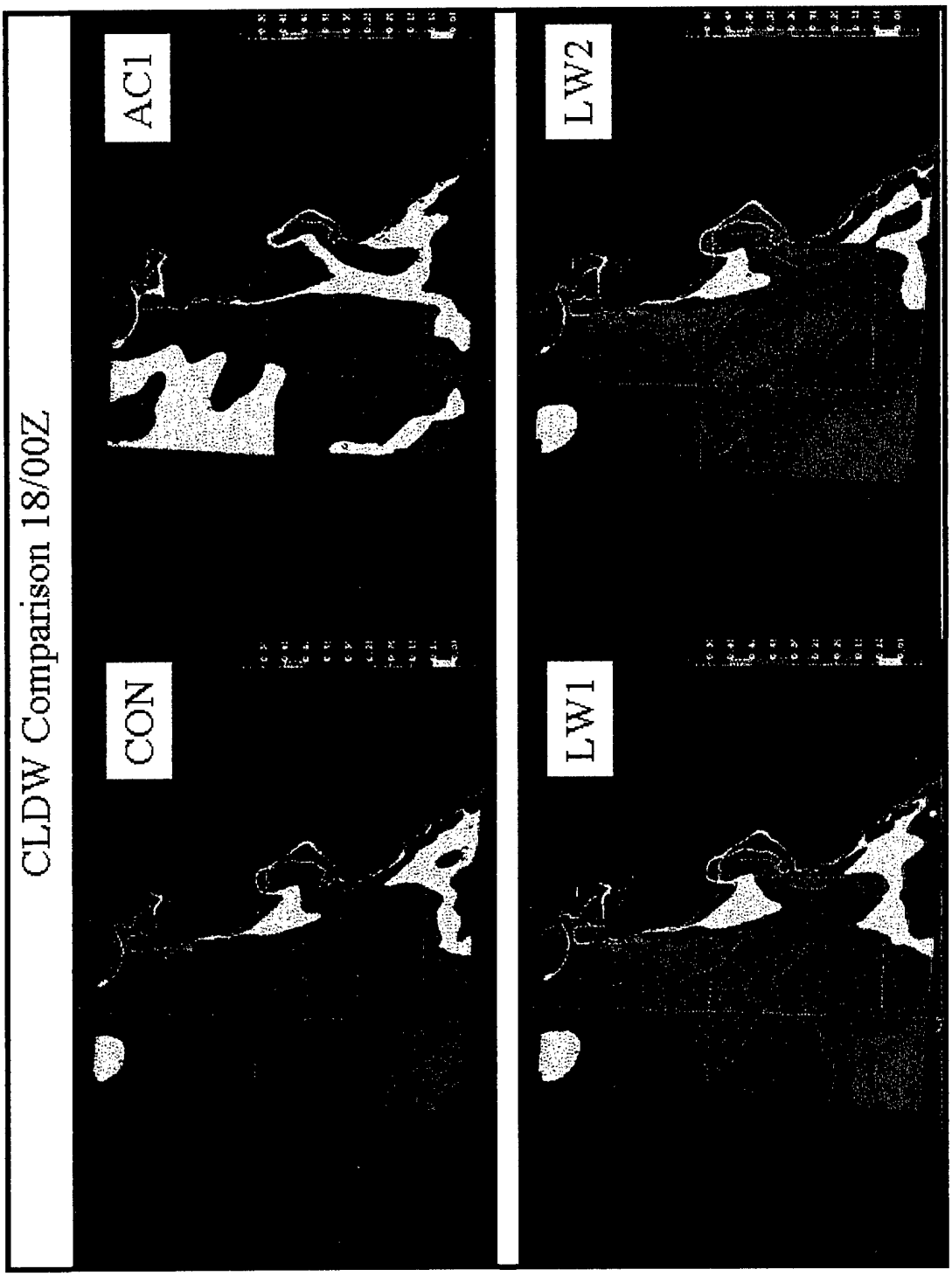

Figure 4-3: CLDW Comparison: CON, AC1, LW1, LW2 at 18/00Z

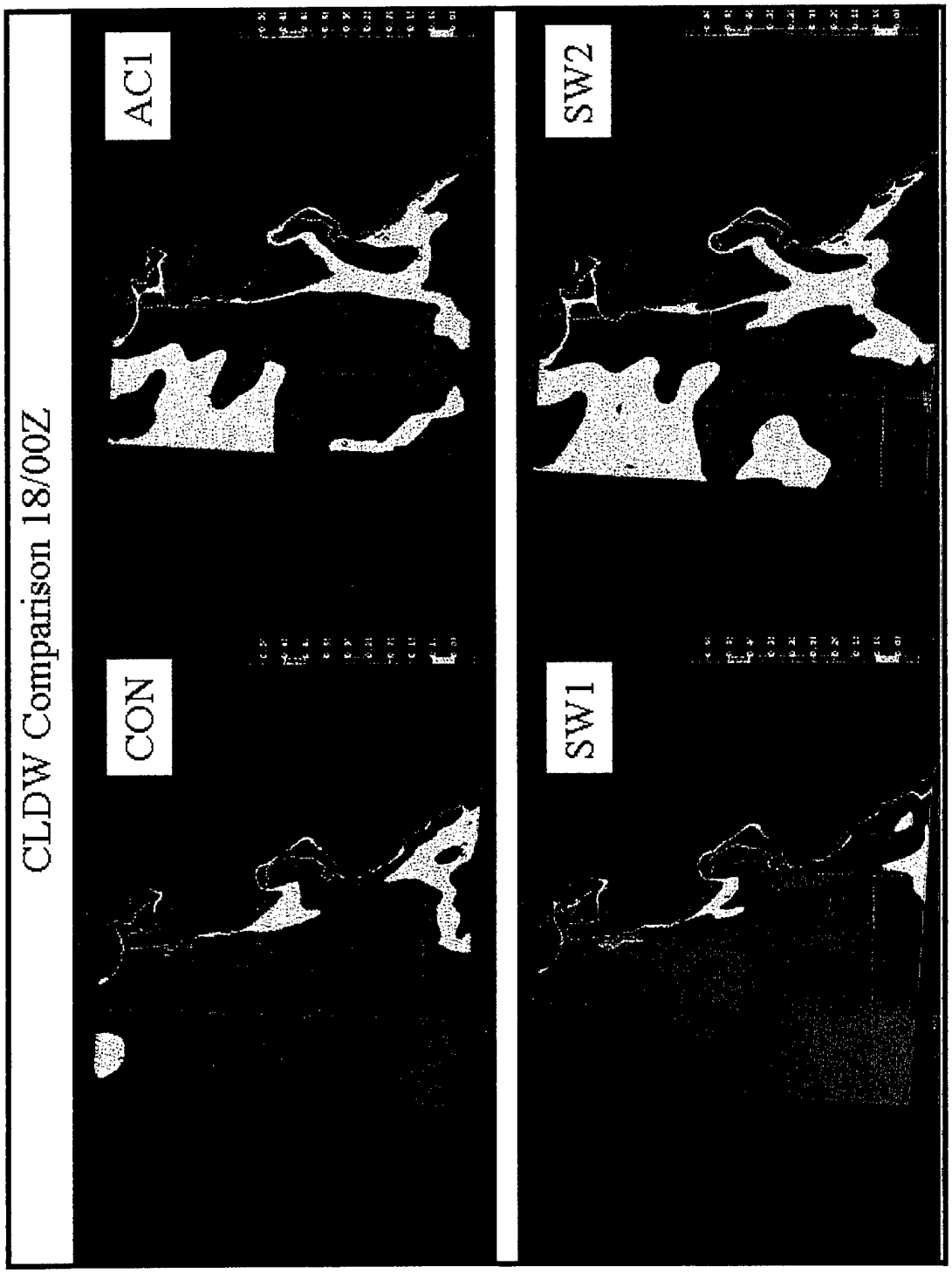

Figure 4-4: CLDW Comparison: CON, AC1, SW1, SW2 at 18/00Z

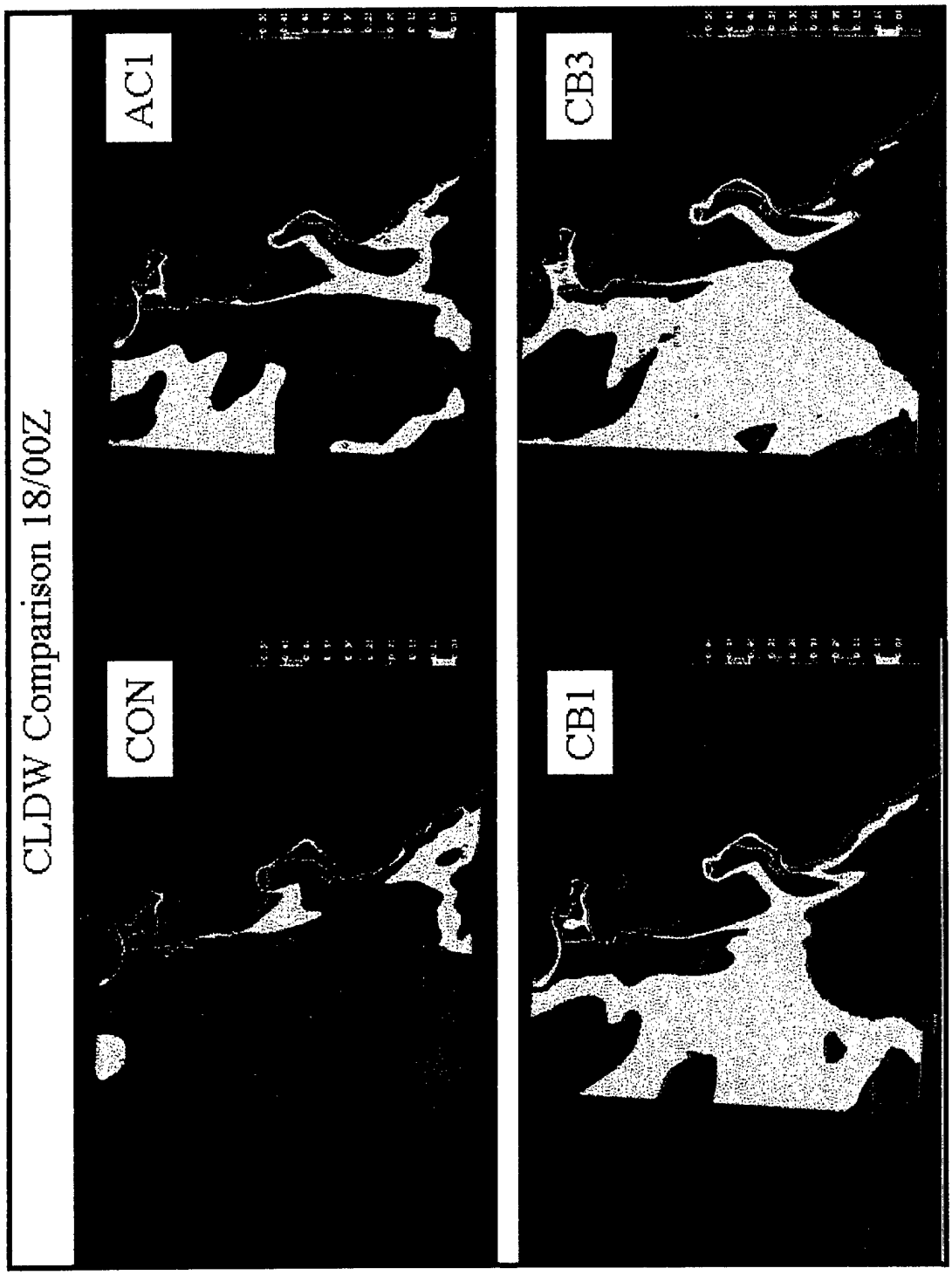

Figure 4-5: CLDW Comparison: CON, AC1, CB1, CB3 at 18/00Z

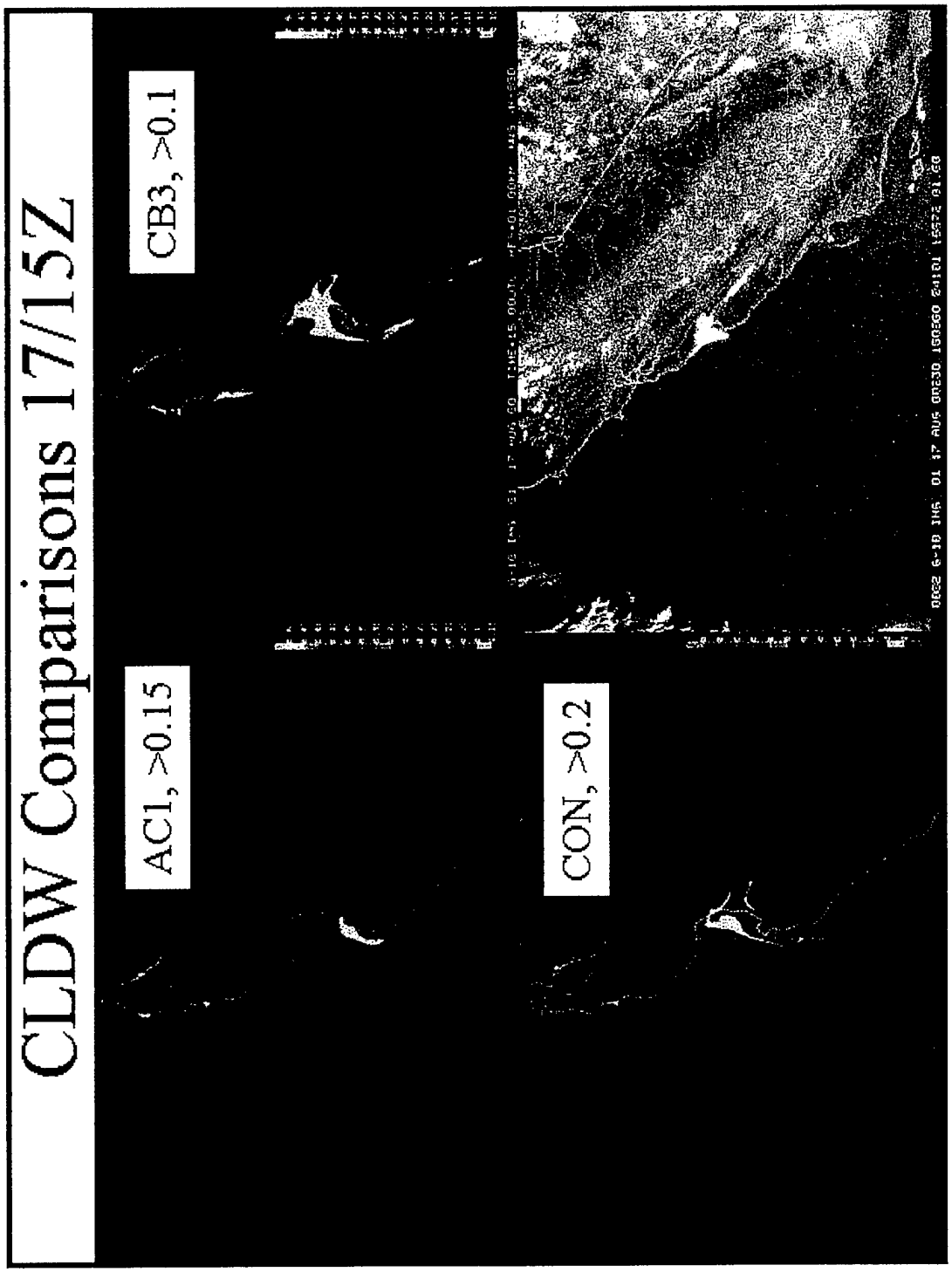

Figure 4-6: CLDW Comparison at 17/15Z

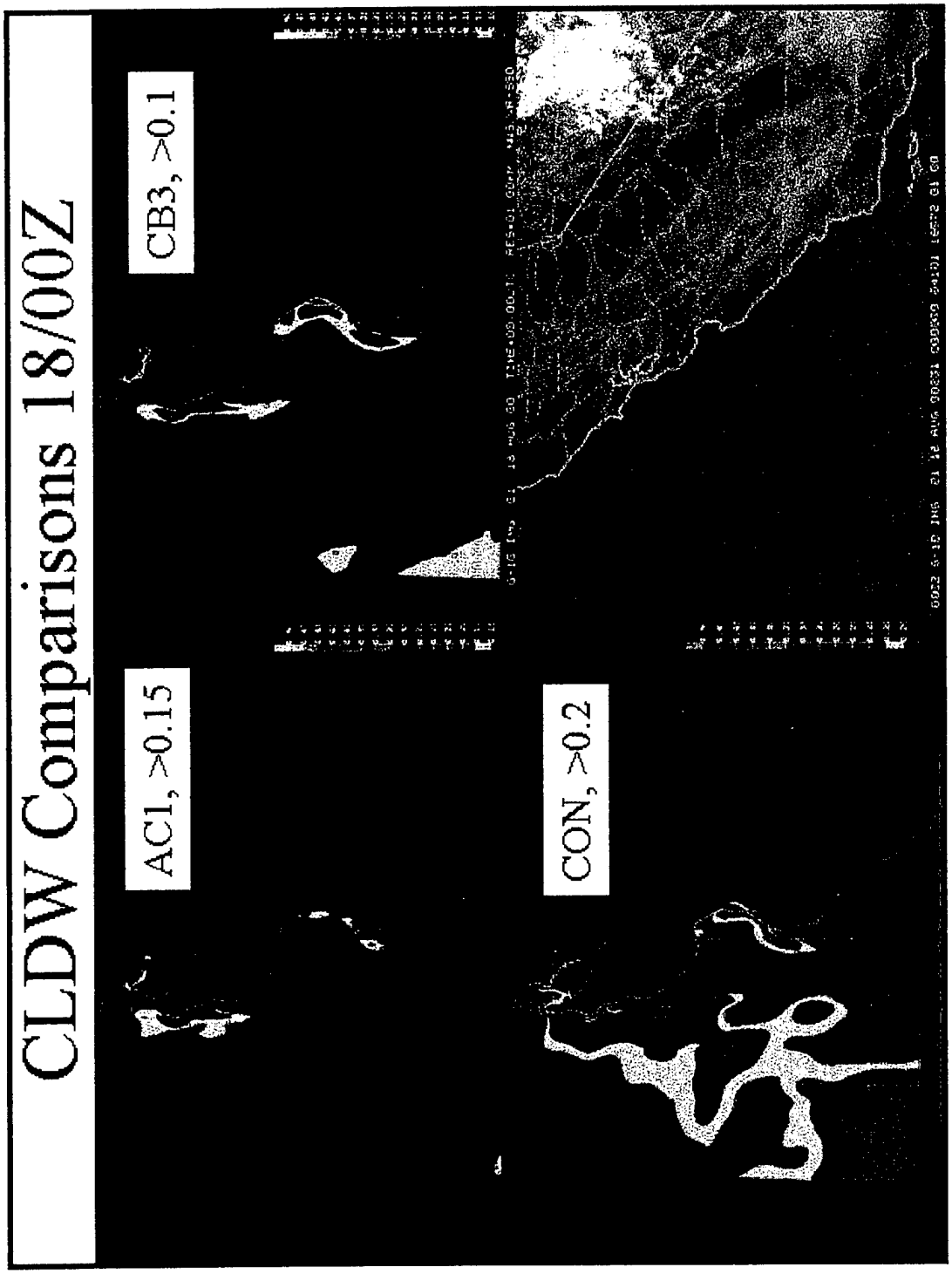

Figure 4-7: CLDW Comparison at 18/00Z

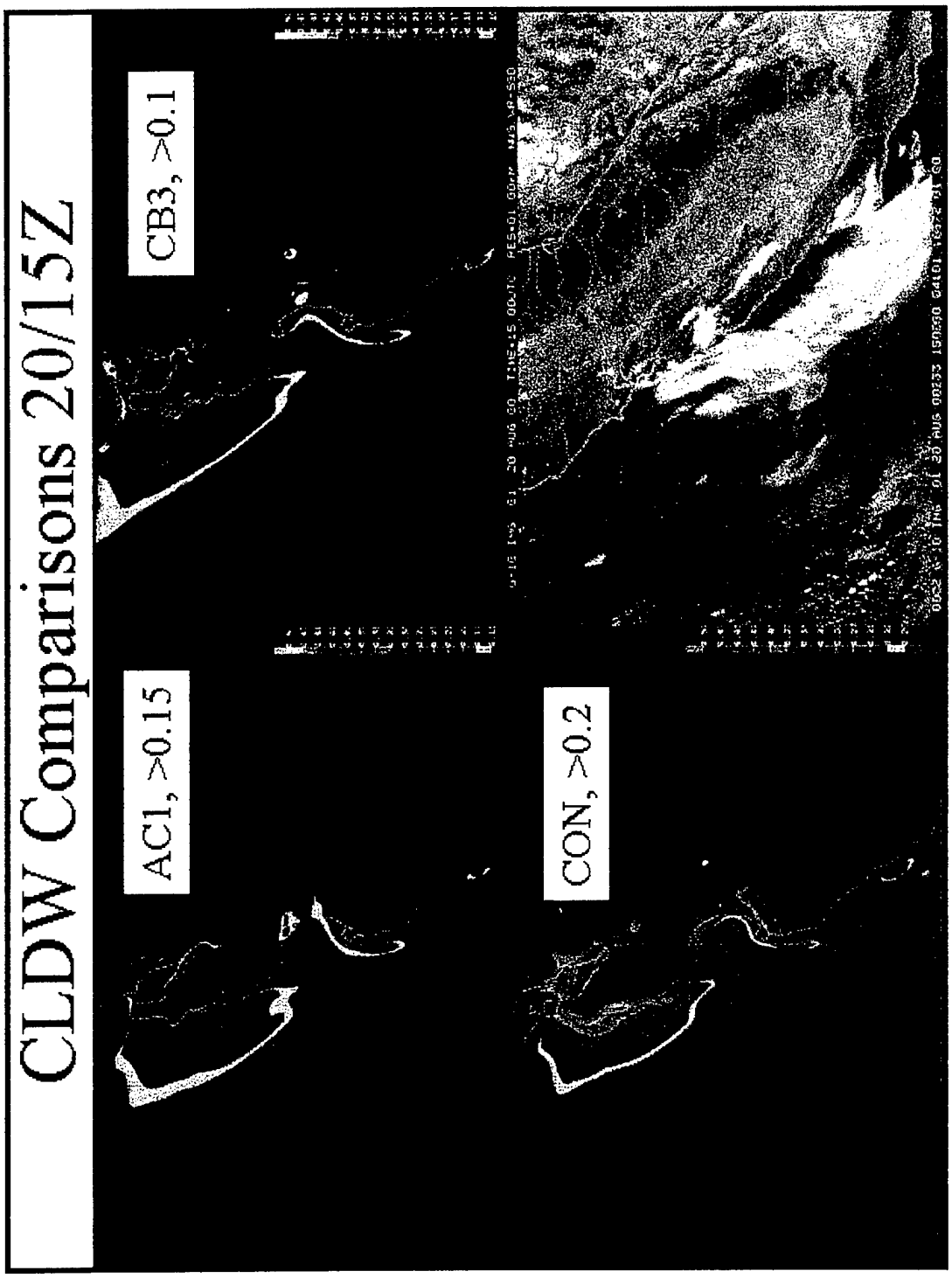

Figure 4-8: CLDW Comparison at 20/15Z

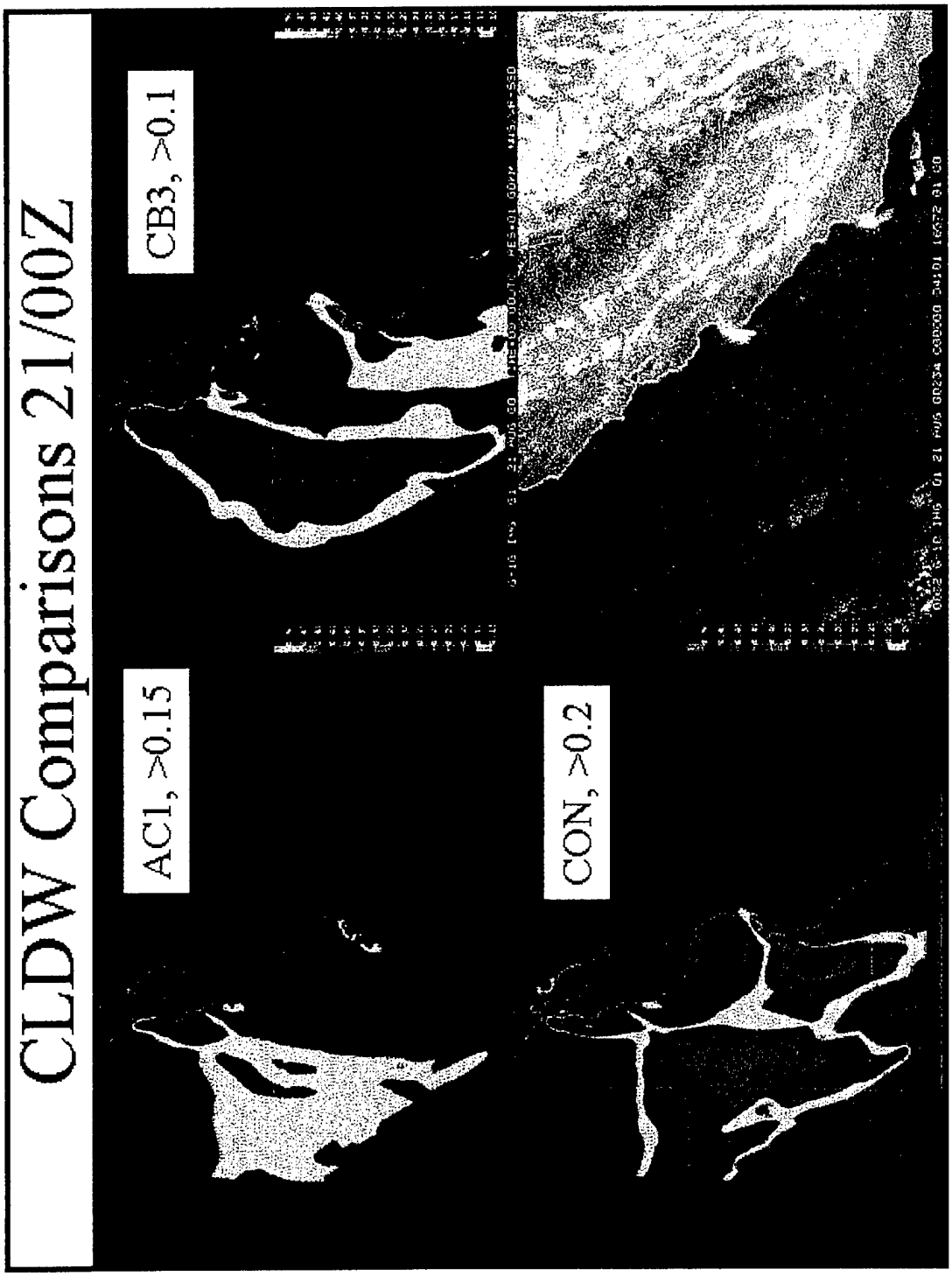

Figure 4-9: CLDW Comparison at 21/00Z

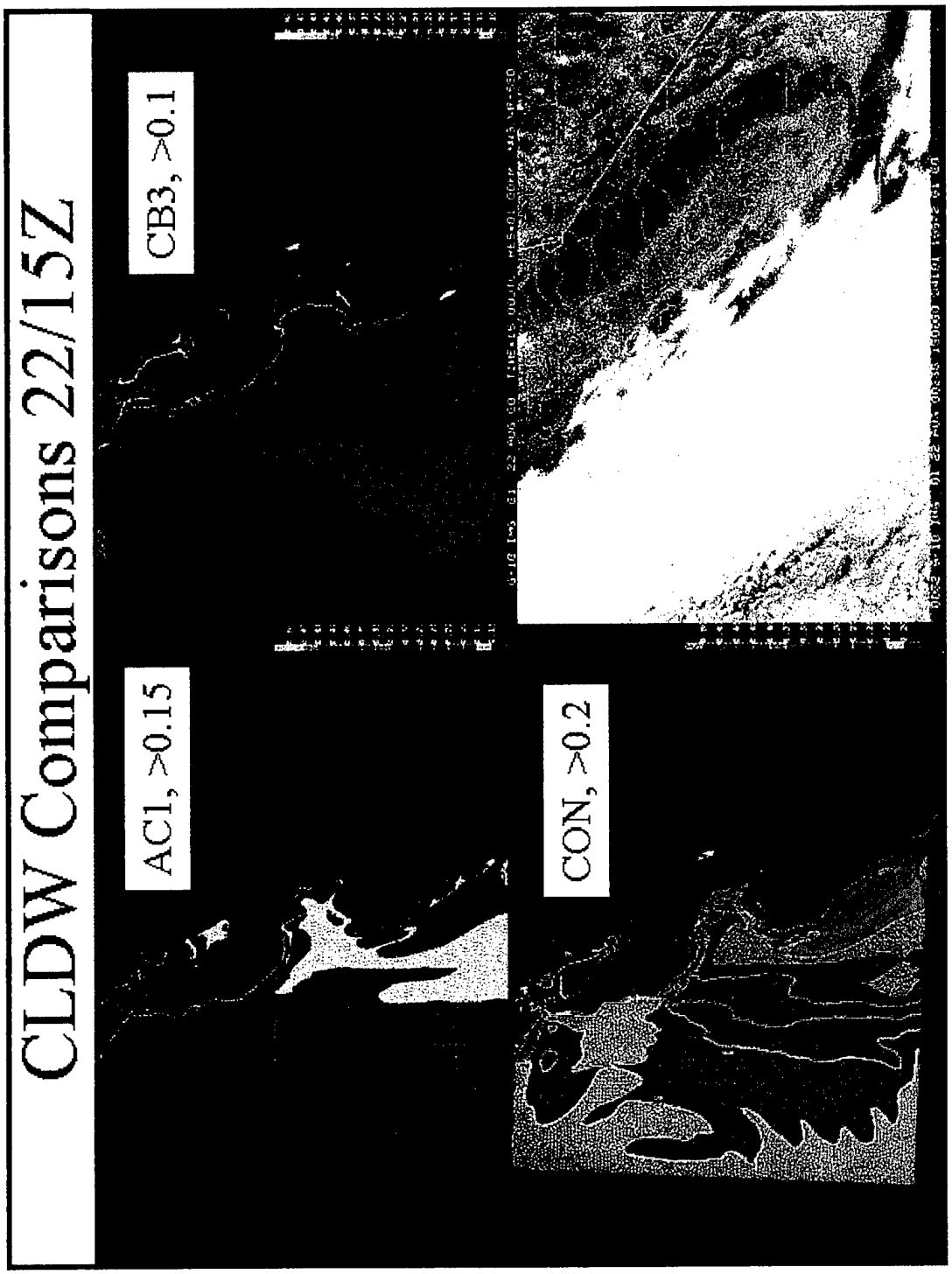

Figure 4-10: CLDW Comparison at 22/15Z

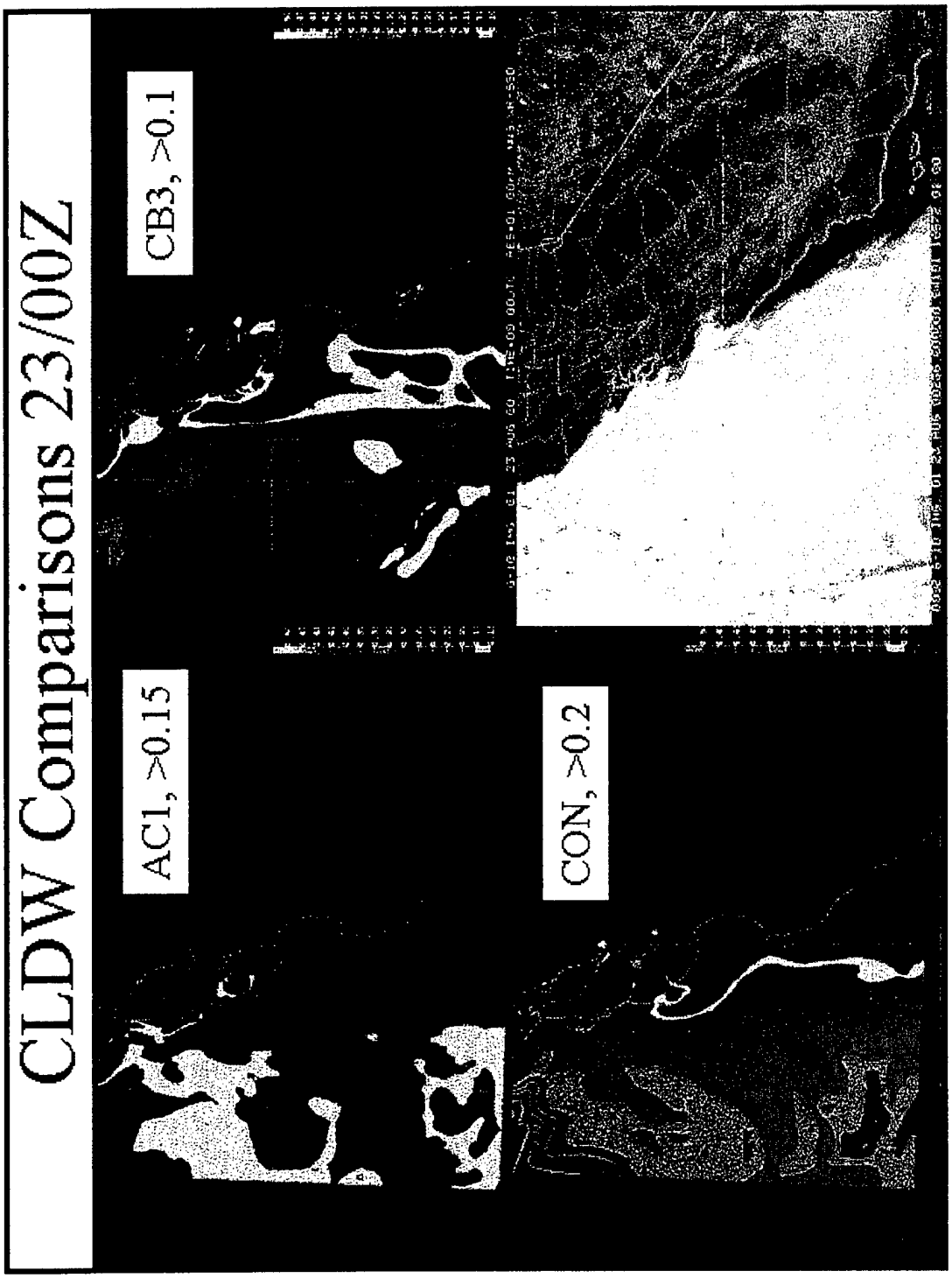

Figure 4-11: CLDW Comparison at 23/00Z

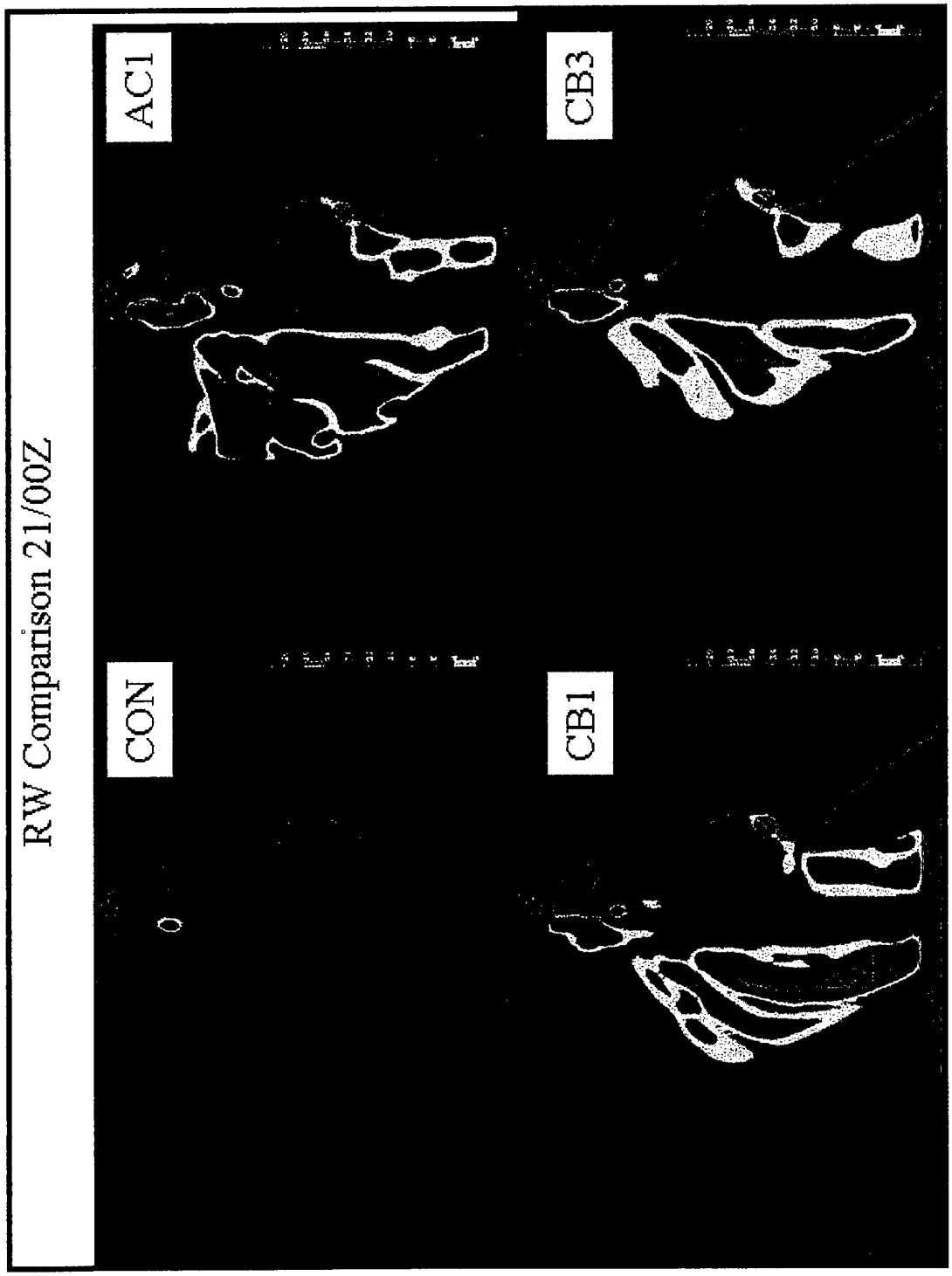

Figure 4-12: Rain Water Comparison at 21/00Z

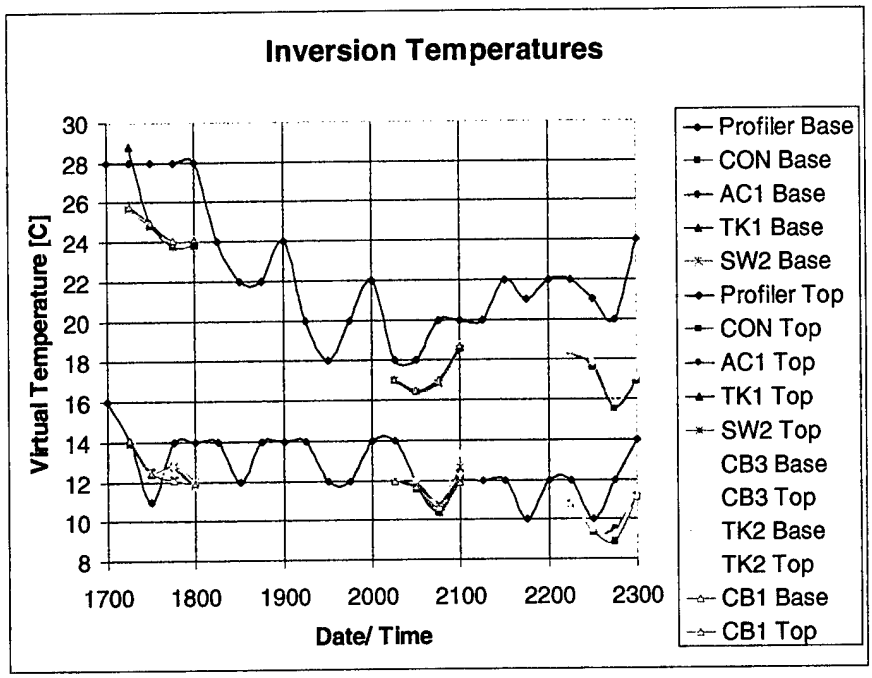

Figure 4-13: Inversion Temperature Comparison Plot

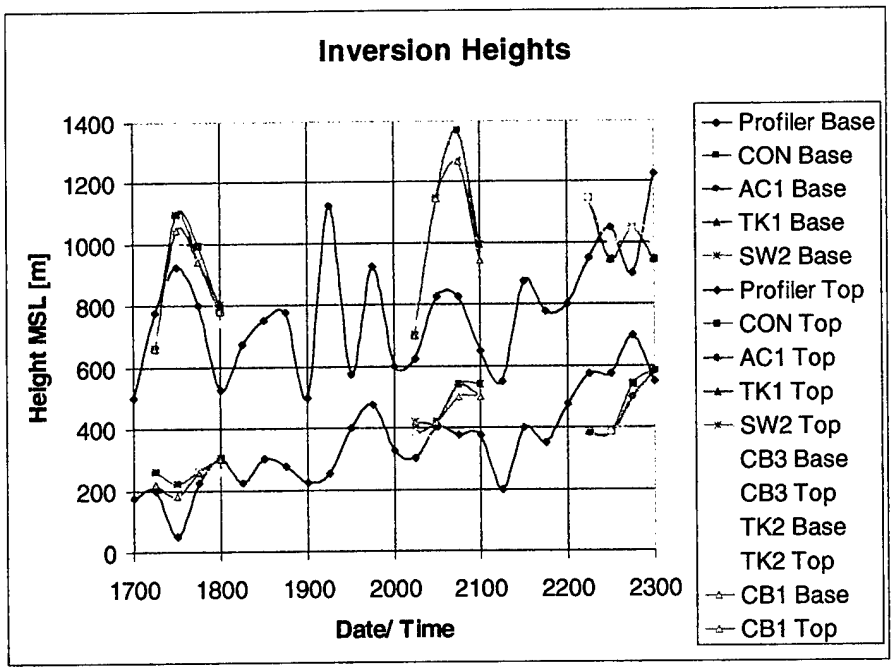

Figure 4-14: Inversion Height Comparison Plot

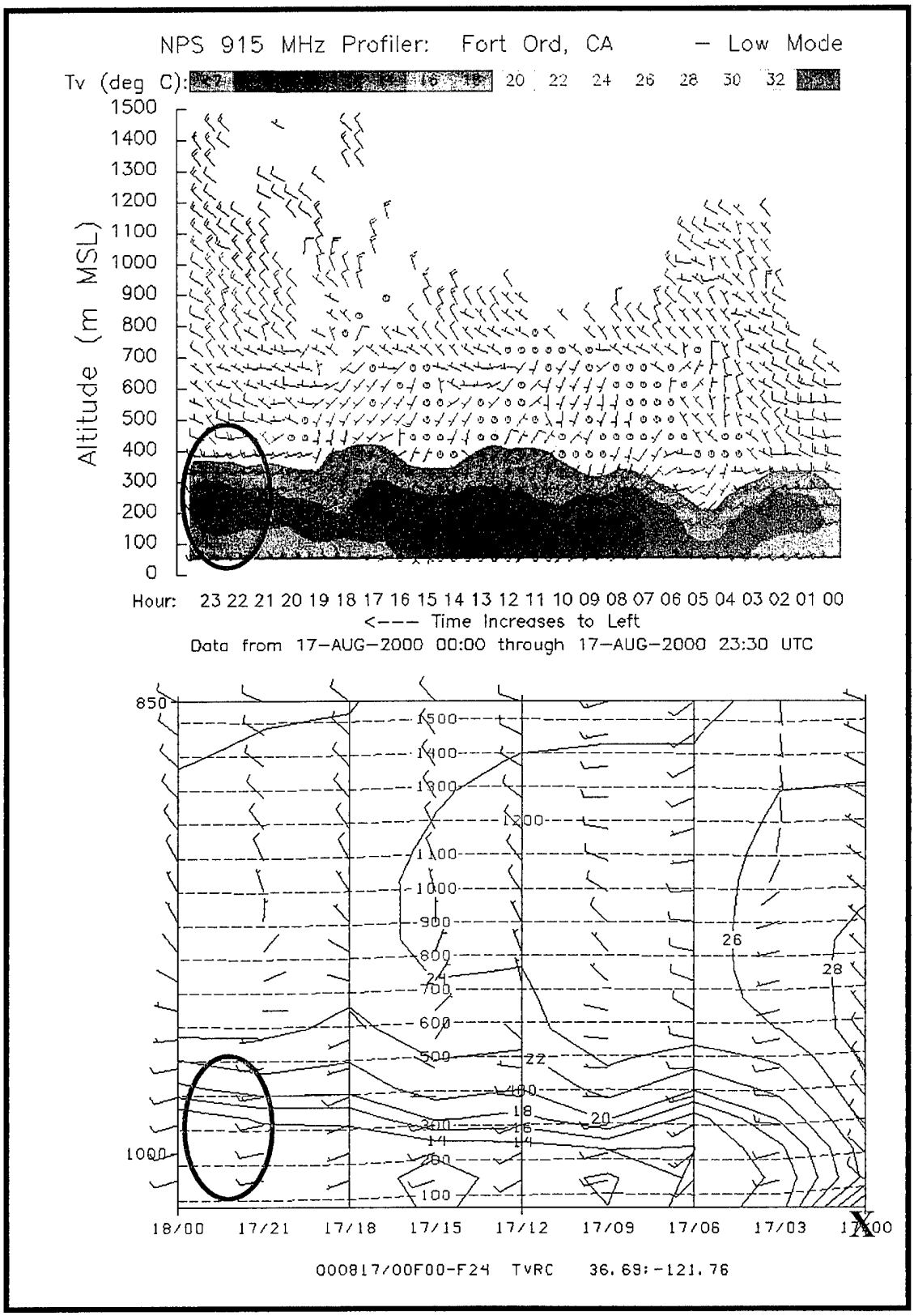

Figure 4-15: Profiler vs. CON Model on 17Aug

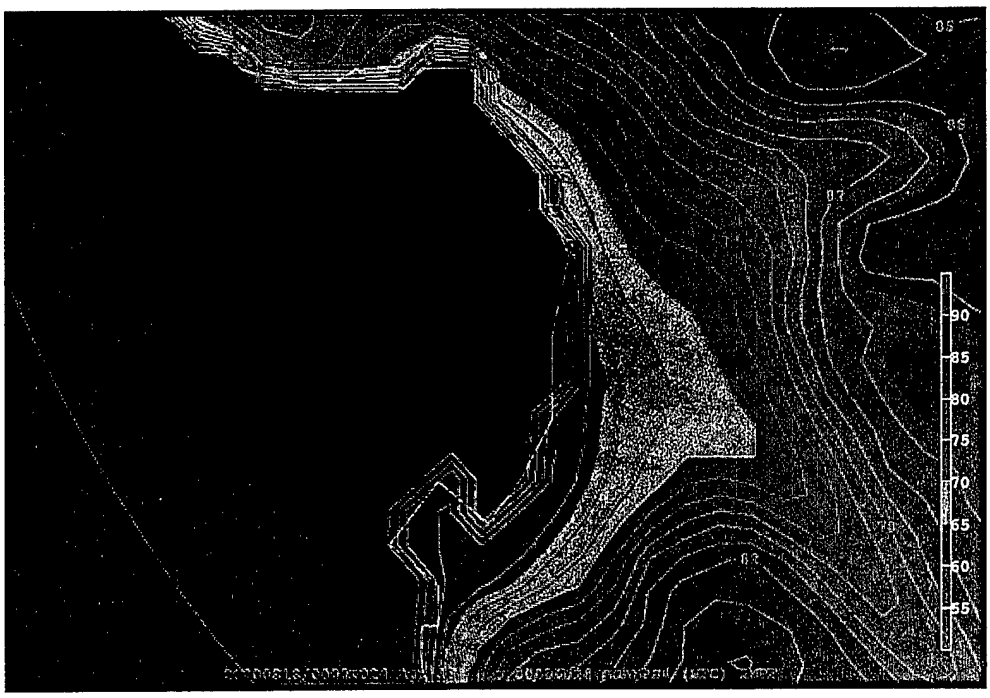

Figure 4-16: SST of the CON Model at 18/00Z

Figure 4-17: 10m Air Temperature of the CON Model at 18/00Z

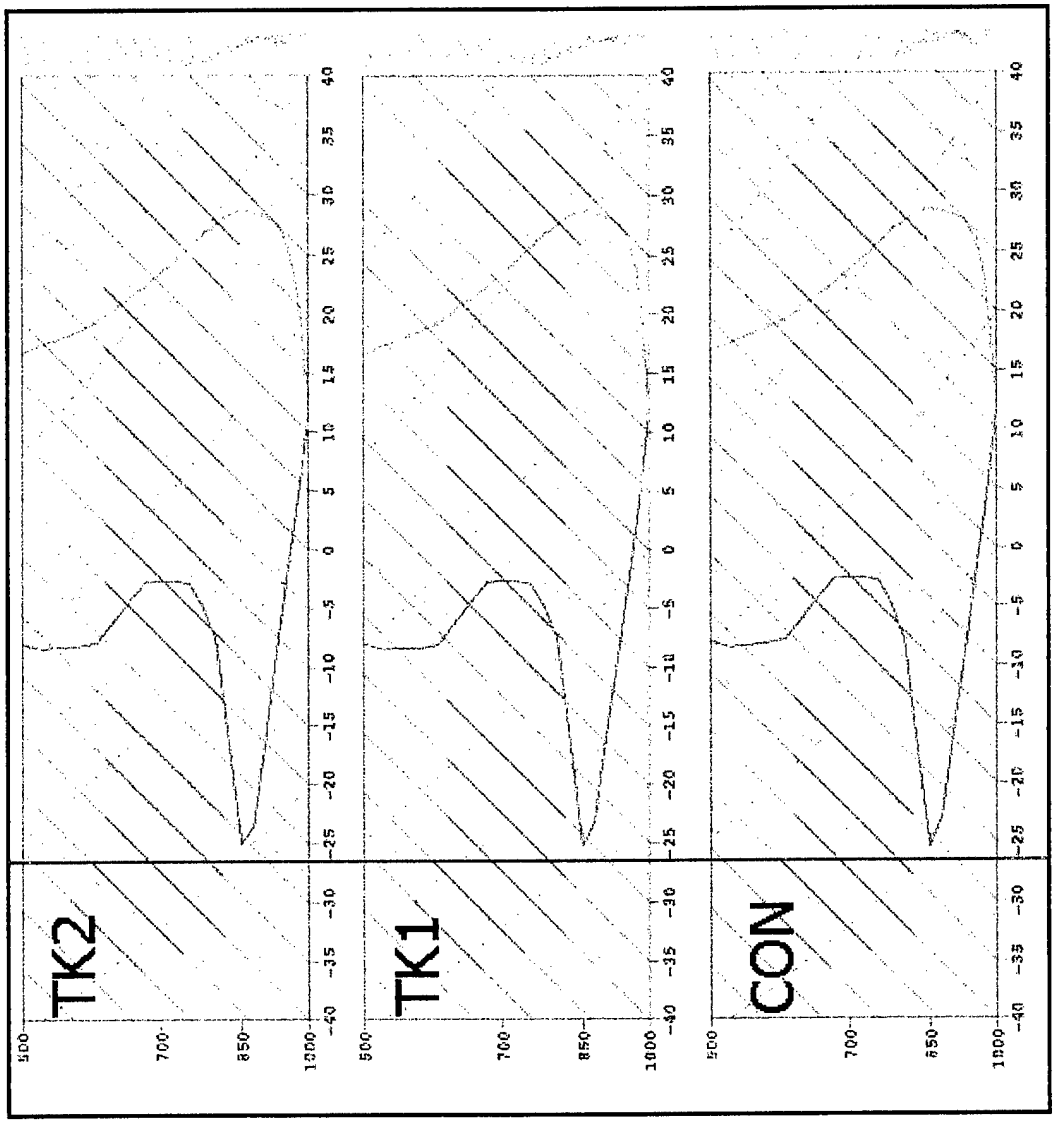

Figure 4-18: Skew-T Diagram Showing the Change from CON toTK1 to TK2

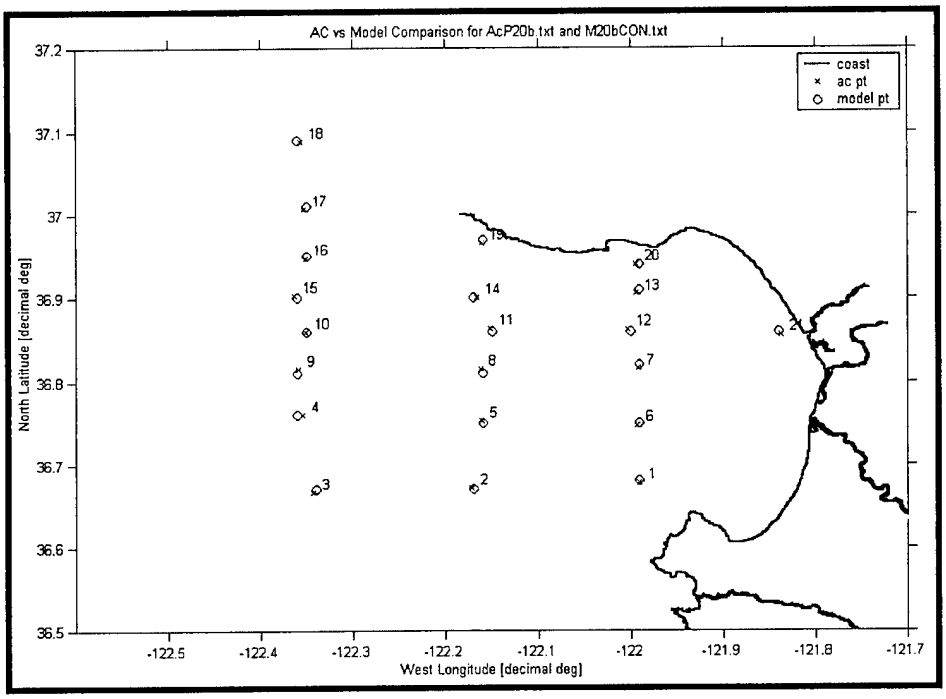

Figure 4-19: The Position of the Chosen Points for Flight 20b

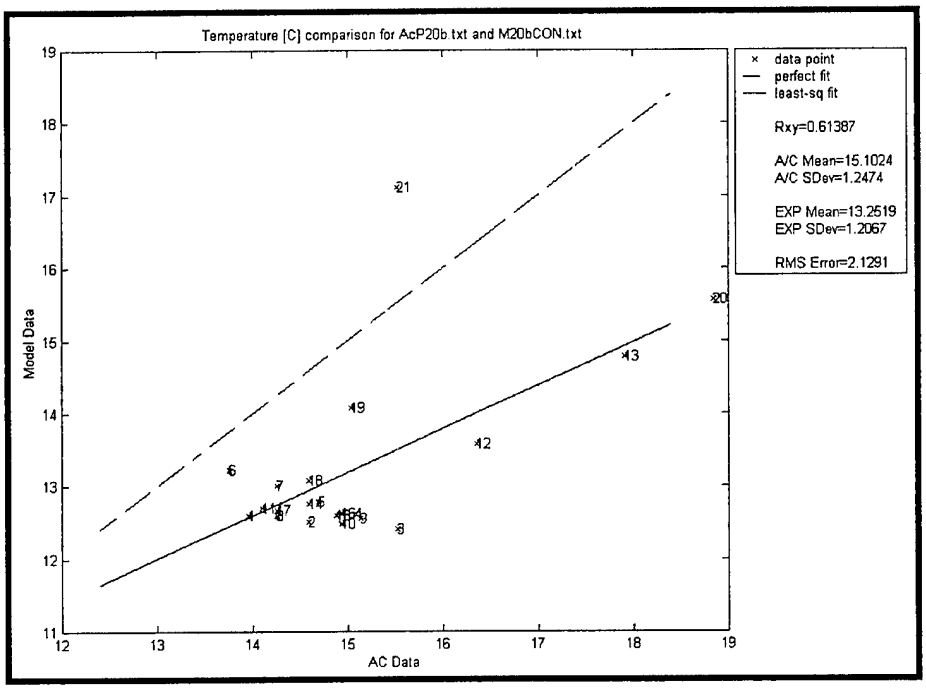

Figure 4-20: Correlation of Temperature Data, CON for Flight 20b

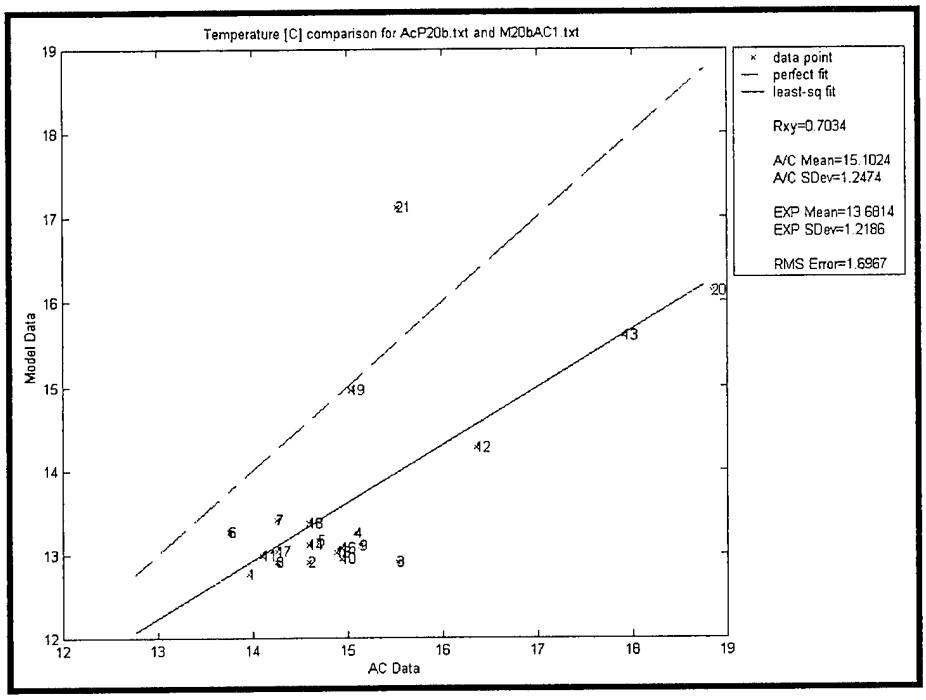

Figure 4-21: Correlation of Temperature Data, AC1 for Flight 20b

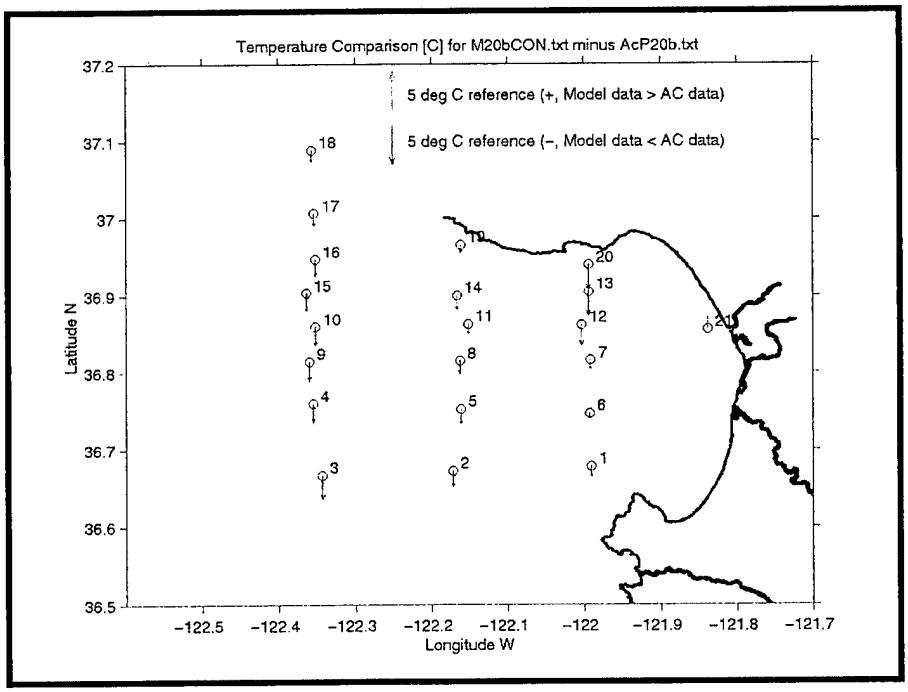

Figure 4-22: Temperature Difference Plot for CON and Flight 20b

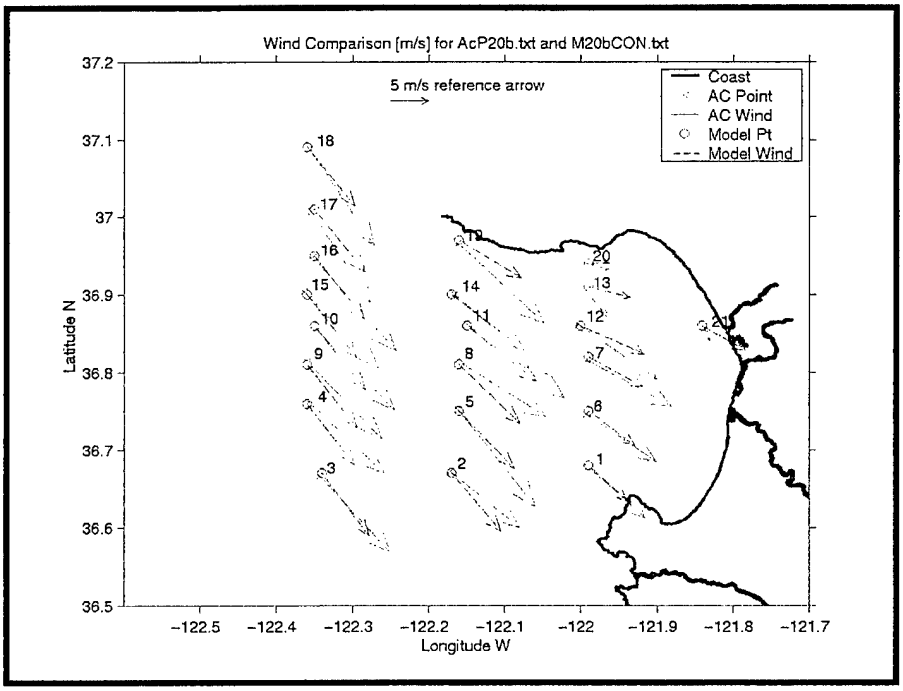

Figure 4-23: Wind Difference Plot for CON and Flight 20b

THIS PAGE INTENTIONALLY LEFT BLANK

APPENDIX C: ADDITIONAL FIGURES

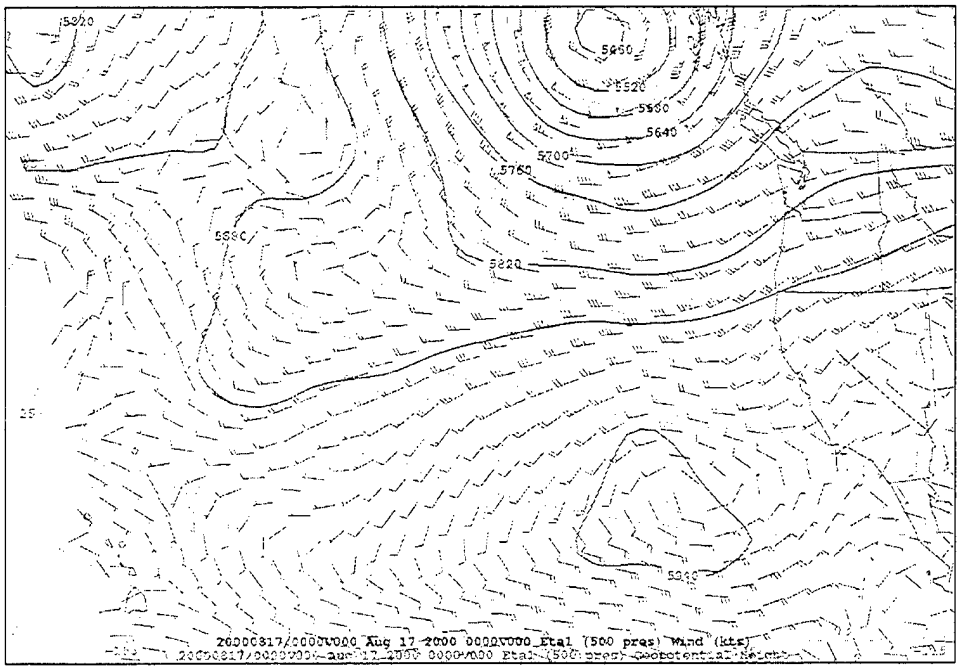

Figure C-1: The Synoptic Picture, ETA Model 500mb at 17/00Z

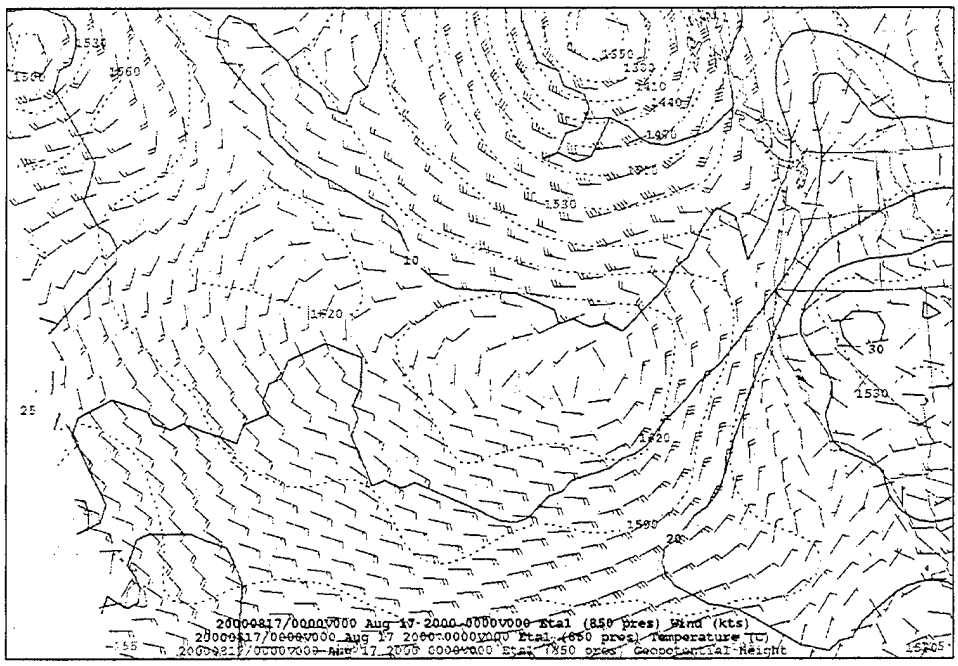

Figure C-2: The Synoptic Picture, ETA Model 850mb at 17/00Z

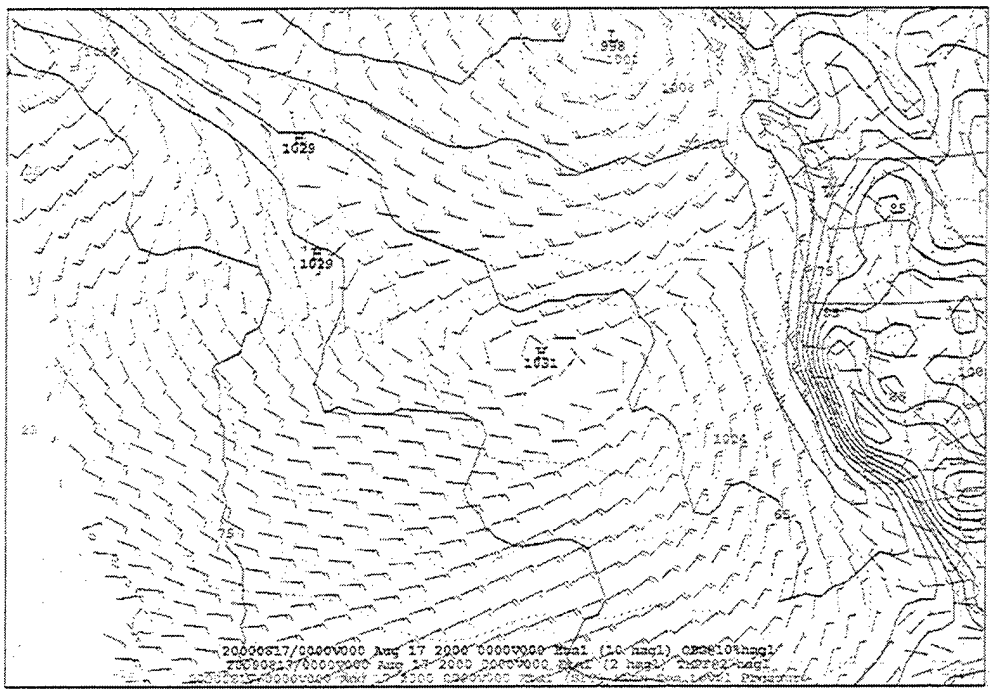

Figure C-3: The Synoptic Picture, ETA Model SFC at 17/00Z

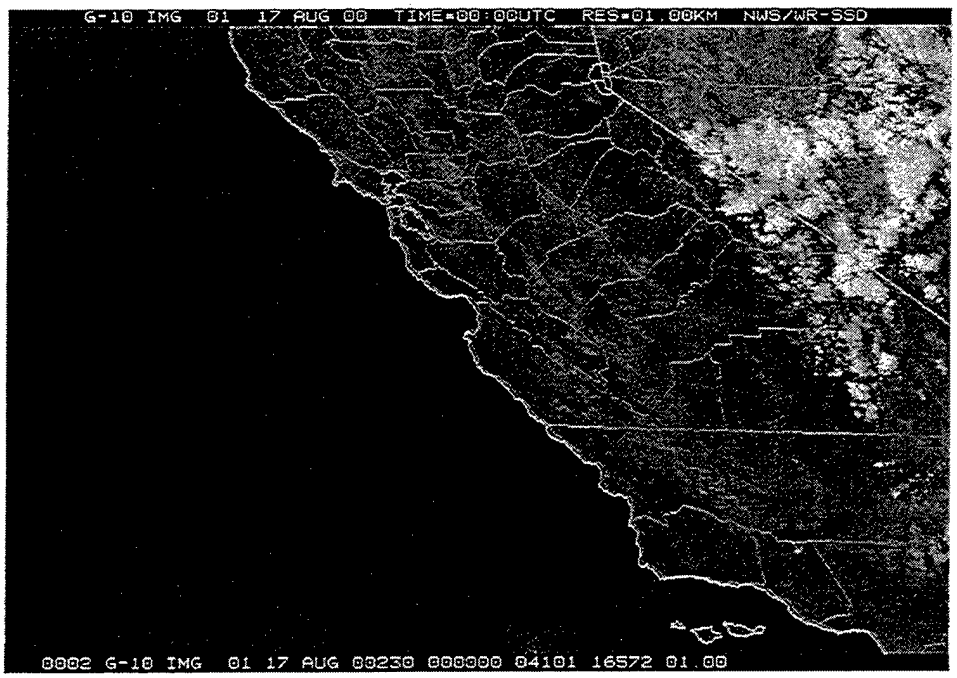

Figure C-4: The Synoptic Picture, GOES-10 1m Vis. Image at 17/00Z

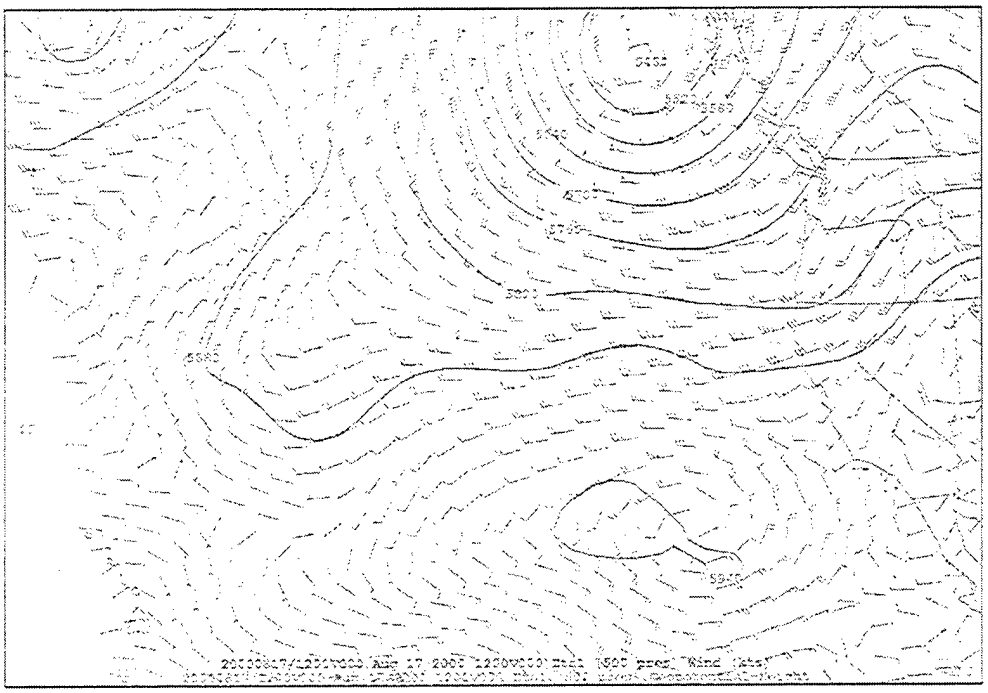

Figure C-5: The Synoptic Picture, ETA Model 500mb at 17/12Z

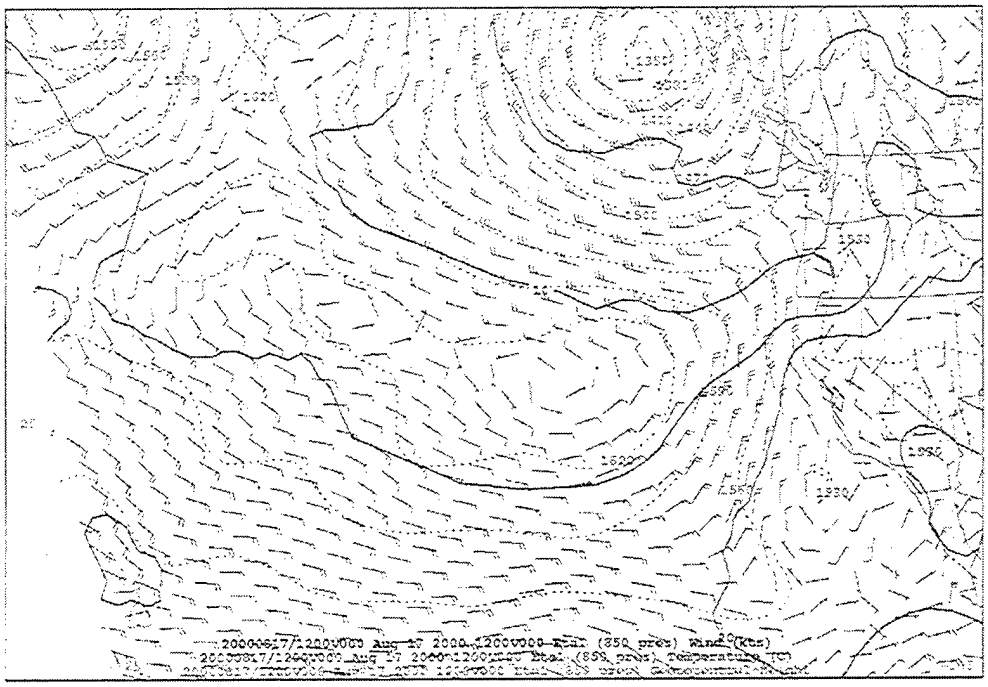

Figure C-6: The Synoptic Picture, ETA Model 850mb at 17/12Z

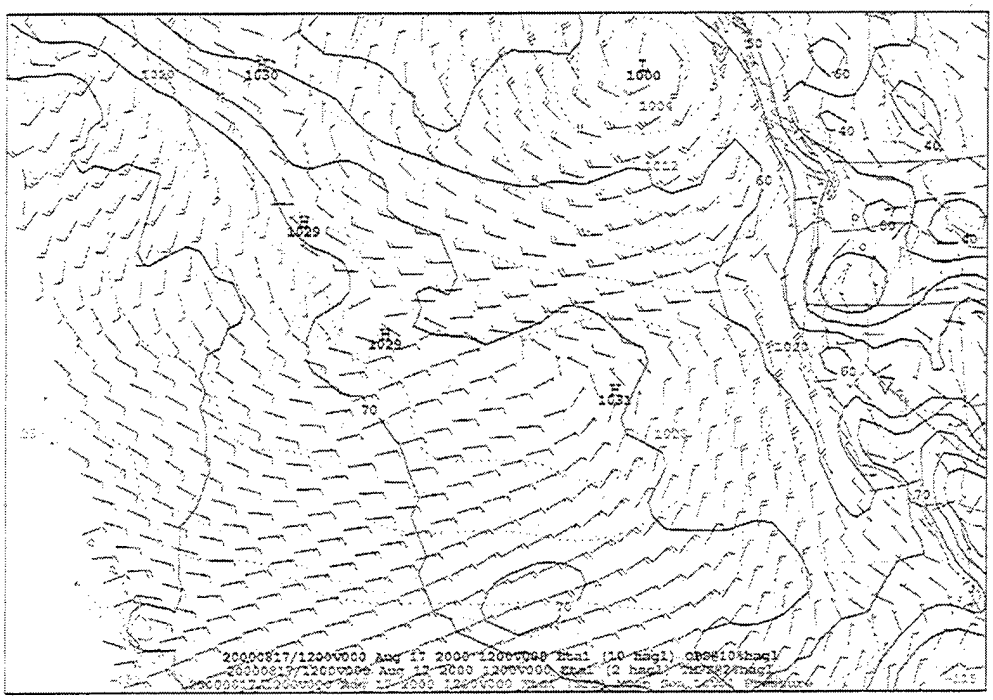

Figure C-7: The Synoptic Picture, ETA Model SFC at 17/12Z

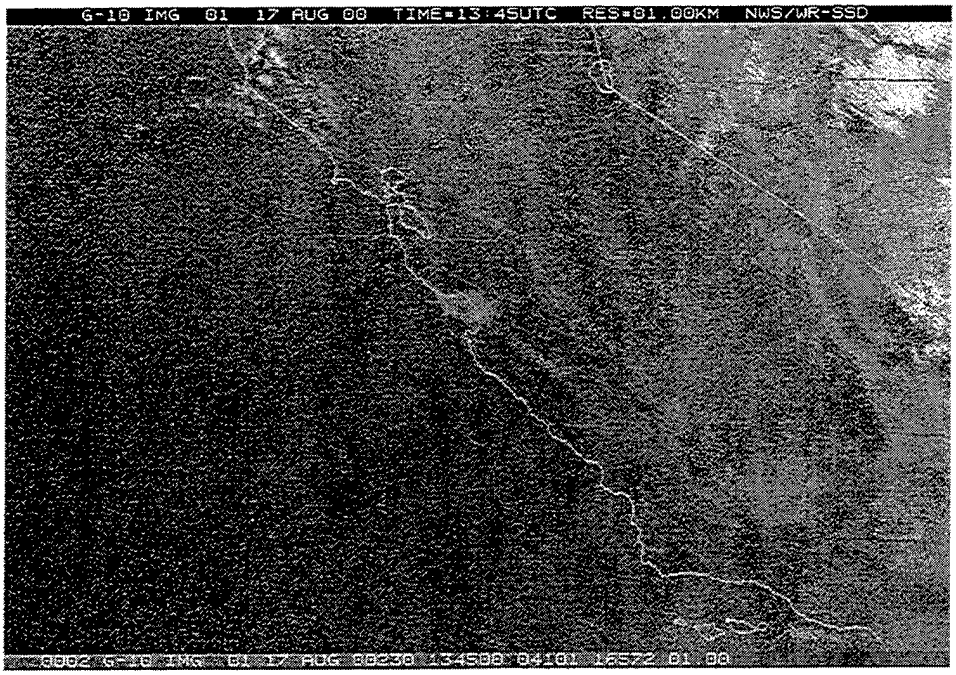

Figure C-8: The Synoptic Picture, GOES-10 1m Vis. Image at 17/1345Z

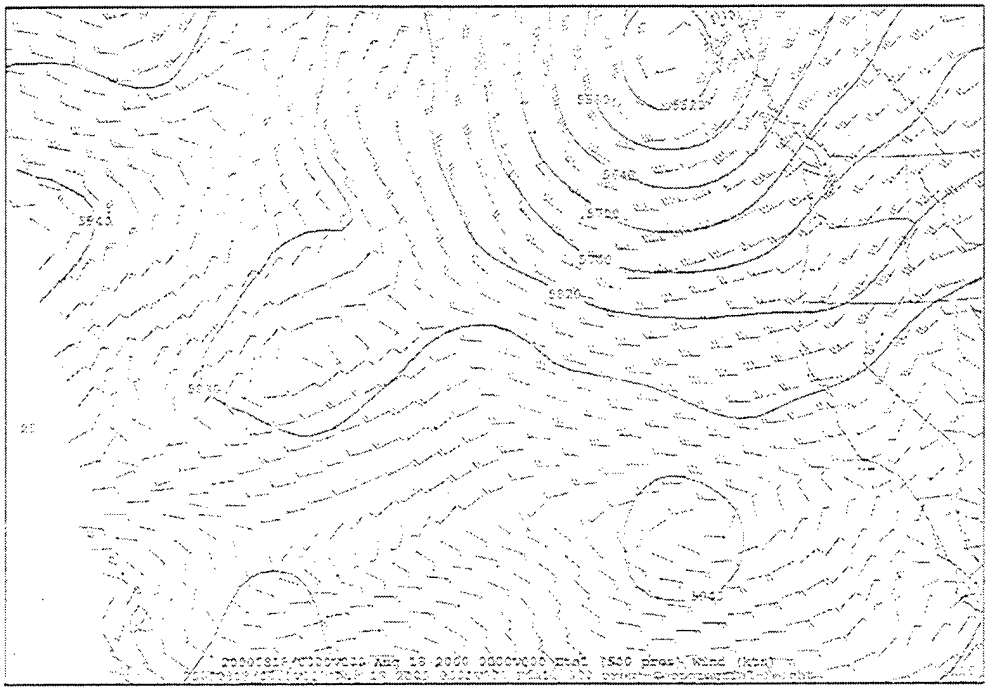

Figure C-9: The Synoptic Picture, ETA Model 500mb at 18/00Z

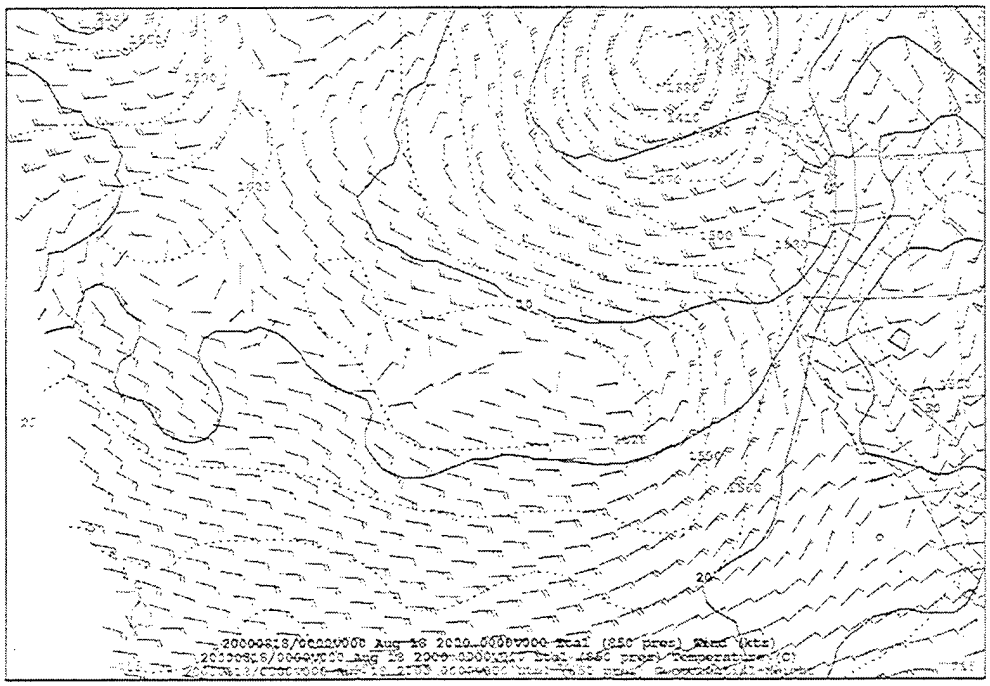

Figure C-10: The Synoptic Picture, ETA Model 850mb at 18/00Z

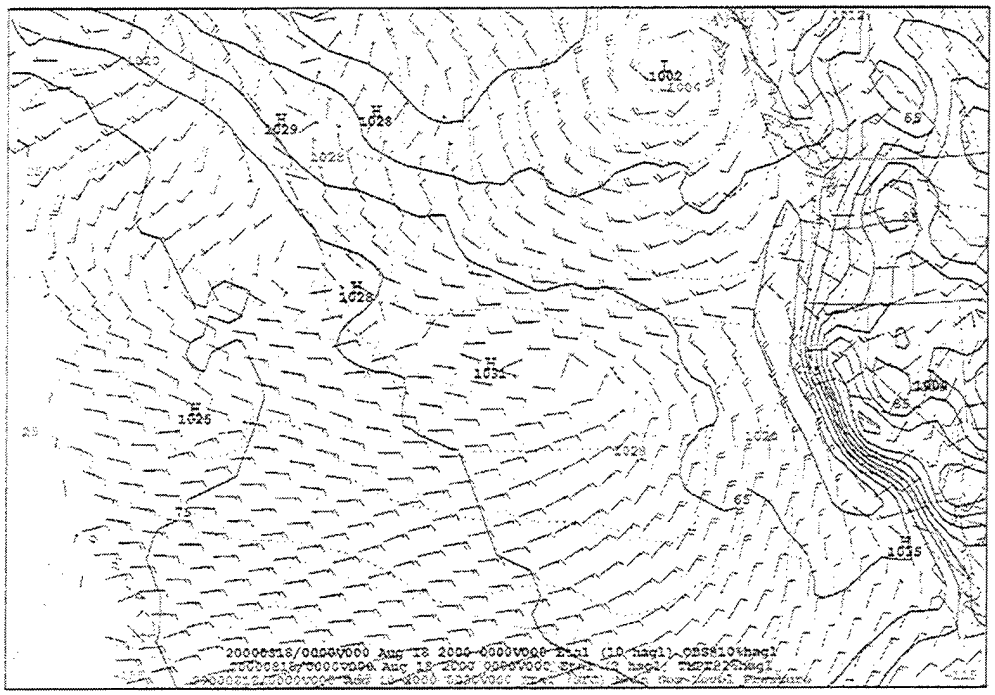

Figure C-11: The Synoptic Picture, ETA Model SFC at 18/00Z

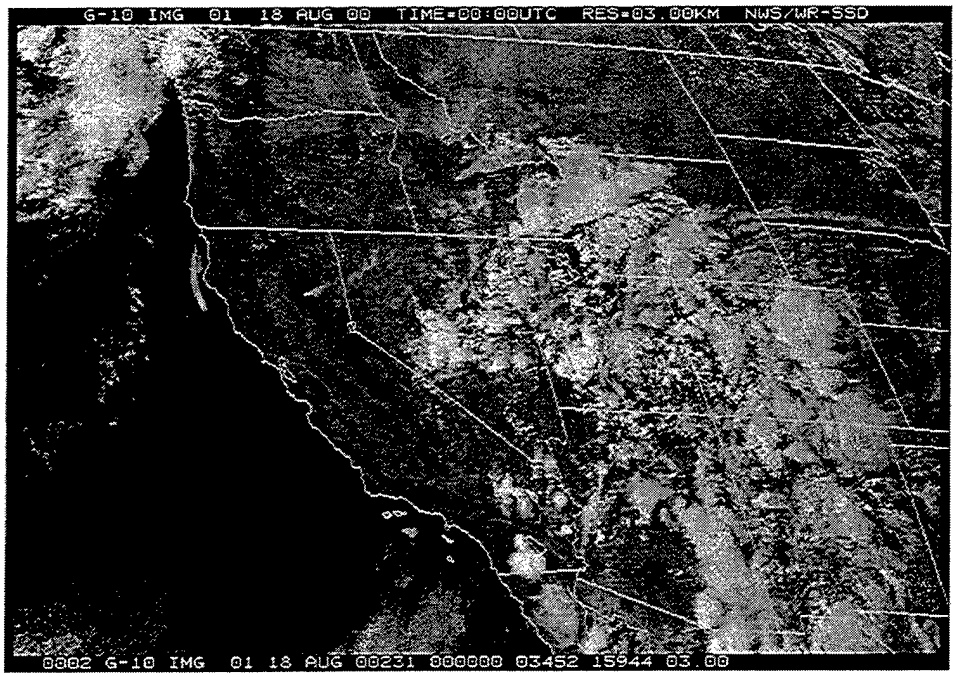

Figure C-12: The Synoptic Picture, GOES-10 1m Vis. Image at 18/00Z

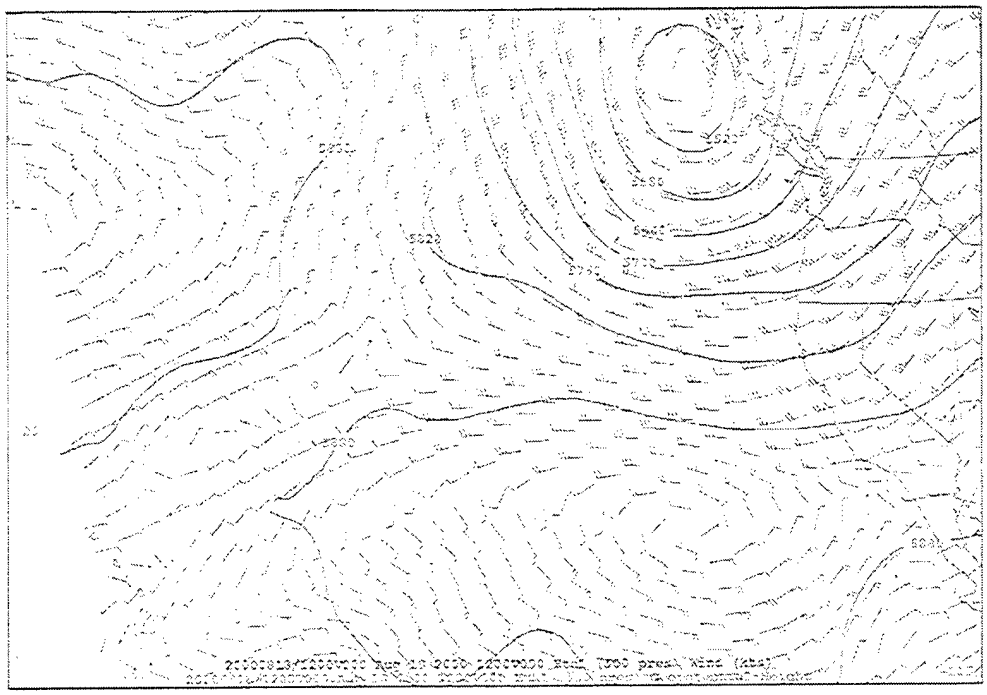

Figure C-13: The Synoptic Picture, ETA Model 500mb at 18/12Z

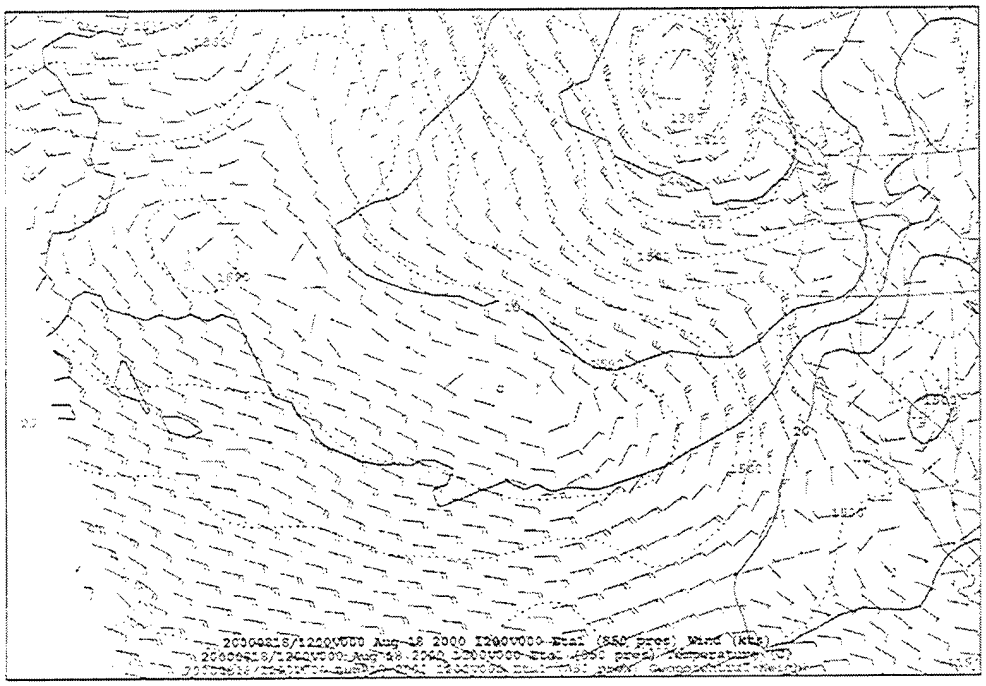

Figure C-14: The Synoptic Picture, ETA Model 850mb at 18/12Z

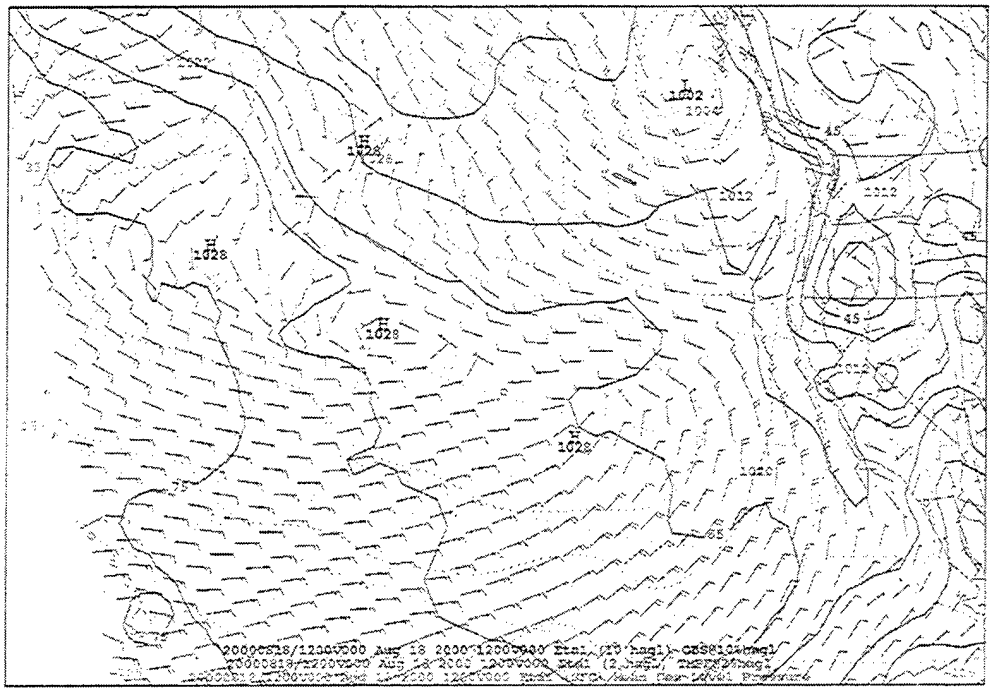

Figure C-15: The Synoptic Picture, ETA Model SFC at 18/12Z

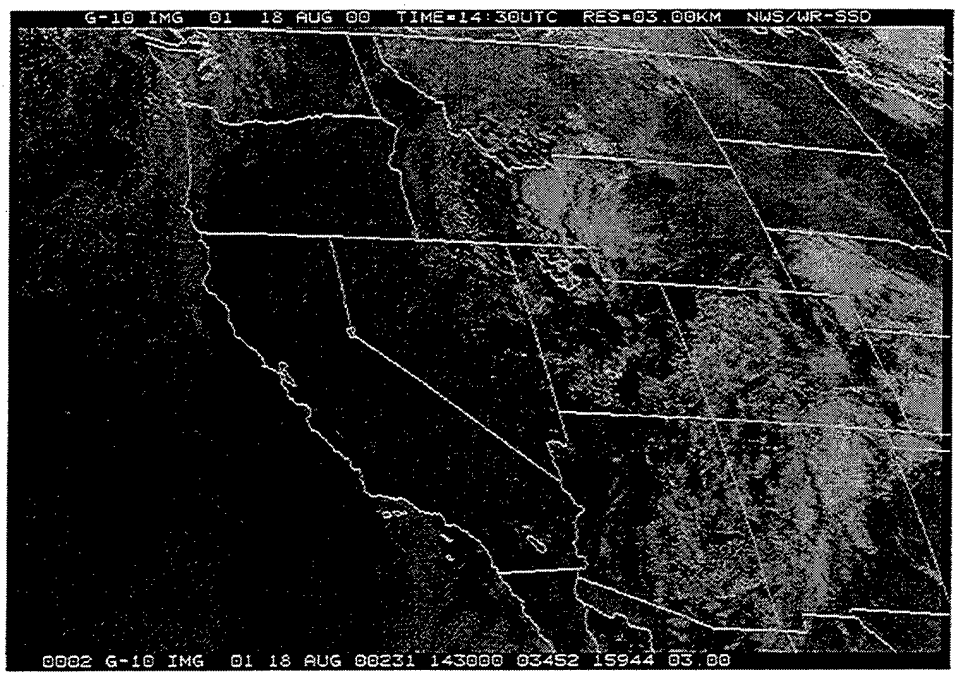

Figure C-16: The Synoptic Picture, GOES-10 1m Vis. Image at 18/1430Z

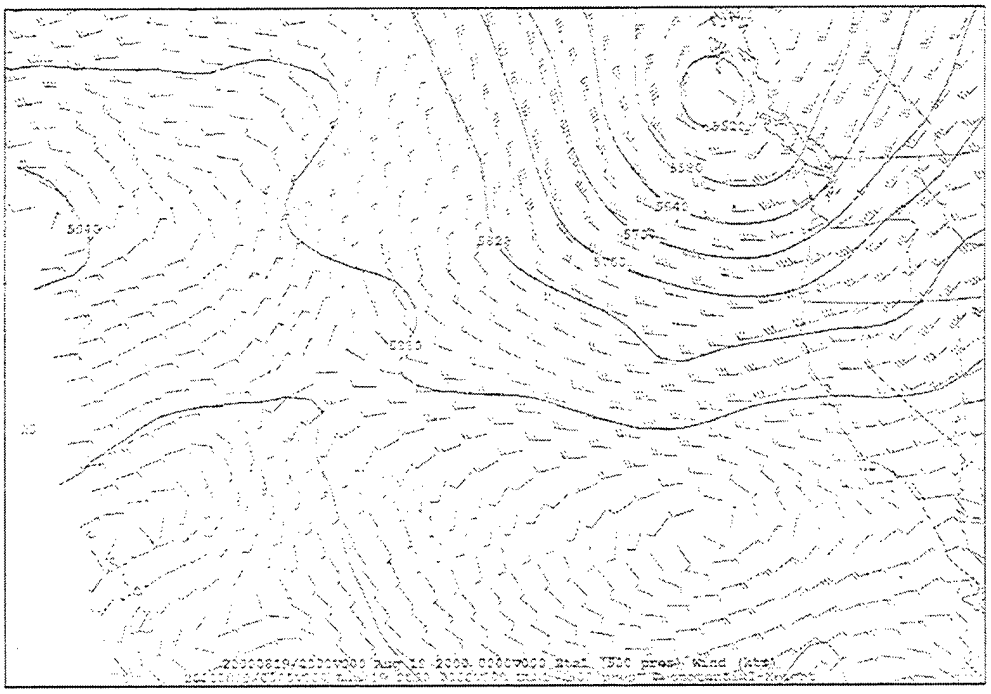

Figure C-17: The Synoptic Picture, ETA Model 500mb at 19/00Z

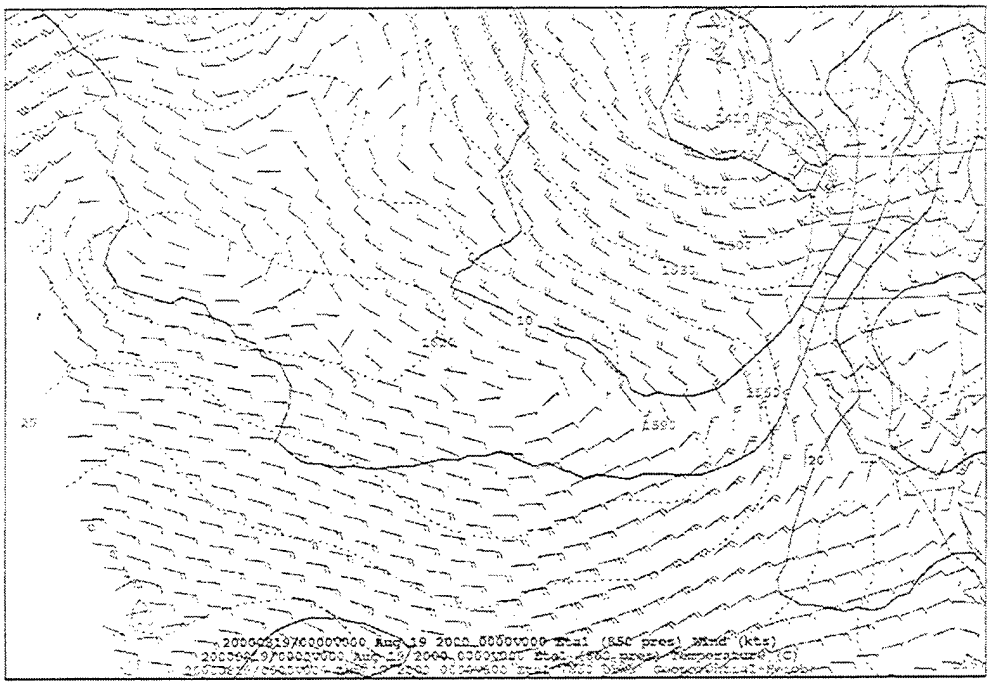

Figure C-18: The Synoptic Picture, ETA Model 850mb at 19/00Z

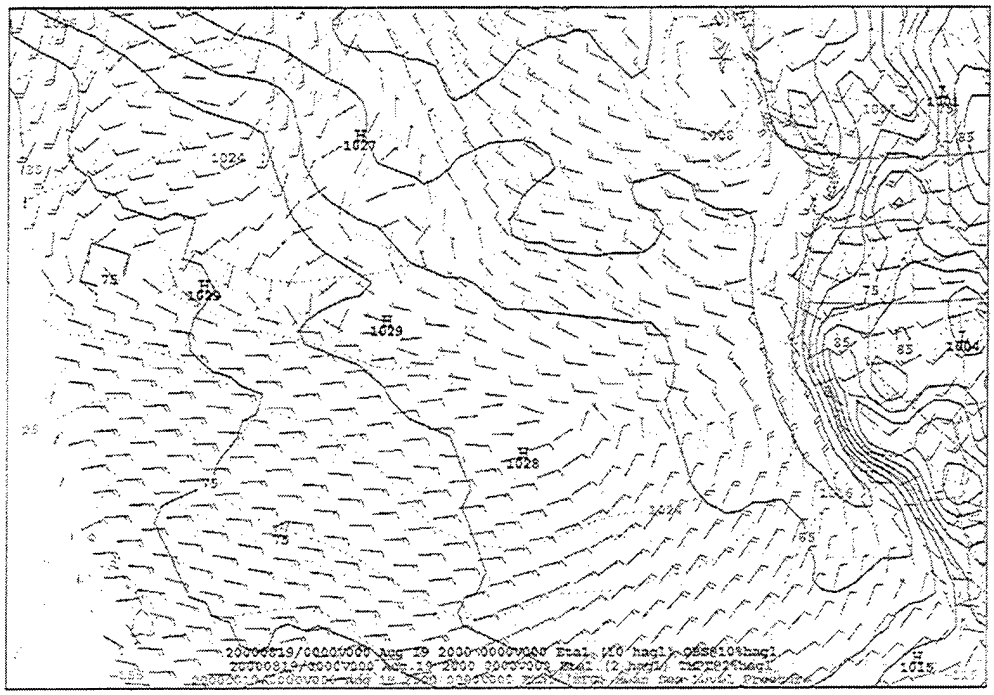

Figure C-19: The Synoptic Picture, ETA Model SFC at 19/00Z

IMAGE NOT AVAILABLE

Figure C-20: The Synoptic Picture, GOES-10 1m Vis. Image at 19/00Z

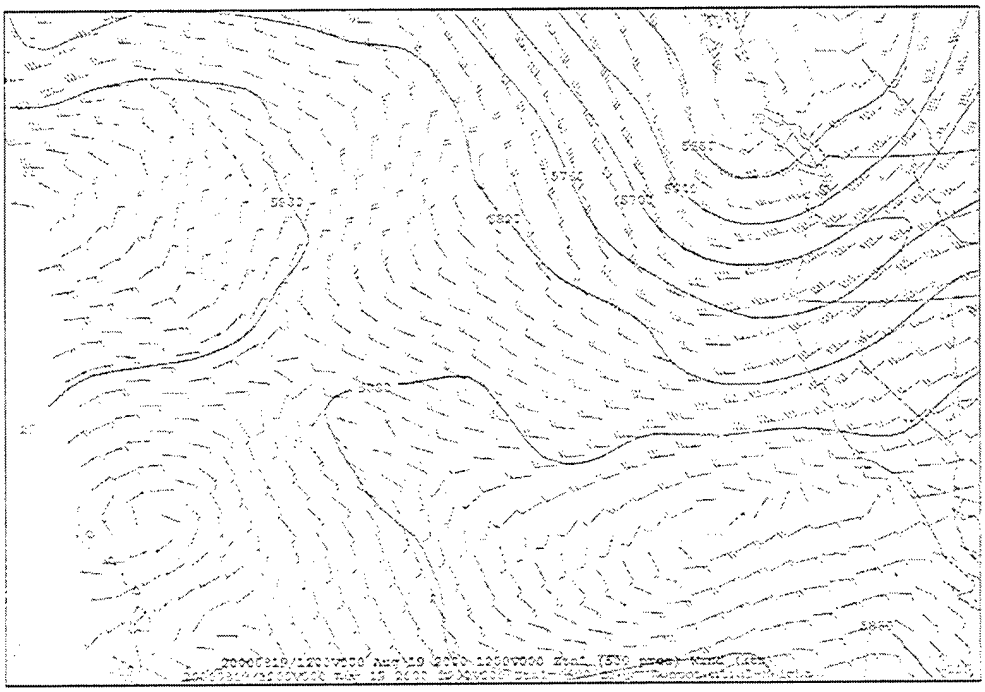

Figure C-21: The Synoptic Picture, ETA Model 500mb at 19/12Z

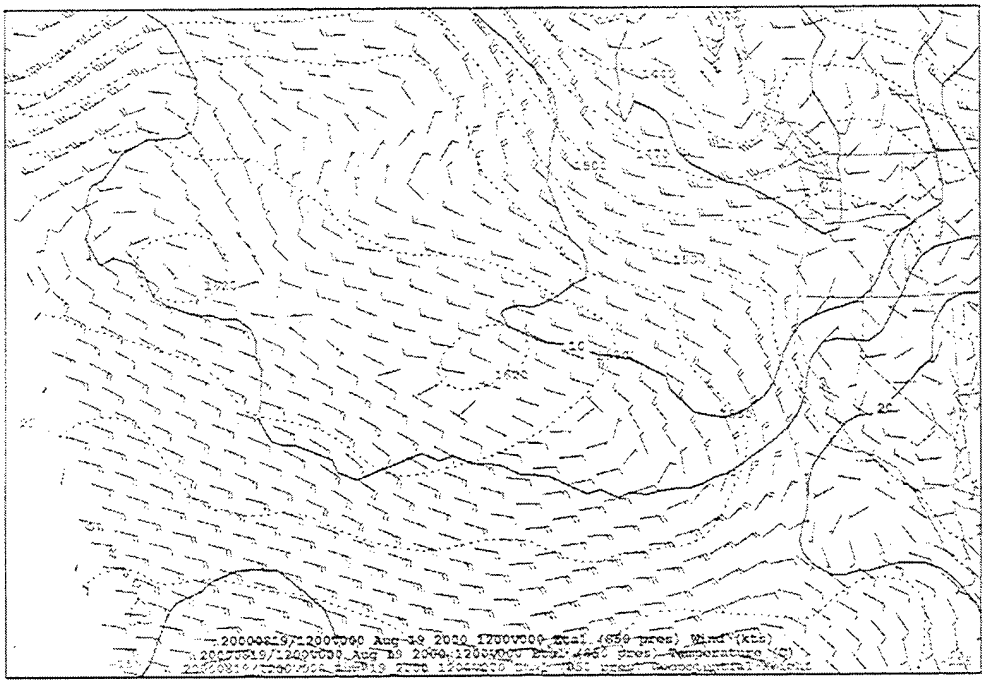

Figure C-22: The Synoptic Picture, ETA Model 850mb at 1912Z

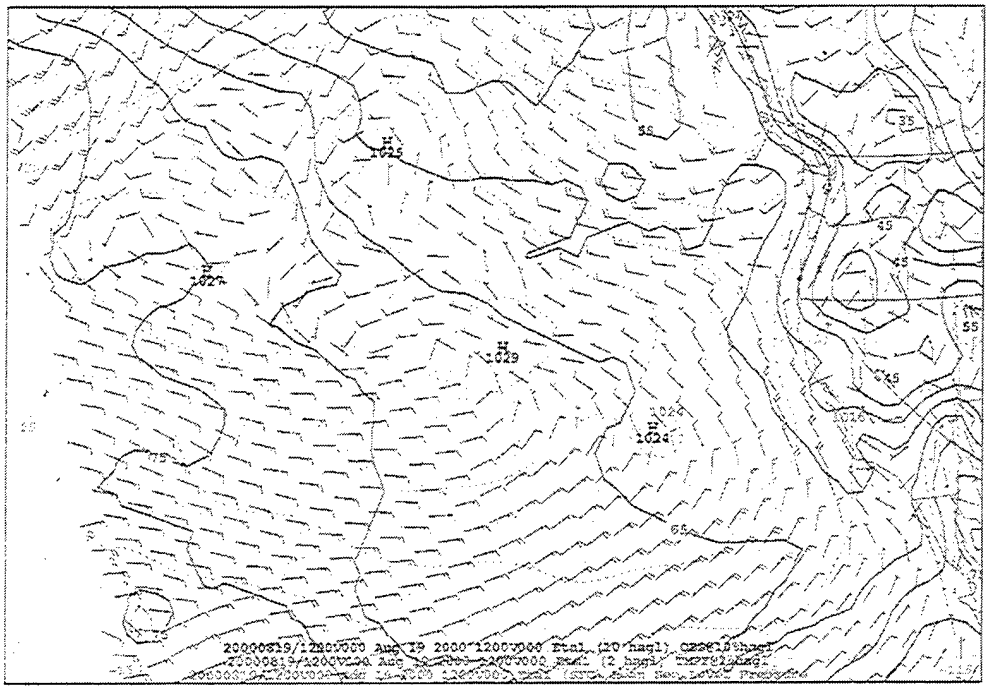

Figure C-23: The Synoptic Picture, ETA Model SFC at 19/12Z

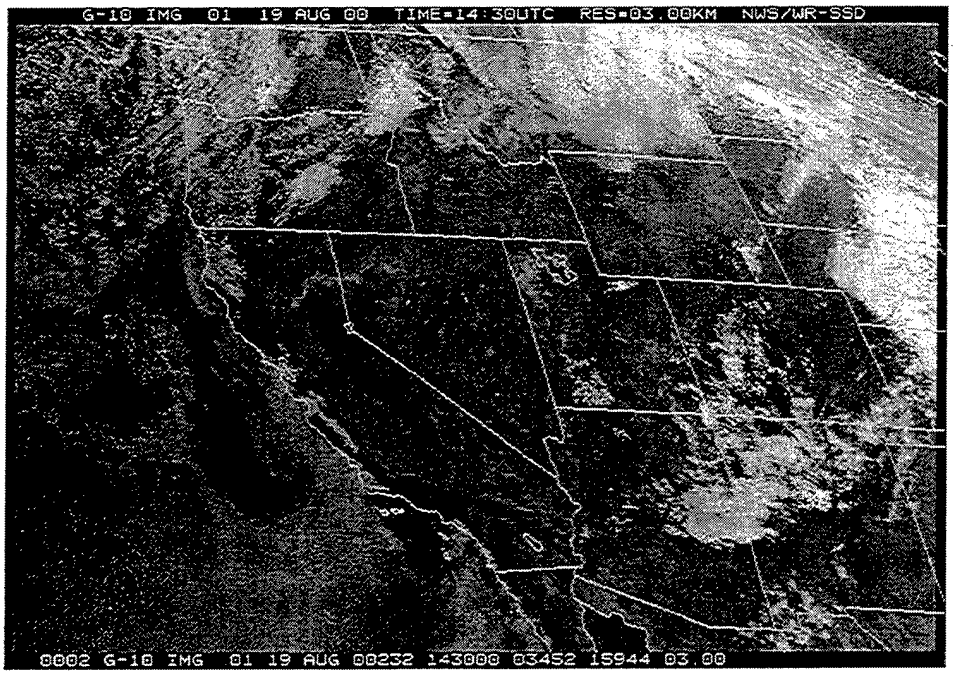

Figure C-24: The Synoptic Picture, GOES-10 1m Vis. Image at 19/1430Z

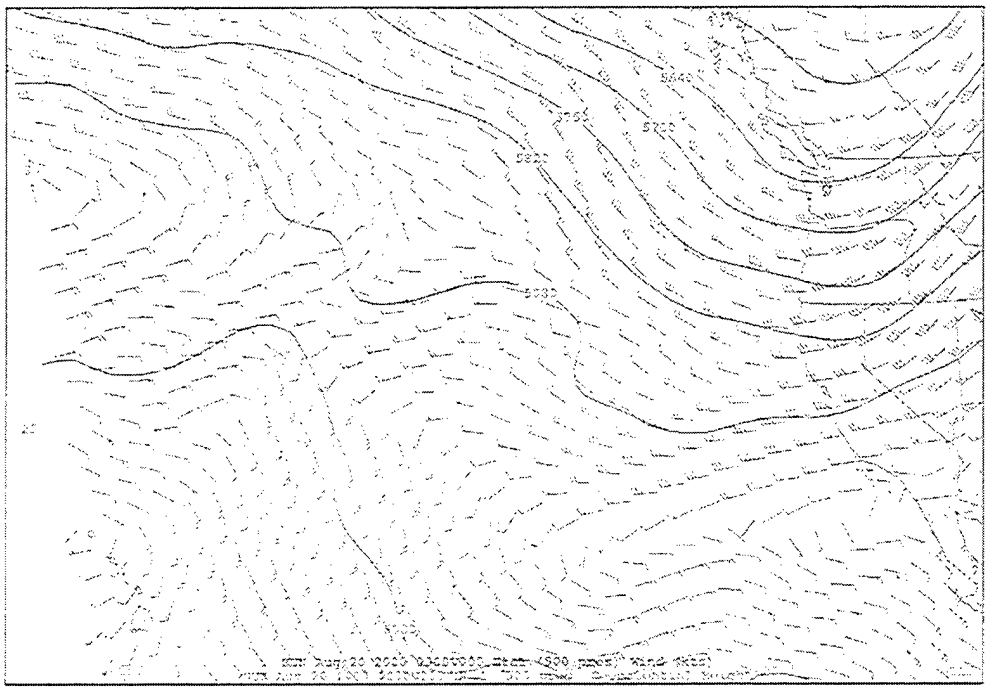

Figure C-25: The Synoptic Picture, ETA Model 500mb at 20/00Z

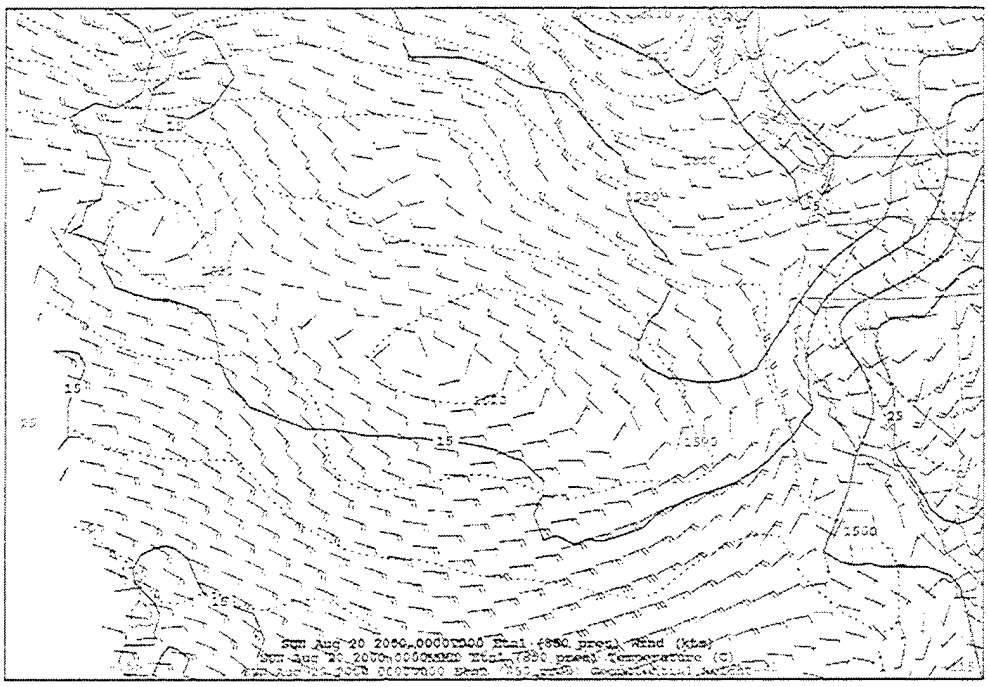

Figure C-26: The Synoptic Picture, ETA Model 850mb at 20/00Z

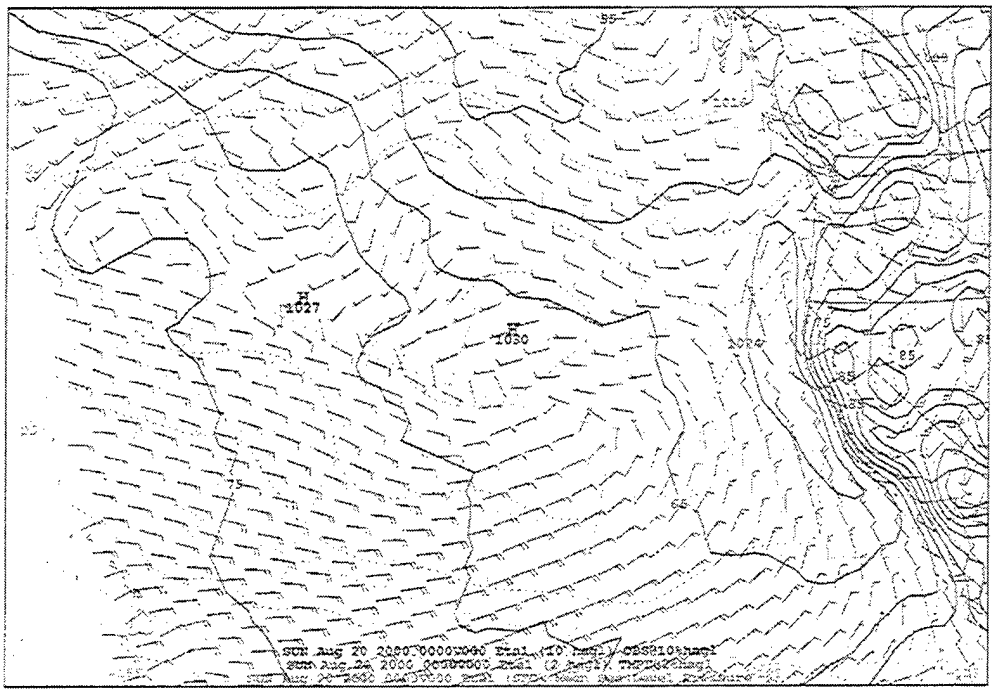

Figure C-27: The Synoptic Picture, ETA Model SFC at 20/00Z

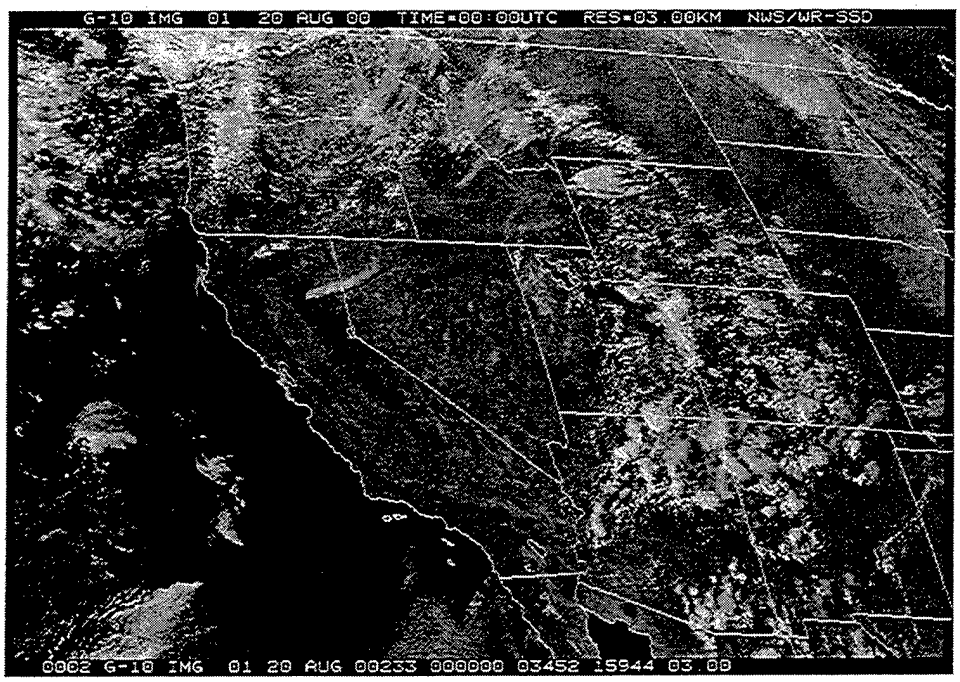

Figure C-28: The Synoptic Picture, GOES-10 1m Vis. Image at 20/00Z

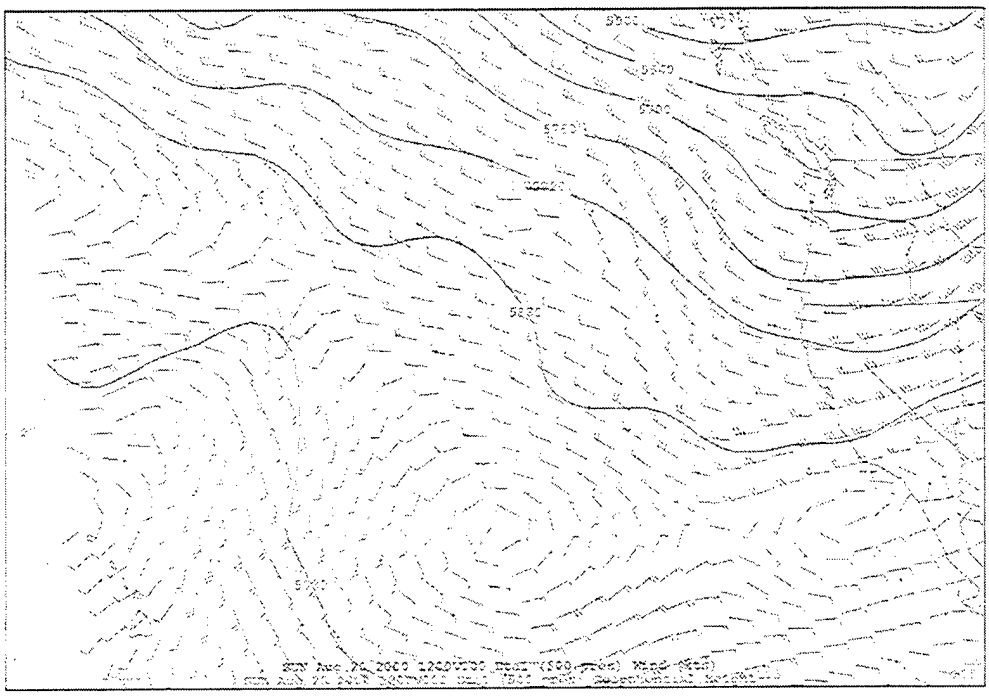

Figure C-29: The Synoptic Picture, ETA Model 500mb at 20/12Z

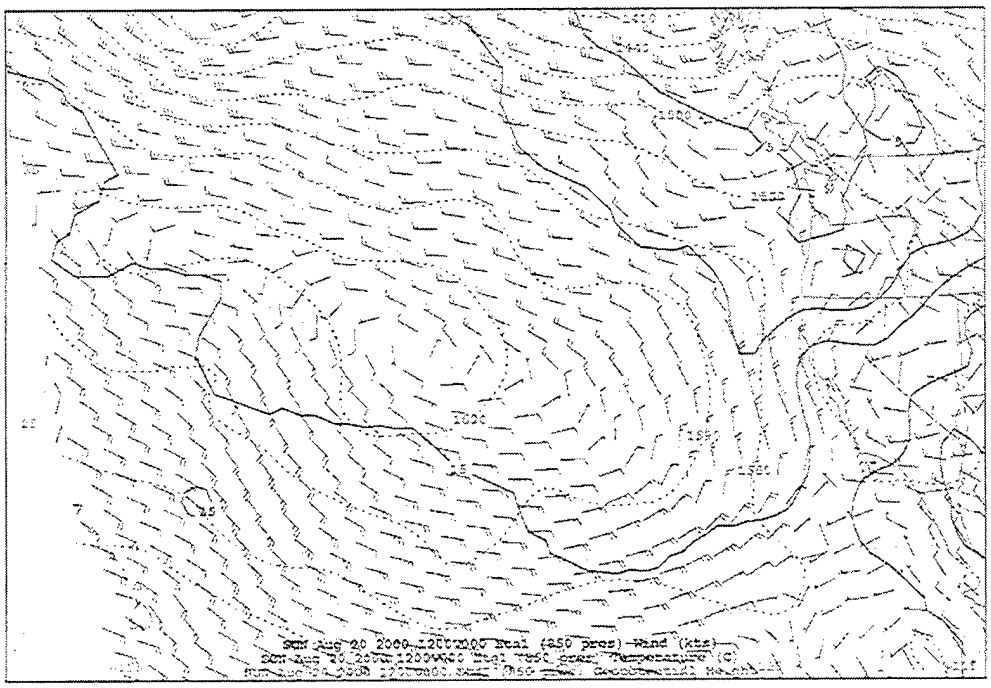

Figure C-30: The Synoptic Picture, ETA Model 850mb at 20/12Z

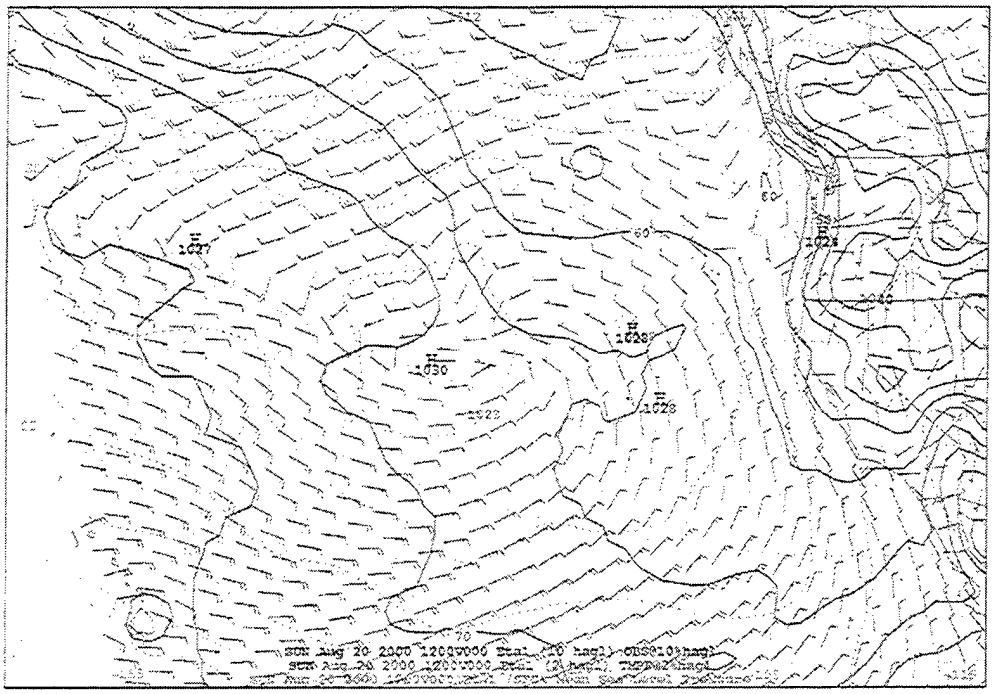

Figure C-31: The Synoptic Picture, ETA Model SFC at 20/12Z

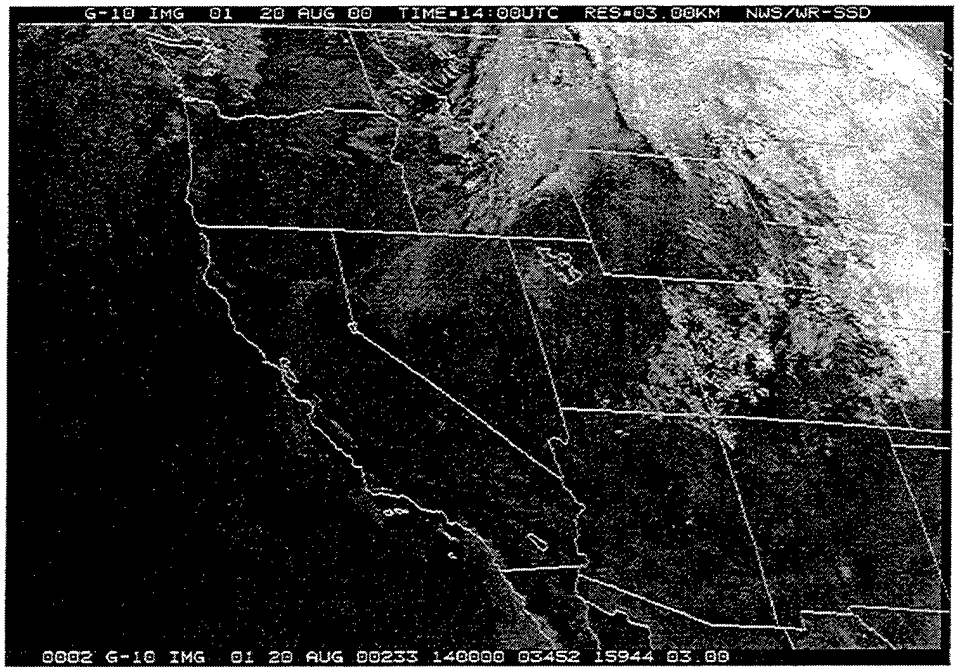

Figure C-32: The Synoptic Picture, GOES-10 1m Vis. Image at 20/1400Z

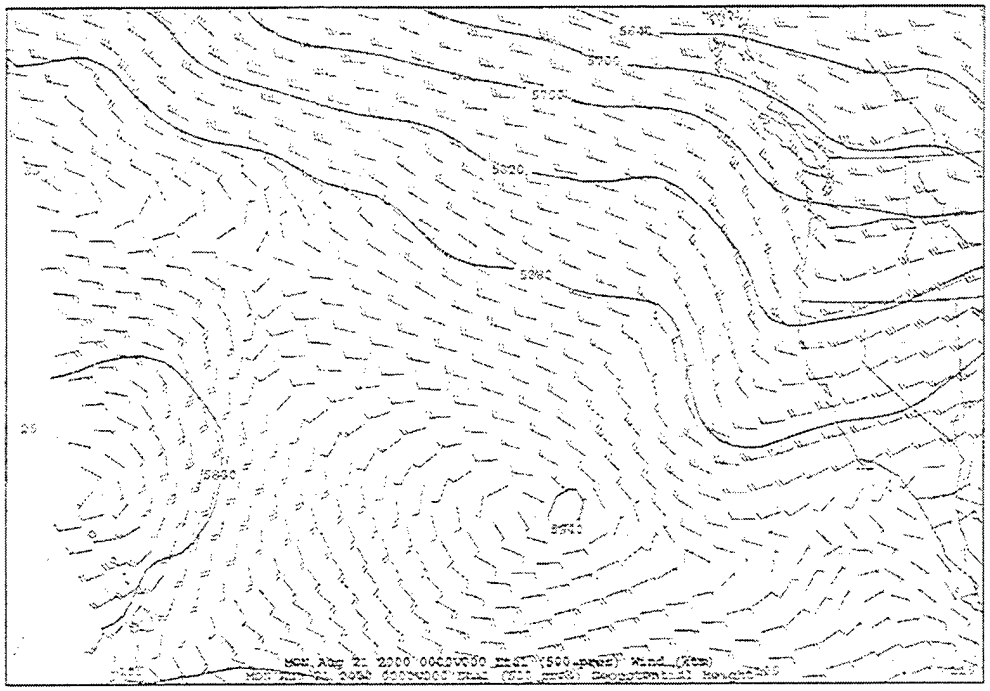

Figure C-33: The Synoptic Picture, ETA Model 500mb at 21/00Z

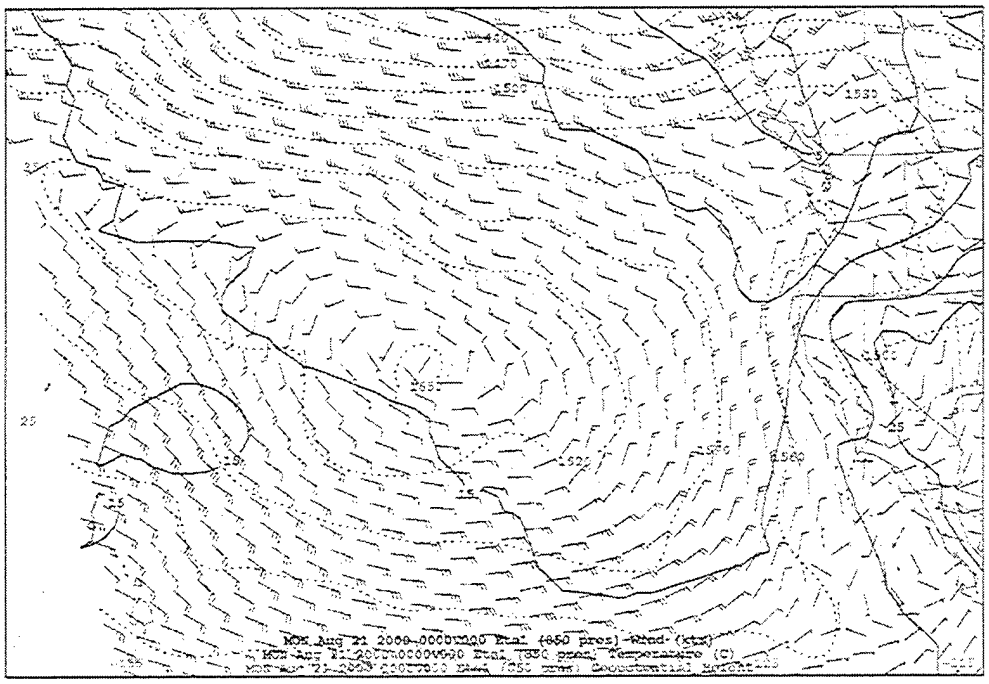

Figure C-34: The Synoptic Picture, ETA Model 850mb at 21/00Z

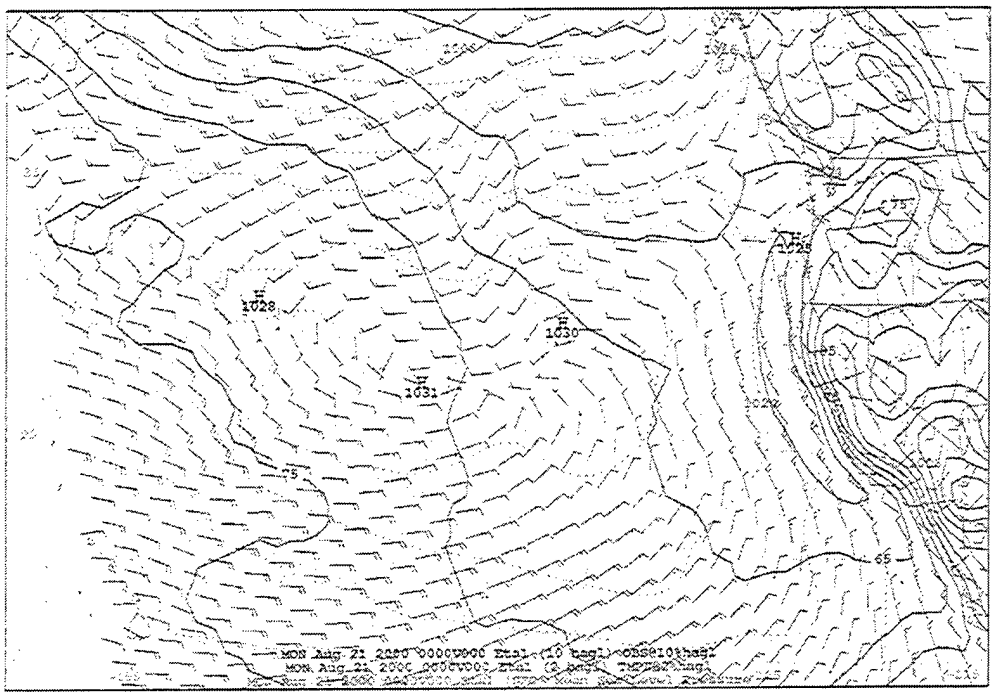

Figure C-35: The Synoptic Picture, ETA Model SFC at 21/00Z

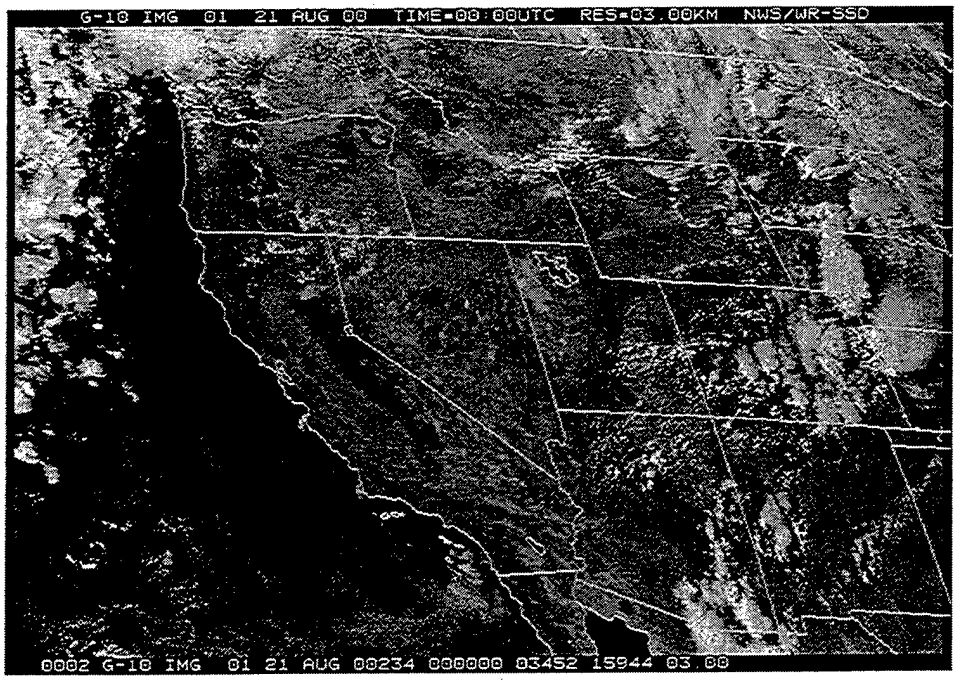

Figure C-36: The Synoptic Picture, GOES-10 1m Vis. Image at 21/00Z

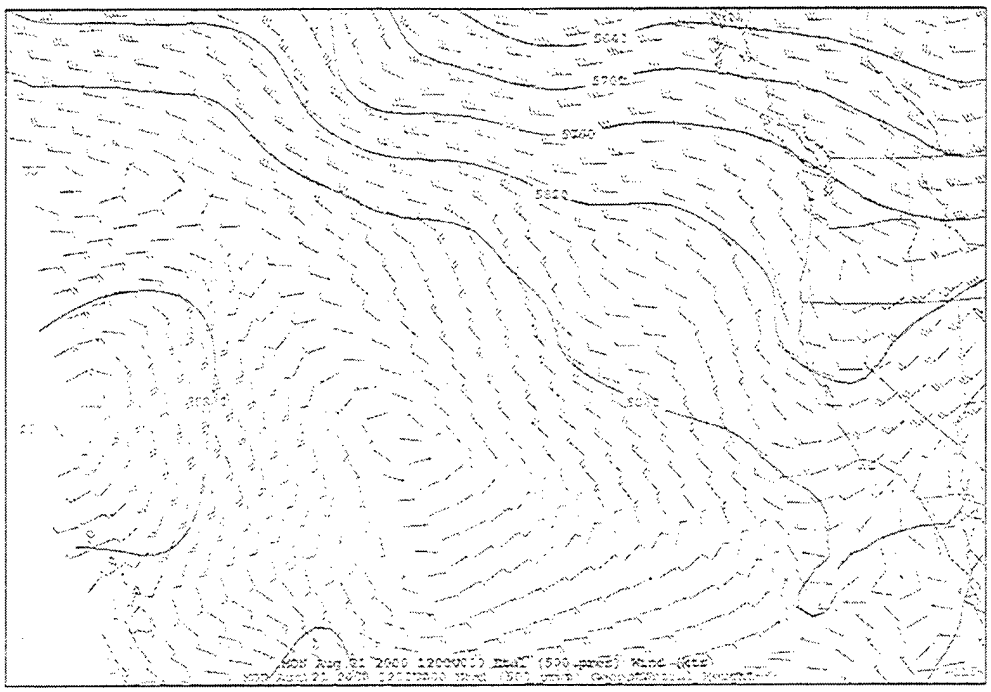

Figure C-37: The Synoptic Picture, ETA Model 500mb at 21/12Z

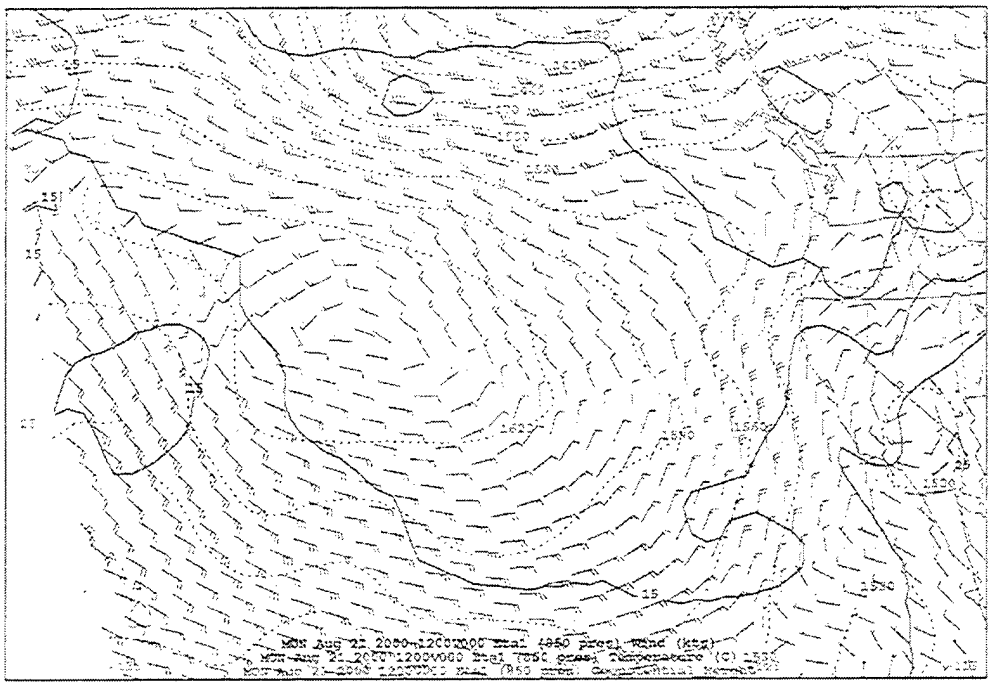

Figure C-38: The Synoptic Picture, ETA Model 850mb at 21/12Z

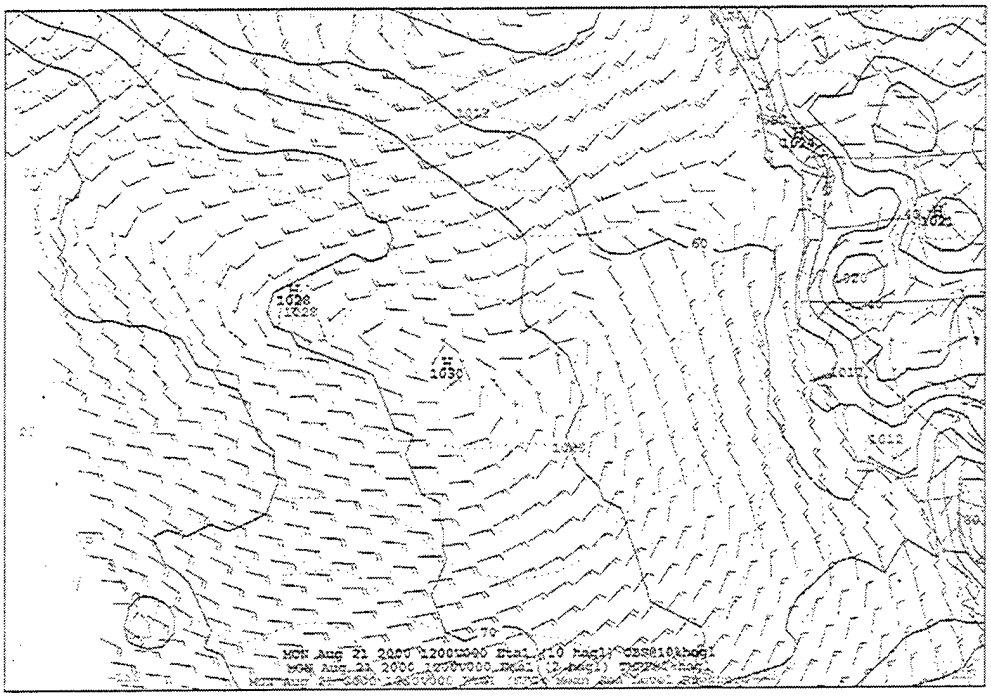

Figure C-39: The Synoptic Picture, ETA Model SFC at 21/12Z

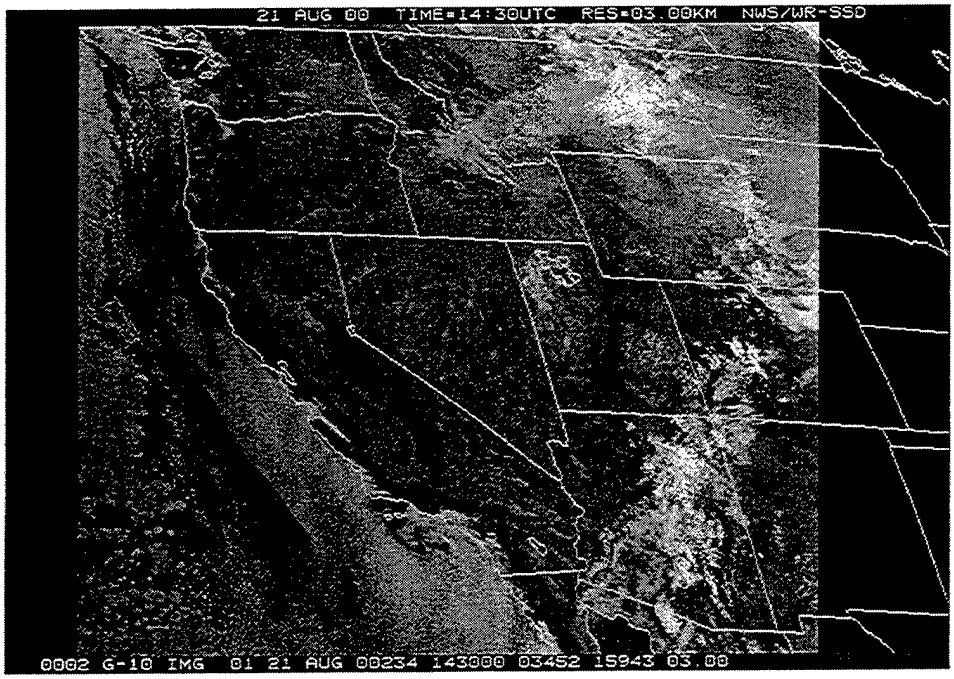

Figure C-40: The Synoptic Picture, GOES-10 1m Vis. Image at 21/1430Z

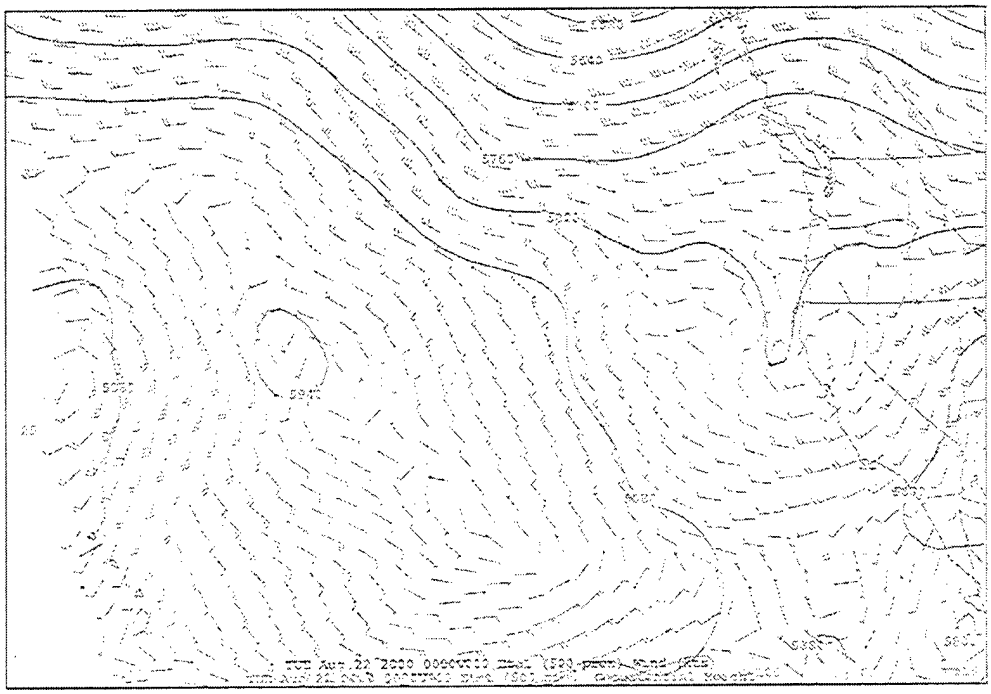

Figure C-41: The Synoptic Picture, ETA Model 500mb at 22/00Z

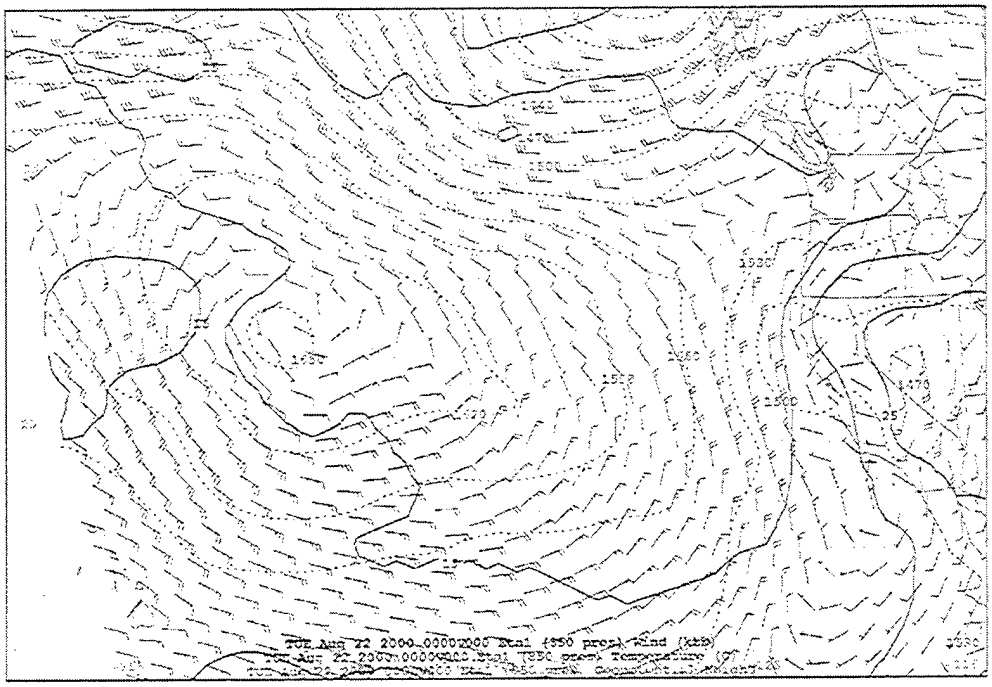

Figure C-42: The Synoptic Picture, ETA Model 850mb at 22/00Z

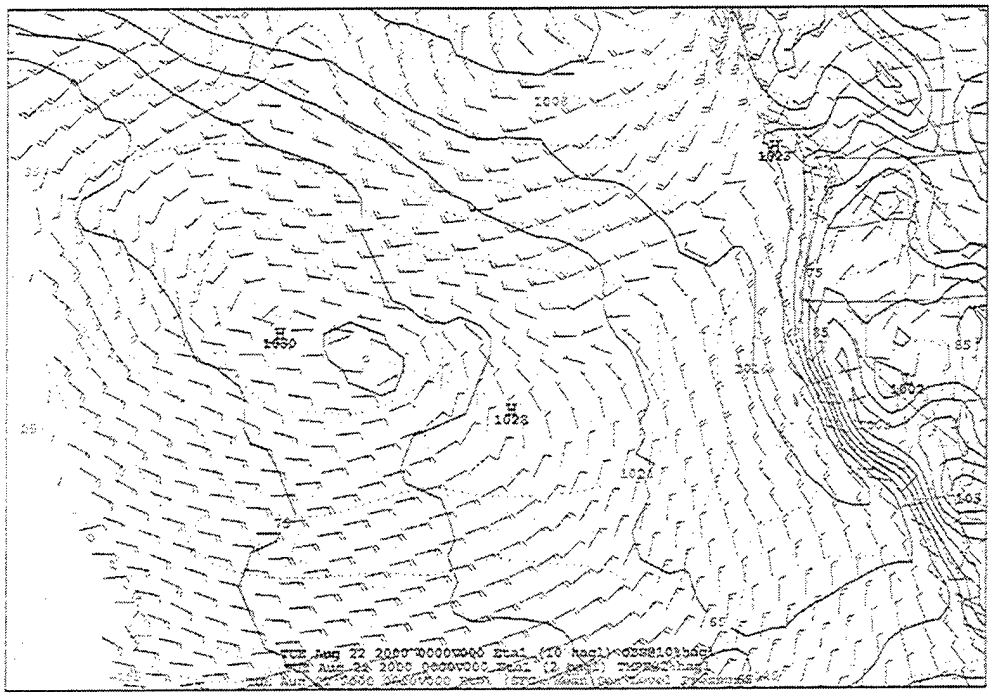

Figure C-43: The Synoptic Picture, ETA Model SFC at 22/00Z

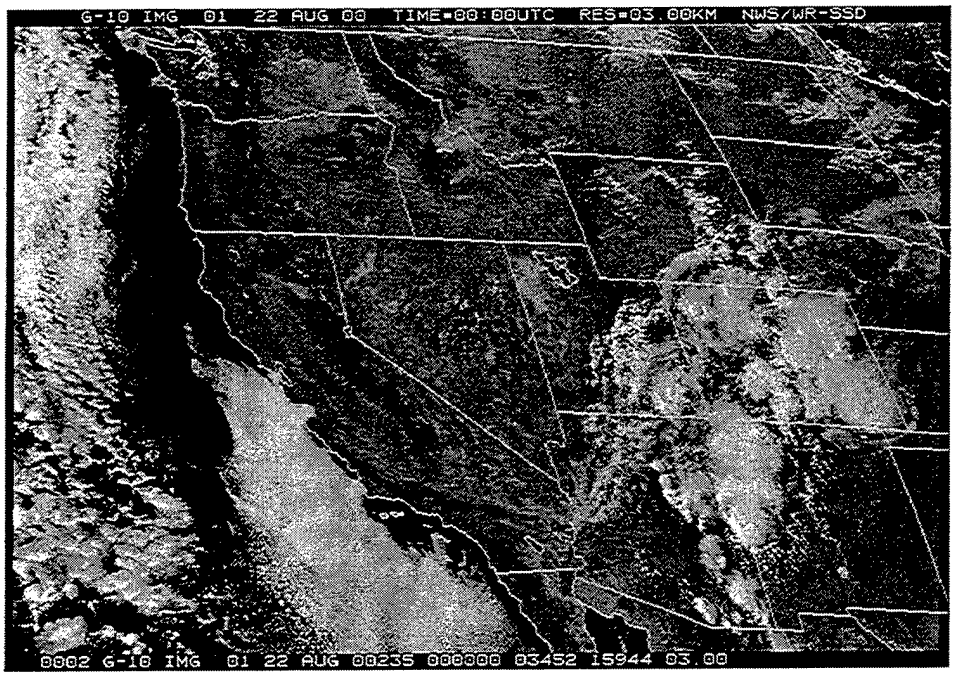

Figure C-44: The Synoptic Picture, GOES-10 1m Vis. Image at 22/00Z

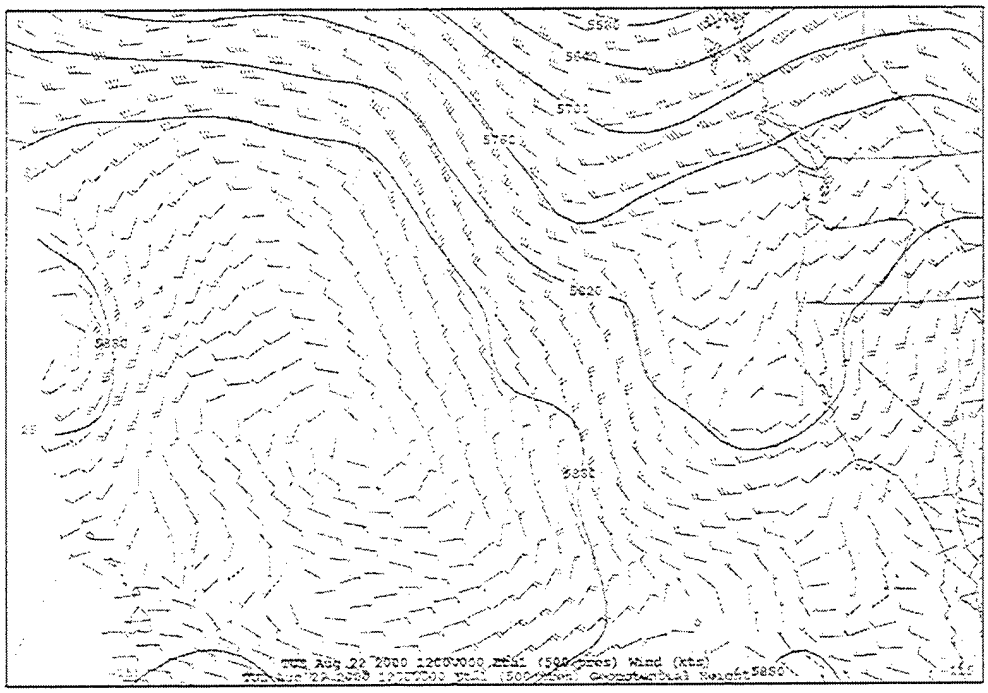

Figure C-45: The Synoptic Picture, ETA Model 500mb at 22/12Z

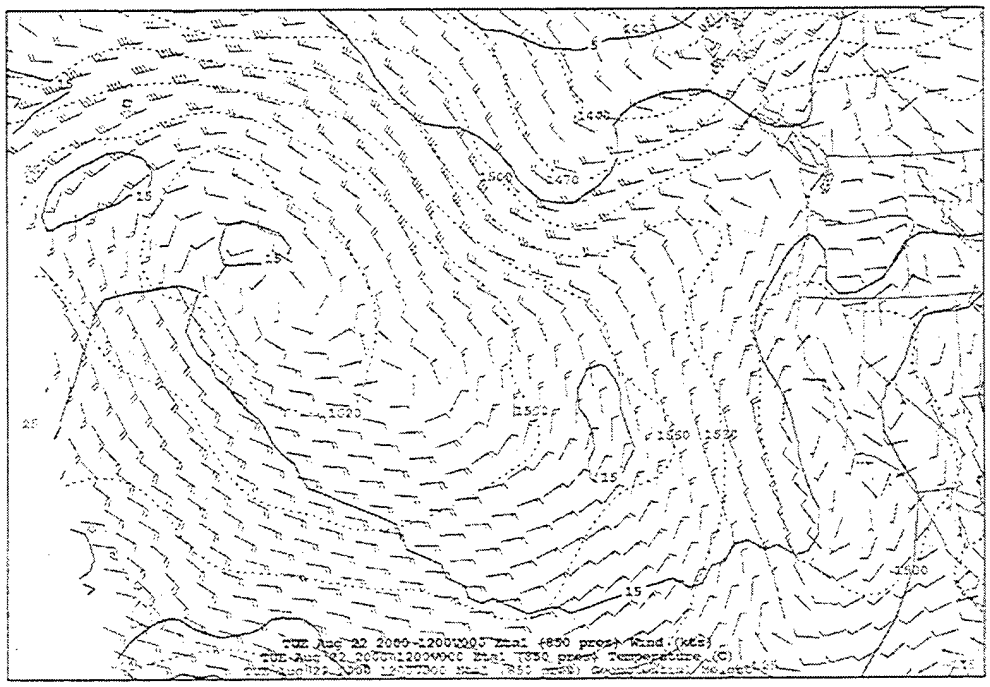

Figure C-46: The Synoptic Picture, ETA Model 850mb at 22/12Z

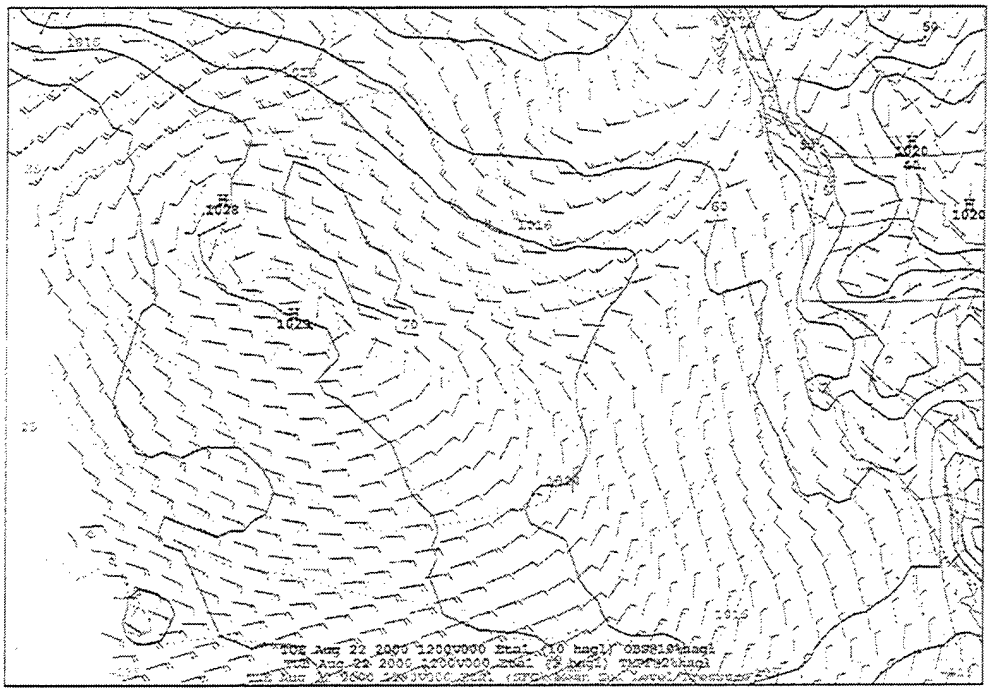

Figure C-47: The Synoptic Picture, ETA Model SFC at 22/12Z

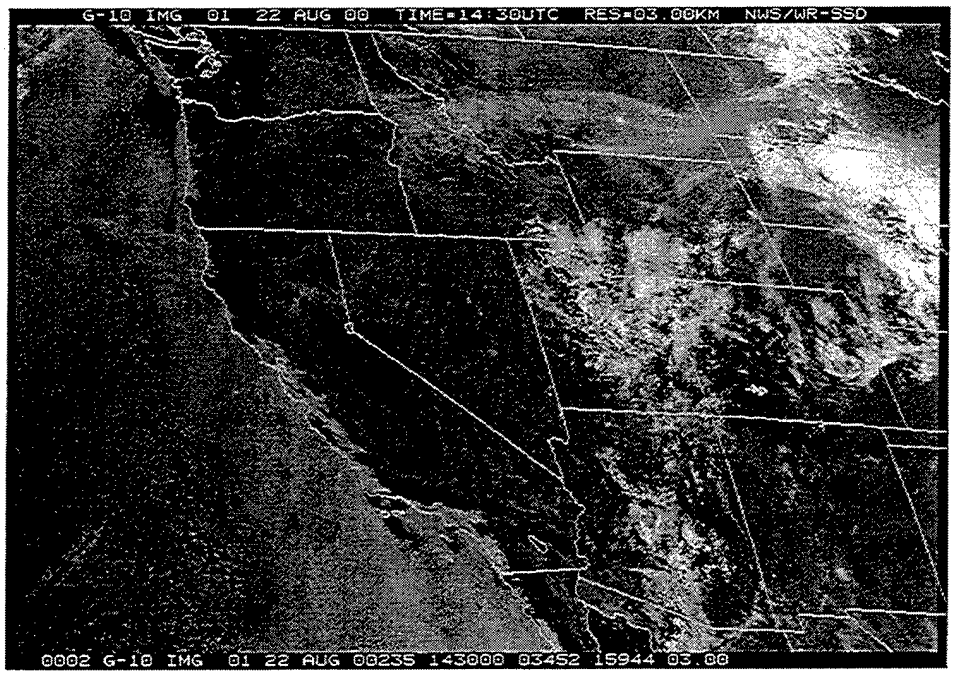

Figure C-48: The Synoptic Picture, GOES-10 1m Vis. Image at 22/1430Z

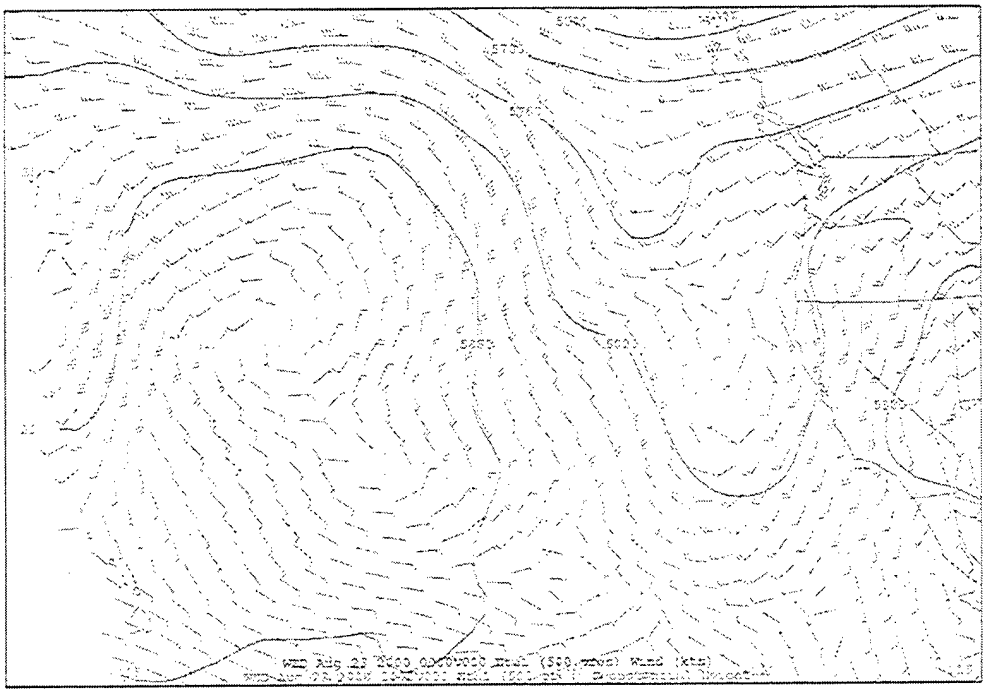

Figure C-49: The Synoptic Picture, ETA Model 500mb at 23/00Z

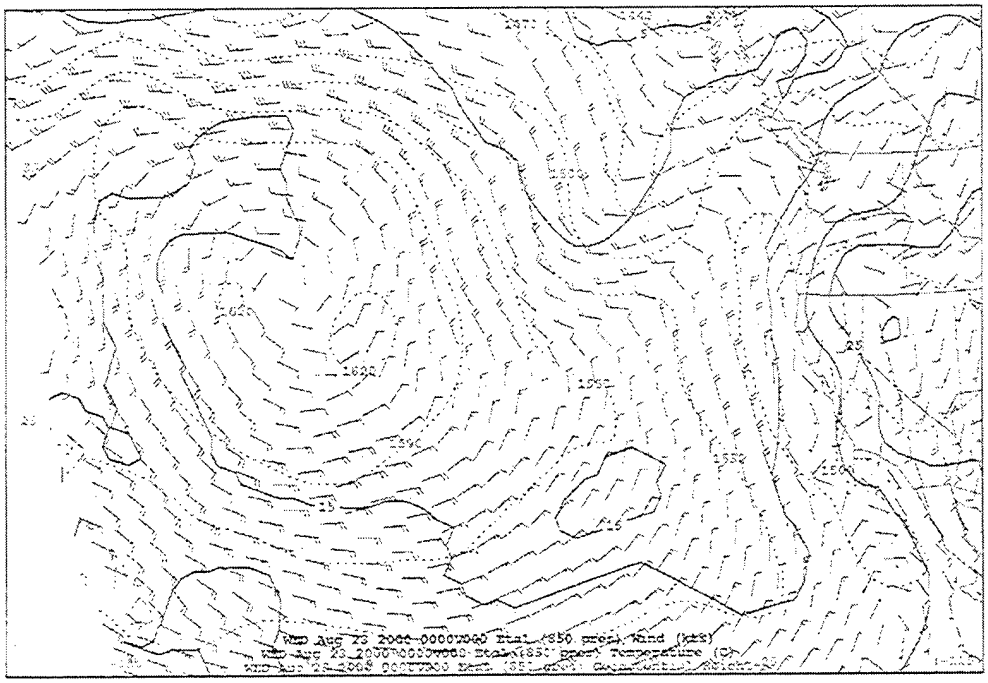

Figure C-50: The Synoptic Picture, ETA Model 850mb at 23/00Z

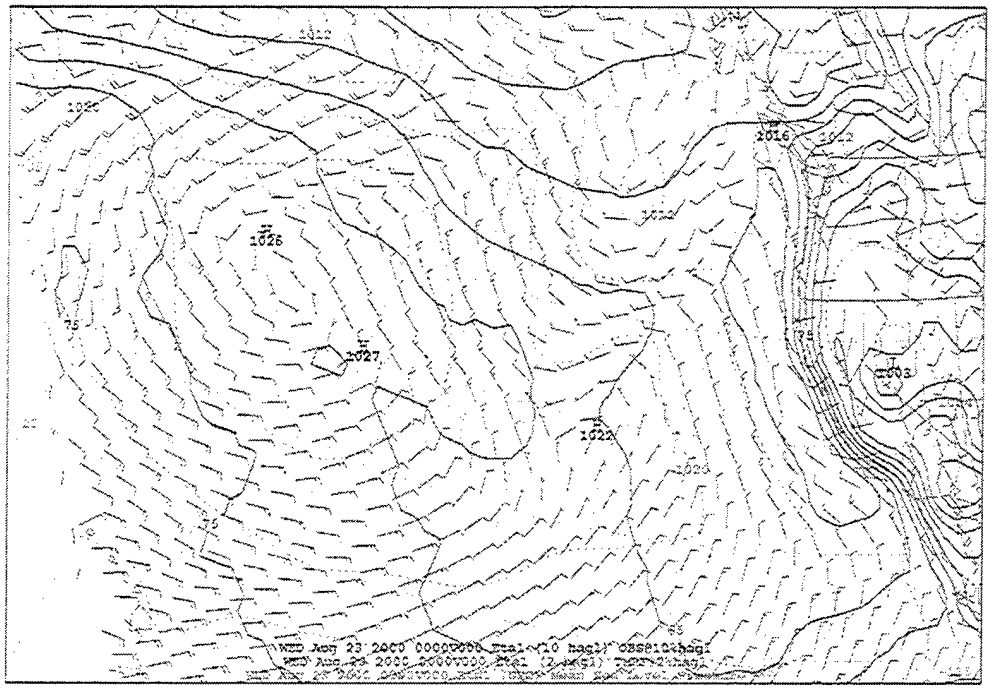

Figure C-51: The Synoptic Picture, ETA Model SFC at 23/00Z

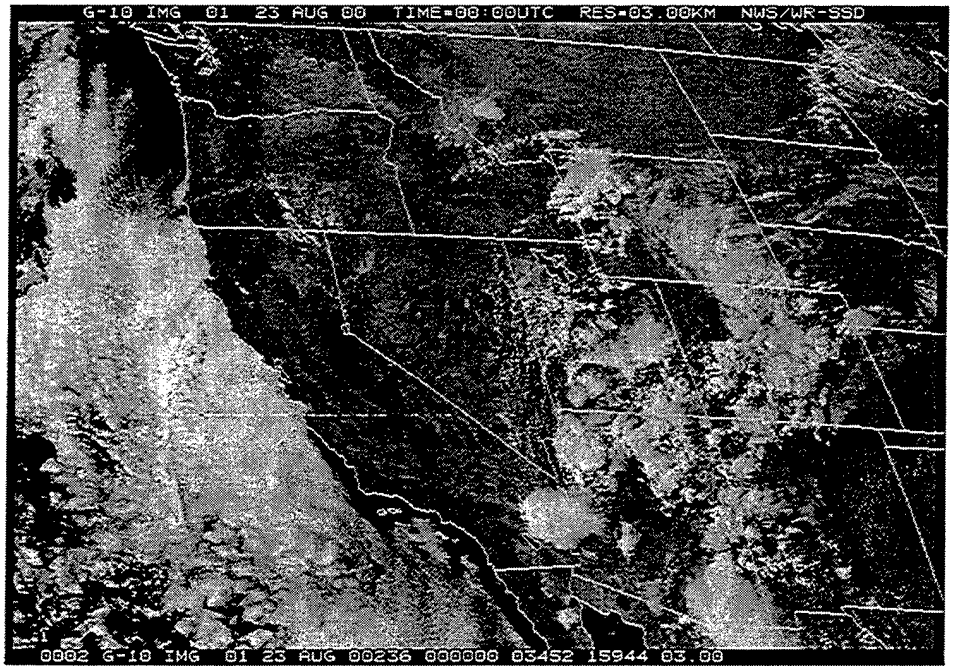

Figure C-52: The Synoptic Picture, GOES-10 1m Vis. Image at 23/00Z

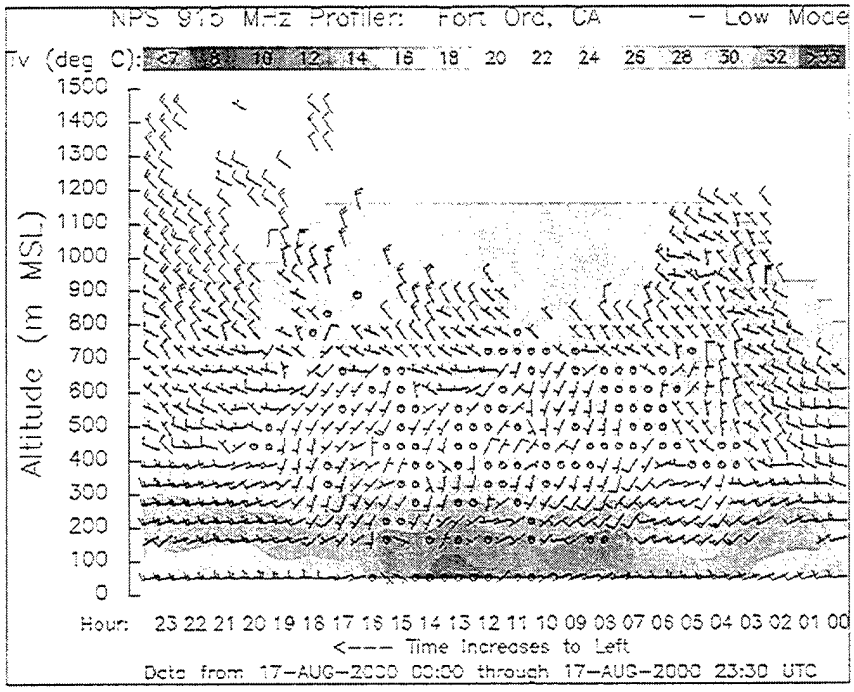

Figure C-53: Ft. Ord Profiler for 17 August

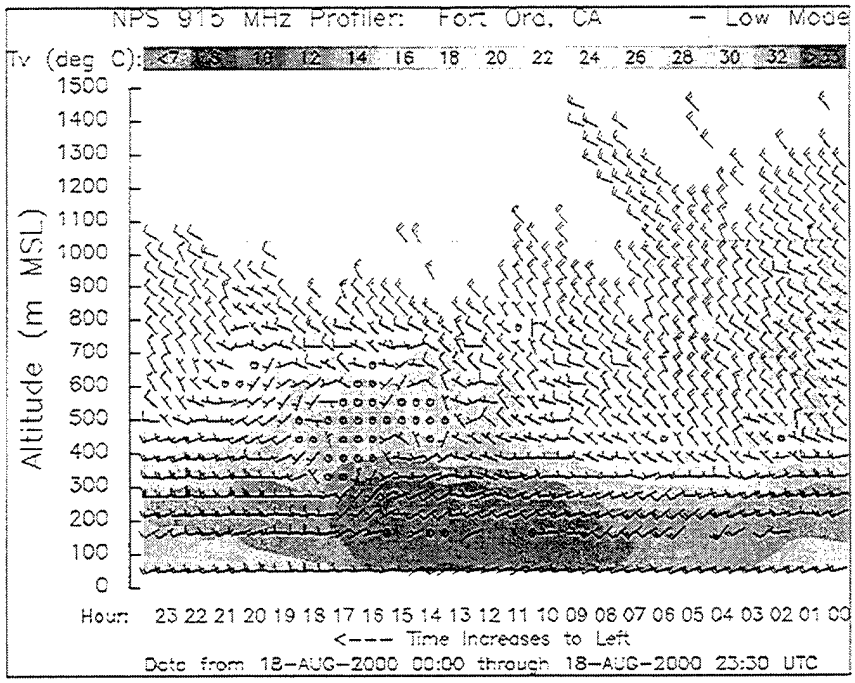

Figure C-54: Ft. Ord Profiler for 18 August

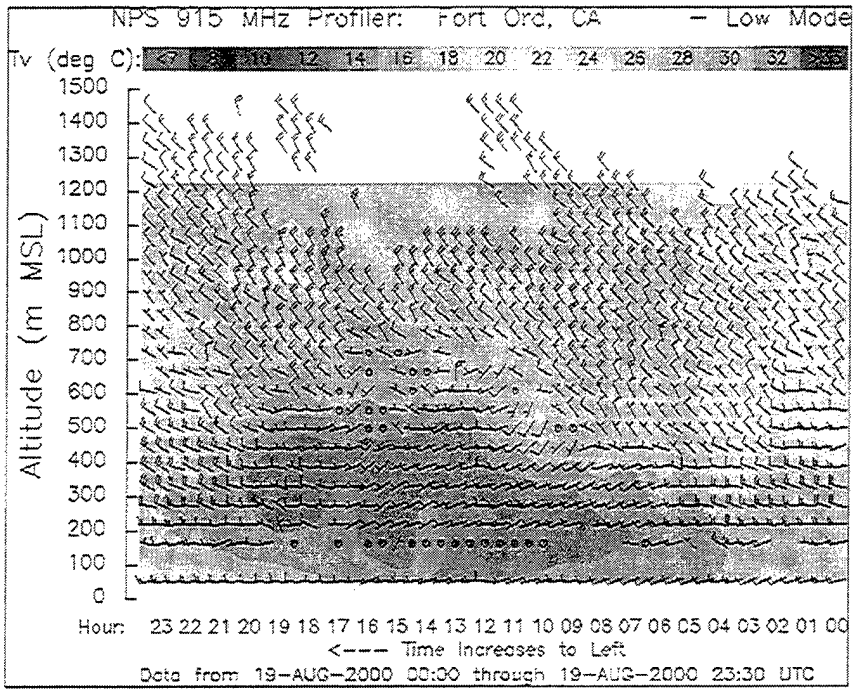

Figure C-55: Ft. Ord Profiler for 19 August

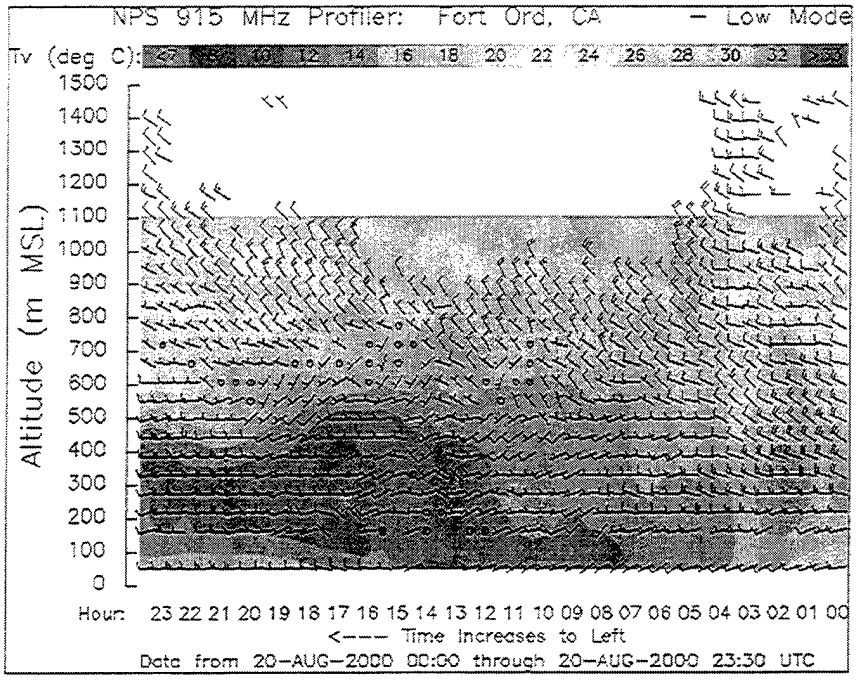

Figure C-56: Ft. Ord Profiler for 20 August

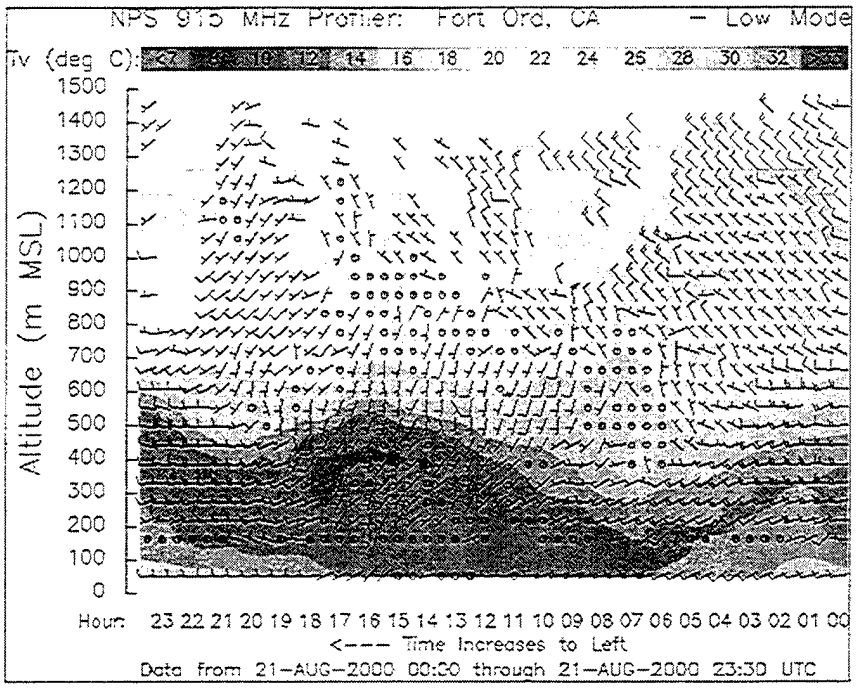

Figure C-57: Ft. Ord Profiler for 21 August

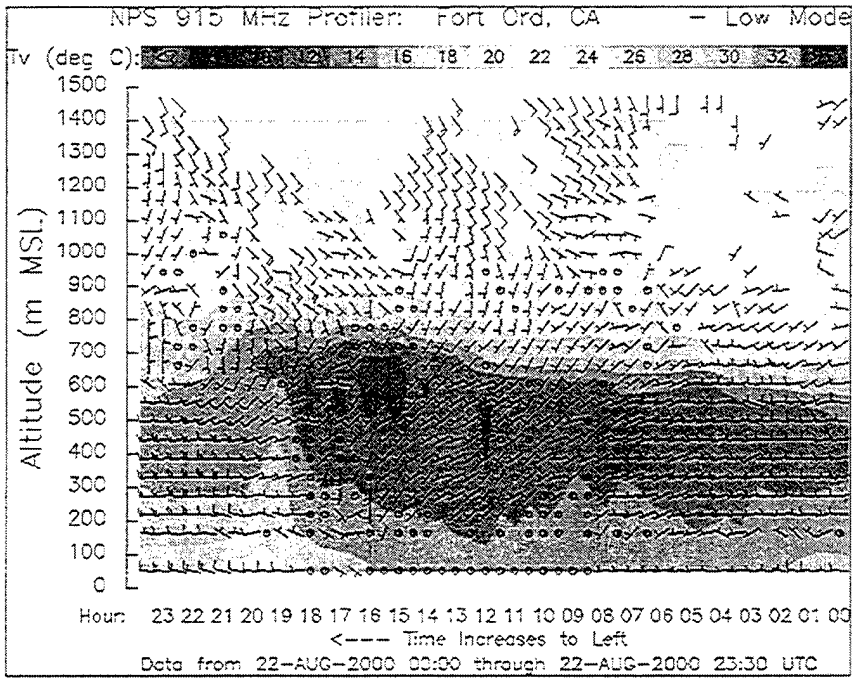

Figure C-58: Ft. Ord Profiler for 22 August

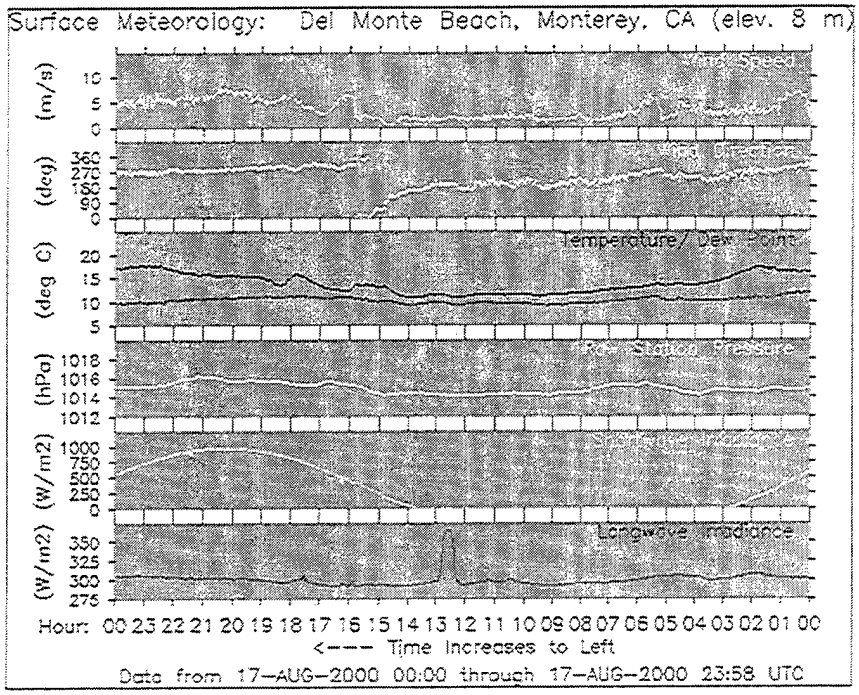

Figure C-59: Del Monte Beach Station Plot for 17 August

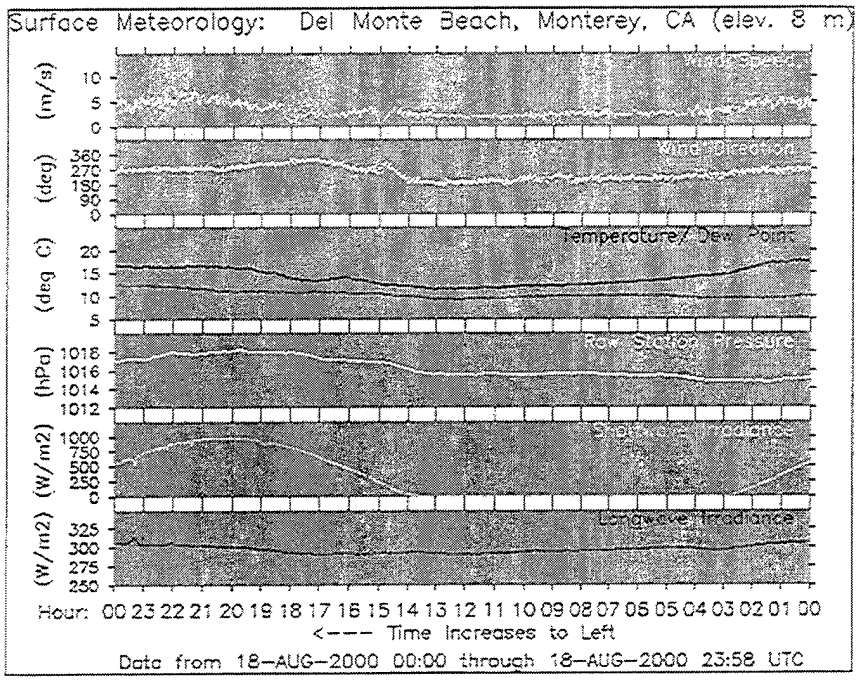

Figure C-60: Del Monte Beach Station Plot for 18 August

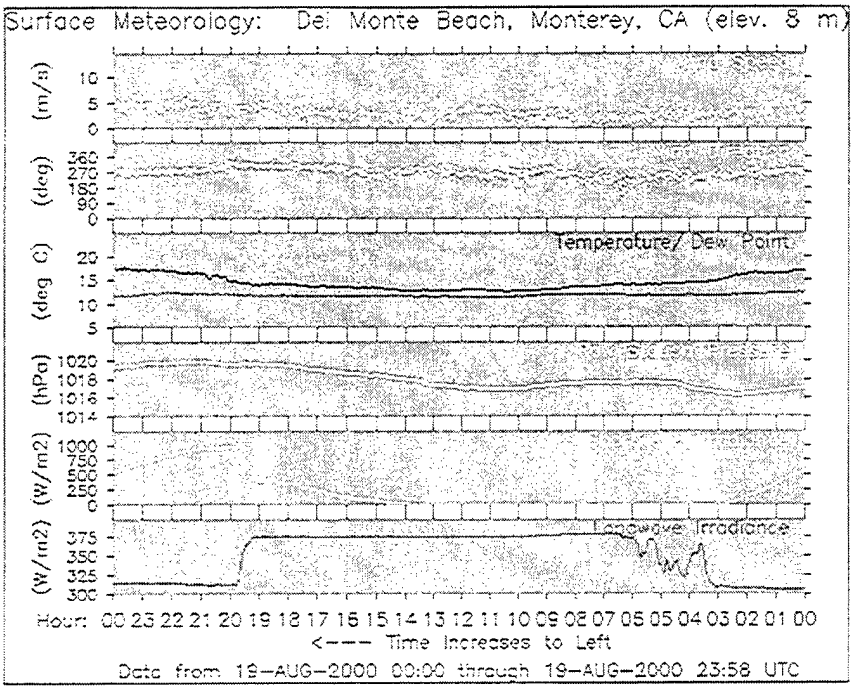

Figure C-61: Del Monte Beach Station Plot for 19 August

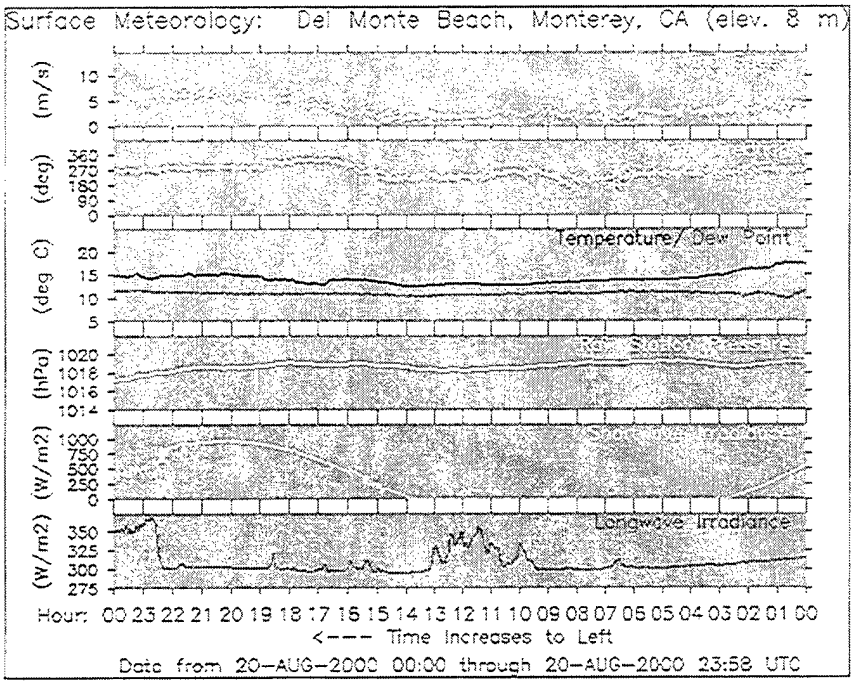

Figure C-62: Del Monte Beach Station Plot for 20 August

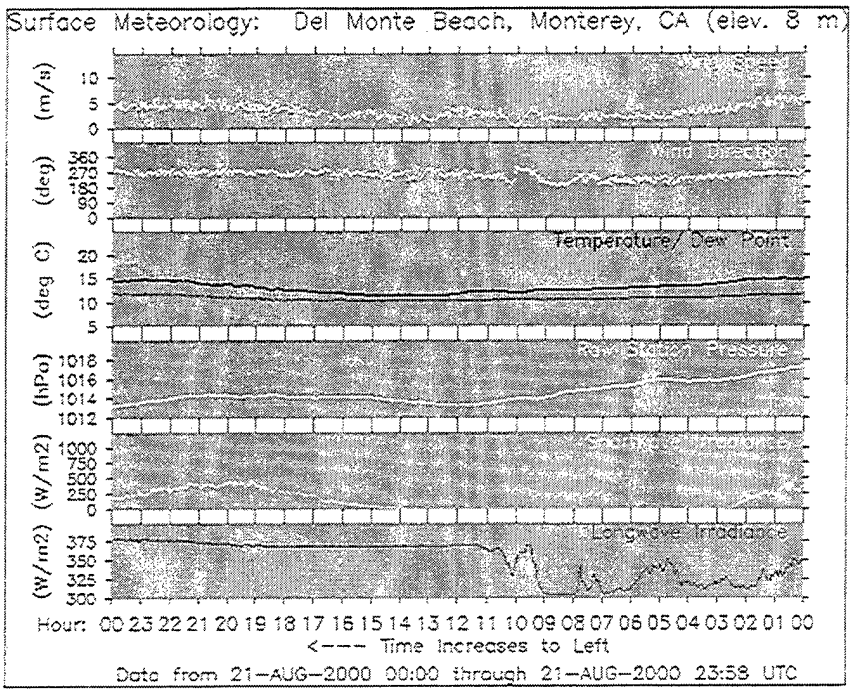

Figure C-63: Del Monte Beach Station Plot for 21 August

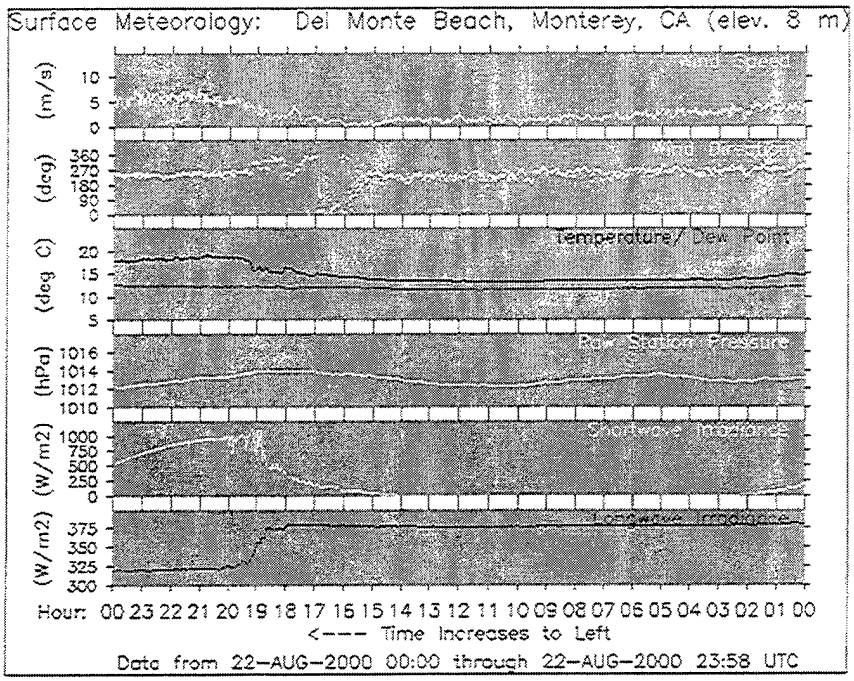

Figure C-64: Del Monte Beach Station Plot for 22 August

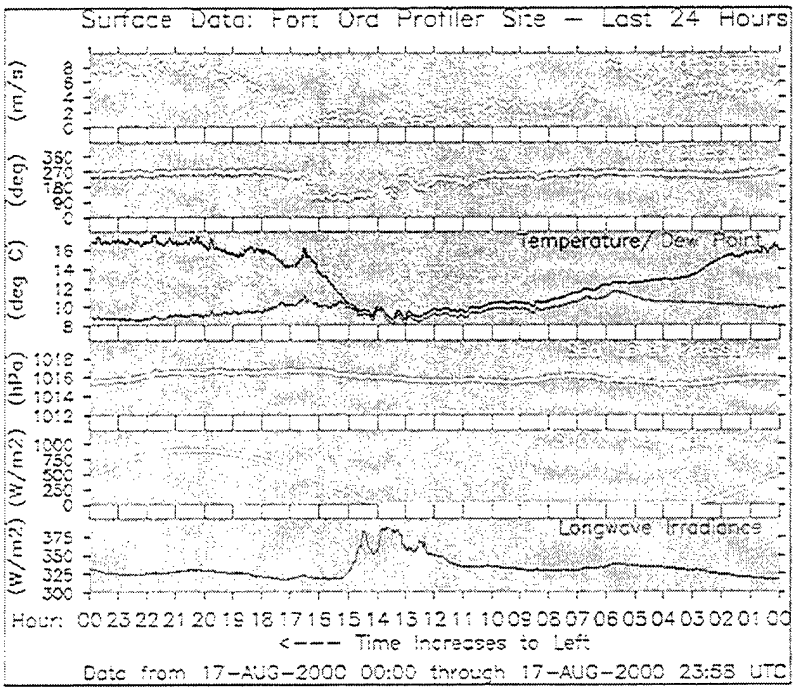

Figure C-65: Ft. Ord Surface Station Plot for 17 August

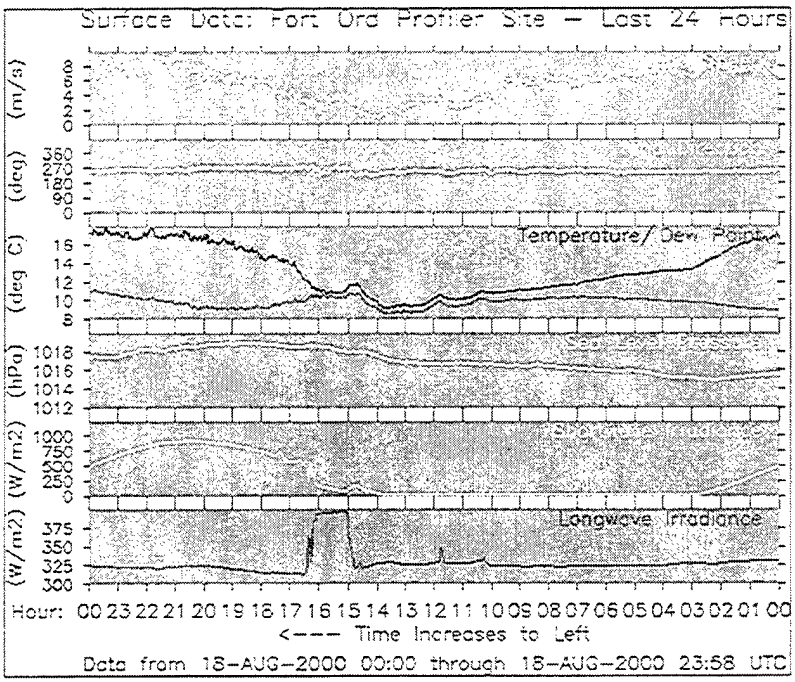

Figure C-66: Ft. Ord Surface Station Plot for 18 August

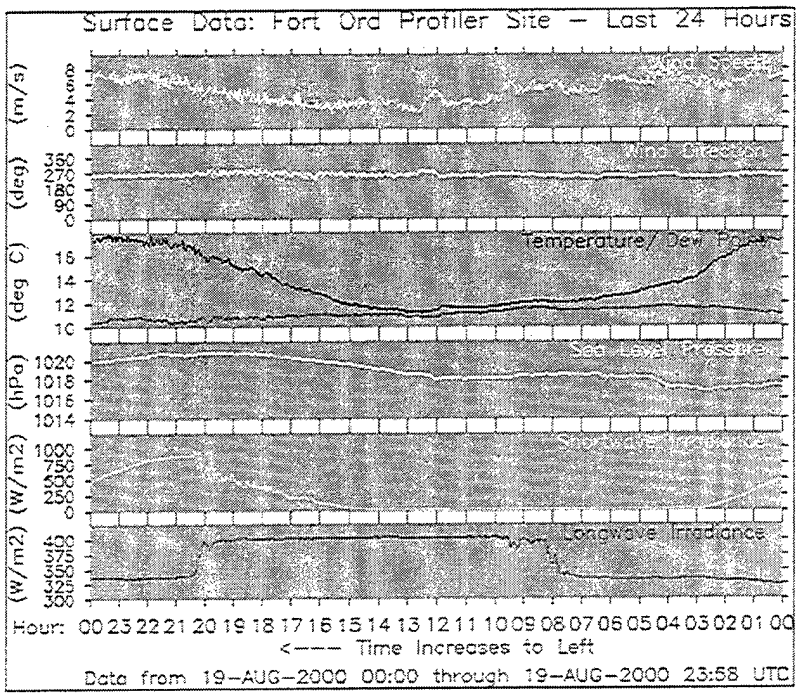

Figure C-67: Ft. Ord Surface Station Plot for 19 August

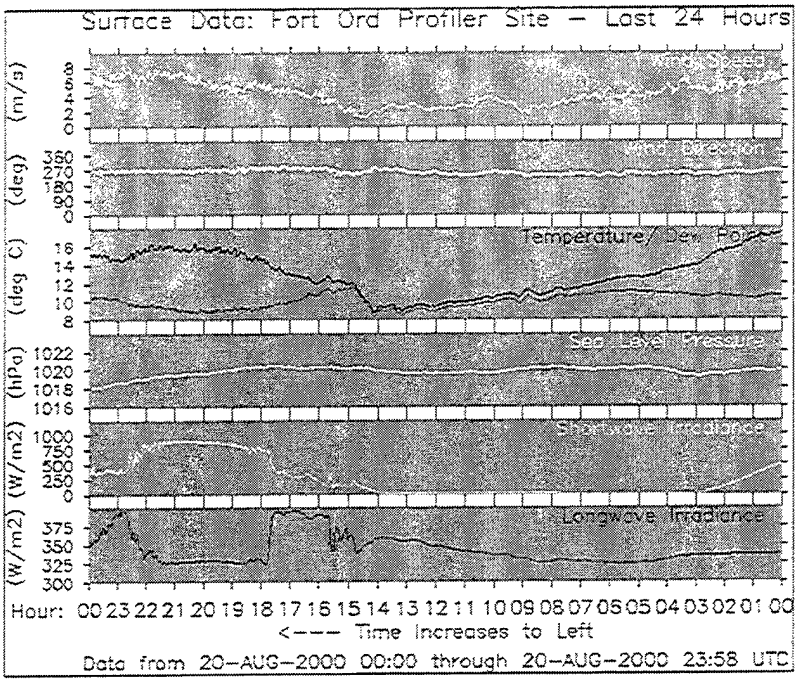

Figure C-68: Ft. Ord Surface Station Plot for 20 August

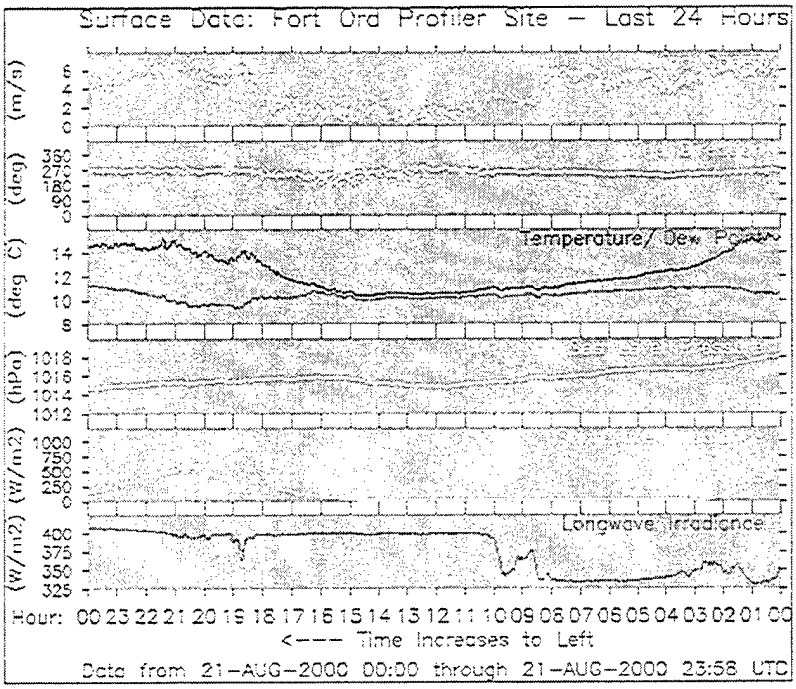

Figure C-69: Ft. Ord Surface Station Plot for 21 August

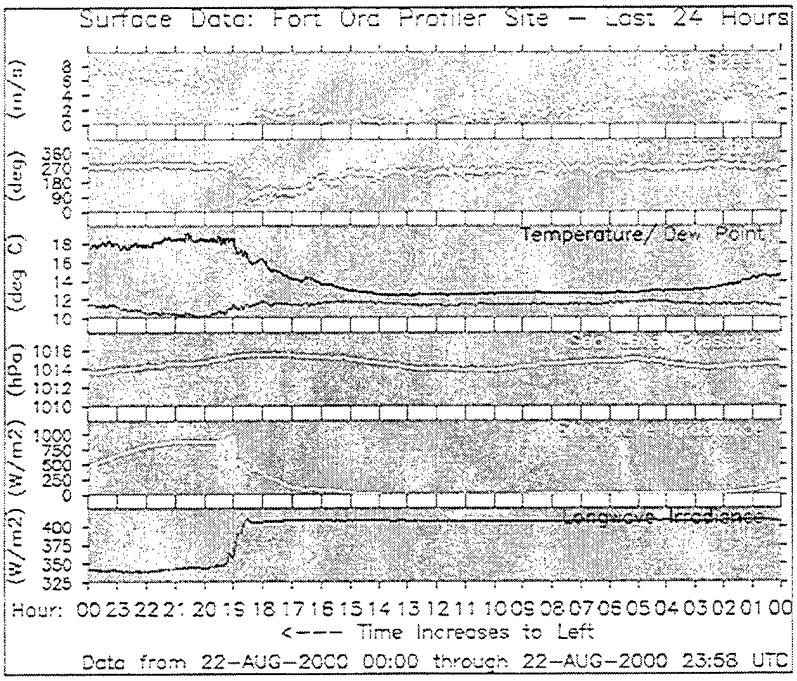

Figure C-70: Ft. Ord Surface Station Plot for 22 August

THIS PAGE INTENTIONALLY LEFT BLANK

LIST OF REFERENCES

Anderson, J.B., "Observations from Airplanes of Cloud and Fog Conditions Along the Southern California Coast," *Monthly Weather Review*, v. 59, pp264-270, 1931.

Backes, Douglas, *Santa Ana Associated Offshore Fog: Forecasting with a Sequential Model*, Master's Thesis, Naval Postgraduate School, Monterey, California, September 1977.

Blake, D., "Temperature inversions at San Diego, as deduced from aerographic observations by airplane," *Monthly Weather Review*, v. 56, pp221-224, 1928.

Chou, Ming-Dah and Peng, Li, "A Parameterization of the Absorption in the 15μm CO_2 Spectral Region with Application to Climate Sensitivity Studies," *Journal of the Atmospheric Sciences*, v. 40, pp. 2183-2192, September 1983.

Chou, Ming-Dah, "Broadband Water Vapor Transmission Functions for Atmospheric IR Flux Computations," *Journal of the Atmospheric Sciences*, v. 41, pp. 1775-1778, May 1984.

CNMOC, "Naval Meteorology and Oceanography Command Strategic Plan," May, 1997.

Durkee, P., Interview between P. Durkee, Professor, Naval Postgraduate School, Monterey, CA, and the author, 9 March 2001.

FNMOC, "The Fleet Numerical Meteorology and Oceanography Center Home Page." [http://www.fnmoc.navy.mil], 2001.

Haack, Tracy, Email from T. Haack, Naval Research Laboratory, Monterey, CA, and the author, 10 January 2001.

Harshvardhan, *et al.*, "A Fast Radiation Parameterization for Atmospheric Circulation Models," *Journal of Geophysical Research*, v. 92, pp. 1009-1016, January 1987.

Hodur, Richard M., "The Naval Research Laboratory's Coupled Ocean / Atmosphere Mesoscale Prediction System (COAMPS)," *Monthly Weather Review*, v. 125, pp. 1414-1430, July 1997.

Hogan, Timothy, Email from Dr. T. Hogan, Naval Research Laboratory, Monterey, CA, and the author, 31 December 2000.

Kong, Fanyou, "A Study of Marine Stratus and Fog Events Using COAMPS Model," paper presented at the American Meteorological Society's Third Conference on Coastal Prediction, New Orleans, LA, 3-5 November 1999.

Koracin, Darko R. *et al.*, "Observations and Modeling of Offshore Fog along the California Coast," paper submitted to the *Journal of Atmospheric Sciences*, 1999.

Koracin, Darko R. *et al.*, "Transition of Stratus into Fog Along the California Coast: Observations and Modeling," paper accepted by the *Journal of Atmospheric Sciences*, 2000.

Lacis, Andrew and Hansen, James, "A Parameterization for the Absorption of Solar Radiation in the Earth's Atmosphere," *Journal of the Atmospheric Sciences*, v. 31, pp. 118-133, January 1974.

Leipper, Dale F., "Fog Development at San Diego California," *Journal of Maritime Research*, v. VII, pp. 337-346, 1948.

Leipper, Dale F., "Fog on the U.S. West Coast: A Review," *Bulletin of the American Meteorological Society*, v. 75, pp. 229-240, February 1994.

Leipper, Dale F., "Fog Forecasting Objectively in the California Coastal Area Using LIBS," *Weather and Forecasting*, v. 10, pp. 741-762, December 1995.

Liou, Chi Sann, Email from Dr. C.S. Liou, Naval Research Laboratory, Monterey, CA, and the author, 22 December 2000.

Lorenz, E.N., *The Essence of Chaos*, University of Washington Press, Seattle, 227pp., 1993.

Mass, Clifford F. and Steenburgh, W. James, "An Observational and Numerical Study of an Orographically Trapped Wind Reversal along the West Coast of the United States," *Monthly Weather Review*, v. 128, pp. 2363-2396, July 2000.

Mechem, David and Kogan, Yefim, "Simulations of Coastal StratoCu Using COAMPS with a New Cloud Microphysical Parameterization," Navy Research Lab Seminar, Monterey, CA, November 2000.

NRL, "The Naval Research Laboratory, Monterey Home Page." [http://www.nrlmry.navy.mil], 2001.

Nuss, W. A., Class notes for MR3262, *Operational Weather Prediction*, Department of Meteorology, Naval Postgaduate School, 86pp, 2000.

Nuss, W. A. and Titley, D. W.,"Use of Multiquadric Interpolation for Meteorological Analysis," *Monthly Weather Review*, v. 122, pp1611-1631, 1994.

Paduan, Jeffrey D. and Ramp, Steven, "Aerial SST and Wind Mapping During MUSE." [http://www.oc.nps.navy.mil/~icon/collaborations/muse_overflights.htm], August 2000.

Petterssen, Sverre, "On the Causes and the Forecasting of the California Fog," *Bulletin of the American Meteorological Society*, v. 19, pp. 49-55, February 1938.

Pelié, R. J., *et al.*, "The Formation of Marine Fog and the Development of Fog-Stratus Systems along the California Coast," *Journal of Applied Meteorology*, v. 18, pp. 1275-1286, October 1979.

Rogers R. R. and Yau, M. K., *A Short Course in Cloud Physics (3rd Edition).* pp. 81-149, Butterworth-Heinemann, 1989.

Sterbis, Christopher, *An Analysis of Short-Term Mesoscale Forecasts in the Los Angeles Basin Using Southern Coast Ozone Study 1997 Data.* Master's Thesis, Naval Postgraduate School, Monterey, California, September 2000.

Tag, Paul and Peak, James, "Machine Learning of Maritime Fog Forecast Rules," *Journal of Applied Meteorology*, v. 35, pp. 714-724, May 1996.

Tjernstrom, Michael, "Turbulence Length Scale in Stably Stratified Free Shear Flow Analyzed from Slant Aircraft Profiles," *Journal of Applied Meteorology*, v. 32, pp. 948-963, May 1993.

Walters, D. L. and D. K. Miller, "Evolution of an Upper-Tropospheric Turbulence Event - Comparison of Observations to Numerical Simulations," paper presented at the 13th Symposium on Boundary Layers and Turbulence, Dallas, Texas, 10-15 January, 1999.

Zwack, Peter and Tardiff, Robert, "The COBEL One-Dimensional Atmospheric Boundary Layer Model." [http://people.sca.uqam.ca/~tardif/COBEL/cobel_main_fr.htm]. 1999.

THIS PAGE INTENTIONALLY LEFT BLANK

INITIAL DISTRIBUTION LIST

1. Defense Technical Information Center 2
   8725 John J. Kingman Road, Suite 0944
   Ft. Belvoir, VA 22060-6218

2. Dudley Knox Library 2
   Naval Postgraduate School
   411 Dyer Road
   Monterey, CA 93943-5101

3. Chairman, Code MR/Wx 1
   Department of Meteorology
   Naval Postgraduate School
   Monterey, CA 93943-5101

4. Chairman, Code OC/Ga 1
   Department of Oceanography
   Naval Postgraduate School
   Monterey, CA 93943-5101

5. Professor Robert L. Haney 1
   Department of Meteorology
   Naval Postgraduate School
   Monterey, CA 93943-5101

6. Professor Douglas K. Miller 1
   Department of Meteorology
   Naval Postgraduate School
   Monterey, CA 93943-5101

7. Professor Wendell Nuss 1
   Department of Meteorology
   Naval Postgraduate School
   Monterey, CA 93943-5101

8. Professor Jeffrey Paduan 1
   Department of Oceanography
   Naval Postgraduate School
   Monterey, CA 93943-5101

9. Dr. Richard M. Hodur 1
   Marine Meteorology Division
   Naval Research Laboratory
   7 Grace Hopper Avenue
   Monterey, CA 93943-5502

10. Dr. Darko Koracin 1
Desert Research Institute
2215 Raggio Parkway
Reno, NV 89512-1095

11. Commander 1
Naval Meteorology and Oceanography Command
1020 Bach Boulevard
Stennis Space Center, MS 39529-5005

12. Models Department Head 1
Fleet Numerical Meteorology and Oceanography Center
7 Grace Hopper Avenue
Monterey, CA 93943

13. LCDR John L. Dumas 4
7517 John Henry Lane
Roseville, CA 95747